THE CATALYTIC HYDROGENATION OF CARBON-CARBON AND CARBON-NITROGEN MULTIPLE BONDS BY A COBALT(I) COMPLEX

BY

KENAN TOKMIC

DISSERTATION

Submitted in partial fulfillment of the requirements
for the degree of Doctor of Philosophy in Chemistry
in the Graduate College of the
University of Illinois at Urbana-Champaign, 2018

Urbana, Illinois

Doctoral Committee:

Assistant Professor Alison R. Fout, Chair
Professor Thomas B. Rauchfuss
Professor Kenneth S. Suslick
Assistant Professor Josh Vura-Weis

ABSTRACT

The widespread use of homogenous late second- and third-row transition metal complexes for the catalytic hydrogenation of carbon-carbon multiple bonds can be attributed to the well-defined reactivity, stability and overall high activity of such catalytic systems. The development of sustainable, more abundant and relatively less toxic late first-row transition metal complexes to parallel such catalysis is an attractive alternative and has gained much interest. However, due to the inherent electronic structure of these metals, common first-row transition metal complexes have a propensity to undergo one-electron or radical reactivity, which can be detrimental to the desired reactivity. Toward this end, an electron-rich monoanionic bis(carbene) aryl pincer ligand, ^{Mes}CCC, was chosen study two-election chemistry with cobalt.

With the ^{Mes}CCC pincer ligand platform well-suited to stabilize a range of oxidation states of cobalt (Co(III), Co(II), and Co(I)), studies into the room temperature metalation of the ligand precursor salt, $[H_3(^{Mes}CCC)]Cl_2$, resulted in the formation $(^{Mes}CCC)CoCl_2py$. Furthermore, the reduction of $(^{Mes}CCC)CoCl_2py$ with one or two reducing electron equivalents yielded the corresponding Co(II) and Co(I) complexes, respectively. Characterization of these complexes by ^1H and ^{13}C NMR, EPR, and FT-IR spectroscopies, as well as single crystal X-ray crystallography is described. The interconversion between a series of low-spin cobalt complexes in the +3, +2 and +1 oxidation states provides a platform for which to study two-electron chemistry with cobalt.

The reactivity of the low-valent $(^{Mes}CCC)Co(N_2)(PPh_3)$ towards dihydrogen resulted in a reversible H_2 coordination to the cobalt center and based on multinuclear NMR studies, a nonclassical binding mode of H_2 was established, $(^{Mes}CCC)Co(H_2)(PPh_3)$. The scrambling of H_2 and D_2 by the Co(I)-(H_2) species suggests a Co(III)-$(H_2)(H)_2$ intermediate may be involved. Furthermore, the competency of the Co-(H_2) complexes towards the catalytic hydrogenation of alkenes was also investigated. The hydrogenation of terminal olefins proceeded selectivity at room temperature, while more sterically demanding 1,2-disubstitued olefins proceeded at elevated temperatures. Mechanistic studies based on multinuclear and *para*hydrogen (*p*-H_2) induced polarization (PHIP) transfer NMR reveled a Co(I)/Co(III) redox process was operative.

Based on the mechanistic studies of the olefin hydrogenation studies, the hydrogenation utility of $(^{Mes}CCC)Co(N_2)(PPh_3)$ was extended toward the semi-hydrogenation of a broad scope of alkynes with excellent selectivity toward *E*-alkenes. Mechanistic studies of the alkyne hydrogenation process using

^{1}H, ^{2}H and PHIP transfer NMR spectroscopy enabled the identification of key reaction intermediates and established that *cis*-hydrogenation occurs first, followed by *trans*-isomerization under a H_2 atmosphere.

The catalytic utility of the (^{Mes}CCC)Co complexes was extended to the selective hydrogenation nitriles to primary amines. The active catalyst was generated by the *in situ* reduction of a bench-stable Co(III) precatalyst, (^{Mes}CCC)$CoCl_2$py, using $NaHBEt_3$. The resulting BEt_3 was found to be vital to the observed catalysis, acting as Lewis acid. Based on the PHIP transfer NMR studies, the role of BEt_3 was proposed to facilitate a side-on coordination of the nitrile to cobalt center, thus permitting a pairwise transfer of H_2 through a Co(I/III) redox process to proceed.

Given the robust functional group tolerance and enhancement of the ^{1}H NMR resonances in the hydrogenation products using PHIP, the low-valent (^{Mes}CCC)Co complex were shown to effectively hyperpolarize the ^{13}C NMR signals using *p*-H_2. Comparisons of the carboxylate ^{13}C signal enhancement of ethyl propionate using [(dppb)Rh(COD)]BF_4 and (^{Mes}CCC)Co-py, showed that the cobalt complex hyperpolarization efficiency is comparable with the rhodium system, demonstrating that the monoanionic bis(carbene) pincer ligand supports noble-metal reactivity with cobalt.

Lastly, stoichiometric oxidative addition and reductive elimination chemistry with the ^{Mes}CCC ligand platform demonstrate the viability of a Co(I)/Co(III) redox couple in the proposed catalytic hydrogenation reactions. The preparation of cationic cobalt(III)-hydride dinitrogen phosphine complexes served as a platform to study migratory insertion of alkenes, as well as, the scrambling of H_2 and D_2. These studies also demonstrate that the ^{Mes}CCC ligand system not only supports the hydrogenation activity but has the proper spectroscopic features to elucidate key mechanistic steps involved.

Za Moju Porodicu

Denmark 1994

ACKNOWLEDGEMENTS

I would like to thank my family first. My father, mother, and older brother have supported me and each other throughout our migration within Europe that eventually led us to the United States of America. Without them, I would not have made it to this point.

I would also like to thank my advisor, Professor Alison Fout. Her door has always been open for a "quick" chat that usually ended about an hour later. I will always appreciate her continued support and insightful discussions which have helped move my research project forward and even spur new ones to explore. Also, I would to like to thank my committee members Professors Tom Rauchfuss, Ken Suslick, and Josh Vura-Weis for their time and guidance.

I am also very thankful for the support of current: *Gabriel Espinosa Martinez, Courtney Ford, Bailey Jackson, Micheal Drummond, Tabitha Miller, Joe Nugent, Safiyah Muhammad, Clare Leahy and Daniel Najera* and past: *Dr. Ellen Matson, Dr. Marshall Brennan, Dr. Yun Ji Park, Dr. Abdulrahman Ibrahim, Jack Killion, and Dr. Zach Gordon* members of the Fout Group. I really enjoyed working with everyone over the past couple of years. During my time in graduate school I have also had the opportunity to mentor and work with the two amazing undergraduate students, Andrea Salazar and Rianna Greer. I am very grateful for all their help.

I would also like to thank Dr. Lingyang Zhu for her patience and help with the PHIP NMR studies. In addition, Charlie Markus and Prof. Benjamin McCall have been very helpful for the generation of *p*-H_2. Dr. Danielle Gray, Dr. Jeffery Bertke and Dr. Toby Woods have been very supportive of modeling disorder in my crystal structures. I would also like to thank Dr. Mark Nilges for helping me with EPR studies.

Lastly, I would like to thank my girlfriend, Lisa Della Ripa, for all her continued support and advice throughout our exciting time at Illinois. Even though at the end of the day we both leave the lab, our trade always continued in the kitchen, by exploring new recipes of the freshly caught fish and enjoying a glass of wine.

TABLE OF CONTENTS

CHAPTER 1: INTRODUCTION

The current emphasis of employing Earth abundant transition metals in favor of noble metals to catalyze chemical reactions is not a novel concept. Historically, osmium was first used to catalyze the hydrogenation of N_2 to ammonia, but today, catalysts featuring iron are highly efficient and are widely employed in the Haber-Bosch process.[1] However, in the case of another industrially momentous process, hydroformylation or also referred to as the oxo process,[2] the opposite is true. The reaction was initially catalyzed by a cobalt(I) carbonyl species, $HCo(CO)_4$,[3] however, catalysts based on more expensive rhodium metal are currently used to mediate these transformations since the rhodium catalytic system is more active and operates under lower pressures and temperatures.[4,5]

That trend has continued, as currently numerous synthetic transformations are dominated by homogenous catalytic systems featuring late second- and third-row transition metals.[6] The integration of stability, well-defined reactivity and high-efficiency are some of the traits generally associated with dominance of noble metal systems.[7] Of the characteristics, well-defined and predictable two-electron reactivity such as oxidative addition, insertion, and reductive elimination is inherently ubiquitous in these metal systems and as result they have occupied a prominent position in numerous synthetic methodologies.[6,8] Vaska's complex, $IrCl(CO)(PPh_3)_2$,[9] readily undergoes oxidative addition of H_2 to give the Ir(III)-dihydride species and has been used as a platform to study two-electron processes (Scheme 1.1). Comparatively straightforward characterization of catalytic intermediates is an additional feature of precious metal complexes. For instance, mechanistic studies of rhodium hydrogenation catalysts[10] revealed numerous reaction intermediates and ultimately these insights led to the development of a more active complexes.[11,12] Despite being featured in numerous catalytic processes, questions into the long-term dependability on noble metals from a sustainability viewpoint arise.

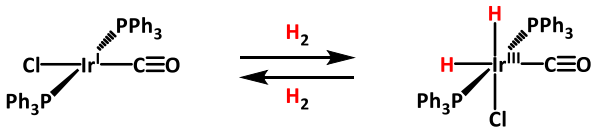

Scheme 1.1 Reversible reactivity of Vaska's compound with H_2.

From a sustainability view, isoelectronic late first-row transition metals can be considered as attractive alternatives to second- and third-row transition metal complexes. Despite being more abundant and generally less toxic, due to the innate electronic structure of common late first-row transition metal complexes, single-electron reactivity dominates. One-electron reactivity often results in side reactivity if two-electron chemistry is sought. Efforts toward promoting noble-metal reactivity on transition metal

complexes featuring base-metals have relied on leveraging ligand systems to circumvent one-electron reactivity.

1.1 Redox-active ligand approach to two-electron reactivity

Much like Nature's own way of furnishing two-electron reactivity[13] with Earth-abundant metals, the incorporation of supporting ligand platforms which can undergo redox changes themselves in addition to the metal center have proven to be an effective strategy to facilitate two-electron reactivity[14] in iron and cobalt complexes. Application of such an approach yielded the discovery of a catalytically active hydrogenation iron catalyst featuring a tridentate aryl-substituted pyridine(diimine) (PDI) ligand platform.[15,16] Subsequent reactivity studies of the cleavage of C-C bonds in biphenylene by the iron complex revealed a one-electron oxidation event at the metal center as well as a one-electron oxidation

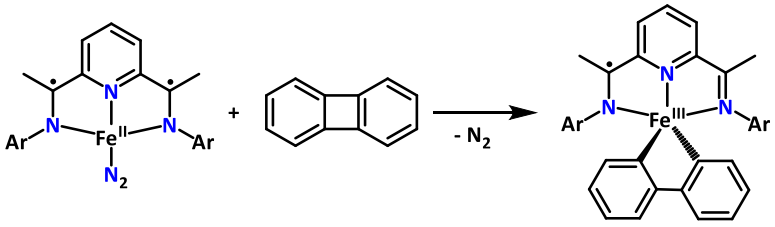

Scheme 1.2 Oxidative addition of biphenylene by ($^{Ar}PDI^{2-}$)Fe(II)-N_2 to give ($^{Ar}PDI^{1-}$)Fe(III)-biphenyl.

of the ligand platform, thus enabling an overall two-electron process to transpire (Scheme 1.2).[17] Adapting a cooperative ligand-metal approach, the hydrogenation of mono and disubstituted alkenes was extended to include square planar PDI cobalt complexes,[18] as well as, C_1-symmetric PDI cobalt derivates,[19] which were active for the asymmetric hydrogenation of prochiral olefins. Incorporating N-heterocyclic carbenes into tridentate redox-active ligands platforms, such as in ^{iPr}CNC-cobalt complexes, (^{iPr}CNC = 2,6-(2,6-$^{i}Pr_2$-C_6H_3-imadazol-2-ylidene)2-C_5H_3N),[20] furnished more electron-rich cobalt complexes than the PDI derivatives and as a result, were highly active for the reduction of unactivated olefins and even challenging tri- and tetra-substituted alkenes. Despite this success of this approach to circumvent one-electron reactivity, unexpected deactivation pathways resulting from the ligand centered radicals can arise and have been shown to hamper catalysis.[20] Nevertheless, redox-active ligands have proven to be an effective approach to yield two-electron reactivity on late first-row transition metal complexes.

1.2 Strong-field ligand approach toward two-electron reactivity

Unlike with the redox active ligand approach, the incorporation of strong-field ligands into late first-row transition metal complexes is focused on maximizing field-strengths to disfavor one-electron reactivity at the metal center. Based on angular overlap studies, carbon-based ligands are well matched

to impart a strong field on late first-row transition metals.[21,22] For example, cyclopentadienyl ligands have been used to sustain low-spin iron(II) configurations in ferrocene[23] and a combination of carbonyl and phosphine ligands have supported low-spin iron(0) complexes, such as (dppe)$Fe(CO)_3$ (dppe = $Ph_2PCH_2CH_2PPh_2$).[24] However, due to the coordinative saturation around the iron center, two-electron reactivity studies with ferrocene are limited. In the case of (dppe)$Fe(CO)_3$[24] dissociation of a strong field CO ligand results in the formation of a high-spin complex. Thus, supporting ligands must be preserved in the metal complex and prevented from taking part in reactivity to maintain a strong-field ligand environment.

Electron-rich pincer ligands are versatile platforms to study two-electron chemistry with base metals due the inherent stability upon complexation, the degree which the electronic and steric parameters can be tuned[25] and the meridional binding of the pincer system generally allows for up to 3 coordination sites for substrate binding. Recent examples of oxidative addition of H_2 onto square planar cobalt complexes (^{iPr}PNP)$CoCH_3$ (^{iPr}PNP = 2,6-bis-(diisopropylphosphino-methyl)-pyridine) (Scheme 1.3)[26] and (HPNP)CoCl (HPNP = $HN(CH_2CH_2PiPr_2)_2$)[27] as well as, three coordinate cobalt centers in ^{tBu}PNPCo (^{tBu}PNP = $(\{^tBu_2PCH_2SiMe_2\}_2N$-)[28] demonstrate the feasibility of using electron-rich pincer systems to study two-

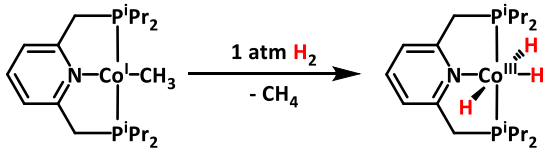

Scheme 1.3 Oxidative addition of H_2 with (^{iPr}CNC)Co(I)-CH_3 to give (^{iPr}CNC)Co(III)-$(H)_3$.

electron chemistry. Additionally, low-spin cobalt(II) complexes featuring electron-rich bidentate phosphine and alkyl ligands were shown to be active for hydrogenation of alkenes[29] and subsequent mechanistic studies of this system demonstrated a Co(0)/Co(II) process was operative.[30] Our group has recently reported an electron-rich low coordinate cobalt complex mediating the amination of aryl halides (Scheme 1.4), demonstrating that multi-electron redox with late first-row transition metals is plausible with the appropriate ligand environment.[31]

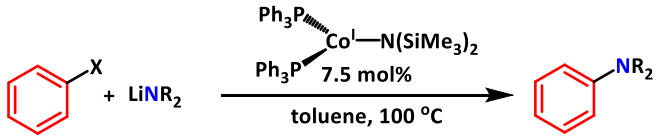

Scheme 1.4 $(PPh_3)_2Co(I)N(SiMe_3)_2$ catalyzed amination of aryl halides.

1.3 Monoanionic bis(NHC) CCC pincer ligand

Encouraged by the successful use of electron-rich ligands to promote effective two-electron reactivity from first-row transition metal centers,[26-28,32] we surveyed the literature to select a robust and electron-

rich ligand platform. Given the enhanced stability and performance observed with transition metal catalysts upon the substitution of phosphines with *N*-heterocyclic carbenes,[33,34] as well as studies suggesting carbon based supporting ligands are best suited to impart an electron-rich environment on a first-row transition metal,[22,23] we decided to employ the monoanionic bis(N-heterocyclic carbene), ^{Mes}CCC (Mes = 2,4,6-trimethylphenyl), pincer ligand platform, of which the imidazolium precursor, $[H_3(^{Mes}CCC)]Cl_2$, was previously reported by Chianese and coworkers[35] (Figure 1.1). We hypothesized that greater orbital overlap between the metal center and the anchoring anionic aryl carbon and the two N-heterocyclic carbene carbon atoms of the pincer ligand would impose a strong-field ligand environment to support two-electron processes in the resulting complexes. Furthermore, the ligand system features mesityl groups on the ligand periphery which serves to provide a ^{1}H and ^{13}C NMR spectroscopic handle,

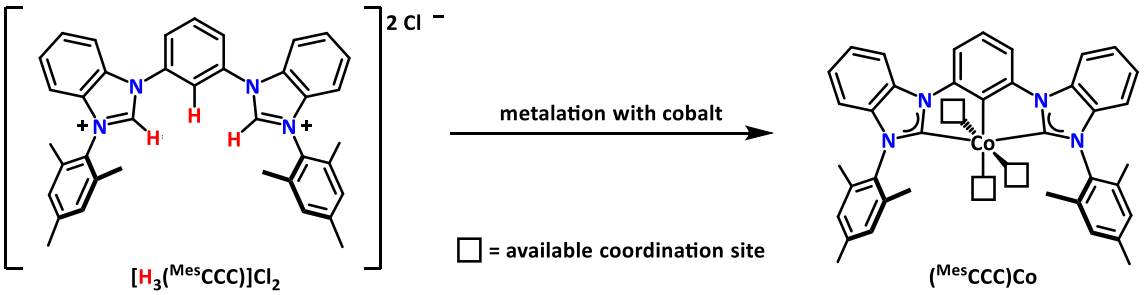

Figure 1.1 (^{Mes}CCC)Co pincer platform to study two-electron reactivity.

aid in the solubility of the complexes in organic solvents and ehance steric protection to the metal center.

The initial aims of our research efforts were focused on developing ^{Mes}CCC-Co complexes to study stoichiometric two-electron chemistry. Initial studies focused on the reactivity of the low-valent cobalt complexes with simple molecules such H_2. The results from these studies may provide insights into the ability of the cobalt complex to undergo oxidative addition, akin to the two-electron chemistry observed in Vaska's complex, $IrCl(CO)(PPh_3)_3$ (PPh_3 = triphenyl phosphine)[9,36] and Wilkinson's catalyst, $RhCl(PPh_3)_3$ with H_2.[37,38] Based on the mechanistic insights gleaned from such reactivity studies, the application of the cobalt complexes in the catalytic hydrogenation of carbon-carbon multiple bonds were envisioned and subsequently carried out.

In the ensuing mechanistic studies of the catalytic hydrogenation of carbon-carbon and carbon-nitrogen multiple bonds (*vide infra*) using the cobalt complexes, we turned our attention to using *para*hydrogen induced polarization (PHIP) transfer NMR spectroscopy. PHIP transfer NMR spectroscopy has been used widely used to study catalytic hydrogenation reactions using homogenous transition metal compounds and for the detection of intermediates involving metal-hydride complexes using *p*-H_2.[39] Due to the intrinsic requirements for the observation of ^{1}H NMR signals (*vide infra*) arising from *p*-H_2 addition

onto a metal complex, as in the formation of a M-$(H)_2$, or in the catalytic addition of *p*-H_2 to a unsaturated bond, such as in the hydrogenation of an olefin via transition metal catalyst, PHIP transfer NMR spectroscopy provides a powerful tool to study the stochiometric and catalytic reactivity of ^{Mes}CCC cobalt complexes with H_2. Moreover, this technique allows us to make direct comparisons between the mechanistic pathways (oxidative addition, migratory insertion and reductive elimination) invoked in the hydrogenation catalysis of homogenous rhodium(I) complexes[40-43] and the ^{Mes}CCC-Co system.

1.4 Mechanistic studies involving PHIP NMR spectroscopy

PHIP transfer NMR spectroscopy studies involve the use of *p*-H_2 in lieu of the "normally occurring" H_2. The H_2 molecule exists as two different nuclear spin isomers, *p*-H_2 (25%) is the antisymmetric isomer, αβ-βα, and *ortho*hydrogen, *o*-H_2, (75%) is the symmetric isomer with nuclear spin configurations αα, ββ and αβ+βα (Figure 1.2).[44,45] To use PHIP transfer NMR to study the catalytic hydrogenations with the ^{Mes}CCC

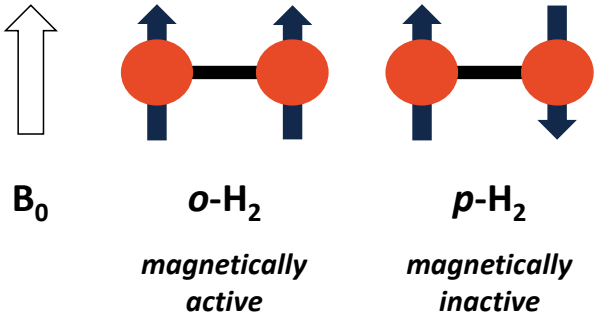

Figure 1.2 Spin isomers of dihydrogen.

cobalt complexes, the percentage of the *p*-H_2 isomer must be increased by converting *o*-H_2 to *p*-H_2. Because of the differences in the rotational state symmetry between the two H_2 spin isomers, *p*-H_2 is inherently more stable because it accesses lower energy rotational states than *o*-H_2.[46] At lower temperatures the equilibrium between the two spin-isomers is shifted toward *p*-H_2, however the conversion between the two isomers can only occur by an interaction of H_2 with a paramagnetic catalyst or impurity, such as O_2, since the interconversion between the two spin states would involve both a rotational and a nuclear spin state change, which is spin forbidden.[46]

In our studies, hydrogen gas was converted to the *p*-H_2 spin isomer using a *para*-H_2 converter developed by the McCall group.[47] At temperatures around 15K using a closed-cycle helium cryostat, hydrogen gas was passed over the hydrous ferric oxide catalyst resulting in the conversion of *p*-H_2 to 99%.[47] Based on the *p*-H_2 to *o*-H_2 back conversion measurements by McCall and coworkers,[47] the *p*-H_2 was stored in a lecture bottle and subsequently used in the PHIP NMR studies within 2 months of being generated (Figure 1.3).

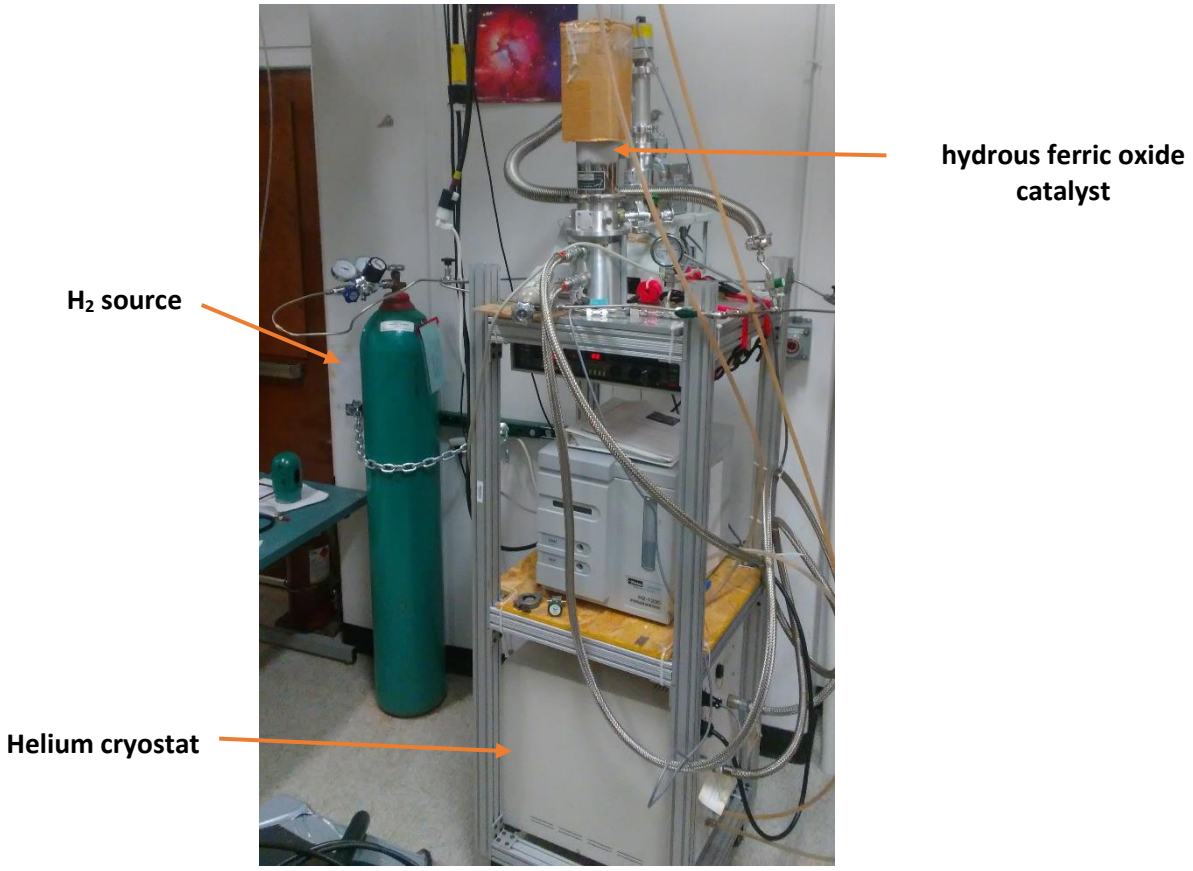

Figure 1.3 Photograph of the parahydrogen generator used to convert H_2 to *p*-H_2 (99.99%).

For the effects of PHIP to be observed by NMR spectroscopy, the symmetry of *p*-H_2 must be broken first because *p*-H_2 by itself is silent toward characterization by ^{1}H NMR spectroscopy since the two nuclear spins in each H atom are aligned in the opposite direction, whereas, the opposite is true for *o*-H_2 (Figure 1.2).[48,49] Moreover, the addition process of *p*-H_2 in hydrogenation reactions or addition to a metal center must occur in a pairwise manner to magnetically distinct positions, while maintaining the spin correlation of *p*-H_2 in the product or the resulting $M(H)_2$ species.[48,49] Furthermore, the addition process must occur faster than the relaxation period of the added hydrogen atoms. For these reasons the choice of the

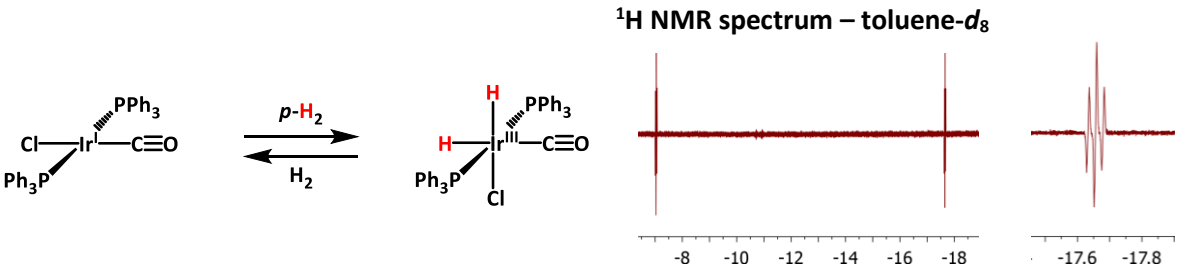

Figure 1.4 Oxidative addition of *p*-H_2 onto $IrCl(CO)(PPh_3)_2$ (left) and resulting ^{1}H NMR spectrum of the upfield region (right) in toluene-d_8.

transition metal complex used to carry out the hydrogenation reactions is important.[48,49] When the conditions are met, such in the concerted oxidative addition of *p*-H_2 onto $IrCl(CO)(PPh_3)_3$, antiphase resonances in the ^1H NMR spectrum are observed (Figure 1.4).

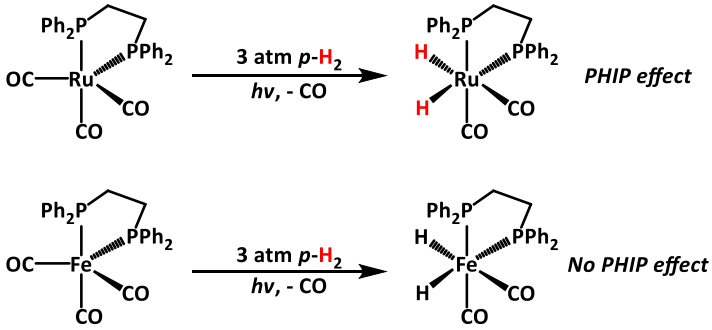

Figure 1.5 Oxidative addition of *p*-H_2 onto $(dppe)M(CO)_3$ (M = Ru, Fe).

The photochemical reaction of $(dppe)M(CO)_3$ with *p*-H_2 yielded PHIP effects for the hydride signals in the ^1H NMR spectrum of M = Ru (Figure 1.5, top), but not M = Fe (Figure 1.5, bottom). The differing behavior is related to the spin state of the $(dppe)M(CO)_2$ intermediates: $(dppe)Fe(CO)_2$ adopts a triplet ground state, whereas a singlet ground state remains in $(dppe)Ru(CO)_2$.[24] When *p*-H_2 is added to the irradiated 16-electron iron complex (S =1), no signal enhancement is observed because of the longer reaction time needed arising from the spin crossover to produce an S = 0 iron center and loss of spin encoding.[24,50] The ruthenium complex maintains a singlet state (S = 0) throughout the hydrogenation process, and spin encoding remains throughout, which results in the observation of antiphase signals in the ^1H NMR spectrum from the added *p*-H_2 molecule on the metal center.[24]

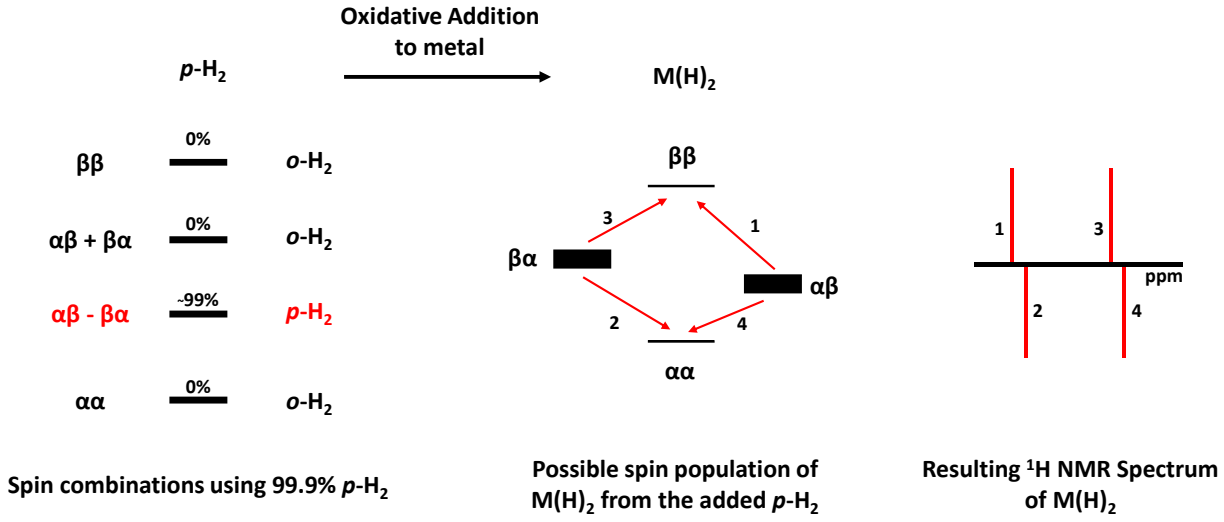

Figure 1.6 Spin populations of *p*-H_2 (left), the spin configurations of an AX system that are populated (middle) and the resulting ^1H NMR spectrum (right).

The antiphase ^{1}H NMR signals in the products of hydrogenation using *p*-H_2 arise because of the non-Boltzmann distribution of spin populations in the product. For example, when the oxidative addition of H_2 (consisting of both *p*-H_2 and *o*-H_2) following the conditions stated above to a metal center occurs, all four possible spin states of the product are equally populated, and only the differences between the Boltzmann governed spin populations energy levels are observed by ^{1}H NMR spectroscopy (Figure 1.6). When purely *p*-H_2 is used in the hydrogenation reaction, only the αβ or βα spin states are populated in the resulting product, therefore a non-Boltzmann distribution of spins is observed, and intense antiphase ^{1}H NMR signals result from those population differences[39] (Figure 1.7).

The magnetic field at which the hydrogenation occurs is also evident in the resulting ^{1}H NMR spectrum.[51] When the symmetry of *p*-H_2 is broken at high field, such as inside the NMR spectrometer (Figure 1.8, middle), four antiphase signals separated by the coupling constant between the protons arise.[49] This effects is known as Parahydrogen And Synthesis Allow Dramatically Enhanced Nuclear Alignment (PASADENA).[49] When the symmetry of the *p*-H_2 molecule is broken at low magnetic field, such as Earth's magnetic field, and the sample is subsequently transferred to the strong magnetic field, only the lower energy βα spin isomer is populated (Figure 1.8, right). In this case, Adiabatic Longitudinal Transport After Dissociation Engenders Net Alignment (ALTADENA) is observed and only 2 antiphase signals are observed.[52]

In 1987 Weitekamp and coworkers reported the first ^{1}H NMR showcasing the antiphase resonances arising from the *para*hydrogenation of acrylonitrile using Wilkinson's catalyst.[49] Only a few months later, Eisenberg and coworkers reported on the hyperpolarization of styrene resulting from the hydrogenation

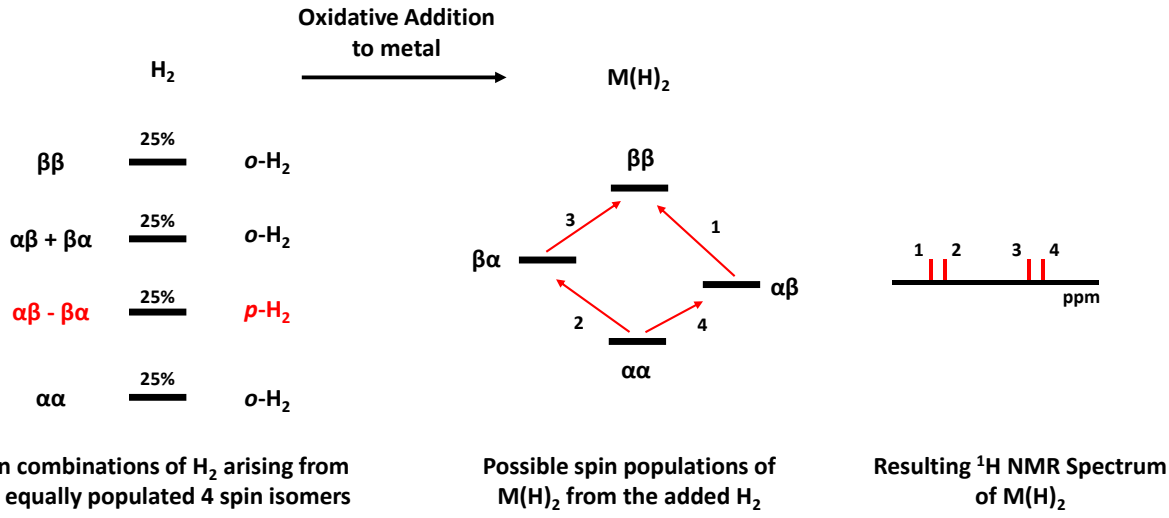

Figure 1.7 Spin populations of H_2 (left), the spin configurations of an AX system that are populated (middle) and the resulting ^{1}H NMR spectrum (right).

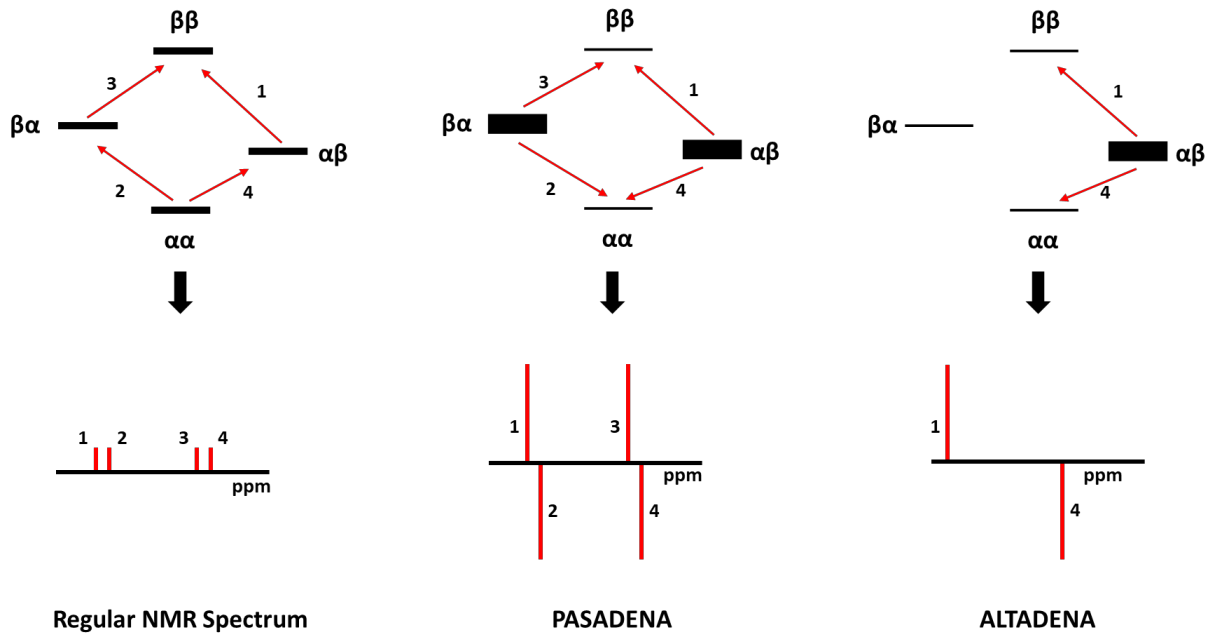

Figure 1.8 Spin configurations populated in an AX system using H_2 (top left), *p*-H_2 at high-field (top middle) and *p*-H_2 at low-field (top right). The resulting ^{1}H NMR spectra are shown below.

of phenylacetylene using $[Rh_3Cl_2H_2(CO)_2((Ph_2PCH_2)_2\text{-}PPh)_2]^+$ or $Pd_2Cl_2(PPh_2PCH_2PPh_2)_2$ as the catalyst and *p*-H_2.[51] Furthermore, in their studies, Eisenberg and coworkers demonstrated that the oxidative addition of *p*-H_2 onto IrX(CO)dppe (X = CN and Br; dppe = 1,2-bis(diphenylphosphino)ethane) generates hyperpolarized ^{1}H NMR resonances assigned to the *cis*-dihydride ligands on the iridium center. Interestingly, in their studies, H_2 was converted to 50% *p*-H_2 by allowing their reaction mixture stand under an H_2 atmosphere in liquid nitrogen for at least 8 hours.[51] While the percentage of *p*-H_2 is increased using this method via the slow exchange of the gas phase H_2 with the transition metal complexes in their studies, conversion of H_2 to *p*-H_2 is typically carried out before introducing the enriched gas to the reaction system of study.

These pioneering studies laid the foundation showing that PHIP transfer NMR spectroscopy is powerful technique to study the heterogenous[53-57] and homogenous[39,58-61] catalytic hydrogenation of organic substrates, H_2 reactivity with transition metal complexes and even more recently metal free compounds.[62,63] Mechanistic studies with PHIP have mainly centered on rhodium and iridium complexes[39] but have also expanded to include systems featuring palladium,[51,61,64] platinum,[65,66] and ruthenium[24,60,67,69] metal centers. Early transition metal complexes such as tantalum[69] and tungsten[70] have been demonstrated to react with *p*-H_2 in a pairwise manner yielding hyperpolarized ^{1}H NMR resonances. PHIP transfer NMR studies using late first-row transition metals remains limited.[71,72] Duckett and coworkers have used PHIP transfer NMR spectroscopy to elucidate key reaction intermediates in the cobalt-catalyzed

hydroformylation of alkenes.[71,72] Unlike the previous PHIP NMR studies with iron carbonyl phosphine complexes,[24] the cobalt hydroformylation system demonstrated that with the appropriate strong-field ligands around the metal center, the spin-correlation of *p*-H_2 can be maintained throughout the catalytic process.

Herein, the synthesis and characterization of cobalt derivatives of the ^{Mes}CCC pincer ligand platform in the +1, +2 and +3 oxidation states are described. The reactivity of low-valent complexes towards dihydrogen resulted in a nonclassical coordination mode of H_2 to the metal center. Further studies, showed Co(I)-(H_2) facilities the scrambling of H_2 and D_2 and is proposed to involve a two-electron redox event at the metal center. The competency of the Co-(H_2) complex towards the catalytic hydrogenation of carbon-carbon multiple bonds was also investigated. The hydrogenation of alkynes resulted in the selective formation of *E*-alkenes. Multinuclear and PHIP transfer NMR spectroscopic studies were employed to elucidate catalytically relevant intermediates in the hydrogenation process and based on these studies, a Co(I)/Co(III) redox process was proposed to be operative. Additionally, the selectivity for *E*-alkenes was found to arise from the *cis*-hydrogenation of the alkyne, followed by *trans*-isomerization under an H_2 atmosphere. In pursuit of using an air-stable Co(III) precatalyst for the selective hydrogenation of nitriles to primary amines, the *in situ* activator ($NaHBEt_3$), generated the catalytically active species and the resulting BEt_3 was found to be vital to the observed catalysis, acting as a Lewis acid. Mechanistic studies stemming from PHIP transfer NMR studies suggested a Co(I)/Co(III) redox cycle was also operative in nitrile hydrogenation. The viability of the low-valent (^{Mes}CCC)Co complex to hyperpolarize ^{1}H and ^{13}C NMR signals in the hydrogenation products of butyl, ethyl and methyl acrylate using *p*-H_2 is discussed. Comparisons of the carboxylate ^{13}C signal enhancement of ethyl propionate using [(dppb)Rh(COD)]BF_4 and (^{Mes}CCC)Co-py, demonstrated that the hyperpolarization efficiency using the cobalt complex is comparable with the rhodium system. Lastly, stoichiometric oxidative addition and reductive elimination chemistry with the ^{Mes}CCC ligand platform demonstrate the viability of a Co(I)/Co(III) redox couple in the proposed catalytic hydrogenation reactions.

1.5 References

1. Kandemir, T.; Schuster, M. E.; Senyshyn, A.; Behrens, M.; Schlogl, R. The Haber-Bosch Process Revisited: On the Real Structure and Stability of “Ammonia Iron” under Working Conditions. *Angew. Chem. Int. Ed.* **2013**, *52*, 12723-12726.
2. In Kirk-Othmer Encyclopedia of Chemical Technology; Stanley, G. G., Ed.; John Wiley and Sons inc: 2017.

3. Cornils, B.; Herrmann, W. A.; Rasch, M. Otto Roelen, Pioneer in Industrial Homogeneous Catalysis. *Angew. Chem. Int. Ed.* **1994**, *33*, 2144-2163.
4. Osborn, J. A.; Wilkinson, G.; Young, J. F. Mild Hydroformylation of Olefins using Rhodium Catalysts. *Chem. Commum.* **1965**, 17.
5. Wang, X. Recent Advances in Continuous Rhodium-Catalyzed Hydroformylation. *J. Flow. Chem.* **2015**, *5*, 125-132.
6. In Organotransition Metal Chemistry: From Bonding to Reactivity; Hartwig, J. F., Ed.; University Science Books: Sausalito, CA, 2010.
7. Ludwig, J. R.; Schindler, C. S. Catalyst: Sustainable Catalysis. *Chem*, **2017**, *2*, 313-316.
8. R. H. Crabtree, *The Organometallics Chemistry of the Transition Metals*, 5th ed., John Wiley & Sons, Hoboken, New Jersey, 2009.
9. Vaska, L.; DiLuzio, J. W.; Activation of Hydrogen by a Transition Metal Complex at Normal Conditions Leading to a Stable Molecular Dihydride. *J. Am. Chem. Soc.* **1962**, *84*, 679-680.
10. Kirss, R. U.; Eisenberg, R. *Para*-hydrogen-induced polarization in rhodium complex-catalyzed hydrogenation reactions. *J. Organomet. Chem.* **1989**, *359*, C22-C26.
11. Sánchez-Delgado, R. A.; Rosales, M. Kinetic studies as a tool for the elucidation of the mechanisms of metal complex-catalyzed homogeneous hydrogenation reactions. *Coord. Chem. Rev.* **2000**, *196*, 249–280.
12. Giernoth, R.; Heinrich, H.; Adams, N. J.; Deeth, R. J.; Bargon, J.; Brown, J. M. PHIP Detection of a Transient Rhodium Dihydride Intermediate in the Homogeneous Hydrogenation of Dehydroamino Acids. *J. Am. Chem. Soc.* **2000**, *122*, 12381–12382.
13. Stubbe, J.; van der Donk, W. A. Protein Radicals in Enzyme Catalysis. *Chem. Rev.* **1998**, *98*, 705-762.
14. Chirik, P. J.; Wieghardt, K. Radical Ligands Confer Nobility on Base-Metal Catalysts. *Science* **2010**, *327*, 794-795.
15. Bart, S. C.; Lobkovsky, E.; Chirik, P. J. Preparation and Molecular and Electronic Structures of Iron(0) Dinitrogen and Silane Complexes and Their Application to Catalytic Hydrogenation and Hydrosilation. *J. Am. Chem. Soc.* **2004**, *126*, 13794-13807.
16. Trovitch, R. J.; Lobkovsky, E.; Bill, E.; Chirik, P. J. Functional Group Tolerance and Substrate Scope in Bis(imino)pyridine Iron Catalyzed Alkene Hydrogenation. *Organometallics* **2008**, *27*, 1470-1478.

17. Darmon, J. M.; Stieber, S. C. E.; Sylvester, K. T.; Fernández, I.; Lobkovsky, E.; Semproni, S. P.; Bill, E.; Wieghardt, K.; DeBeer, S.; Chirik, P. J. Oxidative Addition of Carbon-Carbon Bonds with a Redox-Active Bis(imino)pyridine Iron Complex. *J. Am. Chem. Soc.* **2012**, *134*, 17125-17137.
18. Knijnenburg, Q.; Horton, A. D.; van der Heijden, H.; Kooistra, T. M.; Hetterscheid, D. G. H.; Smits, J. M. M.; de Bruin, B.; Budzelaar, P. H. M.; Gal, A. W. Olefin hydrogenation using diimine pyridine complexes of Co and Rh. *J. Mol. Catal A: Chem*. **2005**, *232*, 151-159.
19. Monfette, S.; Turner, Z. R.; Semproni, S. P.; Chirik, P. J. Enantiopure C_1-Symmetric Bis(imino)pyridine Cobalt Complexes for Asymmetric Alkene Hydrogenation. *J. Am. Chem. Soc.* **2012**, *134*, 4561-4564.
20. Yu, R. P.; Darmon, J. M.; Milsmann, C.; Margulieux, G. W.; Stieber, S. C. E.; DeBeer, S.; Chirik, P. J. Catalytic Hydrogenation Activity and Electronic Structure Determination of Bis(arylimidazol-2-ylidene)pyridine Cobalt Alkyl and Hydride Complexes. *J. Am. Chem. Soc.* **2013**, *135*, 13168−13184.
21. Volpe, E. C.; Manke, D. R.; Bartholomew, E. R.; Wolczanski, P. T.; Lobkovsky, E. B. Aryl-Oxazoline Chelates of First-Row Transition Metals: Structures of {*κ*-C,N-(*o*-C_6H_4)CMe_2($COCH_2CMe_2N$)}FeCl(py) and [(*κ*-C,N-(*o*-C_6H_4)CMe_2($COCH_2CMe_2N$)}Cr(μ -Cl)]$_2$ *Organometallics* **2010**, *29*, 6642-6652.
22. Hirsekorn, K. F.; Hulley, E. B.; Wolczanski, P. T.; Cundari, T. R. Olefin Substitution in (silox)$_3$M(olefin) (silox = tBu_3SiO; M = Nb, Ta): The Role of Density of States in Second vs Third Row Transition Metal Reactivity. *J. Am. Chem. Soc.,* **2008**, *130*, 1183-1196.
23. Wilkinson, G.; Rosenblum, M.; Whiting, M. C.; Woodward, R. B. THE STRUCTURE OF IRON BIS-CYCLOPENTADIENYL. *J. Am. Chem. Soc.* **1952**, *74*, 2125-2126.
24. Schott, D.; Callaghan, P.; Dunne, J.; Duckett, S. B.; Godard, C.; Goicoechea, J. M.; Harvey, J. N.; Lowe, J. P.; Mawby, R. J.; Müller, G.; Perutz, R. N.; Poli, R.; Whittlesey, M. K. The reaction of M(CO)$_3$($Ph_2PCH_2CH_2PPh_2$)(M = Fe, Ru) with parahydrogen: probing the electronic structure of reaction intermediates and the internal rearrangement mechanism for the dihydride products. *Dalton Trans.* **2004**, 3128-3224.
25. Lawrence, M. A. W.; Green, K.; Nelson, P. N.; Lorraine, S. C. Review: Pincer ligands – Tuneable, versatile and applicable. *Polyhedron,* **2018**, *143*, 11-27.
26. Semproni, S. P.; Atienza, C. C. H.; Chirik, P. J. Oxidative addition and C-H activaition chemistry with a PNP pincer-ligated cobalt complex. *Chem. Sci.* **2014**, *5*, 1956-1960.
27. Rozenel, S. S.; Padilla, R.; Camp, C.; Arnold, J. Unusual activation of H_2 by reduced cobalt complexes supported by a PNP pincer ligand. *Chem. Commun.* **2014**, *50*, 2612-2614.

28. Ingleson, M.; Fan, H.; Pink, M.; Tomaszewski, J.; Caulton, K. G. Three-Coordinate Co(I) Provides Access to Unsaturated Dihydrido-Co(III) and Seven-Coordinate Co(V). *J. Am. Chem. Soc.* **2006**, *128*, 1804-1806.
29. Friedfeld, M. R.; Margulieux, G. W.; Schaefer, B. A.; Chirik, P. J. Bis(phosphine)cobalt Dialkyl Complexes for Directed Catalytic Alkene Hydrogenation. *J. Am. Chem. Soc.* **2014**, *136*, 13178-13181.
30. Ma, X.; Lei, M. Mechanistic Insights into the Directed Hydrogenation of Hydroxylated Alkene Catalyzed by Bis(phosphine)cobalt Dialkyl Complexes. *J. Org. Chem.* **2017**, *82*, 2703-2712.
31. Brennan, M. R.; Kim, D.; Fout, A. R. A Synthetic and Mechanistic Investigation into the cobalt(i) catalyzed amination of aryl halides. *Chem. Sci.* **2014**, *5*, 4831-4839.
32. Hebden, T. J.; St. John, A. J.; Gusev, D. G.; Kaminsky, W.; Goldberg, K. I.; Heinekey, D. M. Preparation of a dihydrogen complex of cobalt. *Angew. Chem.* **2011**, *123*, 1913− 1916.
33. Hopkinson, M. N.; Richter, C.; Schedler, M.; Glorius, F. An Overview of N-heterocyclic Carbenes. *Nature* **2014**, *510*, 485-496.
34. Strassner, T. The role of NHC Ligands in Oxidation Catalysis. *Top. Organomet. Chem.* **2007**, *22*, 125-148.
35. Chianese, A. R.; Mo, A.; Lampland, N. L.; Swartz, R. L.; Bremer, P. T. Iridium complexes of CCC-pincer N-heterocyclic Carbene Ligands: Synthesis and Catalytic C-H Functionalization. *Organometallics* **2010**, *29*, 3019-3026.
36. Hasnip, S. K.; Duckett, S. B.; Sleigh, C. J.; Taylor, D. R.; Barlow, G. K.; Taylor, M. J. New products in an old reaction: isomeric products from H_2 addition to Vaska's complex and its analogues. *Chem. Commun.* **1999**, 1717-1718.
37. Ducket, S. B.; Newell, C. L.; Eisenberg, R. Observation of New Intermediates in Hydrogenation Catalyzed by Wilkinson's Catalyst, $RhCl(PPh_3)_3$, Using Parahydrogen-Induced Polarizatiton. *J. Am. Chem. Soc.* **1994**, *116*, 10548-10556.
38. Morran, P. D.; Duckett, S. B.; Howe, P. R.; McGrady, J. E.; Colebrooke, S. A.; Eisenberg, R.; Partridge, M. G.; Lohman, J. B. Activation of H_2 by halogenocarbonylbis(phosphine)rhodium(I) complexes. The use of parahydrogen induced polarisation to detect species present at low concentration. *J. Chem. Soc., Dalton Trans.* **1999**, 3949-3960.
39. Duckett, S. B.; Mewis, R. E. Application of *Para*hydrogen Induced Polarization Techniques in NMR Spectroscopy and Imaging. *Acc. Chem. Res.* **2012**, *45*, 1247− 1257 and references therein.

40. Ducket, S. B.; Newell, C. L.; Eisenberg, R. Observation of New Intermediates in Hydrogenation Catalyzed by Wilkinson's Catalyst, $RhCl(PPh_3)_3$, Using Parahydrogen-Induced Polarizatiton. *J. Am. Chem. Soc.* **1994**, *116*, 10548-10556.
41. Morran, P. D.; Duckett, S. B.; Howe, P. R.; McGrady, J. E.; Colebrooke, S. A.; Eisenberg, R.; Partridge, M. G.; Lohman, J. B. Activation of H_2 by halogenocarbonylbis(phosphine)rhodium(I) complexes. The use of parahydrogen induced polarisation to detect species present at low concentration. *J. Chem. Soc., Dalton Trans.* **1999**, 3949-3960.
42. Sánchez-Delgado, R. A. ; Rosales, M. Kinetic studies as a tool for the elucidation of the mechanisms of metal complex-catalyzed homogeneous hydrogenation reactions. *Coord. Chem. Rev.* **2000**, *196*, 249–280.
43. Giernoth, R.; Heinrich, H.; Adams, N. J.; Deeth, R. J.; Bargon, J.; Brown, J. M. PHIP Detection of a Transient Rhodium Dihydride Intermediate in the Homogeneous Hydrogenation of Dehydroamino Acids. *J. Am. Chem. Soc.* **2000**, *122*, 12381–12382.
44. Sandler, Y. L. The Adsorption and the Magnetic Ortho–Para Conversion of Hydrogen on Diamagnetic Solids. I. Some Experiments in Surface Paramagnetism. *J. Phys. Chem.* **1954,** *58*, 54–57.
45. Sandler, Y. L. Hindered Rotation in Adsorbed Hydrogen. Adiabatic Cooling by Adsorbed Parahydrogen. *J. Chem. Phys.* **1956**, *29*, 97-99.
46. Buljubasich, L.; Franzoni, M. F.; Münnemann, K. parahydrogen Induced Polarization by Homogenous Catalysis: Theory and Applications. *Top. Curr. Chem.* **2013**, *338*, 33-74 and references therein.
47. Tom, B. A.; Bhasker, S.; Miyamoto, Y.; Momose, T.; McCall, B. J. Producing and quantifying enriched *para*-H_2. *Rev. Sci. Instrum.* **2009**, *80*, 016108.
48. Bowers, C. R.; Weitekamp, D. P. Transformation of Symmetrization Order to Nuclear-Spin Magnetization by Chemical Reaction and Nuclear Magnetic Resonance. *Phys. Rev. Lett.* **1986**, *57*, 2645-2648.
49. Bowers, C. R.; Weitekamp, D. P. Parahydrogen and synthesis allow dramatically enhanced nuclear alignment. *J. Am. Chem. Soc.* **1987**, *109*, 5541-5542.
50. Nilsson, T.; Kowalewski, J. Low-field theory of nuclear spin relaxation in paramagnetic low-symmetry complexes for electron spin systems of S = 1, 3/2, 2, 5/2, 3 and 7/2. *Mol. Phys.* **2000**, *98*, 1617-1638.

51. Eisenschmid, T. C.; Kirss, R. U.; Deutsch, P. P.; Hommeltoft, S. I.; Eisenberg, R.; Bargon, J.; Lawler, R. G.; Balch, A. L. Para hydrogen induced polarization in hydrogenation reactions. *J. Am. Chem. Soc.* **1987**, *109*, 8089-8091.
52. Pravica, M. G.; Weitekamp, D. P. Net NMR alignment by adiabatic transport of parahydrogen addition products to high magnetic field. *Chem. Phys. Lett.* **1988**, *145*, 255−258.
53. Kovtunov, K. V.; Beck, I. E.; Bukhtiyarov, V. I.; Koptyug, I. V. Observation of Parahydrogen-Induced Polarization in Heterogeneous Hydrogenation on Supported Metal Catalysts. *Angew. Chem., Int. Ed.* **2008**, *47*, 1492−1495.
54. Balu, A. M.; Duckett, S. B.; Luque, R. Para-hydrogen induced polarisation effects in liquid phase hydrogenations catalysed by supported metal nanoparticles. *Dalton Trans.* **2009**, 5074−5076.
55. Irfan, M.; Eshuis, N.; Spannring, P.; Tessari, M.; Feiters, M. C.; Rutjes, F. P. J. T. Liquid-Phase Parahydrogen-Induced Polarization (PHIP) with Ligand-Capped Platinum Nanoparticles. *J. Phys. Chem. C* **2014**, *118*, 13313−13319.
56. Burueva, D. B.; Salnikov, O. G.; Kovtunov, K. V.; Romanov, A. S.; Kovtunova, L. M.; Khudorozhkov, A. K.; Bukhtiyarov, A. V.; Prosvirin, I. P.; Bukhtiyarov, V. I.; Koptyug, I. V. Hydrogenation of Unsaturated Six-Membered Cyclic Hydrocarbons Studied by the Parahydrogen-Induced Polarization Technique. *J. Phys. Chem. C* **2016**, *120*, 13541−13548.
57. Salnikov, O. G.; Liu, H.; Fedorov, A.; Burueva, D. B.; Kovtunov, K. V.; Copéret, C.; Koptyug, I. V. Pairwise hydrogen addition in the selective semihydrogenation of alkynes on silica-supported Cu catalysts. *Chem. Sci.* **2017**, *8*, 2426−2430.
58. Eisenberg, R. Parahydrogen-induced polarization: a new spin on reactions with molecular hydrogen. *Acc. Chem. Res.* **1991**, *24*, 110−116.
59. Duckett, S. B.; Wood, N. J. Parahydrogen-based NMR methods as a mechanistic probe in inorganic chemistry. *Coord. Chem. Rev.* **2008**, *252*, 2278− 2291.
60. Leutzsch, M.; Wolf, M. L.; Gupta, P.; Fuchs, M.; Thiel, W.; Farès, C.; Fürstner, A. Formation of Ruthenium Carbenes by *gem*-Hydrogen Transfer to Internal Alkynes: Implications for Alkyne *trans*-Hydrogenation. *Angew. Chem., Int. Ed.* **2015**, *54*, 12431−12436.
61. Guan, D.; Holmes, A. J.; Lopez-Serrano, J.; Duckett, S. B. Following palladium catalyzed methoxycarbonylation by hyperpolarized NMR spectroscopy: a parahydrogen based investigation. *Catal. Sci. Technol.* **2017**, *7*, 2101−2109.

62. Zhivonitko, V. V.; Telkki, V. V.; Chernichenko, K.; Repo, T.; Leskela, M.; Sumerin, V.; Koptyug, I. V. Tweezers for Parahydrogen: A Metal-Free Probe of Nonequilibrium Nuclear Spin States of H_2 Molecules. *J. Am. Chem. Soc.* **2014**, *136*, 598−601.
63. Longobardi, L. E.; Russell, C. A.; Green, M.; Townsend, N. S.; Wang, K.; Holmes, A. J.; Duckett, S. B.; McGrady, J. E.; Stephan, D. W. Hydrogen Activation by an Aromatic Triphosphabenzene. *J. Am. Chem. Soc.* **2014**, *136*, 13453−13457.
64. Permin, A. B.; Eisenberg, R. One-hydrogen polarization in hydroformylation promoted by platinum-tin and iridium carbonyl complexes: A new type of parahydrogen-induced effect. *J. Am. Chem. Soc.* **2002**, *124*, 12406–12407.
65. Deibele, C.; Permin, A. B.; Petrosyan, V. S.; Bargon, J. A Study of the Mechanism of Platinum(II)/Tin(II) Dichloride Mediated Hydrogenation of Alkynes and Alkenes Employing Parahydrogen-Induced Polarization. *Eru. J. Inorg. Chem.* **1998**, 1915-1923.
66. Millar, S. P.; Jang, M.; Lachicotte, R. J.; Eisenberg, R. Hydride complexes of platinum(II) containing unsymmetrical di(phosphine) ligands: synthesis, characterization and evidence for pairwise addition of hydrogen based on parahydrogen induced polarization. *Inorganica Chem. Acta* **1998**, *270*, 363-375.
67. Schleyer, D.; Niessen, H. G.; Bargon, J. *In situ* ^{1}H-PHIP-NMR studies of the stereoselective hydrogenation of alkynes to (*E*)-alkenes catalyzed by a homogeneous $[Cp^*Ru]^+$ catalyst. *New J. Chem.* **2001**, *25*, 423−426.
68. Guthertz, A.; Leutzsch, M.; Wolf, L. M.; Gupta, P.; Rummelt, S. M.; Goddard, R.; Farés, C.; Thiel, W.; Fürstner, A. Half-Sandwich Ruthenium Carbene Complexes Link *trans*-Hydrogenation and *gem*-Hydrogenation of Internal Alkynes. *J. Am. Chem. Soc.* **2018**, *140*, 3156-3169.
69. Millar, S. P.; Zubris, D. L.; Bercaw, J. E.; Eisenberg, R. On the Mechanism of Dihydrogen Addition to Tantalocene Complexes. *J. Am. Chem. Soc.* **1998**, *120*, 5329-5330.
70. Eguillor, B.; Caldwell, P. J.; Cockett, M. C. R.; Duckett, S. B.; John, R. O.; Lynam, J. M.; Sleigh, C. J.; Wilson, I. Detection of Unusual Reaction Intermediates during the Conversion of $W(N_2)_2(dppe)_2$ to $W(H)_4(dppe)_2$ and of H_2O into H_2. *J. Am. Chem. Soc.* **2012**, *134*, 18257-18265.
71. Godard, C.; Duckett, S. B.; Polas, S.; Tooze, R.; Whitwood, A. C. An NMR study of cobalt-catalyzed hydroformylation using *para*-hydrogen induced polarization. *Dalton Trans.* **2009**, 2496−2509.
72. Godard, C.; Duckett, S. B.; Polas, S.; Tooze, R.; Whitwood, A. C. Detection of Intermediates in Cobalt-Catalyzed Hydroformylation Using *para*-Hydrogen-Induced Polarization. *J. Am. Chem. Soc.* **2005**, *127*, 4994−4995.

CHAPTER 2: SYNTHESIS AND CHARACTERIZATION OF LOW-SPIN COBALT(I-III) COMPLEXES FEATURING A CCC-PINCER BIS(N-HETEROCYCLIC CARBENE) LIGAND[†]

2.1 Introduction

Generally speaking, the incorporation of electron-rich ligands into pincer complexes of the late first-row transition metals has supported a wide variety of noteworthy catalytic and stoichiometric reactivity. In the case of PNP (PNP = bis(phosphine) pyridine),[1] ^{tBu}PNP (^{tBu}PNP = (^{t}Bu$_2$PCH$_2$SiMe$_2$)$_2$N$^-$)[2] and HPNP (HPNP = HN(CH$_2$CH$_2$P^{i}PR$_2$)[3] cobalt complexes, the oxidative addition of H_2 was favorable and the resulting products were amenable toward crystallographic characterization. Furthermore, these complexes were employed for inert C–H bond activation,[1] hydrogenation of olefins[1,2] and activation of a phenylsilane[2] and these processes are thought to proceed through 2 electron oxidative addition. In this regard, the development of electron-rich pincer cobalt complexes bearing strongly-donating N-heterocyclic carbene ligands was pursued to build upon the two-electron paradigm for cobalt.

2.2 Preparation of [H$_3$(^{Mes}CCC)]Cl$_2$

Prior to metalation and studying the subsequent proposed two-electron redox processes with the new cobalt complexes, the ligand precursor, [H$_3$(^{Mes}CCC)]Cl$_2$ (Mes = bis(2,4,6-trimethylphenyl-benzimidazol-2-ylidene)phenyl), to support such reactivity, was synthesized following a modification of the synthetic procedure reported by Chianese and coworkers[4] (Figure 2.1). Using Pd(PPh$_3$)$_4$ in place of Pd$_2$(dba)$_3$ for the two sequential Buchwald-Hartwig amination steps increased the overall yield of the tetraamine product to 89% from the reported 55% and one column chromatography purification step was circumvented. Following the cyclization of the tetraamine in triethylorthoformate in the presence of excess hydrochloric acid, the imidazolium salt was isolated as an off-white solid. While the ^{1}H NMR of the imidazolium salt matched the published data, resonances corresponding to water and unidentified contaminants were also observed in the ^{1}H NMR spectrum, indicating the ligand precursor required additional purification steps before metalation with cobalt was attempted. The crude mixture was dissolved in dichloromethane and placed under 4 Å molecular sieves for 24 h to remove the residual water. After filtration, copious amounts of hexanes were added to the dichloromethane solution, resulting in the precipitation of a white solid, which was subsequently isolated in in 77% yield. Characterization of

[†] Portions of this chapter are reproduced from the following publications with permission from the authors. (1) Ibrahim, A. D.; Tokmic, K.; Brennan, M. B.; Kim, D. Matson, E. M.; Nilges, M. J.; Bertke, J. A.; Fout, A. R. Monoanionic bis(carbene) pincer complexes featuring cobalt(I-III) oxidation states. *Dalton Trans.* **2016**, *45*, 9805-9811. (2) Tokmic, K.; Markus, C. R.; Zhu, L.; Fout, A. R. Well-Defined Cobalt(I) Dihydrogen Catalyst: Experimental Evidence for a Co(I)/Co(III) Redox Process in Olefin Hydrogenation. *J. Am. Chem. Soc.* **2016**, *138*, 11907-11913.

the white product, $[H_3(^{Mes}CCC)]Cl_2$, by ^1H NMR spectroscopy in $CDCl_3$ only displayed resonances corresponding to the desired product.

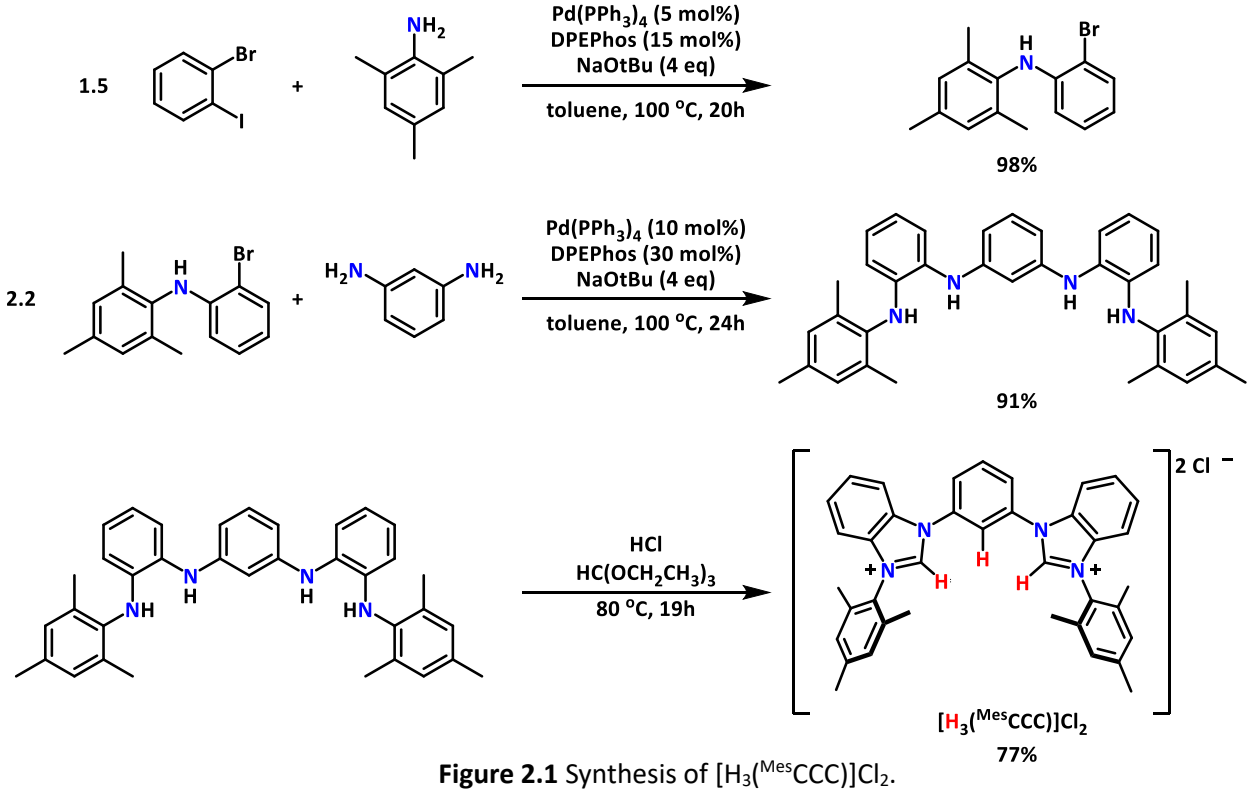

Figure 2.1 Synthesis of $[H_3(^{Mes}CCC)]Cl_2$.

2.3 Synthesis and characterization of $(^{Mes}CCC)CoCl_2py$

With the purified ligand precursor in hand, several approaches to install cobalt onto the ligand platform were investigated. To accomplish this task, the cleavage of three C–H bonds was required. The two imidazolium protons of the ligand precursor can be readily deprotonated by the addition of an appropriate base to generate the two N-heterocyclic carbenes, while the selective activation of the central C–H bond requires an electrophile.[5] Metalation of $[H_3(^{Mes}CCC)]Cl_2$ with iridium was successfully accomplished by the *in situ* deprotonation of the imidazolium protons using excess base, followed by the addition of an iridium(I) source.[4] Following this strategy, 2 equivalents of lithium hexamethyldisilazide ($LiN(SiMe_3)$) were used to deprotonate the imidazolium protons *in situ*, followed by addition of a cobalt(I) source ($(PPh_3)_3CoCl$ or $(PPh_3)_2CoN(SiCH_3)_2$).[6] This strategy, however, led to the formation of mixtures, which proved difficult toward characterization and, thus, alternative routes toward metalation were pursued.

Metalation of a related CCC pincer platform, $[H_3(^{DIPP}CCC)]Cl_2$ (DIPP = bis(2,6-diisopropylphenyl-benzimidazol-2-ylidene)phenyl), employing nickel salts featuring multiple equivalents of an internal base,

dichlorotetrakis(pyridine) nickel(II), and 2 equivalents of $LiN(SiMe_3)$, proved to be an effective strategy for placing a base metal in the electron-rich ligand system.[7] To this end, a similar strategy was attempted toward the metalation of $[H_3(^{Mes}CCC)]Cl_2$ by using 2 equivalents of $LiN(SiMe_3)$, dichlorotetrakis(pyridine) cobalt(II) and one equivalent of an oxidant, $ClCPh_3$, in the effort to furnish a low-spin cobalt(III) species. While this protocol proved to be successful, the low yields (<50%) of the target complex encountered upon isolation regarded this approach synthetically ineffective.

In effort to improve the metalation protocol of the imidazolium salt, other cobalt sources featuring internal bases to generate the desired complexes were explored. Work by Hollis and coworkers[5,8,9] demonstrated that the use of group 4 metal amido complexes, tetrakis(dimethylamido)metal(IV) (M = Ti, Zr, Hf), resulted in the successful preparation of $(^{Bu}CCC)MX_3$ (M = Ti, Zr, Hf; X = NMe_2, I, Cl; Bu = *n*-butyl). Following the metalation procedure utilized by Danopoulos and coworkers[10] for the preparation of related CNC (CNC = 2,6-bis(arylimidazol-2-ylidene), aryl = 2,6-$Pr^i_2C_6H_3$) cobalt bis(carbene) complexes, a derivative of cobalt(II) amido complex, $[Co(N(SiMe_3)_2)]_2$,[11,12] $Co(N(SiMe_3)_2)(py)_2$[13] was selected as the metalating agent.

A sequential treatment of a suspension of $[H_3(^{Mes}CCC)]Cl_2$ and $LiN(SiMe_3)$ in THF with $Co(N(SiMe_3)_2)(py)_2$ and $ClCPh_3$, followed by stirring of the mixture at room temperature for 18 h, resulted in the formation of a green solution (Scheme 2.1). Following workup, the product, **$(^{Mes}CCC)CoCl_2py$**, was isolated as a green solid in excellent yield (93%). Characterization of **$(^{Mes}CCC)CoCl_2py$** in $CDCl_3$ by ^1H NMR spectroscopy revealed the disappearance of the singlet at 12.17 ppm corresponding to the benzimidazolium protons of the ligand precursor and the formation of a diamagnetic C_2-symmetric Co(III) compound with 12 resonances assigned to the target complex (Figure 2.2). Two singlets in the upfield region integrating to 12H and 6H, respectively, were located at 1.83 and 2.19 ppm, corresponding to the mesityl methyl moieties of the flanking aryl substituents. The remaining resonances integrating to 20H between 6.52 and 8.79 ppm were assigned to the aryl backbone of the CCC ligand and the bound pyridine ligand. Additional characterization of **$(^{Mes}CCC)CoCl_2py$** by ^{13}C NMR spectroscopy showed signals at 195.74 and 151.33 ppm (C_{NHC} and C_{Ar} carbons, respectively) are shifted from those of analogues cobalt complex with a ligand derivative[14] featuring 2,6-diisopropylphenyl flanking groups, $(^{DIPP}CCC)CoCl_2py$, but are consistent with the previously reported nickel complex.[7]

To support the assignment of **$(^{Mes}CCC)CoCl_2py$** by ^1H NMR spectroscopy, single crystals suitable for X-ray structure determination were grown from a concentrated solution of a 1:1 mixture of chloroform and benzene. The cobalt center adopts an octahedral geometry with the chloride ligands bound *trans* to each other in the apical position of the CCC-pincer framework and the pyridine ligand bound *trans* to the Co-

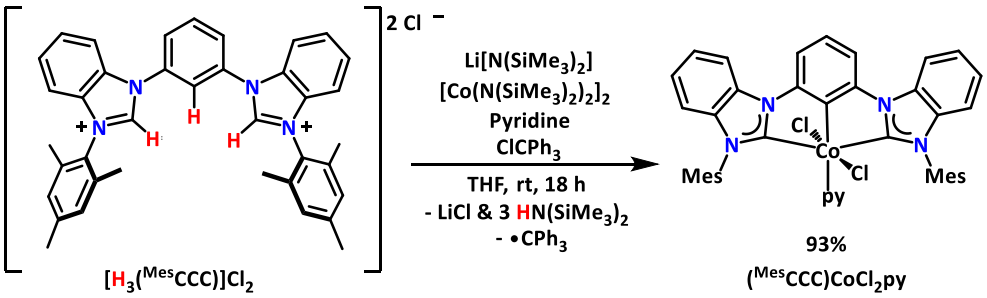

Scheme 2.1 Synthesis of **(^{Mes}CCC)CoCl$_2$py**.

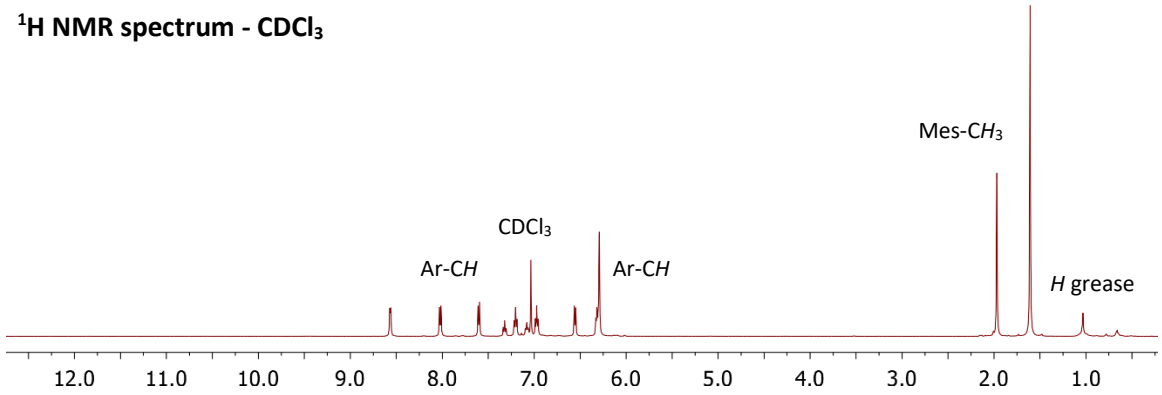

Figure 2.2 ^{1}H NMR spectrum of **(^{Mes}CCC)CoCl$_2$py**.

C_{Ar} bond in equatorial plane (Figure 2.6, Table 2.1 and 2.3). The two Co–C_{NHC} bond lengths of 1.961(4) and 1.958(4) Å, are comparable to those of (^{DIPP}CCC)CoCl$_2$py (1.981(2) and 2.000(2) Å),[14] (CNC)CoBr$_3$ (1.962(7) and 1.962(7) Å), reported by Danopoulos and coworkers[10] and within the range reported for Co(III)–C_{NHC} bonds, 1.815 Å–2.012 Å.[15,16] Similarly, the Co–C_{Ar} bond length of 1.871(4) Å is within the range of Co(III)–C_{Ar} bonds, which range from 1.845–2.057 Å,[14,17] but are shorter than the bond length, (1.937(1) Å, for the analogous Co^{III} species, (PCP^{Me}-^{i}Pr)CoCl$_2$ (PCP = N,N'-bis(diisopropylphosphino)-N,N'-dimethyl-1,2-diaminobenzene),[18] likely as a result of the more rigid CCC ligand framework. The Co–Cl bond lengths, 2.2751(13) and 2.2651(12) Å, are similar to those found in (^{DIPP}CCC)CoCl$_2$py (2.2787(6) and 2.3175(6) Å)[14] and both fall within the regime of recently reported Co(III) complexes featuring an anionic Co–C_{Ar} linkage, 2.229–2.429 Å.[19,20] Finally, the C_{Ar}–Co–N_{py} and C_{Ar}–Co–Cl bond angles, 179.13(16) and 90.11(12)°, signify a nearly idealized octahedral geometry at cobalt and are within error of the same bond angles present in (^{DIPP}CCC)CoCl$_2$py.[14]

Monoanionic pincer ligands containing a Co-C_{Ar} linkage are rare. The report of (C_6H_3(CH_2NMe_2)$_2$)CoClpy by Van Koten and coworkers[21] in 1986 was one of the first reported examples of cobalt pincer complexes featuring a meridional ECE pincer ligand (E = donor group). It was not until 19 years later until the second example of a ECE-cobalt pincer complex was reported.[20] More recently, Nishiyama and coworkers reported the synthesis of NCN–Co complexes containing bis-

(oxazolinyl)phenyl(phebox) as auxiliary ligands.[17] Similarly, the work of Sun,[22] Heinekey,[23] Wass,[24] and Kirchner[18,25] has been instrumental in establishing facile synthetic protocols to cobalt complexes featuring monoanionic PCP pincer ligands. Finally, work by Hollis and coworkers[26] established a supplemental route toward the synthesis of CCC-NHC pincer cobalt complexes via transmetalation from CCC-NHC zirconium complexes. Nevertheless, due to the difficulty in metalating these ligands with first-row transition metals such compounds remain largely underexplored.

2.4 Synthesis and characterization of (^{Mes}CCC)CoClpy

Interested in examining if lower-oxidation-state cobalt complexes could be accessed and stabilized by the CCC-pincer platform, the preparation of a Co(II) derivate was carried out. The addition of half of an equivalent a two-electron reductant, 9,10-dihydro-9,10-anthracendiyl-tris(THF)magnesium, to a THF solution containing **(^{Mes}CCC)CoCl$_2$py** resulted in the formation of an orange solid, **(^{Mes}CCC)CoClpy**, albeit in low-crystalline yield, 28% (Scheme 2.2). Characterization of **(^{Mes}CCC)CoClpy** by ^{1}H NMR spectroscopy proved ineffective due the paramagnetic nature of species and only residual solvent resonances were discerned. The complex was thus considered to be NMR silent, which is distinct from the broaden, but discernable ^{1}H NMR resonances observed in (^{DIPP}CCC)CoCl$_2$py.[14]

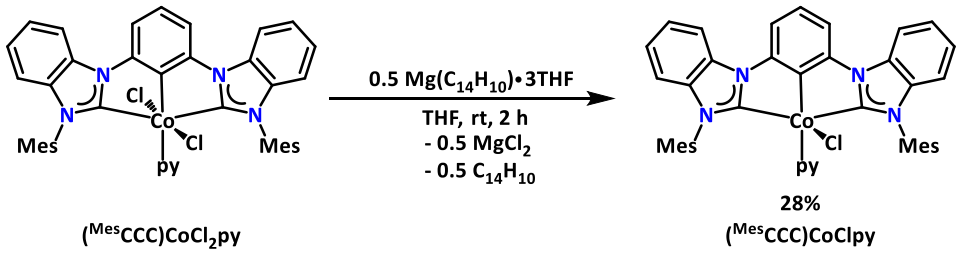

Scheme 2.2 Synthesis of **(^{Mes}CCC)CoClpy**.

In efforts to understand the electronic structure of the paramagnetic complex, **(^{Mes}CCC)CoClpy**, EPR spectroscopy was employed. The X-band EPR spectrum of crystalline **(^{Mes}CCC)CoClpy** obtained from a 1:1 toluene : THF glass at 77 K is depicted in Figure 2.3. The EPR parameters for **(^{Mes}CCC)CoClpy** (g_x = 2.380, g_y = 2.259, and g_z = 1.985) are consistent with the expected low-spin d^7 S = 1/2 molecule,[27] given the strongly donating monoanionic bis(*N*-heterocyclic carbene) ligand. Additionally, the hyperfine interaction to the ^{59}Co nucleus (S = 7/2) is not the sole contributor to the hyperfine coupling observed (A_{Co} (*x*,*y*,*z*) = 224 MHz, 132 MHz, 355 MHz). Superhyperfine coupling to the ^{35}Cl and ^{37}Cl (S = 3/2) nuclei was also observed (A_{Cl}(x,y,z) = 10 MHz, 10 MHz, 41 MHz).

Intriguingly, a comparison of EPR parameters to (^{DIPP}CCC)CoCl$_2$py (g_x = 2.259, g_y = 2.215, and g_z = 1.995; A_{Co} (*x*,*y*,*z*) = 9 MHz, 7 MHz, 266 MHz)[14] revealed notable differences between the two ligand variants.

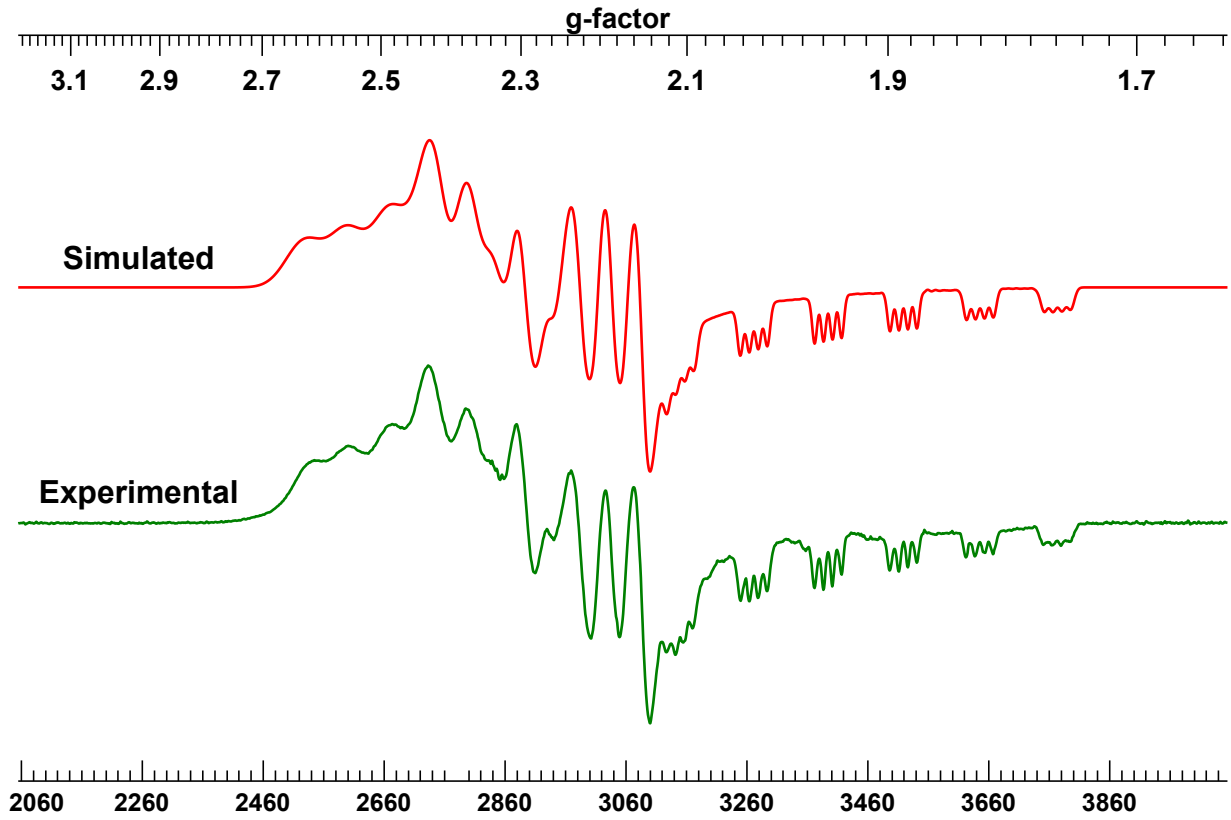

Figure 2.3 EPR spectra of **(^{Mes}CCC)CoClpy** recorded in toluene : THF (1 : 1) glass at 77 K. EPR parameters for **(^{Mes}CCC)CoClpy** (1.60 × 103 gain; 4.00 G modulation amplitude; 20.00 dB power; microwave frequency = 9.2907 GHz).

Unlike the EPR spectrum of **(^{Mes}CCC)CoClpy**, the EPR spectrum of (^{DIPP}CCC)$CoCl_2py^{14}$ revealed weakly resolved superhyperfine coupling interactions to the ^{14}N nuclei (A_N (x,y,z) = 24 MHz, 27 MHz, 31 MHz). Moreover, no resolved superhyperfine coupling to the ^{35}Cl and ^{37}Cl nuclei in (^{DIPP}CCC)$CoCl_2py^{14}$ was observed. Such differences between the ligand variants may be linked to the spatial orientation of the chloride ligand. In the case of **(^{Mes}CCC)CoClpy**, it is likely that the chloride ligand binds *trans* to the Co–C_{Ar} bond in the solution state, in contrast to its apical position in the solid state, while (^{DIPP}CCC)$CoCl_2py^{14}$ maintains the structure observed in the solid state.

To unambiguously identify the structure of **(^{Mes}CCC)CoClpy**, crystals suitable for X-ray diffraction studies from a saturation solution of the target complex in THF at room temperature. Crystallographic characterization of **(^{Mes}CCC)CoClpy** confirmed the formation of the target complex, revealing a square pyramidal geometry (τ = 0.13) about a Co(II) center with the chloride ligand occupying the apical position (Figure 2.6, Table 2.1 and 2.3). The two Co–C_{NHC} bond lengths of 1.948 (3) and 1.930(3) of **(^{Mes}CCC)CoClpy** are very similar to those reported for [*trans*-(CNC)Co(κ^1-CF_3-SO_3)$_2$(py)], 1.942(6) and 1.941(6) Å,[10] and

typical for Co(II)–C_{NHC} bonds (1.845–2.127 Å).[29] In contrast, the Co–C_{Ar} bond length of 1.872(3) Å is noticeably shorter than typical Co(II)–C_{Ar} bonds reported in the literature (1.9020–2.0570 Å)[29-31] and shorter than those observed in the [Co(II)(PCP^{Me}–^{i}Pr)] complexes recently reported by Kirchner and coworkers (1.919 to 1.953 Å)[18] or the ^{R}POCOP^{R}Co(I) complex reported by Heinekey (1.924(4) Å).[23] The Co–Cl bond length of 2.4561(10) Å also differ considerably from the bond lengths in the [Co(II)(PCP^{Me}–^{i}Pr)][18] and [Co(PCP–^{t}Bu)Cl][25] complexes (2.234(1)–2.3103(4) Å) and 2.260(1) Å, respectively. Furthermore, the pyridine ligand lies in the basal position with a Co–N_{py} bond length of 2.011(3) Å, in contrast to the apical position of the pyridine ligand observed in the analogous PCP system (Co–N: 2.1417(8) Å).[18] Finally, the C_{Ar}–Co–N_{py} and Cl–Co–N_{py} bond angles (166.81(13)° and 96.58(9)°) are distorted from an idealized square pyramidal geometry, as indicated by the τ_5 parameter,[28] but similar to those reported for (PCPMe-^{i}Pr)Co(py)Cl (166.89(3)° and 96.28(3)°).[18]

2.5 Electrochemical studies of (^{Mes}CCC)CoClpy

Seeking to investigate the accessibility of a Co(I) derivative of the ^{Mes}CCC ligand platform, the electrochemical properties of **(^{Mes}CCC)CoClpy** were studied using cyclic voltammetry (Figure 2.4). The study was carried out in a 1 mM solution of **(^{Mes}CCC)CoClpy** in acetonitrile with 0.1 M [NBu_4][PF_6] as electrolyte. At a scan rate of 100 mV s^{-1}, a single reversible redox event assigned to the Co(II)/Co(I) redox couple was observed in the window between −1.1 and −1.9 V with an $E_{1/2}$ at −1.56 V vs. Fc/Fc+, respectively. The cyclic voltammogram suggests that the Co(II) species may be amenable to chemical reduction with an appropriate reducing agent.

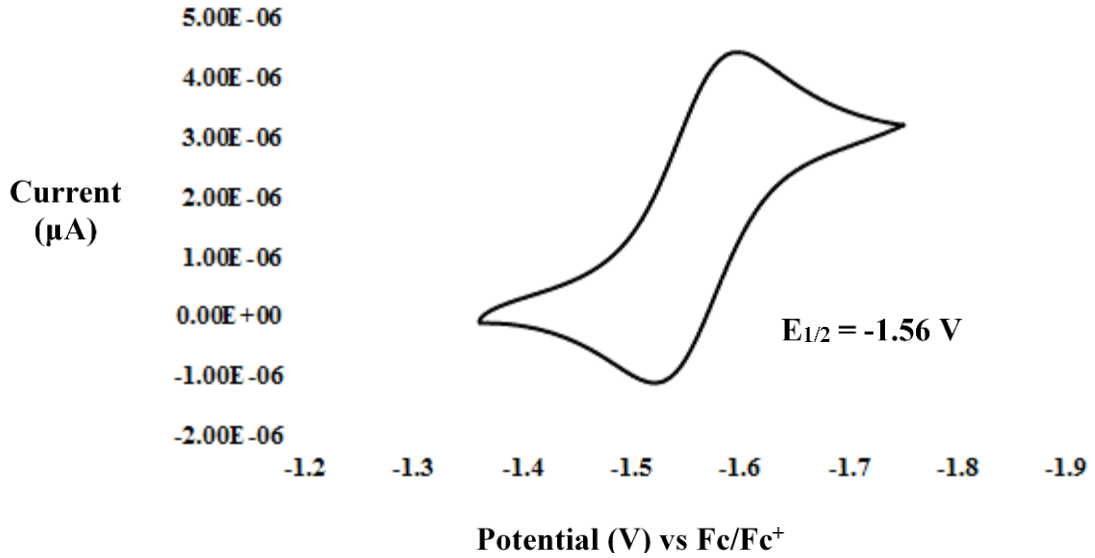

Figure 2.4 Cyclic voltammogram of **(^{Mes}CCC)CoClpy** in acetonitrile at 100 mVs^{-1}. Conditions: 1 mM **(^{Mes}CCC)CoClpy**. 0.1 M [NBu_4][PF_6] in acetonitrile using platinum working electrode.

2.6 Synthesis and characterization of (^{Mes}CCC)Co(N_2)(PPh_3)

Encouraged by these results and interested in the synthesis of low-valent complexes featuring the ^{Mes}CCC ligand platform, the chemical reduction of **(^{Mes}CCC)CoClpy** was carried out. Initial effort to achieve this goal applied the same approach used to prepare **(^{Mes}CCC)CoClpy**. Following the procedure employed for the one-electron reduction of (^{DIPP}CCC)CoClpy,[14] the addition of half an equivalent of 9,10-dihydro-9,10-anthracendiyltris(THF)magnesium to **(^{Mes}CCC)CoClpy** yielded a brown solution. Characterization of the brown solid by ^{1}H NMR spectroscopy revealed broadened resonances, however sufficient information in the ^{1}H NMR spectrum to identify the compound was not present. The use of alternative reducing agents, such sodium amalgam provided the same result. Given the isolation and extensive characterization of a square planar Co(I) dinitrogen compound with the diisopropyl variant of the ligand platform, (^{DIPP}CCC)Co(N_2),[14] IR spectroscopy was employed in order to assay the presence of a dinitrogen ligand. Characterization of the brown solid by IR spectroscopy did not reveal absorptions corresponding to a coordinated dinitrogen ligand. Nevertheless, the possibility of a symmetric dimer bridging N_2 cannot be ruled out given that examples of these arrangements have been reported.[32-37] On this basis, it was

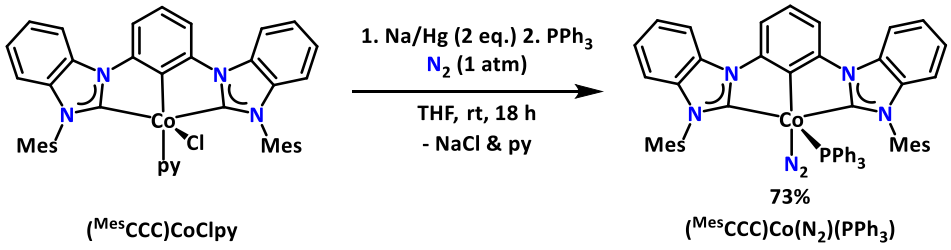

(^{Mes}CCC)CoClpy (^{Mes}CCC)Co(N_2)(PPh_3)

Scheme 2.3 Synthesis of **(^{Mes}CCC)Co(N_2)(PPh_3)**.

^{1}H NMR spectrum – C_6D_6

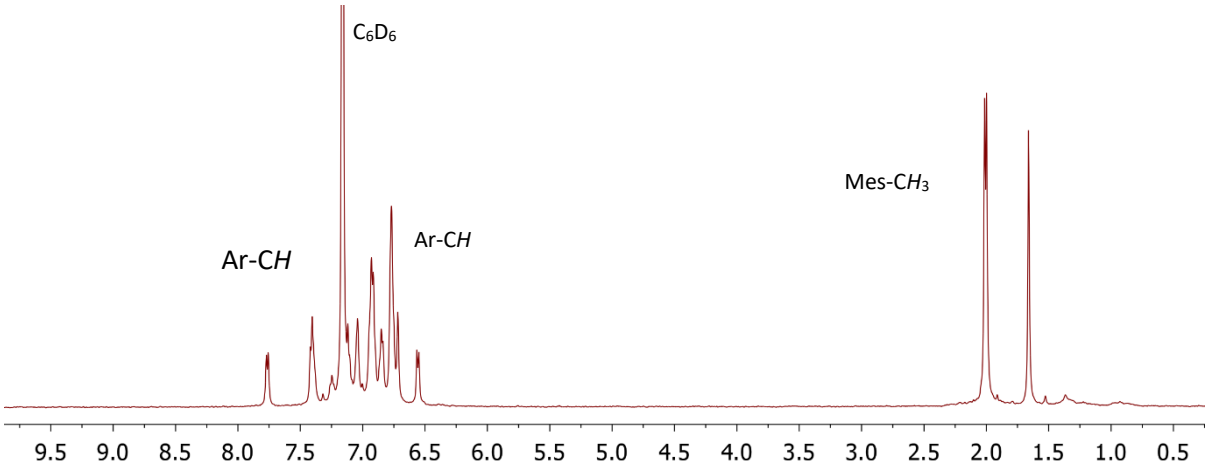

Figure 2.5 ^{1}H NMR spectrum of **(^{Mes}CCC)Co(N_2)(PPh_3)**.

reasoned that the addition of PPh_3 to a presumably 16-electron compound would likely provide a monomeric and diamagnetic species amenable to further characterization. Upon addition of PPh_3 the formation of a dark red solution was observed, and following workup, **(^{Mes}CCC)Co(N_2)(PPh_3)** was isolated as red solid in good yields (73%, Scheme 2.3).

Although the yield of the reduction was impressive, improvements to the long reaction time and use of mercury were considered disadvantageous toward the future reactivity studies of the low-valent complex. To this end, the use of an alternative reducing agents, such as KC_8, was investigated. Employing KC_8 in lieu of Na/Hg resulted in the isolation of the target complex, **(^{Mes}CCC)Co(N_2)(PPh_3)**, in improved yields, 88%, and shorter reaction time.

Characterization of the red solid by ^{1}H NMR spectroscopy confirmed the formation of a diamagnetic species, consistent with the predicted cobalt(I) product, **(^{Mes}CCC)Co(N_2)(PPh_3)**. The presence of 12 resonances in the ^{1}H NMR spectrum (Figure 2.5), shifted from **(^{Mes}CCC)CoCl$_2$py**, indicated a C_s symmetric complex and the presence of triphenyl phosphine. Resonances in the aryl region, shifted from those of free triphenylphosphine, further corroborate this assignment. ^{1}H NMR resonances located at 1.66, 2.00

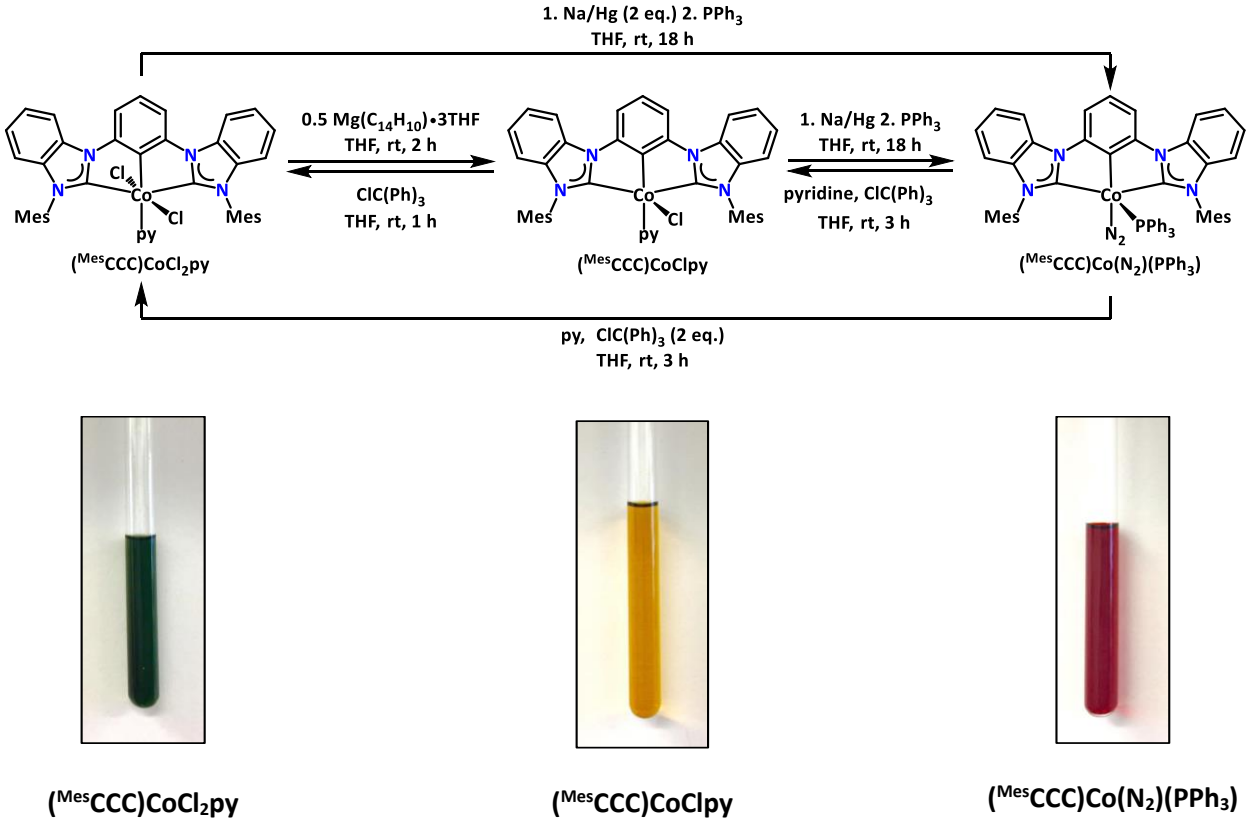

Scheme 2.4 The interconversion between Co(III), Co(II), and Co(I) oxidation states of the ^{Mes}CCC pincer (top) and the corresponding color of the complexes in solution (bottom).

and 2.01 ppm and integrating to 6H each, were assigned to the methyls of the mesityl moiety. Characterization by ^{31}P NMR spectroscopy revealed no resonances, likely attributed a broaden signal arising from the coupling of the phosphorous ligand to the ^{59}Co nucleus (I = 7/2, 100% abundance).

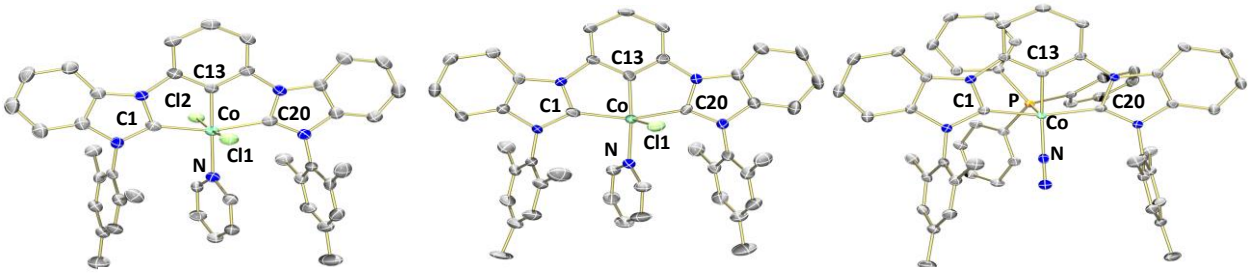

(^{Mes}CCC)CoCl$_2$py **(^{Mes}CCC)CoClpy** **(^{Mes}CCC)Co(N$_2$)(PPh$_3$)**

Figure 2.6 Molecular structures of **(^{Mes}CCC)CoCl$_2$py**, **(^{Mes}CCC)CoClpy**, and **(^{Mes}CCC)Co(N$_2$)(PPh$_3$)** with 50% probability ellipsoids. Solvent molecules and hydrogen atoms have been omitted for clarity.

Table 2.1 Selected bond distances and angles for **(^{Mes}CCC)CoCl$_2$py**, **(^{Mes}CCC)CoClpy**, and **(^{Mes}CCC)Co(N$_2$)(PPh$_3$)**.

	(^{Mes}CCC)CoCl$_2$py	**(^{Mes}CCC)CoClpy**	**(^{Mes}CCC)Co(N$_2$)(PPh$_3$)**
Bond Distances (Å)			
Co – C1	1.961(4)	1.948(3)	1.9147(13)
Co – C13	1.871(4)	1.872(3)	1.8750(13)
Co – C20	1.958(4)	1.930(3)	1.9001(13)
Co – Cl1	2.2751(13)	2.4561(10)	N/A
Co – Cl2	2.2651(12)	N/A	N/A
Co – N	2.090(3)	2.011(3)	1.8270(12)
Co – P	N/A	N/A	2.2483(4)
N – N	N/A	N/A	1.1005(16)
Bond Angles (°)			
C13-Co-N5	179.13(16)	166.81(13)	157.89(5)
C1-Co-C13	80.29(18)	96.60(10)	79.14(5)
C13-Co-C20	80.44(18)	79.53(13)	79.21(5)
C1-Co-C20	160.73(17)	159.07(13)	152.73(4)
C1-Co-Cl	173.28(5)	N/A	N/A
N5-Co-P	N/A	N/A	106.68(4)

Additional characterization of **(^{Mes}CCC)Co(N_2)(PPh_3)** by IR spectroscopy revealed an intense absorption at 2112 cm^{-1}, indicative of a weakly activated dinitrogen ligand bound to the 18-electron cobalt complex. A comparison to the N_2 absorption (2117 cm^{-1}) found in the diisopropyl analogue, (^{DIPP}CCC)Co(N_2)(PPh_3), suggests the mesityl and diisopropyl ligand derivatives impart a similar electronic effect on the metal center, with the mesityl ligand analogue being slightly more electron-rich. Furthermore, differences in reactivity between two ligands derivatives likely arises due to steric factors.

It was hypothesized that the presence of the dinitrogen ligand along with the steric demands of the triphenylphosphine moiety would ensure the formation of a monomeric complex. Molecular structure determination of single crystals suitable for X-ray diffraction studies of **(^{Mes}CCC)Co(N_2)(PPh_3)** confirmed this hypothesis. The cobalt center adopts a square pyramidal geometry ($\tau = 0.09$)[28] with the N_2 ligand bound *trans* to the Co-C_{Ar} bond (Figure 2.6, Table 2.1 and 2.4). The two Co–C_{NHC} bond lengths of 1.9147(13) and 1.9001(13) Å and the Co–C_{Ar} bond length of 1.8750(13) Å are comparable to those of complex (^{DIPP}CCC)Co-N_2.[14] Similarly, the N_2 bond length of 1.100 5(16) Å indicated a largely unactivated dinitrogen ligand in agreement with the IR stretch observed for the complex. **(^{Mes}CCC)Co(N_2)(PPh_3)** represents a rare example of a five coordinate, mononuclear cobalt complex featuring a dinitrogen ligand. There have been only nine examples reported in the CSD thus far, eight of which feature phosphine ligands.[37-43]

As depicted in Scheme 2.4, the interconversion of these molecules was readily achieved by using stoichiometric one electron oxidation or reduction agents. Oxidation of the Co(I), **(^{Mes}CCC)Co(N_2)(PPh_3)**, to the Co(II), **(^{Mes}CCC)CoClpy**, analogue was accomplished by the addition of pyridine and one equivalent of $ClCPh_3$ as the oxidant and subsequent formation of Gomberg's dimer. The addition of one equivalent of $ClPh_3$ to the Co(II), **(^{Mes}CCC)CoClpy**, furnished the Co(III), **(^{Mes}CCC)$CoCl_2$py**, and the subsequent formation of Gomberg's dimer.

2.7 Synthesis of (^{Mes}CCC)$Co(CO)_2$

Comparison between the (^{Ar}CCC)Co(N_2)(PPh_3) (Ar = Mes and DIPP) dinitrogen stretching frequencies via IR spectroscopy suggested the mesityl analogue of the ligand is slightly more electron-rich than the diisopropyl derivative. Seeking to further examine the ^{Ar}CCC ligand influences on the metal center, the synthesis of cobalt-carbonyl complexes was investigated. Since the C≡O IR stretching frequency correlates well with the donor-strength of the metal center, as in the case of widely studied phosphine ligands using the Tolman electronic parameter,[44] these studies would provide an additional parameter to probe the electronic effects of the two derivatives of the ^{Ar}CCC pincer ligands examined in our group. To this end, **(^{Mes}CCC)$CoCl_2$py** was reduced following the previously mentioned protocol using 2 equiv of KC_8 and CO (1

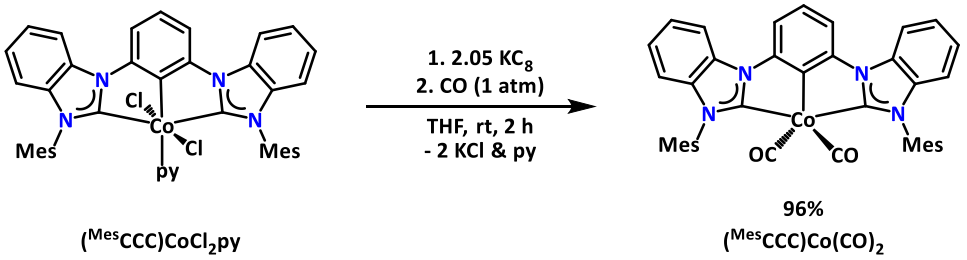

(^{Mes}CCC)CoCl$_2$py (^{Mes}CCC)Co(CO)$_2$

Scheme 2.5 Synthesis of **(^{Mes}CCC)Co(CO)$_2$.**

atm) was added to the reduced species (Scheme 2.5). Following workup, the yellow solid, **(^{Mes}CCC)Co(CO)$_2$**, was isolated in 96% yield.

Characterization of **(^{Mes}CCC)Co(CO)$_2$** by ^{1}H NMR spectroscopy in C_6D_6 revealed 8 resonances, consistent with a low-spin complex. One singlet integrating to 18H in the aliphatic region at 1.95 ppm was assigned to mesityl methyl groups. Additional resonances integrating to 15H between 6.5 ppm and 7.9 ppm were assigned to the aryl backbone of the CCC ligand. The ^{13}C NMR spectrum showed signal for the bound CO ligand at 207.4 ppm. Furthermore, the presence of 17 additional resonances in the ^{13}C NMR spectrum are consistent with the proposed complex.

Characterization of **(^{Mes}CCC)Co(CO)$_2$** by single crystal X-ray diffraction established the identity of the compound. Yellow crystals suitable for analysis were grown from a saturated solution of the target complex in THF at -35 °C, confirming the addition of two carbon monoxide ligands, resulting in the formation of a five-coordinate species with a distorted-trigonal-bipyramidal geometry ($\tau = 0.55$)[28] about the metal center (Figure 2.7 and Table 2.2 and 2.4). The two Co-C_{NHC} bond distances of 1.9119(15) Å are similar to those found in **(^{Mes}CCC)Co(N$_2$)(PPh$_3$)** and the Co-C_{Ar} bond length, 1.910(2) Å, of **(^{Mes}CCC)Co(CO)$_2$** is slightly elongated compared to **(^{Mes}CCC)Co(N$_2$)(PPh$_3$)**. The Co-C_{Ar} bond distance is shorter than the bond lengths for analogues cobalt(I) dicarbonyl PCP pincer complexes reported by Kirchner,[25] Heinekey[45] and Wass,[24] likely as result of the increased rigidity of the CCC ligand backbone compared to the PCP systems. The Co-C_{CO} bond lengths, 1.7776(19) Å, falls within the range of reported cobalt(I) dicarbonyl complexes, 1.743(2)-1.799(2) Å.[24,25,45]

Additional characterization of **(^{Mes}CCC)Co(CO)$_2$** by IR spectroscopy revealed two intense absorption bands at 1918 cm^{-1} and 1973 cm^{-1} corresponding to the CO stretching frequencies. These values are at lower energy compared to the diisopropyl derivative of the ligand system, (^{DIPP}CCC)Co(CO)$_2$ (1939 cm^{-1} and 1992 cm^{-1}, respectively), indicating the mesityl derivative of the metal complex imparts stronger back-donation from the metal to the carbonyl ligands, and is thus more electron-rich and is also in agreement with the Co-dinitrogen IR data between the ligand derivatives. A comparison to analogous PCP cobalt

dicarbonyl complexes IR stretching frequencies, 1906-1926 cm^{-1} and 1963 and 1982 cm^{-1},[24,25,45] indicates that the ^{Ar}CCC pincer ligands promote a similar electronic effect on the cobalt center.

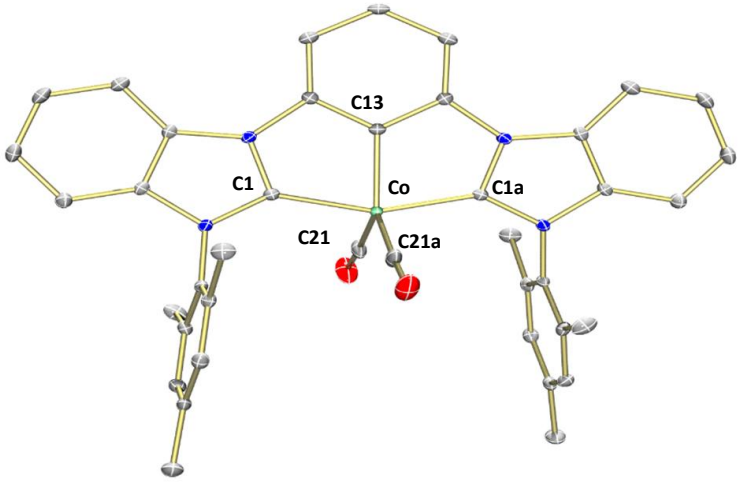

Figure 2.7 Molecular structures of **(^{Mes}CCC)Co(CO)$_2$** with 50% probability ellipsoids. Hydrogen atoms have been omitted for clarity.

Table 2.2 Selected bond distances and angles for **(^{Mes}CCC)Co(CO)$_2$**.

	(^{Mes}CCC)Co(CO)$_2$
Bond Distances (Å)	
Co – C1	1.9119(15)
Co – C13	1.910(2)
Co – C1a	1.9119(15)
Co – C21	2.2787(6)
Co – C21a	2.3175(6)
Bond Angles (°)	
C1-Co-C1a	156.27(10)
C1-Co-C11	78.14(5)
C1-Co-C21	98.15(7)
C1a-Co-C21	94.15(7)
C11-Co-C21	123.54(7)
C21-Co-C21a	112.93(14)

2.8 Conclusion

In conclusion, a series of cobalt pincer complexes featuring the electron-rich, monoanionic bis(carbene) (^{Mes}CCC) ligand have been synthesized. The Co(I-III) derivatives of these compounds have been prepared in good yields, including the room temperature synthesis of a Co(III) derivative, **(^{Mes}CCC)CoCl$_2$py**, from the benzimidazolium salt precursor, [H$_3$(^{Mes}CCC)]Cl$_2$. In contrast to traditional routes that make use of lithiation and subsequent addition of cobalt halide compounds,[23] this room temperature synthesis utilizes Co(II) source featuring multiple equivalents of internal base for the room temperature aryl C–H bond cleavage. A suite of characterization techniques was used to identify and study these complexes, including ^{1}H and ^{13}C NMR, EPR, and FT-IR spectroscopies, as well as single crystal X-ray crystallography. IR studies of the N_2 and carbonyl complexes indicate that the mesityl derivative is slightly more electron-rich than the diisopropyl ligand derivative. Such complexes provide an interesting platform from which to study two-electron processes with cobalt, particularly given the extensively characterized nature of the different oxidation states of cobalt with the ligand platform.

2.9 Experimental section

General Considerations. All manipulations of air- and moisture-sensitive compounds were carried out in the absence of water and dioxygen in an MBraun inert atmosphere drybox under a dinitrogen atmosphere except where specified otherwise. All glassware was oven dried for a minimum of 8 h and cooled in an evacuated antechamber prior to use in the drybox. Solvents for sensitive manipulations were dried and deoxygenated on a Glass Contour System (SG Water USA, Nashua, NH) and stored over 4 Å molecular sieves purchased from Strem following a literature procedure prior to use.[46] Chloroform-*d*, and benzene-d_6 were purchased from Cambridge Isotope Labs and were degassed and stored over 4 Å molecular sieves prior to use. Lithium hexamethyldisilazane was purchased from Sigma-Aldrich and recrystallized from toluene under an inert atmosphere prior to use. Celite® 545 (J. T. Baker) was dried in a Schlenk flask for 24 h under dynamic vacuum while heating to at least 150˚C prior to use in a glovebox. DPEPhos (>99%) and $CoCl_2$ (99% anhydrous) were purchased from Strem and used as received. $PdCl_2$ was purchased from Pressure Chemicals. [Co(N(SiMe$_3$)$_2$)$_2$]$_2$•THF[11,12] and Pd(PPh$_3$)$_4$[47] were prepared by literature procedures. NMR Spectra were recorded at room temperature on a Varian spectrometer operating at 500 MHz (^{1}H NMR) and 126 MHz (^{13}C NMR) (U500, VXR500, UI500NB) and referenced to the residual $CHCl_3$ and C_6D_5H resonance (δ in parts per million, and *J* in Hz). Solid-state infrared spectra were recorded using a PerkinElmer Frontier FT-IR spectrophotometer equipped with a KRS5 thallium bromide/iodide universal attenuated total reflectance accessory. Elemental analyses were performed by

the University of Illinois at Urbana−Champaign School of Chemical Sciences Microanalysis Laboratory in Urbana, IL. Electrospray ionization mass spectrometry (ESI) was recorded on a Water Q-TOF Ultima ESI instrument. Cyclic voltammetry studies were collected on CH Instruments 1410C potentiostat. EPR samples were prepared in an MBraun glovebox. The sample concentration is approximately 10mM in tetrahydrofuran/toluene (1:1) mixture. EPR spectra were recorded on a Varian E-line 12" Century series X-band CW spectrometer and the spectra were simulated using the program SIMPOW6.[48,49] EPR parameters for (^{Mes}CCC)CoClpy (1.60E+3 gain; 4.00G modulation amplitude; 20.00dB power; microwave frequency = 9.2907GHz).

Modified Ligand Procedure

Synthesis of N-(2-bromophenyl)-2,4,6-trimethylaniline: A 20 mL scintillation vial charged with $Pd(PPh_3)_4$ (0.404 g, 0.35 mmol) and DPEPhos (0.566 g, 1.05 mmol) was stirred at 80°C for 20 minutes in toluene (20 mL). The DPEPhos/$Pd(PPh_3)_4$ solution was then filtered through a pad of celite into a 150 mL Schlenk bomb and 2-bromoiodobenzene (2.97 g, 10.5 mmol), 2,4,6-trimethylaniline (0.947 g, 7 mmol) and sodium *tert*-butoxide (2.69 g, 28 mmol) were added and the mixture was diluted with 80 mL of toluene. After stirring the mixture at 100°C for 20 h, the suspension was allowed to cool to ambient temperature and then filtered through a plug of silica, eluting with 500 mL of Et_2O. The filtrate was concentrated to an oil under reduced pressure and filtered through a pad of silica, eluting with 800 mL of hexanes. Under reduced pressure, the filtrate was concentrated to an oil, taken up in *ca.* 10 mL hot ethanol, and upon cooling, the product was obtained as a white solid (2.00 g, 6.89 mmol, 98%). The ^{1}H and ^{13}C NMR spectra match those of the reported compound.[4]

Synthesis of N^1,$N^{1'}$-(1,3-phenylene)bis(N^2-mesityl-1,2-diamine): A 20 mL scintillation vial charged with $Pd(PPh_3)_4$ (0.550 mg, 0.476 mmol) and DPEPhos (0.800 g, 1.48 mmol) was stirred at 80°C for 20 minutes in toluene (20 mL). The DPEPhos/$Pd(PPh_3)_4$ solution was then filtered through a pad of celite into a 250 mL Schlenk bomb and N-(2-bromophenyl)-2,4,6-trimethylaniline (3.00 g, 10.34 mmol), 1,3-diaminobenzene (0.502 g, 4.64 mmol) and sodium *tert*-pentoxide (2.500 g, 22.7 mmol) were added and the mixture was diluted with *ca.* 120 mL of toluene. After stirring at 100°C for 24 h, the suspension was allowed to cool to ambient temperature and then filtered through a plug of silica, eluting with 500 mL of Et_2O. The solvent was removed under reduced pressure, the residue adsorbed on 30 g of dry silica and loaded onto a silica gel column. The product is separated with a stepwise gradient of 2-5% ethyl acetate/hexanes, yielding a green powder. This powder is further recrystallized from hexanes to give the desired compound (2.23 g, 4.24 mmol, 91%). The ^{1}H and ^{13}C NMR spectra match those of the reported compound.[4]

Synthesis of 1,1'-(1,3-phenylene)bis(3-mesityl-1H-benzo[d]imidazole-3-ium) chloride, $[H_3(^{Mes}CCC)]Cl_2$: $N^1,N^{1'}$-(1,3-phenylene)bis(N^2-mesitylbezene-1,2-diamine) (2.245 g, 4.24 mmol) was suspended in 55 mL triethyl orthoformate and heated to reflux under an N_2 atmosphere. Concentrated hydrochloric acid (37% w/w, 0.8 mL, 9.7 mmol) was added dropwise and the color of the suspension turned off-white. After stirring for 19 h, the suspension was allowed to cool to ambient temperature and treated with 55 mL of Et_2O, followed by 165 mL of hexanes. After stirring for 20 min, the solid was collected by filtration and washed with excess ether. The off-white solid was taken into the drybox, dissolved in *ca.* 100 mL of DCM and stored under 4 Å molecular sieves for 24 h. The solution was decanted, and *ca.* 120 mL of hexanes was added, and a white solid was isolated by filtration (2.015 g, 3.25 mmol, 77%). The ^1H and ^{13}C NMR spectra match those of the reported compound.[4]

Synthesis of Metal Complexes

Synthesis of $(^{Mes}CCC)CoCl_2py$: A mixture in a 20 mL scintillation vial charged with $[H_3(CCC^{Mes})]Cl_2$ (0.050 g, 0.08 mmol) in *ca.* 5 mL of THF and a THF solution of lithium hexamethyldisilazide (0.013 g, 0.08 mmol) was stirred at ambient temperature for 5 min. A THF solution of $[Co(N(SiMe_3)_2)_2]_2$•THF (0.036 g, 0.08 mmol) and 4 drops of anhydrous pyridine were added to the reaction mixture. A solution of trityl chloride (0.023 g, 0.83 mmol) in *ca.* 2 mL THF was added to the reaction mixture. After stirring for 18 h at ambient temperature, the volatiles were removed under reduce pressure and the green solid was washed with hexanes (2 × 10 mL), dissolved in DCM (10 mL), filtered over a plug of Celite, and the solvent was removed under reduced pressure to give a green solid (0.057 g, 0.075 mmol, 93%). Crystals suitable for X-ray diffraction were grown from slow evaporation of a concentrated solution of complex $(^{Mes}CCC)CoCl_2py$ in benzene and chloroform at room temperature. Anal. Calcd for $(^{Mes}CCC)CoCl_2py*C_6H_6/CH_2Cl_2$ ($C_{50}H_{45}Cl_4CoN_5$): C, 65.51; H, 4.95; N, 7.64. Found: C, 65.54; H, 4.6; N, 7.64. ^1H NMR (500 MHz, $CDCl_3$) δ 8.79 (d, J = 6.0, 2H), 8.25 (d, J = 8.0, 2H), 7.83 (d, J = 8.0, 2H), 7.55 (t, J = 7.8, 1H), 7.43 (t, J = 7.5, 2H), 7.31 (t, J = 7.8, 1H), 7.20 (t, 7.5, 2H), 6.78 (d, J = 8.0, 2H), 6.56-6.50 (m, 6H), 2.19 (s, 6H), 1.83 (s, 12H). ^{13}C NMR ($CDCl_3$): δ 195.7, 151.3, 147.8, 137.6, 135.8, 135.7, 135.4, 132.3, 131.6, 131.5, 131.3, 129.7, 128.5, 128.1, 127.5, 127.4, 124.0, 122.8, 122.1, 121.7, 111.2, 109.5, 109.3, 20.1, 17.2.

Alternative synthesis of $(^{Mes}CCC)CoCl_2py$ from $(^{Mes}CCC)Co(N_2)(PPh_3)$: A solution of trityl chloride (0.063 mg, 0.226 mmol) in *ca*. 5 mL of THF was added to a 20 mL scintillation vial charged with a suspension of **$(^{Mes}CCC)Co(N_2)(PPh_3)$** (0.101 g, 0.113 mmol) and 5 drops of anhydrous pyridine in *ca.* 5 mL THF. After stirring the mixture for 3 h at ambient temperature, the volatiles were removed under reduced pressure to give a green solid mixture. The crude product was washed with Et_2O (2 × 5 mL), pumped to dryness *in*

vacuo, taken up in *ca*. 10 mL DCM and filtered over a plug of Celite. Removal of the solvent under reduced pressured resulted in a green powder (0.070 g, 0.0882 mmol, 78%).

Alternative synthesis of (^{Mes}CCC)CoCl$_2$py from (^{Mes}CCC)CoClpy: A solution of trityl chloride (0.004 mg, 0.014 mmol) in *ca*. 5 mL of THF was added to a 20 mL scintillation vial charged with a pre-stirred suspension of **(^{Mes}CCC)CoClpy** (0.010 g, 0.014 mmol) in *ca.* 5 mL THF. After stirring the mixture for 1 h at ambient temperature, the volatiles were removed under reduced pressure to give a green solid mixture. The crude product was triturated with Et_2O (2 × 5 mL), pumped to dryness *in vacuo*, taken up in *ca*. 10 mL DCM and filtered over a plug of Celite. Removal of the solvent under reduced pressured resulted in a green powder (0.009 g, 0.0119 mmol, 85%).

Synthesis of (^{Mes}CCC)CoClpy: A suspension of Mg($C_{14}H_{10}$)•3THF (0.142mg, 0.068 mmol) in ca. 2 mL of THF was added to a 20 mL scintillation vial charged with a pre-stirred solution of **(^{Mes}CCC)CoClpy** (0.100 g, 0.136 mmol) in approximately 3 mL of THF. The resulting reaction was stirred for 2 h at room temperature and then pipette-filtered over Celite. Removal of volatiles from the filtrate under reduced pressure yielded a solid residue, which was washed with THF (2 × 1 mL) to give an orange solid. Further washing with hexanes (2 × 1 mL), followed by the removal of solvents under reduced pressure afforded 6 mg of pure compound. A second cropping from the THF washes provided an additional 21 mg of the crystalline orange product (0.027 g, 0.038 mmol, 28 %). Crystals suitable for X-ray diffraction were grown from these THF washes, as well as recrystallization of the compound from THF. The product is ^{1}H NMR silent. HRMS (ESI), calc. for $C_{43}H_{38}ClCoN_5$ $(M)^+$: 718.2148; found 718.2137.

Alternative synthesis of (^{Mes}CCC)CoClpy from (^{Mes}CCC)Co(N$_2$)(PPh$_3$): A solution of trityl chloride (0.004 mg, 0.015 mmol) in *ca*. 2 mL of THF was added to a 20 mL scintillation vial charged with a pre-stirred suspension of **(^{Mes}CCC)Co(N$_2$)(PPh$_3$)** (0.015 g, 0.017 mmol) and 2 drops of anhydrous pyridine in *ca.* 5 mL THF. After stirring the mixture for 3 h at ambient temperature, the volatiles were removed under reduced pressure to give an orange residue. The crude product was washed with Et_2O (2 × 5 mL), pumped to dryness *in vacuo*, taken up in *ca*. 5 mL of THF and filtered over a plug of Celite. Removal of the solvent under reduced pressured resulted in an orange powder (0.009 g, 0.0128 mmol, 85%).

Synthesis of (^{Mes}CCC)Co(N$_2$)(PPh$_3$): A 20 mL scintillation vial was charged with **(^{Mes}CCC)CoCl$_2$py** (0.108 g, 0.141 mmol) and THF (10 mL). After stirring for 10 min, the green suspension was transferred to a THF suspension (5 mL) of freshly prepared sodium amalgam (Na: 0.012 g, 0.53 mmol; Hg 3.80 g). After stirring the mixture at ambient temperature for 18 h, the dark suspension was filtered over Celite and to the filtrate, triphenylphosphine (0.037 g, 0.141 mmol) was added, resulting in the color change of the mixture to dark red. After stirring the solution for 2 h, the THF was removed under reduced pressure. The product

was then extracted into benzene (3 x 5 mL), filtered over Celite and concentrated to a red solid. The solid was triturated with hexane (10 mL) and concentrated under vacuum to give a fine red powder (0.094 g, 0.105 mmol, 73%). Crystals suitable for X-ray diffraction were grown from slow evaporation of a concentrated solution of complex **(^{Mes}CCC)Co(N_2)(PPh_3)** in benzene layered with hexanes at room temperature. NMR data (in benzene-d_6, 25 °C): ^{1}H δ = 7.76 (d, J = 8.0, 2H), 7.41 (d, J = 7.5, 2H), 7.25 (t, J = 7.5, 2H), 7.12 (t, J = 7.8, 2H), 6.95-6.89 (m, 8H), 6.85 (t, J = 7, 3H), 6.79-6.74 (m, 8H), 6.71 (s, 1H), 6.55 (d, J = 8, 2H), 2.01 (s, 6H), 2.00 (s, 6H), 1.66 (s, 6H); ^{13}C δ = 208.9, 164.9,143.8, 138.5, 138.4, 137.1, 136.9, 136.7, 134.4, 133.0, 132.9, 132.4, 129.9, 121.9, 121.7, 119.4, 109.7, 108.5, 105.8, 21.1, 18.2, 17.8. HRMS (ESI), calc. for $C_{56}H_{49}CoN_4P$ $(M)^+$: 867.3027; found 867.2997. IR: 2112 cm^{-1} (N_2).

Synthesis of (^{Mes}CCC)Co(N_2)(PPh_3) using KC_8: A 20 mL scintillation vial was charged with **(^{Mes}CCC)CoCl_2py** (0.094 g, 0.124 mmol) and THF (10 mL). A suspension of KC_8 (0.035 g, 0.259 mmol) in THF (5 mL) was added to the mixture. After stirring for 2 hours, the dark brown suspension was filtered over Celite and to the filtrate, PPh_3 (0.033 g, 0.124 mmol) was added, resulting in the change of the mixture to dark red. The THF was removed under reduced pressure after stirring the solution for 1 h. The product was then extracted into benzene (3 x 5 mL), filtered over Celite and concentrated under reduced pressure to a red solid. The solid was triturated with hexane (10 mL) and concentrated *in vacuo* to give a fine red powder (0.097 g, 0.109 mmol, 88%). NMR data (in toluene-d_8, 25 °C): 1H δ = 7.72 (d, J = 8.0, 2H), 7.33 (d, J = 7.5, 2H), 7.16 (t, J = 7.0, 1H), 7.12 (d, J = 8.0, 2H), 6.89 (t, J = 7.5, 2H), 6.87-6.81 (m, 7H), 6.77-6.68 (m, 12H), 6.52 (d, J = 7.5, 2H), 2.03 (s, 6H), 1.92 (s, 6H), 1.62 (s, 6H) The ^{1}H and ^{13}C NMR spectra in benzene-d_6 match that of the reported compound.

Alternative synthesis of (^{Mes}CCC)Co(N_2)(PPh_3) from (^{Mes}CCC)CoClpy: A 20 mL scintillation vial was charged with **(^{Mes}CCC)CoClpy** (0.027 g, 0.0375 mmol) and *ca.* 5 mL of THF. After stirring for 10 min, the orange solution was transferred to a *ca*. 5 mL THF suspension of freshly prepared sodium amalgam (Na: 0.010 g, 0.43 mmol; Hg 1.61 g). After stirring the mixture at ambient temperature for 17 h, the dark suspension was filtered over Celite and to the filtrate, triphenylphosphine (0.010 g, 0.038 mmol) was added, resulting in the change of the mixture to dark red. After stirring the solution for 1 h, the THF was removed under reduced pressure. The product was then extracted into benzene (3 x 5 mL), filtered over Celite and concentrated to a red solid. The solid was triturated with hexane (10 mL) and concentrated under vacuum to give a fine red powder (0.025 g, 0.028 mmol, 75%).

Synthesis of (^{Mes}CCC)Co$(CO)_2$: A 20 mL scintillation vial was charged with **(^{Mes}CCC)CoCl_2py** (0.025 g, 0.0331 mmol) and THF (10 mL). A suspension of KC_8 (0.009 g, 0.0679 mmol) in THF (5 mL) was added to the mixture. After stirring the suspension for 1h, the mixture was filtered into a 50 mL storage vessel and 1

atm of CO was added. The volatiles were removed under reduced pressure after stirring for 2 h. The resulting crude mixture was washed with hexanes (10 mL) and the product was extracted in benzene (15 mL), filtered and concentrated to a yellow solid. The solid was triturated with hexanes (10 mL) and concentrated under vacuum to give a fine yellow power (0.021 g, 0.0316 mmol, 96%). ^{1}H NMR (500 MHz, C_6D_6) δ = 7.82 (d, J = 7.8, 2H), 7.74 (d, J = 7.8, 2H), 7.50 (t, 7.6, 1H), 7.07 (t, 7.8, 2H), 6.90 (t, 7.8, 2H), 6.65 (s, 4H), 6.56 (d, 6.6, 2H), 1.95 (s, 18H). ^{13}C NMR (125 MHz, THF-d_8) δ = 207.4, 205.8, 170.9, 145.8, 139.9, 137.7, 134.0, 132.1, 130.3, 129.0, 123.6, 123.4, 121.3, 111.5, 110.2, 107.4, 21.3, 17.8. HRMS (ESI), calc. for $C_{38}H_{34}CoN_4$ $(M)^+$: 605.2115; found 605.2115. IR: 1918 and 1973 cm^{-1} (C≡O).

Table 2.3 Crystallographic parameters for **(^{Mes}CCC)CoCl$_2$py**, **(^{Mes}CCC)CoClpy**, and **(^{Mes}CCC)Co(N$_2$)(PPh$_3$)**.

	(^{Mes}CCC)CoCl$_2$Py bm27vsa1	(^{Mes}CCC)CoClPy cm69jsaq1	(^{Mes}CCC)CoN$_2$(PPh$_3$) cd62hsa
Empirical Formula	C47 H42 Cl5 Co N5	C51 H54 Cl Co N5 O2	C56 H48 Co N6 P
Formula Weight	913.04	863.07	894.90
Temperature	183(2) K	296(2) K	100(2) K
Wavelength	0.71073 Å	0.71073 Å	0.71073 Å
Crystal system	Monoclinic	Monoclinic	Triclinic
Space group	P 21/n	P 21/c	P-1
Unit Cell Dimensions	a = 9.069(2) Å b = 22.886(6) Å c = 20.280(5) Å α= 90° β= 92.301(4)° γ = 90°	a = 14.4441(18) Å b = 20.502(3) Å c = 16.521(2) Å α = 90° β = 98.680(8)° γ = 90°	a = 12.3483(6) Å b = 13.3152(7) Å c = 16.1489(9) Å α = 107.661(3)° β = 90.213(2)° γ = 115.791(2)°
Volume	4206.0(18) Å^3	4836.5(11) Å^3	2249.4(2) Å^3
Z	4	4	2
Reflections collected	46522	8946	115626
Independent reflections	7747	8946	13805
Goodness-of-fit on F2	1.005	0.901	1.030
Final R indices [I>sigma(I)]	R1 = 0.0532 wR2 = 0.0953	R1 = 0.0596 wR2 = 0.1394	R1 = 0.0371 wR2 = 0.0862

Table 2.4 Crystallographic parameters for **(^{Mes}CCC)Co(CO)$_2$**.

	(^{Mes}CCC)Co(CO)$_2$ cd99da
Empirical Formula	C40 H33 Co N4 O2
Formula Weight	660.63
Temperature	105(2) K
Wavelength	0.71073 Å
Crystal system	Monoclinic
Space group	C 2/c
Unit Cell Dimensions	a = 23.7349(9) Å b = 14.5175(6) Å c = 9.3849(4) Å α= 90° β= 102.0336(14)° γ = 90°
Volume	3162.7(2) Å^3
Z	4
Reflections collected	61292
Independent reflections	3497
Goodness-of-fit on F2	1.053
Final R indices [I>sigma(I)]	R1 = 0.0325 wR2 = 0.0854

2.10 References

1. Semproni, S. P.; Atienza, C. C. H.; Chirik, P. J. Oxidative addition and C–H activaition chemistry with a PNP pincer-ligated cobalt complex. *Chem. Sci.* **2014**, *5*, 1956-1960.
2. Ingleson, M.; Fan, H.; Pink, M.; Tomaszewski, J.; Caulton, K. G. Three-Coordinate Co(I) Provides Access to Unsaturated Dihydrido-Co(III) and Seven-Coordinate Co(V). *J. Am. Chem. Soc.* **2006**, *128*, 1804-1806.
3. Rozenel, S. S.; Padilla, R.; Camp, C.; Arnold, J. Unusual activation of H_2 by reduced cobalt complexes supported by a PNP pincer ligand. *Chem. Commun.* **2014**, *50*, 2612-2614.
4. Chianese, A. R.; Mo, A.; Lampland, N. L.; Swartz, R. L.; Bremer, P. T. Iridium Complexes of CCC-Pincer N-Heterocyclyic Carbene Ligands: Synthesis and Catalytic C–H Functionalization. *Organometallics* **2010**, *29*, 3019-3026.
5. Rubio, R. J.; Andavan, G. T. S.; Bauer, E. B.; Hollis, T. K.; Cho, J.; Tham, F. S.; Donnadieu, B. Toward a general method for CCC N-Heterocyclic carbene pincer synthesis: Metallation and transmetallation strategies for concurrent activation of three C–H bond. *J. Organomet. Chem.* **2005**, *690*, 5353-5364.
6. Brennan, M. B.; Kim, D.; Fout. A. R. A synthetic and mechanistic investigation into the cobalt(I) catalyzed amination of aryl halides. *Chem. Sci.* **2014**, *5*, 4831-4839.
7. Matson, E. M.; Espinosa-Martinez, G.; Ibrahim, A. D.; Jackson, B. J.; Bertke, J. A.; Fout, A. R. Nickel(II) Pincer Carbene Complexes: Oxidative Addition of an Aryl C–H Bond to Form a Ni(II) Hydride. *Organometallics* **2015**, *34*, 399-407.
8. Halgert, T. R.; Hollis, T. K.; Valente, E. J. Synthesis of Titanium CCC-NHC Pincer Complexes and Catalytic Hydroamination of Unactivated Alkenes. *Organometallics* **2012**, *31*, 3002-3009.
9. Cho, J.; Hollis, K.; Valente, E. J.; Trate, J. M. CCC-N-heterocyclic carbene pincer complexes: Synthesis, characterization and hydroamination activity of a hafnium complex. *J. Organomet. Chem.* **2012**, *696*, 373-377.
10. Danopoulos, A. A.; Wright, J. A.; Motherwell, W. B.; Ellwood, S. N-Heterocyclic "Pincer" Dicarbene Complexes of Cobalt(I), Cobalt(II), and Cobalt(III). *Organometallics* **2014**, *23*, 4807-4810.
11. Bürger, H.; Wannagat, U. Silylamido-Derivate von Eisen und Kobalt. *Monatsh. Chem.* **1963**, *94*, 1007-1012.
12. Eichhöfer, A.; Lan, Y.; Mereacre, V.; Bodenstein, T.; Weigend, F. Slow Magnetic Relaxation in Trigonal-Planar Mononuclear Fe(II) and Co(II) Bis(trimethylsilyl)amido Complexes-A Comparative Study. *Inorg. Chem.* **2014**, *53*, 1962-1974.

13. Panda, A.; Stender, M.; Olmstead, M. M.; Klavins, P.; Power, P. P. Reactions of M{N($SiMe_3$)}$_2$ (M = Mn, Fe, or Co) with pyridine and 4,4'-bipyridyl: structural and magnetic studies. *Polyhedron* **2003**, *22*, 67-73.
14. Ibrahim, A. D.; Tokmic, K.; Brennan, M. B.; Kim, D. Matson, E. M.; Nilges, M. J.; Bertke, J. A.; Fout, A. R. Monoanionic bis(carbene) pincer complexes featuring cobalt(I-III) oxidation states. *Dalton Trans.* **2016**, *45*, 9805-9811.
15. Xi, Z.; Liu, B.; Lu, C.; Chen, W. Cobalt(III) complexes bearing bidentate, tridentate, and tetradentate N-heterocyclic carbene: synthesis, X-ray structures and catalytic activities. *Dalton Trans.* **2009**, 7008– 7014.
16. Scepaniak, J. j.; Margarit, C. G.; Bontchev, R. P.; Smith, J. M. Cobalt azide complexes with a tris(carbene)borate ligand scaffold. Acta Cryst. **2013**, *C69*, 968–971.
17. Hosokawa, S.; Ito, J.; Nishiyama, H. NCN-Pincer Cobalt Complexes Containing Bis(oxazolinyl)phenyl Ligands. *Organometallics* **2013,** *32*, 3980-3985.
18. Murugesan, S.; Stöger, B.; Carvalhos, M. D.; Ferreira, L. P.; Pittenauer, E.; Allmaier, G.; Veiros, L. F.; Kirchner, K. Synthesis and Reactivity of Four- and Five-Coordinate Low Spin Cobalt(II) PCP Pincer Complexes and Nickel(II) Analogues. *Organometallics* **2014**, *33*, 6132-6140.
19. Zheng, T.; Sun, H. Dichlorido[2,3,5,6-tetrafluoro-4-(trifluoromethyl)phenyl-kC1] bis(trimethylphosphine-kP)cobalt(III). *Acta Cryst.* **2010**, *E66*, m574.
20. Robitzer, M.; Bouamaïed, I.; Sirlin, C.; Chase, P. A.; Koten, G. V.; Pfeffer, M. Transmetalation of Aryl Units from Gold(I) to Cobalt(III): A Clean Route to the Synthesis of Anion Cobaltoreceptors. *Organometallics* **2005**, *24*, 1756-1761.
21. Van der Zeijden, A. A. H.; Van Koten, G. Monoarylcobalt(II) compounds stabilized by bis ortho chelation. *Inorg. Chem.* **1986**, *25*, 4723-4725.
22. Zhu, G.; Li, X.; Xu, G.; Wang, L.; Sun, H. A new PC(Sp^3)P ligand and its coordination chemistry with low-valent iron, cobalt and nickel complexes. *Dalton Trans.* **2014**, *43*, 8595-8598.
23. Hebden, T. J.; St. John, A.; Gusev, D. G.; Kaminsky, W.; Goldberg, K.; Heinekey, D. M. Preparation of Dihydrogen Complex of Cobalt. *Angew. Chem.* **2011**, *123*, 1913-1916.
24. Kent, M. A.; Woodall, C. H.; Haddow, M. F.; McMullin, C. L.; Pringle, P. G.; Wass, D. F. Cobalt PCP Pincer Complexes via an Unexpected Sequence of Ortho Metalations. *Organometallics* **2014**, *33*, 5686-5692.
25. Murugesan, S.; Stöger, B.;Weil, M.; Veiros, L. F.; Kirchner, K. Synthesis, Structure, and Reactivity of Co(II) and Ni(I) PCP Pincer Borohydride Complexes. *Organometallics* **2015**, *34*, 1364-1372.

26. Reily, S. W.; Webster, C. E.; Hollis, T. K.; Valle, H. U. Transmetallation from CCC-NHC pincer Zr complexes in the synthesis of air-stable CCC-NHC pincer Co(III) complexes and initial hydroboration trials. *Dalton Trans.* **2016**, *45*, 2823-2828.
27. Morton, J. R.; Preston, K. F.; Page, Y. L.; Krusic, P. J. Electron paramagnetic resonance spectra of the $Fe_2(CO)^-$ radical trapped in single crystals of $PPN^+FeCo(CO)^-$. *J. Chem. Soc., Faraday Trans 1.* **1989**, *85*, 4019-4030.
28. Addison, A. W.; Rao, T. N.; Reedijk, J.; Van Rijn, J.; Verschoor, G. C. Synthesis, structure, and spectroscopic properties of copper(II) compounds containing nitrogen–sulphur donor ligands; the crystal and molecular structure of aqua[1,7-bis(N-methylbenzimidazol-2'-yl)-2,6-dithiaheptane]copper(II) perchlorate. *J. Chem. Soc., Dalton Trans.* **1986**, 1349-1356.
29. Allen, F. H. The Cambridge Structural Database: a quarter of a million crystal structures and rising. *Acta Cryst.* **2002**, *B58*, 380-388.
30. Theopold, K. H.; Silvestre, J.; Byrne, E. K.; Richeson, D. S. Homoleptic mesityl complexes of cobalt(II). Synthesis, crystal structure, and theoretical description of bis(.mu.-mesityl)dimesityldicobalt. *Organometallics* **1989**, *8*, 2001-2009.
31. Li, J.; Li, X.; Wang, Q.; Sun, H. C-Cl bond activation and catalytic hydrodechlorination of hexachlorobenzene by cobalt and nickel complexes with sodium formate as a reducing agent. *Dalton Trans.* **2014**, *43*, 6660-6666.
32. Fout, A. R.; Basuli, F.; Fan, H.; Tomaszewski, J.; Huffman, J. C.; Baik, M.-H.; Mindiola, D. J. A Co_2N_2 Diamond-Core Resting State of Cobalt(I): a Three-Coordinate Co^I Synthon Invoking an Unusual Pincer-Type Rearrangement. *Angew. Chem. Int. Ed.* **2006**, *45*, 3291-3295.
33. Betley, T. a.; Peters, J. C. Dinitrogen Chemistry from Trigonally Coordinated Iron and Cobalt Platforms. *J. Am. Chem. Soc.* **2003**, *125*, 10782-1783.
34. Ding, K.; Pierpont, A. W.; Brennessel, W. W.; Lukat-Rodgers, G.; Rodgers, K. R.; Cundari, T. R.; Bill, E.; Holland, P. L. Cobalt-Dinitrogen Complexes with Weakened N-N Bonds. *J. Am. Chem. Soc.* **2009**, *131*, 9471-9472.
35. Fernández, P.; Sousa-Pedrares, A.; Romero, J.; Durán, M. L.; Sousa, A.; Pérez-Lourido, P.; García-Vázquez, J. A. Synthesis and Structural Characterization of Cobalt, Nickel and Copper Phosphanylthiolato Complexes. *Eur. J. Inorg. Chem.* **2010**, *2010*, 814-823.
36. Suess, D. L. M.; Peters, J. C. H-H and Si Bond Addition to $F{\equiv}NNR_2$ Intermediates Derived from N_2. *J. Am. Chem. Soc.* **2013**, *135*, 4938-4941.

37. Carpenter, A. E.; Margulieux, G. W.; Millard, M. D.; Moore, C. E.; Weidemann, N.; Rheingold, A. L.; Figueroa, J. S. Zwitterionic Stabilization of a Reactive Cobalt Tris-Isocyanide Monoanion by Cation Coordination. *Angew. Chem. Int. Ed.* **2012**, *51*, 9412-9416.
38. Bianchini, C.; Peruzzini, M.; Zanobini, F. Solid-State Organometallic Chemistry of Tripodal (polyphosphine)metal Complexes. Carbon-Hydrogen Activation Reactions at Cobalt(I) Encapsulated into the Tetraphosphine $P(CH_2CH_2PPh_2)_3$. *Organometallics* **1991**, *10*, 3415-3417.
39. Whited, M. T.; Mankad, N. P.; Lee, Y.; Oblad, P. F.; Peters, J. C. Dinitrogen Complexes Supported by tris(phosphino)silyl Ligands. *Inorg. Chem.* **2009**, *48*, 2507-2517.
40. Davis, B. Y. B. R.; Payne, N. C.; Ibers, J. A. The Bonding of Molecular Nitrogen. I. The Crystal and Molecular Structure of Hydridodinitrogentris(triphenylphosphine) cobalt (I) *Inorg. Chem.* **1969**, *8*, 2719-2728.
41. Suess, D. L. M.; Tsay, C.; Peters, J. C. Dihydrogen Binding to Isostructural S = ½ and S = 0 Cobalt Complexes. *J. Am. Chem. Soc.* **2012**, *134*, 14158-14164.
42. Del Castillo, T. J.; Thompson, N. B.; Suess, D. L. M.; Ung, G.; Peters, J. C. Evaluating Molecular Cobalt Complexes for the Conversion of N_2 to NH_3. *Inorg. Chem.* **2015**, *54*, 9256-9262.
43. Nesbit, M. A.; Suess, D. L. M.; Peters, J. C. E-H Bond Activation and Hydrosilylation Catalysis with Iron and Cobalt Metalloboranes. *Organometallics* **2015**, *34*, 4741-4752.
44. Tolman, C. A. Steric effects of phosphorus ligands in organometallic chemistry and homogeneous catalysis. *Chem. Rev.* **1977**, *77*, 313—348.
45. Guard, L. M.; Hebden, T. J.; Linn, D. E.; Heinekey, D. M. Pincer-Supported Carbonyl Complexes of Cobalt(I). *Organometallics* **2017**, *36*, 3104-3109.
46. Pangborn, A.B.; Giardello, M.A.; Grubbs, R. H.; Rosen, R. K.; Timmers, F. J. Safe and Convenient Procedure for Solvent Purification. *Organometallics*, **1996**, *15*, 1518−1520.
47. D. R. Coulson, L. C. Satek and S. O. Grim, *Inorg. Synth.*, 1972, **13**, 121-123.
48. M. J. Nilges, K. Matteson and R. L. Belford, SIMPOW6: a software package for simulation of ESP powder-type spectra.
49. In *ESR Spectroscopy in Membrane Biophysics, Biological Magentic Resonance;* M. A. Hemmings and L. Berlinger, Eds; Springer, New York, 2007.

CHAPTER 3: SYNTHESIS, CHARACTERIZATION, AND REACTVITY OF A WELL-DEFINED COBALT(I) DIHYDROGEN CATALYST: EXPERIMENTAL EVIDENCE FOR A COBALT(I)/COBALT(III) REODOX PROCESS IN OLEFIN HYDROGENATION[†]

3.1 Introduction

Catalytic homogeneous hydrogenation is one of the most atom economical methods employed for the transformation of organic substrates. The abundant use of late second- and third-row transition metal systems in these reactions reflects the high activity, selectivity, and overall function conferred.[1] Detailed mechanistic studies elucidating oxidation state changes at the metal centers over the course of catalysis, as well as the nature of H_2 interaction and substrate binding, have enabled improvements to be made to these catalytic systems.[2]

More recently, there has been a wide interest in employing more sustainable first-row transition metal complexes in the hydrogenation of olefins. Work by Budzelaar,[3] Chirik,[4,5] Hanson,[6-8] and Peters[9,10] in this area clearly demonstrates the potential of ligand-assisted cobalt-based systems as hydrogenation catalysts. However, catalytic complexes featuring exclusively metal-centered reactivity with cobalt are rare.[11,12] As such, a detailed mechanistic study of such systems is necessary. Nonclassical transition-metal dihydride complexes, including those consisting of iron[13-15] and nickel,[16-18] are probable intermediates in a variety of catalytic H_2-producing and -consuming reactions, but further investigations are needed.[19-22]

Due to the inherent thermal instability of Co-(H_2) complexes, few can be studied in catalytic transformations. A recent example by the Peters group features a Co-(H_2) complex characterized by X-ray crystallography, and the thermal stability of the complex permitted equilibrium binding studies of the dihydrogen ligand.[23] Other Co-(H_2) complexes have been reported, but in these cases the thermal instability only allowed for *in situ* characterization at low temperature.[24-26] Interestingly, none of the reported Co-(H_2) complexes have proven to be effective catalysts. In fact, the only evidence of a Co-(H_2) complex directly involved in catalysis was reported in a computational study of the $Co_2(CO)_8$-catalyzed oxo process developed by Ziegler and co-workers,[27,28] as well as in NMR studies of phosphine derivatives of cobalt-hydroformylation catalysts employing *para*hydrogen (p-H_2) induced polarization (PHIP) transfer.[29,30]

[†] Portions of this chapter are reproduced from the following publications with permission from the authors. Tokmic, K.; Markus, C. R.; Zhu, L.; Fout, A. R. Well-Defined Cobalt(I) Dihydrogen Catalyst: Experimental Evidence for a Co(I)/Co(III) Redox Process in Olefin Hydrogenation. *J. Am. Chem. Soc.* **2016**, *138*, 11907-11913.

We recently reported a series of cobalt pincer complexes featuring electron-rich monoanionic bis(carbene) ligands, ^{Mes}CCC and ^{DIPP}CCC (^{Mes}CCC = bis(mesityl-benzimidazol-2-ylidene)phenyl and ^{DIPP}CCC = bis(diisopropylphenyl-benzimidazol-2-ylidene)phenyl).[31] Cleavage of the strong aryl C−H bond was achieved in a one-pot metalation procedure to afford the Co(III) complexes, whereby reduction of these species with the appropriate equivalents of reductant afforded the Co(II) and Co(I) complexes. Interested in further exploring low-valent cobalt catalysts to be employed in Co(I)/Co(III) catalysis,[32] the reactivity of our Co(I)-(N_2) complex, **(^{Mes}CCC)Co(N_2)(PPh_3)**, to effect two-electron chemistry with dihydrogen was investigated. In doing so, we synthesized a Co(I)-(H_2) complex that is catalytically active toward the hydrogenation of olefins under ambient conditions and have successfully identified various intermediates within the catalytic cycle using both multinuclear and PHIP transfer NMR studies. These studies provide compelling evidence for a Co(I)/Co(III) redox process in the catalytic cycle.

3.2 Synthesis and characterization of (^{Mes}CCC)Co(H_2)(PPh_3)

The addition of H_2 (4 atm) to **(^{Mes}CCC)Co(N_2)(PPh_3)** at room temperature in toluene-d_8 resulted in an immediate color change from dark red to red-orange (Scheme 3.1). The ^{1}H NMR spectrum of the resulting species in toluene-d_8 revealed a new diamagnetic product (Figure 3.1). A shift of the three mesityl methyl resonances from 2.03, 1.92, and 1.62 ppm to 2.14, 1.82, and 1.30 ppm was observed and is consistent with a C_s-symmetric complex in solution. An additional broad resonance at −5.56 ppm corresponding to 2H confirmed the addition of dihydrogen to yield **(^{Mes}CCC)Co(H_2)(PPh_3)**. Subsequent exposure of **(^{Mes}CCC)Co(H_2)(PPh_3)** to 1 atm of N_2 resulted in a color change back to dark red, indicating the formation of **(^{Mes}CCC)Co(N_2)(PPh_3)** (Scheme 3.1), which was verified by ^{1}H NMR spectroscopy.

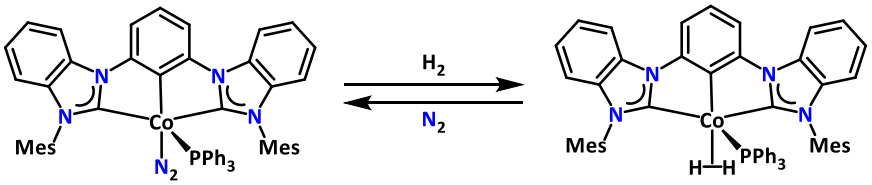

(^{Mes}CCC)Co(N_2)(PPh_3) (^{Mes}CCC)Co(H_2)(PPh_3)

Scheme 3.1 Synthesis of **(^{Mes}CCC)Co(H_2)(PPh_3)** from **(^{Mes}CCC)Co(N_2)(PPh_3)**.

To support the assignment of the resonance at −5.56 ppm as the added dihydrogen, the deuterium analogue of **(^{Mes}CCC)Co(H_2)(PPh_3)** was prepared. Exposure of **(^{Mes}CCC)Co(N_2)(PPh_3)** to 4 atm of D_2 in toluene-d_8 resulted in the formation of a red-orange diamagnetic species with identical pincer ligand resonances to those of **(^{Mes}CCC)Co(H_2)(PPh_3)**, as determined by ^{1}H NMR spectroscopy (Figure 3.1). Moreover, the absence of a broadened upfield resonance around −5.56 ppm in the ^{1}H NMR spectrum and observation of the corresponding resonance at −5.66 ppm in the ^{2}H NMR spectrum (Figure 3.2) confirmed

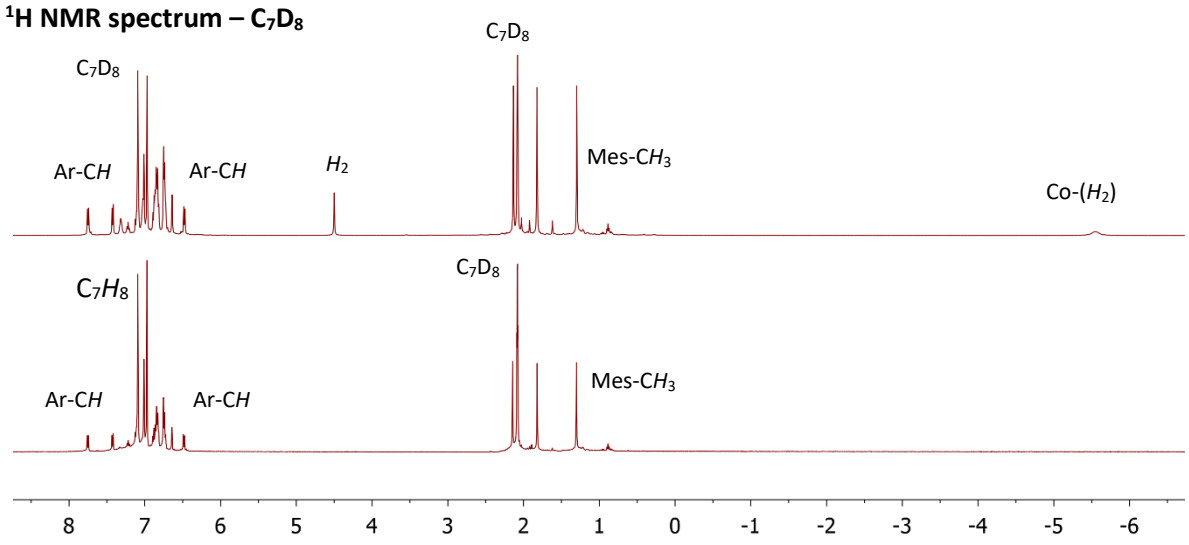

Figure 3.1 ^{1}H NMR spectrum of **(^{Mes}CCC)Co(H_2)(PPh_3)** (top) and **(^{Mes}CCC)Co(D_2)(PPh_3)** (bottom).

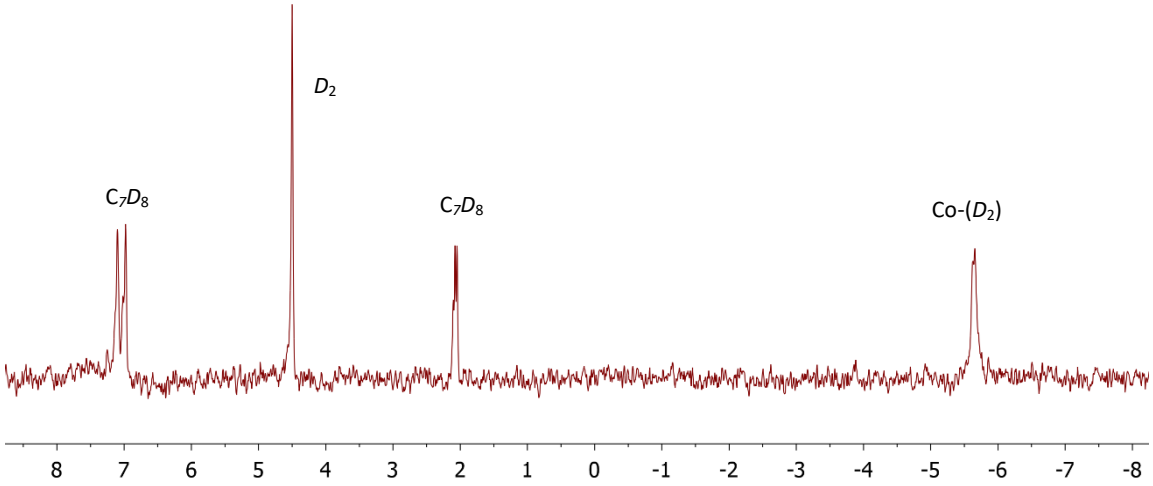

Figure 3.2 ^{2}H NMR spectrum of **(^{Mes}CCC)Co(D_2)(PPh_3)**.

that the dihydrogen gas was the source of this signal. Monitoring this solution over several days by ^{2}H NMR spectroscopy demonstrated that there was no incorporation of deuterium into the pincer ligand framework.

Given the facile and reversible nature of **(^{Mes}CCC)Co(H_2)(PPh_3)** and **(^{Mes}CCC)Co(N_2)(PPh_3)** formation, the possibility that **(^{Mes}CCC)Co(H_2)(PPh_3)** was a nonclassical dihydrogen complex instead of a Co(III)-dihydride was considered. In order to determine the binding mode of H_2, T_1 relaxation studies on **(^{Mes}CCC)Co(H_2)(PPh_3)** were performed. A T_1 study of the resonance at −5.56 ppm in a toluene-d_8 solution of **(^{Mes}CCC)Co(H_2)(PPh_3)** from 203 to 343 K (Figure 3.3) gave the lowest T_1(min) value of 12 ms (253 to 313 K), supporting the formation of a nonclassical cobalt dihydride complex in solution, **(^{Mes}CCC)Co(H_2)(PPh_3)**.

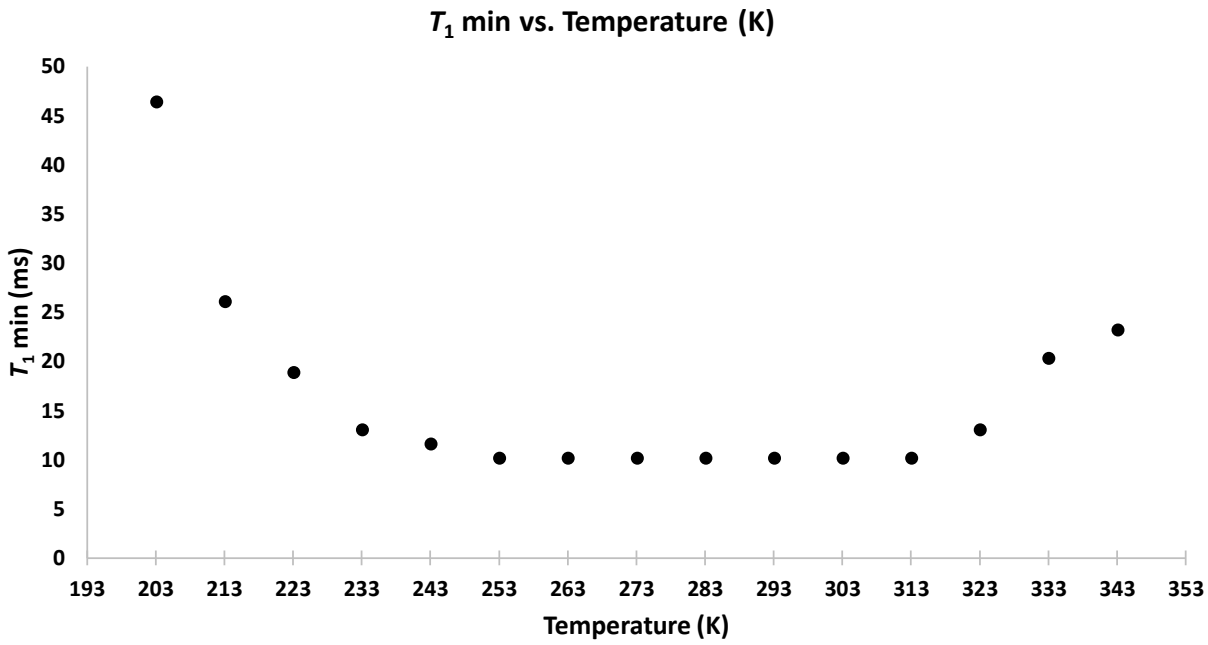

Figure 3.3 Plot of T_1 as a function of temperature (K) for **(^{Mes}CCC)Co(H_2)(PPh_3)**.

The T_1(min) value is consistent with other Co-(H_2) complexes reported in the literature.[23,24] Although this data is consistent with a nonclassical bonding of H_2, Halpern and coworkers[33] reported that differentiating classical and nonclassical bonding of H_2 using the "T_1 criterion" requires a consideration of other NMR active nuclei. The high gyromagnetic ratio of ^{59}Co as well as the additional PPh_3 ligand in our complexes would naturally contribute to the relaxation rate of the bound H_2 ligand. Heinekey and co-workers have demonstrated upon a reinvestigation[34,35] that cationic nonclassical Co-(H_2) complexes[36,37] were more appropriately described as highly dynamic octahedral classical Co-$(H)_2$ molecules. They cited the absence of HD coupling and higher T_1 (min) measurements as a key part in their formulation.

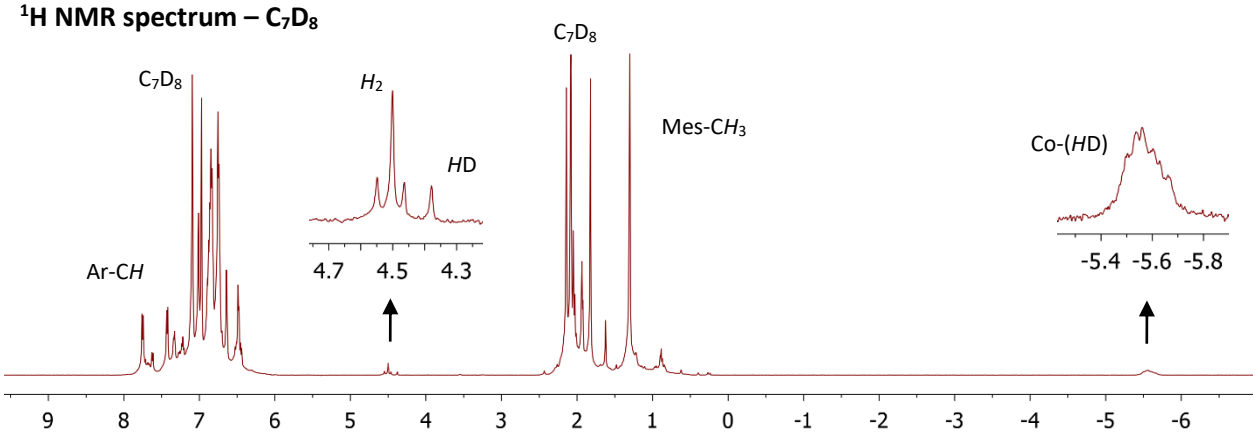

Figure 3.4 ^{1}H NMR spectrum of **(^{Mes}CCC)Co(HD)(PPh_3)**.

In order to further understand the extent of H_2 coordination and activation, **(^{Mes}CCC)Co(N_2)(PPh_3)** was reacted with HD gas. The resulting ^{1}H NMR spectrum of **(^{Mes}CCC)Co(HD)(PPh_3)** in toluene-d_8 displayed two sets of triplets at −5.56 and −5.60 ppm with a J_{HD} coupling constant of 33 Hz each (Figure 3.4). On the basis of previously reported correlations between J_{HD} and r_{HH} values by Morris,[38] the coupling constant corresponds to a r_{HH} of 0.87 Å, which is slightly shorter than other reported cobalt dihydrogen complexes (r_{HH} = 0.95[24] and 0.92[23] Å) and is consistent with a nonclassical binding mode of H_2 (d_{HH} of H_2 = 0.74 Å). Interestingly, the formation of free H_2 gas (4.50 ppm) was also observed in the ^{1}H NMR spectrum (Figure 3.4), suggestive of HD scrambling.

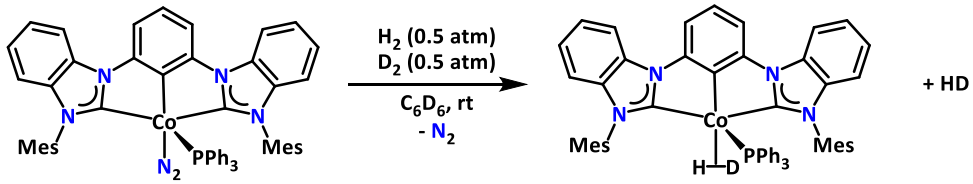

(^{Mes}CCC)Co(N_2)(PPh_3) (^{Mes}CCC)Co(HD)(PPh_3)

Scheme 3.2 Synthesis of **(^{Mes}CCC)Co(HD)(PPh_3)** from **(^{Mes}CCC)Co(N_2)(PPh_3)** and a 1:1 mixture of H_2/D_2.

HD scrambling was probed further by adding a mixture of H_2 and D_2 (0.5 atm each) at 77 K to a degassed benzene-d_6 solution of **(^{Mes}CCC)Co(N_2)(PPh_3)** (Scheme 3.2). Within 10 min of warming to ambient temperature, the resulting ^{1}H NMR spectrum was consistent with the formation of **(^{Mes}CCC)Co(HD)(PPh_3)**, and, in addition, revealed a new triplet at 4.43 ppm (J_{HD} = 43 Hz), corresponding to the formation of HD gas as well as the expected singlet at 4.47 ppm for H_2 gas (Figure 3.5). This result indicates that **(^{Mes}CCC)Co(N_2)(PPh_3)** is capable of facilitating H_2/D_2 exchange, a process that is rare with cobalt,[23,39] and may be mediated by a transient Co(III)-dihydrogen/dihydride species (Figure 3.6). However, Lewis acidic H_2 activation and deprotonation by exogenous base could not be ruled out as pathways for this scrambling process.[40]

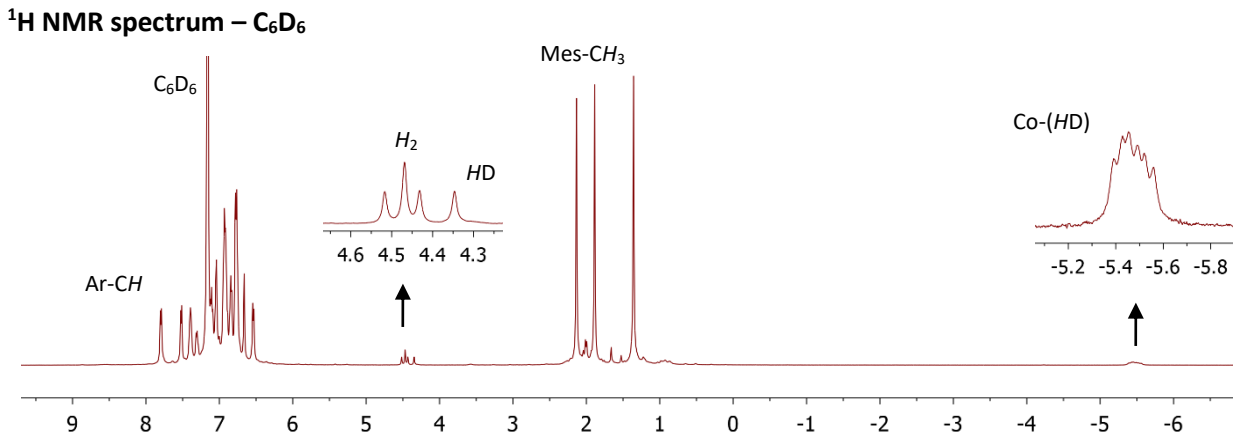

Figure 3.5 ^{1}H NMR spectrum of **(^{Mes}CCC)Co(HD)(PPh_3)**.

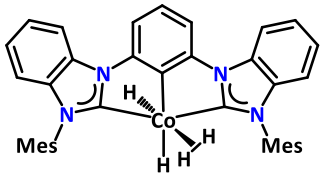

(^{Mes}CCC)Co(H_2)($H)_2$

proposed intermediate

Figure 3.6 Proposed intermediate facilitating H_2/D_2 exchange.

Interested in understanding if the H−H bond was amenable to cleavage, a solution of **(^{Mes}CCC)Co(H_2)(PPh_3)** in toluene-d_8 was monitored by variable temperature ^{1}H NMR spectroscopy from −80 to 80 °C (Figures 3.15 to 3.18). No changes suggesting H−H bond cleavage were observed in the ^{1}H NMR spectrum. Likewise, the dissociation of PPh_3 was not observed in either the ^{31}P or ^{1}H NMR spectrum over this temperature range.

3.3 Synthesis and characterization of (^{Mes}CCC)Co(N_2)(PMe_3)

These results prompted us to understand the role of the PPh_3 in H_2 binding and activation, and therefore, the substitution by a more basic phosphine, PMe_3, was targeted. Reduction of **(^{Mes}CCC)CoCl_2py**[31] with KC_8 in the presence of PMe_3 cleanly afforded **(^{Mes}CCC)Co(N_2)(PMe_3)** in 77% yield (Scheme 3.3). The mesityl methyl resonances of **(^{Mes}CCC)Co(N_2)(PMe_3)** at 2.10, 2.09, and 2.02 ppm in the

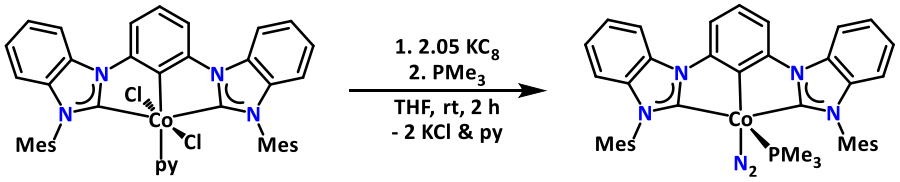

77%

(^{Mes}CCC)CoCl_2py (^{Mes}CCC)Co(N_2)(PMe_3)

Scheme 3.3 Synthesis of **(^{Mes}CCC)Co(N_2)(PMe_3)**.

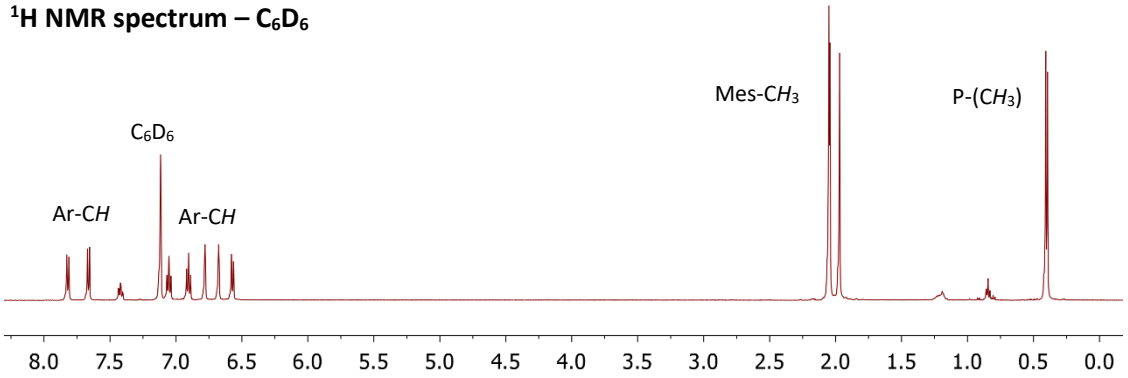

Figure 3.7 ^{1}H NMR spectrum of **(^{Mes}CCC)Co(N_2)(PMe_3)**.

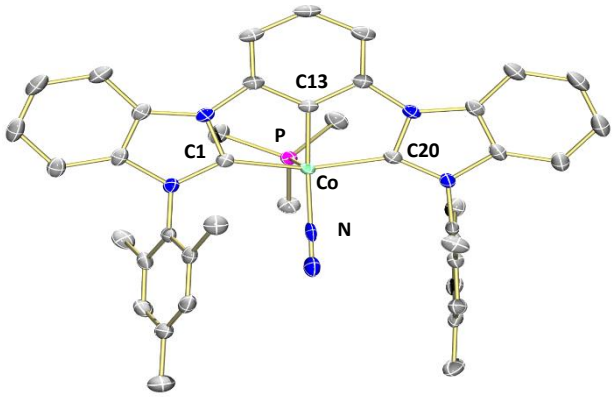

Figure 3.8 Molecular structure of **(^{Mes}CCC)Co(N$_2$)(PMe$_3$)** shown with 50% probability ellipsoids. H atoms have been omitted for clarity.

^{1}H NMR spectrum established a C_s coordination environment about the metal center and are slightly shifted downfield from that of **(^{Mes}CCC)Co(N$_2$)(PPh$_3$)** (Figure 3.7).

X-ray crystallographic characterization (Figure 3.8 and Tables 3.3 and 3.4) further established the connectivity of this square pyramidal ($\tau = 0.16$)[41] Co(I) species. The two Co–C_{NHC} bond lengths of 1.9033(19) and 1.9079(19) Å and the Co–C_{aryl} bond length of 1.8734(19) Å are comparable to those in **(^{Mes}CCC)Co(N$_2$)(PPh$_3$)**.[31] Similarly, the N_2 bond distance of 1.022(2) Å and an IR stretch (2114 cm^{-1}) remain largely unactivated from free N_2 akin to that observed in **(^{Mes}CCC)Co(N$_2$)(PPh$_3$)**.[31]

3.4 Reactivity of (^{Mes}CCC)Co(N$_2$)(PMe$_3$) toward H$_2$

In the presence of a more electron-donating phosphine, it was hypothesized that the H–H bond may be more activated. The addition of H_2 (4 atm) to a degassed benzene-d_6 solution of **(^{Mes}CCC)Co(N$_2$)(PMe$_3$)** resulted in the observation of a new species, **(^{Mes}CCC)Co(H$_2$)(PMe$_3$)**, by ^{1}H NMR spectroscopy, while 40% of the starting compound **(^{Mes}CCC)Co(N$_2$)(PMe$_3$)** remained unreacted. The mesityl methyl resonances are shifted slightly upfield to 2.02, 1.97, and 1.96 ppm, consistent with C_s-symmetry in solution. Similar to **(^{Mes}CCC)Co(H$_2$)(PPh$_3$)**, a low T_1 (min) value of 14 ms was observed for this resonance at 298 K, confirming

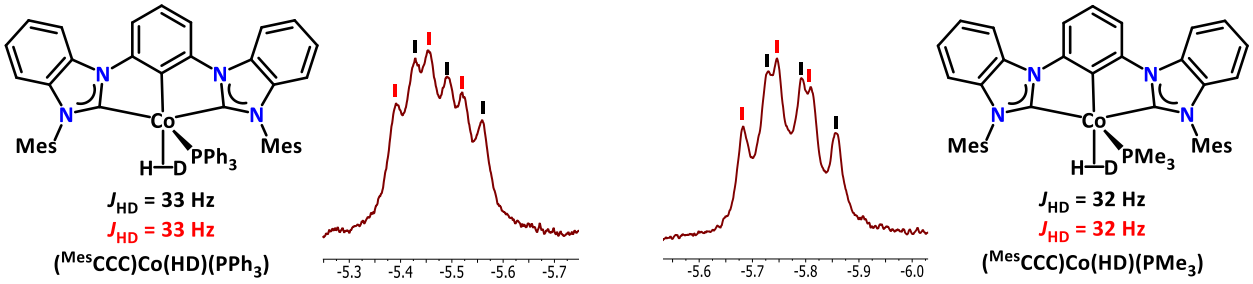

Figure 3.9 Truncated ^{1}H NMR spectrum showing the upfield region of **(^{Mes}CCC)Co(HD)(PPh$_3$)** (left) and **(^{Mes}CCC)Co(H$_2$)(PMe$_3$)** (right).

σ-bound H_2 formulation, **(^{Mes}CCC)Co(H_2)(PMe_3)**. A J_{HD} coupling constant of 32 Hz, obtained from treating **(^{Mes}CCC)Co(N_2)(PMe_3)** with a mixture of H_2 and D_2 (0.5 atm each) at 77 K, correlated[38] to an r_{HH} of 0.89 Å, demonstrating that the use of the more basic PMe_3 resulted in only a marginal elongation of the H−H bond (from 0.87 Å in **(^{Mes}CCC)Co(H_2)(PPh_3)** (Figure 3.9). In comparison to **(^{Mes}CCC)Co(H_2)(PPh_3)**, however, where the conversion to product was essentially quantitative, the use of the more electron-rich phosphine resulted in a lower conversion to **(^{Mes}CCC)Co(H_2)(PMe_3)**, indicating that H_2/N_2 exchange is slower or less favorable in the presence of the more basic phosphine.

3.5 Olefin hydrogenation with the Co(I)-(N_2) complexes

Given the ability of the Co(I)-(N_2) complexes to facilitate the scrambling of H_2/D_2 by accessing higher oxidation states, the competency of the Co(I)-(H_2) complexes toward catalytic hydrogenation of olefins was probed, as transition metal dihydrogen complexes are often considered as transient intermediates in many catalytic hydrogenation reactions. In an effort to understand if **(^{Mes}CCC)Co(H_2)(PPh_3)** is catalytically relevant to the hydrogenation of olefins, a degassed benzene solution of **(^{Mes}CCC)Co(N_2)(PPh_3)** was exposed to H_2 (1 atm) for 10 min to generate **(^{Mes}CCC)Co(H_2)(PPh_3)** *in situ*. To this solution was added 50 equiv of styrene, and within 2 h at room temperature, the full conversion of styrene to ethylbenzene was observed by GC−MS. Additionally, ^{1}H and ^{13}C NMR spectroscopy was used to monitor the hydrogenation studies. Upon addition of 4 atm of H_2 to a degassed benzene-d_6 solution of **(^{Mes}CCC)Co(H_2)(PPh_3)** or **(^{Mes}CCC)Co(H_2)(PMe_3)** (2 mol%) and styrene in a J. Young NMR tube, the color of both of the mixtures changed from dark red to red-orange. Complete conversion to ethylbenzene was readily achieved with **(^{Mes}CCC)Co(N_2)(PPh_3)** (Table 3.1, entry 1), while unsurprisingly **(^{Mes}CCC)Co(N_2)(PMe_3)** was not as active for the hydrogenation of styrene. Only 30% conversion was obtained when using **(^{Mes}CCC)Co(N_2)(PMe_3)**, likely the result of the lack of formation of **(^{Mes}CCC)Co(H_2)(PMe_3)** and phosphine-olefin exchange throughout catalysis (Table 3.1, entry 2). In the case of **(^{Mes}CCC)Co(N_2)(PPh_3)**, **(^{Mes}CCC)Co(H_2)(PPh_3)** was observed upon the completion of the reaction, indicating **(^{Mes}CCC)Co(H_2)(PPh_3)** is the resting state of the catalytic process. This represents the first example of a well-defined homogeneous cobalt dihydrogen complex that has been demonstrated to be an effective hydrogenation catalyst.

To better understand the nature of this catalysis, elemental mercury was added to a catalytic run, and no change in reactivity was observed indicating that this process is homogeneous[42] (Table 3.1, entry 3). The use a cobalt(III) derivative, **(^{Mes}CCC)CoCl$_2$py**, did not yield any hydrogenation activity (Table 3.1, entry 4). Furthermore, the role of PPh_3 in catalysis was probed, as dissociation of PPh_3 is likely to occur given the electronic saturation of **(^{Mes}CCC)Co(N_2)(PPh_3)** and **(^{Mes}CCC)Co(H_2)(PPh_3)**. To this end, the role of PPh_3

Table 3.1 Hydrogenation of styrene and control experiments.

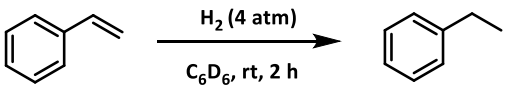

Entry	Additive	conversion[a]
1	(^{Mes}CCC)Co(N_2)(PPh_3) (2 mol%)	>99%
2	(^{Mes}CCC)Co(N_2)(PMe_3) (2 mol%)	30%
3	(^{Mes}CCC)Co(N_2)(PPh_3) (2 mol%) + Hg	>99%
4	(^{Mes}CCC)CoCl_2py (2 mol%)	0%
5	(^{Mes}CCC)Co(N_2)(PPh_3) (2 mol%) + PPh_3 (10 mol%)	50%
6	(^{Mes}CCC)Co(N_2)(PPh_3) (2 mol%) + PPh_3 (25 mol%)	12%
7	(^{Mes}CCC)Co(N_2)(PPh_3) (2 mol%) + PPh_3 (50 mol%)	6%

[a]Conversion was monitored by ^{1}H NMR using mesitylene as an internal standard.

in the catalytic reaction was examined. The addition of 5 mol equiv of PPh_3 with respect to **(^{Mes}CCC)Co(N_2)(PPh_3)** resulted in a diminished conversion of styrene to ethylbenzene (50%) after 2 h at room temperature (Table 3.1, entry 5). Furthermore, the addition of 12.5 and 25 mol equiv of PPh_3 led to 12% and 6% conversion to ethylbenzene, respectively, as determined by ^{1}H NMR spectroscopy (Table 3.1, entries 6 and 7). This diminished conversion is consistent with dissociation of PPh_3 during catalysis.

Encouraged by the ability of **(^{Mes}CCC)Co(H_2)(PPh_3)** to effectively hydrogenate styrene, the substrate scope was expanded to include more sterically hindered olefins. Under catalytic conditions (2 mol % catalyst, 4 atm of H_2 in benzene-d_6 at room temperature) a variety of olefins bearing different functional groups were successfully hydrogenated (Table 3.2, Figures 3.19 to 3.29). The cobalt(I) system readily reduces inactivated terminal olefins such 1-octene, albeit taking longer to reach full conversion than styrene (Table 3.1, entry 1). Furthermore, functionalities such as hydroxyl groups, ketones, anhydrides, and aldehydes did not inhibit catalytic activity and were not reduced (Table 3.2, entries 2-4 and 9). Additionally, 4-vinyl pyridine did not inhibit the catalysis and reached full conversion within 2 h (Table 3.2, entry 5). Interestingly, the hydrogenation of cyclohexene did not proceed well at room temperature, but upon heating to 60 °C, complete conversion to cyclohexane was achieved (Table 3.2, entry 8). Selectivity toward terminal alkenes over internal alkenes was established with 4-vinylcyclohexene. At room

temperature the terminal alkene was reduced, and upon heating to 60 °C, the reduction of the internal C=C bond was achieved (Table 3.2, entry 7).

Table 3.2 Olefin hydrogenation substrate scope.

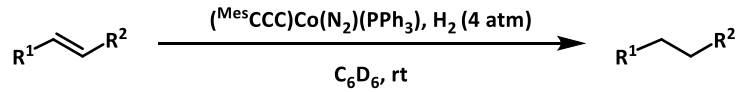

Entry	Substrate	Product	Conversion[a]	Time
1	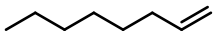	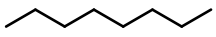	>99%	3 h
2	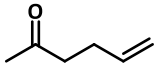	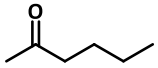	>99%	2 h
3	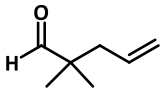	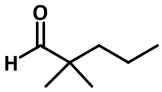	>99%	22 h
4	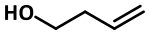	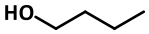	>99%	2 h
5	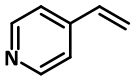	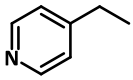	>99%	2 h
6	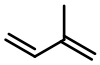		>99%	21 h
7[b]	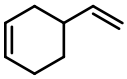	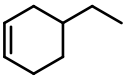	>99%	2 h
8[c]			>99%	22 h
9[c]	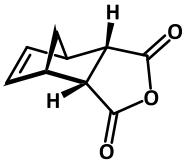	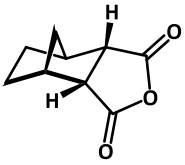	>99%	17 h

[a]Conversion was monitored by H NMR spectroscopy. [b]Alkane product obtained after heating to 60°C for 19h. [c]Reaction was heated to 60°C.

3.6 Mechanistic studies using *para*hydrogen induced polarization

Having established that the reactivity of **(^{Mes}CCC)Co(N_2)(PPh_3)** with H_2 results in an arrested intermediate **(^{Mes}CCC)Co(H_2)(PPh_3)** in the oxidative addition of H_2 rather than a formal oxidation state change by the metal center and reasoning that catalytic activity of these cobalt complexes likely proceeds

through more than one oxidation state, further mechanistic studies were performed to understand the catalytic nature of the cobalt(I) species in the hydrogenation of olefins.

Toward this end, *para*hydrogen (*p*-H_2) was generated,[43] and *para*hydrogen induced polarization (PHIP) NMR spectroscopy was performed to identify reaction intermediates. The use of PHIP NMR spectroscopy has successfully allowed for the detection of organometallic reaction intermediates, especially those employed in hydrogenation reactions, which normally would have been "invisible" toward characterization by conventional methods.[44-46] The PHIP NMR data acquired was obtained by using a 45° pulse and with the use of a double quantum OPSY (only parahydrogen spectroscopy)[47] filter in the ^{1}H NMR spectrum following introduction of *p*-H_2 at low field (following ALTADENA[48] conditions).

The addition of *p*-H_2 (4 atm) to a solution of **(^{Mes}CCC)Co(N_2)(PPh_3)** in benzene-d_6 resulted in an identical ^{1}H NMR spectrum to that of **(^{Mes}CCC)Co(H_2)(PPh_3)**; no polarization of any signals was detected. If polarization did occur, then it would provide direct evidence that the H-H bond is broken and oxidative addition on the metal center has occurred; however, since that is not the case, these results further support our initial formulation, in which **(^{Mes}CCC)Co(H_2)(PPh_3)** is best described as a dihydrogen complex (Figure 3.10).

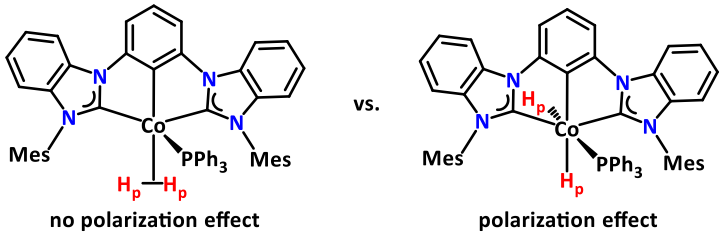

no polarization effect polarization effect

Figure 3.10 Expected PHIP effect of **(^{Mes}CCC)Co(H_2)(PPh_3)** (left) and the oxidative addition product **(^{Mes}CCC)Co(H)$_2$(PPh_3)** (right).

The PHIP studies under catalytic conditions were explored next to probe the mechanism of observed catalysis. Upon the addition of *p*-H_2 (4 atm) to a solution of **(^{Mes}CCC)Co(N_2)(PPh_3)** (2 mol %) and styrene in benzene-d_6, polarization in the aliphatic and vinyl/aryl (sp^2 C–H) regions were observed in the ^{1}H and ^{1}H-OPSY NMR spectra (Figure 3.11 (top) and Figure 3.11 (bottom), respectively). Resonances at 1.07 and 2.44 ppm corresponding to the hydrogenation product of styrene demonstrate that both H atoms of the H_2 molecule add to the substrate in a concerted fashion (Figure 3.11 (top), known as ALTADENA). The polarization effect observed for resonances at 5.07, 5.59, 6.55, and 7.00–7.25 ppm suggests that a reversible exchange process in the hydrogenation reaction is operative (Figure 3.11 (bottom), SABRE). SABRE (signal amplification by reversible exchange) occurs by polarizing a substrate using *p*-H_2 without

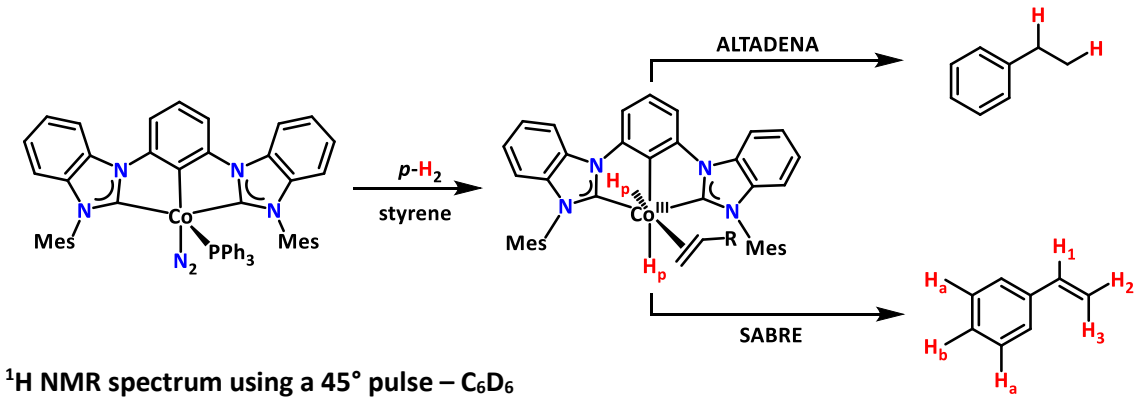

^{1}H NMR spectrum using a 45° pulse – C_6D_6

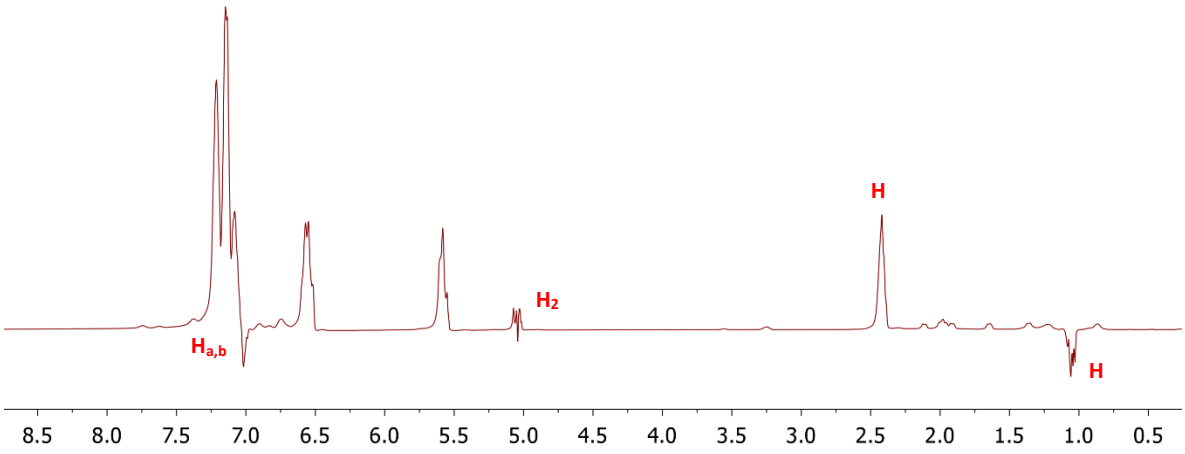

^{1}H-OPSY NMR spectrum – C_6D_6

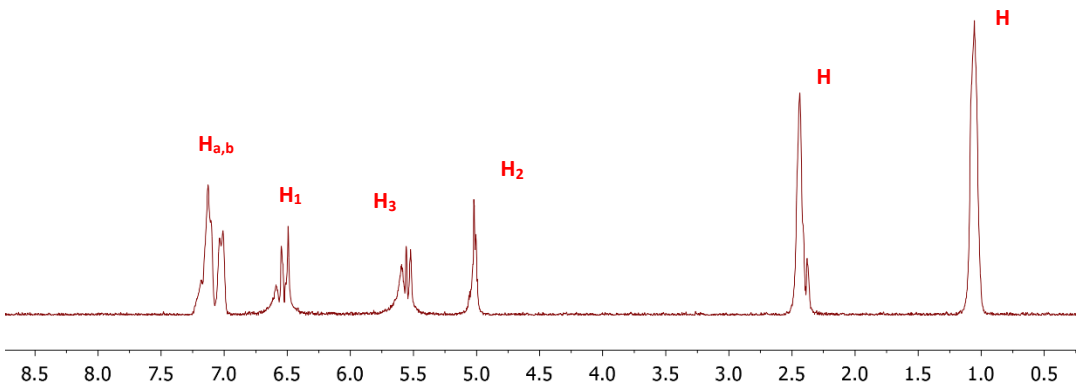

Figure 3.11 ^{1}H NMR spectrum (top) and ^{1}H-OPSY NMR spectrum (bottom) showing the hydrogenation of styrene using **(^{Mes}CCC)Co(N_2)(PPh_3)** with *p*-H_2.

any chemical transformation to the substrate.[49] Duckett and co-workers[49-51] have demonstrated the transfer of nuclear spin polarization to substrates without the incorporation of *p*-H_2, while citing the importance of the reversible binding of the substrate, and, in addition, have provided a theoretical understanding of this process.[52] In the observed studies herein, only some of the nuclear spin polarization

from *p*-H_2 transfer to styrene without chemically modifying the substrates. This indicates that the coordination of styrene and oxidative addition of H_2 onto the Co(I) center proceeds in a joint manner, and that styrene coordination is reversible. Furthermore, this signal enhancement was also observed in the ^{1}H-OPSY NMR spectrum when using 4-vinylcyclohexene as the substrate, suggesting this effect is general and specific to styrene (Figure 3.33).

3.7 Mechanistic studies using D_2

To further examine the reversible exchange process observed in the PHIP studies, the feasibility of deuterium incorporation into styrene was examined. Following the addition of D_2 (4 atm) to a benzene solution of **(^{Mes}CCC)Co(N_2)(PPh_3)** (2 mol %) and styrene, the incorporation of deuterium was observed in the olefinic region (5.05, 5.58, and 6.55 ppm) of styrene and the aliphatic region of the product (ethylbenzene) within 1 h at room temperature, as assayed in the ^{2}H NMR spectrum (Figure 3.12). The observation of **(^{Mes}CCC)Co(H_2)(PPh_3)**, **(^{Mes}CCC)Co(HD)(PPh_3)**, H_2 and HD gas in the ^{1}H NMR spectrum following the completion of the reaction, as well as HD gas in the ^{2}H NMR spectrum, are representative of another reversible reaction occurring over the course of catalysis (Figure 3.13). The observation of H_2 and HD likely occurs via β-hydride elimination from a cobalt-alkyl complex. Deuterium labeling studies with cyclohexene revealed a similar scrambling process, indicating this process is general and not specific to styrene (Figures 3.30 and 3.31).

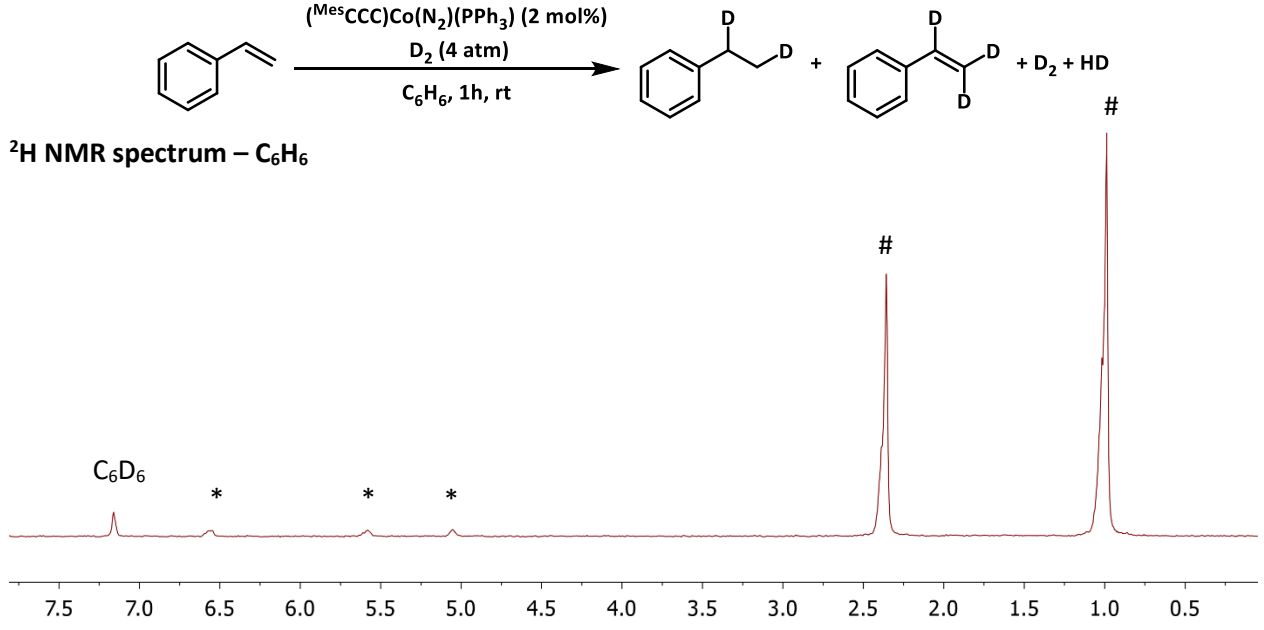

Figure 3.12 ^{2}H NMR spectrum of **(^{Mes}CCC)Co(N_2)(PPh_3)** and styrene under 4 atm of D_2 for 1 h. *denotes styrene olefinic resonances, $^\#$denotes ethylbenzene.

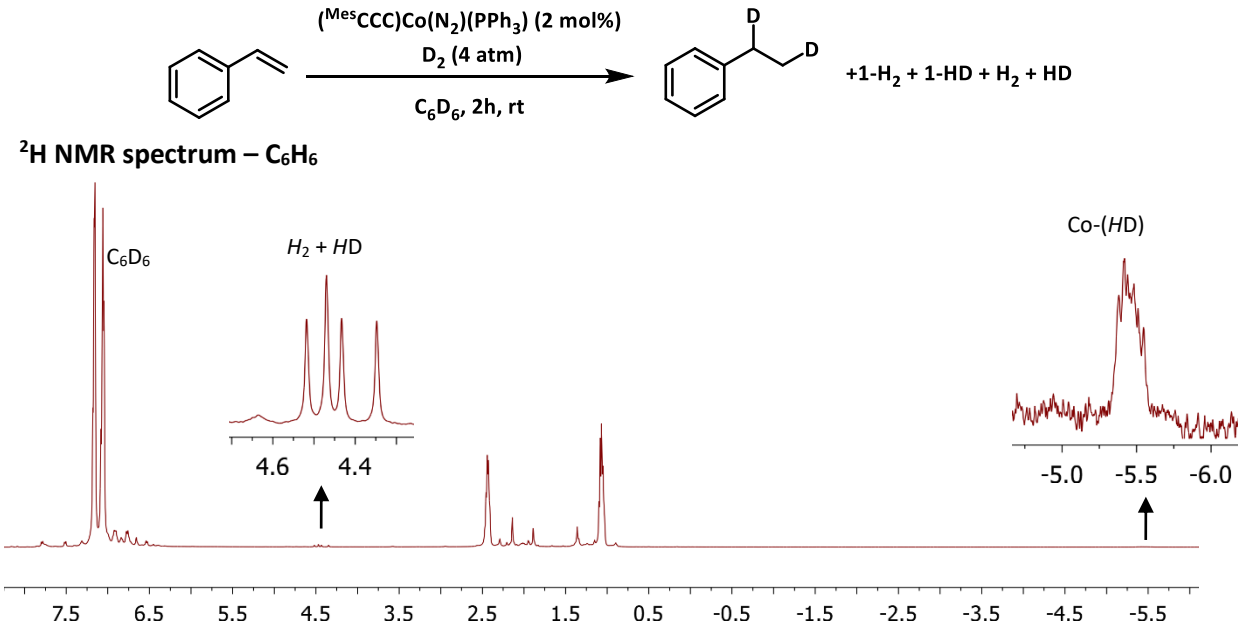

Figure 3.13 ^{1}H NMR spectrum of **(^{Mes}CCC)Co(N_2)(PPh_3)** and styrene under 4 atm of D_2 for after 24 h.

3.8 Proposed mechanism for the catalytic hydrogenation of olefins by (^{Mes}CCC)Co(N_2)(PPh_3)

A comprehensive mechanistic picture of the catalytic hydrogenation process of **(^{Mes}CCC)Co(N_2)(PPh_3)** is proposed (Figure 3.14). T_1 relaxation and HD labeling studies have demonstrated that a dihydrogen complex is generated under an H_2 atmosphere by displacing the N_2 ligand from **(^{Mes}CCC)Co(N_2)(PPh_3)**. Next, PHIP NMR data supports that olefin displacement of the bound phosphine (***I-1***) must occur. No signal enhancements were observed upon the addition of *p*-H_2 to a solution containing only **(^{Mes}CCC)Co(N_2)(PPh_3)**; the olefin must be present for this enhancement to occur. Moreover, the addition of excess PPh_3 inhibits catalytic reactivity. Next, H_2 oxidatively adds onto the metal center to generate a Co(III)-dihydride intermediate, ***I-2***. The polarization of styrene by SABRE indicates that the formations of ***I-1*** and ***I-2***, as well as ***I-1*** and **(^{Mes}CCC)Co(H_2)(PPh_3)**, are reversible and that oxidative addition of H_2 onto the cobalt center does occur. Following ***I-2*** formation, migratory insertion generates a dihydrogen hydride, ***I-3*****.** Detection of partially deuterated substrates is indicative of β-hydride elimination from ***I-3*** to generate ***I-2*****,** accompanied by dissociation of H_2. The observation of HD and H_2 in deuterium studies strongly suggests that HD exchange occurs via complexes ***I-3*** and ***I-4***, and further establishes that β-hydride elimination must be operative. Lastly, **(^{Mes}CCC)Co(H_2)(PPh_3)** is regenerated by reductive elimination of the alkane product and coordination of PPh_3 to the cobalt complex.

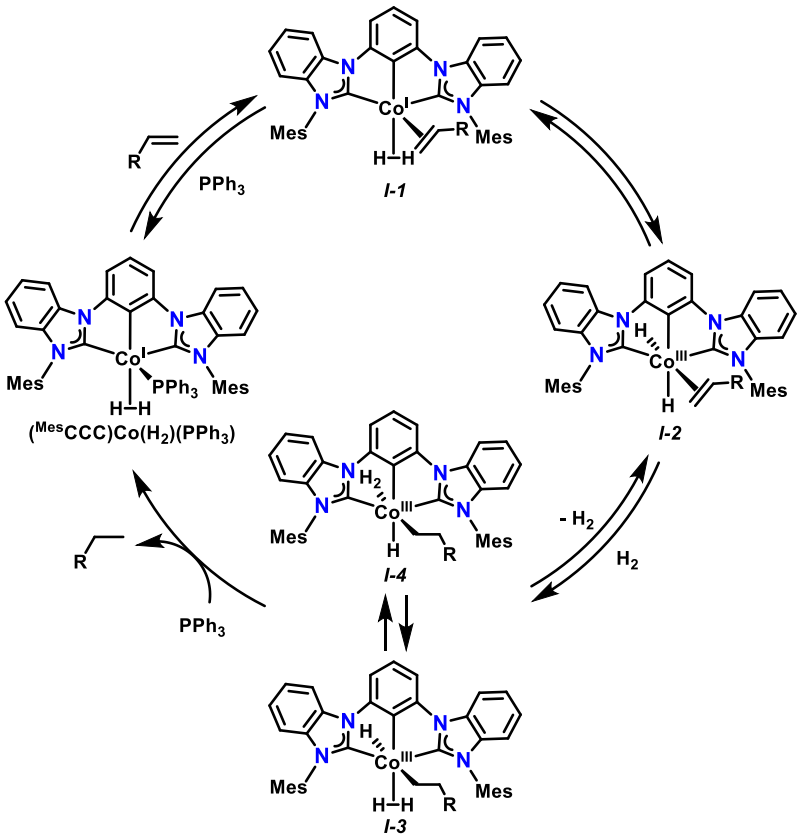

Figure 3.14 Proposed catalytic mechanism for the hydrogenation of olefins with **(^{Mes}CCC)Co(H_2)(PPh_3)**.

3.9 Conclusion

In summary, a "Kubas-type" cobalt dihydrogen complex supported by a monoanionic bis(carbene) ligand platform was prepared and characterized in solution using multinuclear NMR studies. In the course of these studies, it was determined that Co(I)-(N_2) precursors **(^{Mes}CCC)Co(N_2)(PPh_3)** and **(^{Mes}CCC)Co(N_2)(PPh_3)** exchange N_2 for H_2 and are able to facilitate the scrambling of H_2 and D_2, generating HD gas. Furthermore, **(^{Mes}CCC)Co(N_2)(PPh_3)** is competent toward the hydrogenation of olefins in the presence of hydrogen gas. A number of studies suggest the dihydrogen complex, **(^{Mes}CCC)Co(H_2)(PPh_3)**, is the resting state of the active catalyst. Finally, the use of ^{1}H, ^{2}H, and PHIP NMR studies established a Co(I)/Co(III) was operative and has enabled the identification of key reaction intermediates and established the role of the cobalt(I) dihydrogen complex, **(^{Mes}CCC)Co(H_2)(PPh_3)**, in the catalytic hydrogenation of olefins.

3.10 Experimental section

General considerations. All manipulations of air- and moisture-sensitive compounds were carried out in the absence of water and dioxygen in an MBraun inert atmosphere drybox under a dinitrogen atmosphere except where specified otherwise. All glassware was oven dried for a minimum of 8 h and cooled in an evacuated antechamber prior to use in the drybox. Solvents for sensitive manipulations were dried and deoxygenated on a Glass Contour System (SG Water USA, Nashua, NH) and stored over 4 Å molecular sieves purchased from Strem following a literature procedure prior to use.[53] Chloroform-*d*, toluene-d_8 and benzene-d_6 were purchased from Cambridge Isotope Labs and were degassed and stored over 4 Å molecular sieves prior to use. Lithium hexamethyldisilazane was purchased from Sigma-Aldrich and recrystallized from toluene under an inert atmosphere prior to use. Celite® 545 (J. T. Baker) was dried in a Schlenk flask for 24 h under dynamic vacuum while heating to at least 150˚C prior to use in a glovebox. NMR Spectra were recorded at room temperature on a Varian spectrometer operating at 500 MHz (^{1}H NMR) and 126 MHz (^{13}C NMR) (U500, VXR500, UI500NB) and referenced to the residual C_7D_7H, $CHCl_3$ and C_6D_5H resonance (δ in parts per million, and *J* in Hz). Potassium graphite (KC_8),[54] **(^{Mes}CCC)CoCl$_2$py** and **(^{Mes}CCC)Co(N$_2$)(PPh$_3$)**[31] were prepared according to literature procedures.

Synthesis of metal complexes

Preparation of (^{Mes}CCC)Co(H$_2$)(PPh$_3$): A solution of **(^{Mes}CCC)Co(N$_2$)(PPh$_3$)** (0.005 g, 0.006 mmol) in *ca*. ½ mL of benzene-d_6 or toluene-d_8 was transferred to a J. Young tube and sealed. The sample was subjected to three freeze-pump-thaw cycles and exposed to 1 atm of H_2 at 77K and then allowed to warm ambient temperature resulting a color change of the solution to red-orange after agitating the mixture. After subjecting **(^{Mes}CCC)Co(H$_2$)(PPh$_3$)** to a freeze-thump-thaw cycle, the Co(n^2-H_2) complex was unchanged. Upon exposure to an N_2 atmosphere, the gradual formation of **(^{Mes}CCC)Co(N$_2$)(PPh$_3$)** was observed by ^{1}H NMR and the solution turned dark red. Elemental analysis or HRMS (ESI) were not performed since upon exposure to N_2, the H_2 ligand dissociates from the complex. NMR data (in benzene-d_6, 25 °C): ^{1}H δ = 7.80 (d, J = 7.5, 2H), 7.52 (d, J = 7.0, 2 H), 7.39 (m, 2 H), 7.31 (d, J= 7, 1H), 7.10 (t, J = 7.5, 2 H), 7.04 (m, 2H), 6.97-6.88 (m, 7H) 6.86-6.82 (m, 2H), 6.80-6.75 (m, 6H), 6.66 (s, 2H), 6.54 (d, J = 7.5, 2H), 2.13 (s, 6H), 1.89 (s, 6H), 1.36 (s, 6H), -5.48 (s, 2H). ^{13}C δ = 144.7, 139.3, 139.1, 137.9, 137.7, 137.7 137.7, 136.9, 135.3, 133.1, 133.0, 132.7, 129.8, 129.2, 128.0, 127.6, 127.6, 121.6, 121.5, 118.8, 109.5, 108.6, 105.9, 21.1, 19.0, 17.4. NMR data (in toluene-d_8, 25 °C): ^{1}H δ = 7.76 (d, J = 7.5, 2H), 7.42 (d, J = 7.0, 2H), 7.32 (s, 2H), 7.22 (t, J = 6.5, 2H), 6.90-6.80 (m, 12H), 6.77-6.71 (m, 8H), 6.64 (s, 2H), 6.48 (d, J = 10, 2H), 2.14 (s, 6H), 1.82 (s, 6H), 1.30 (s, 6H), -5.56 (s, 2H).

Preparation of (^{Mes}CCC)Co(D_2)(PPh_3):. A solution of **(^{Mes}CCC)Co(N_2)(PPh_3)** (0.008 g, 0.009 mmol) in *ca*. ½ mL of toluene-d_8 or toluene was transferred to a J. Young tube and sealed. The sample was subjected to three freeze-pump-thaw cycles and exposed to 1 atm of D_2 at 77K and allowed to warm to ambient temperature for 15 min. After agitating the mixture, the color of the solution turned orange. ^{1}H NMR data (in toluene-d_8, 25 °C): δ = 7.76 (d, J = 7.5, 2H), 7.42 (d, J = 7.0, 2H), 7.22 (t, J = 6.5, 1H), 6.90-6.80 (m, 13H), 6.77-6.71 (m, 8H), 6.64 (s, 2H), 6.48 (d, J = 10, 2H), 2.14 (s, 6H), 1.82 (s, 6H), 1.30 (s, 6H). ^{2}H NMR data (in toluene, 76.7 MHz, 25 °C): δ = -5.66 (s, 2H).

Preparation of (^{Mes}CCC)Co(HD)(PPh_3): A solution of **(^{Mes}CCC)Co(N_2)(PPh_3)** (0.005 g, 0.006 mmol) in *ca*. ½ mL of toluene-d_8 was transferred to a J. Young tube and sealed. The sample was subjected to three freeze-pump-thaw cycles and exposed to 1 atm of HD (generated from excess $LiAlH_4$ and degassed D_2O*) at 77K and let stand for 10 min at ambient temperature upon which the solution slowly turned red-orange. ^{1}H NMR data (in toluene-d_8, 25 °C): δ = 7.76 (d, J = 7.5, 2H), 7.42 (d, J = 7.0, 2H), 7.32 (s, 2H), 7.22 (t, J = 6.5, 1H), 6.90-6.80 (m, 12H), 6.77-6.71 (m, 7H), 6.64 (s, 2H), 6.48 (d, J = 7.5, 2H), 2.14 (s, 6H), 1.82 (s, 6H), 1.30 (s, 6H), -5.56 (t, J = 33, ½ H) -5.60 (t, J = 33, ½ H). (*This is very exothermic and it is vital that this is carried out in absence of oxygen gas).

Alternative preparation of (^{Mes}CCC)Co(HD)(PPh_3): A solution of **(^{Mes}CCC)Co(N_2)(PPh_3)** (0.005 g, 0.006 mmol) in *ca*. ½ mL of benzene-d_6 was transferred to a J. Young tube and sealed. The sample was subjected to three freeze-pump-thaw cycles and exposed to a mixture of H_2 and D_2 (50:50) at 1 atm and 77K. The solution was warmed to ambient temperature and upon agitating the reaction mixture the color of the solution turned red-orange. ^{1}H NMR data (in benzne-d_6, 25 °C): δ = δ = 7.80 (d, J = 7.5, 2H), 7.52 (d, J = 7.0, 2 H), 7.39 (m, 2 H), 7.31 (d, J= 7, 1H), 7.10 (t, J = 7.5, 2 H), 7.04 (m, 2H), 6.97-6.88 (m, 7H) 6.86-6.82 (m, 2H), 6.80-6.75 (m, 6H), 6.66 (s, 2H), 6.54 (d, J = 7.5, 2H), 2.13 (s, 6H), 1.89 (s, 6H), 1.36 (s, 6H), -5.46 (t, J = 33, ½ H), -5.49 (t, J = 33, ½ H).

Preparation of (^{Mes}CCC)Co(N_2)(PMe_3): A 20 mL scintillation vial was charged with **(^{Mes}CCC)CoCl_2py** (0.222 g, 0.294 mmol) and THF (10 mL). A suspension of KC_8 (0.087 g, 0.647 mmol) in THF (5 mL) was added to the mixture. After stirring for 2 hours, the deep brown suspension was filtered over Celite and to the filtrate PMe_3 (1.0 M in THF, 0.22 mL, 0.22 mmol), was added, resulting in the change of the mixture to dark red. After stirring the solution for 1 h, the THF was removed under reduced pressure. The solid was

taken up in Et_2O (3 x 5 mL), filtered over Celite, concentrated under pressure and triturated with hexanes (10 mL) to yield a red powder (0.160 g, 0.225 mmol, 77%). Crystals suitable for X-ray diffraction were grown from slow evaporation of a concentrated solution of complex **(^{Mes}CCC)Co(N_2)(PMe_3)** in hexanes at room temperature. NMR data (in benzene-d_6, 25 °C): ^{1}H δ = 7.87 (d, J = 7.5, 2H), 7.71 (d, J = 7.5, 2H), 7.46 (t, J = 7.5, 1H), 7.10 (t, J = 7.5, 2H), 6.95 (t, J = 7.8, 2H), 6.83 (s, 2H), 6.72 (s, 2H), 6.62 (d, J = 7.5, 2H), 2.10 (s, 6H), 2.09 (s, 6H), 2.02 (s, 6H), 0.45 (d, $J_{CH3\text{-}P}$ = 6.5, 9H). ^{13}C δ = 209.6, 163.0, 143.1, 138.4, 138.4, 138.2, 135.8, 134.4, 132.2, 130.2, 128.9, 121.8, 121.7, 118.6, 109.7, 108.3, 105.6, 21.1, 18.5, 18.4, 15.6, 15.4. IR: 2114 cm^{-1} (N_2). HRMS (ESI), calc. for $C_{41}H_{42}CoN_4P$ $(M - N_2)^+$: calculated 680.2479; found 680.2507.

Preparation of (^{Mes}CCC)Co(H_2)(PMe_3): A solution of **(^{Mes}CCC)Co(N_2)(PMe_3)** (0.006 g, 0.008 mmol) in *ca*. ½ mL of benzene-d_6 was transferred to a J. Young tube and sealed. The sample was subjected to two freeze-pump-thaw cycles and exposed 1 atm of H_2 at 77K. The reaction was warmed to room temperature for 10 min and after agitating the mixture, the color of the solution turned red. ^{1}H NMR data (in benzene-d_6, 25 °C): 7.88 (d, J = 8.5, 2H), 7.78 (d, J = 7.5, 2 H), 7.52 (t, J = 7.0, 1H), 7.09 (s, 2H), 6.93 (t, J = 8.0, 2H), 6.74 (s, 2H), 6.72 (s, 2H), 6.54 (d, J = 7.5, 2H), 2.02 (s, 6H), 1.97 (s, 6H), 1.96 (s, 6H), 0.56 (d, $J_{CH3\text{-}P}$ = 6.5, 9H), -5.77 (s, 2H). ^{13}C δ = 144.2, 137.7, 137.5, 135.6, 135.3 134.9, 134.2, 132.4, 130.0, 129.1. 128.7, 121.4, 121.3, 118.1, 109.4, 108.2, 105.4, 21.1, 19.4, 19.2, 18.8, 18.5, 18.3. Elemental analysis or HRMS (ESI) were not performed since upon exposure to N_2, the H_2 ligand dissociates from the complex. T_1 (minimum): 14 ms (298K).

Preparation of (^{Mes}CCC)Co(D_2)(PMe_3): A solution of **(^{Mes}CCC)Co(N_2)(PMe_3)** (0.008 g, 0.011 mmol) in *ca*. ½ mL of benzene was transferred to a J. Young tube and sealed. The sample was subjected to two freeze-pump-thaw cycles and exposed 1 atm of D_2 at 77K. The reaction was warmed to room temperature for 10 min and after agitating the mixture, the color of the solution turned red. ^{1}H NMR data (in benzene-d_6, 25 °C): 7.88 (d, J = 8.5, 2H), 7.78 (d, J = 7.5, 2 H), 7.52 (t, J = 7.0, 1H), 7.09 (s, 2H), 6.93 (t, J = 8.0, 2H), 6.74 (s, 2H), 6.72 (s, 2H), 6.54 (d, J = 7.5, 2H), 2.02 (s, 6H), 1.97 (s, 6H), 1.96 (s, 6H), 0.56 (d, $J_{CH3\text{-}P}$ = 6.5, 9H). ^{2}H NMR data (in benzene, 76.7 MHz, 25 °C): -5.86 (s).

Preparation of (^{Mes}CCC)Co(HD)(PMe_3): A solution of **(^{Mes}CCC)Co(N_2)(PMe_3)** (0.009 g, 0.013 mmol) in *ca*. ½ mL of benzene-d_6 was transferred to a J. Young tube and sealed. The sample was subjected to two freeze-pump-thaw cycles and exposed to a mixture of D_2 and H_2 gas (0.5:0.5 atm) at 77K. The reaction was warmed to room temperature for 10 min and after agitating the mixture, the color of the solution turned red. ^{1}H NMR data (in benzene-d_6, 25 °C) 7.88 (d, J = 8.5, 2H), 7.78 (d, J = 7.5, 2 H), 7.52 (t, J = 7.0, 1H), 7.09

(s, 2H), 6.93 (t, J = 8.0, 2H), 6.74 (s, 2H), 6.72 (s, 2H), 6.54 (d, J = 7.5, 2H), 2.02 (s, 6H), 1.97 (s, 6H), 1.96 (s, 6H), 0.56 (d, $J_{CH3\text{-}P}$ = 6.5, 9H), -5.75 (t, J = 32, ½ H), -5.79 (t, J = 32, ½ H).

Determination of T_1: T_1 (minimum): 12 *m*s (253 to 313K). Measurements were obtained on a 500 MHz spectrometer of **(^{Mes}CCC)Co(H_2)(PPh_3)** in toluene-d_8 from 203 K to 343 K by the standard inversion recovery pulse sequence method. T_1 (minimum) of **(^{Mes}CCC)Co(H_2)(PMe_3)** was assumed to behave in a similar manner and only a room temperature T_1 measurement of Co-(H_2) resonance was collected.

Table 3.3 Crystallographic parameters for **(^{Mes}CCC)Co(N_2)(PMe_3)**.

	(^{Mes}CCC)Co(N_2)(PMe_3) cd34w
Empirical Formula	C41 H42 Co N6 P
Formula Weight	708.71
Temperature	100(2) K
Wavelength	0.71073 Å
Crystal system	Monoclinic
Space group	P 21/n
Unit Cell Dimensions	a = 7.8946(3)Å b = 16.5851(5) Å c = 27.3473(10) Å α= 90° β= 94.4478 (12)° γ = 90°
Volume	3569.9(2) Å^3
Z	4
Reflections collected	88825
Independent reflections	7884
Goodness-of-fit on F2	1.098
Final R indices [I>sigma(I)]	R1 = 0.0386 wR2 = 0.0870

Table 3.4 Selected bond lengths and angles for **(^{Mes}CCC)Co(N_2)(PMe_3)**.

	(^{Mes}CCC)Co(N_2)(PMe_3)
Bond Distances (Å)	
Co – C1	1.9033 (19)
Co – C13	1.8734(19)
Co – C20	1.9079(19)
Co – N	1.871(2)
Co – P	2.2131(6)
N – N	1.022(2)
Bond Angles (°)	
C13-Co-N5	162.95(8)
C1-Co-C13	76.18(8)
C13-Co-C20	79.12(8)
C1-Co-C20	153.32(8)
N5-Co-P	101.29(5)

The ^{1}H NMR spectra (toluene-d_8) of the downfield (Figures 3.15 and 3.16) and upfield (Figures 3.17 and 3.18) region of variable temperature studies of (^{Mes}CCC)Co(H$_2$)(PPh$_3$) from 80°C to -80°C are shown below.

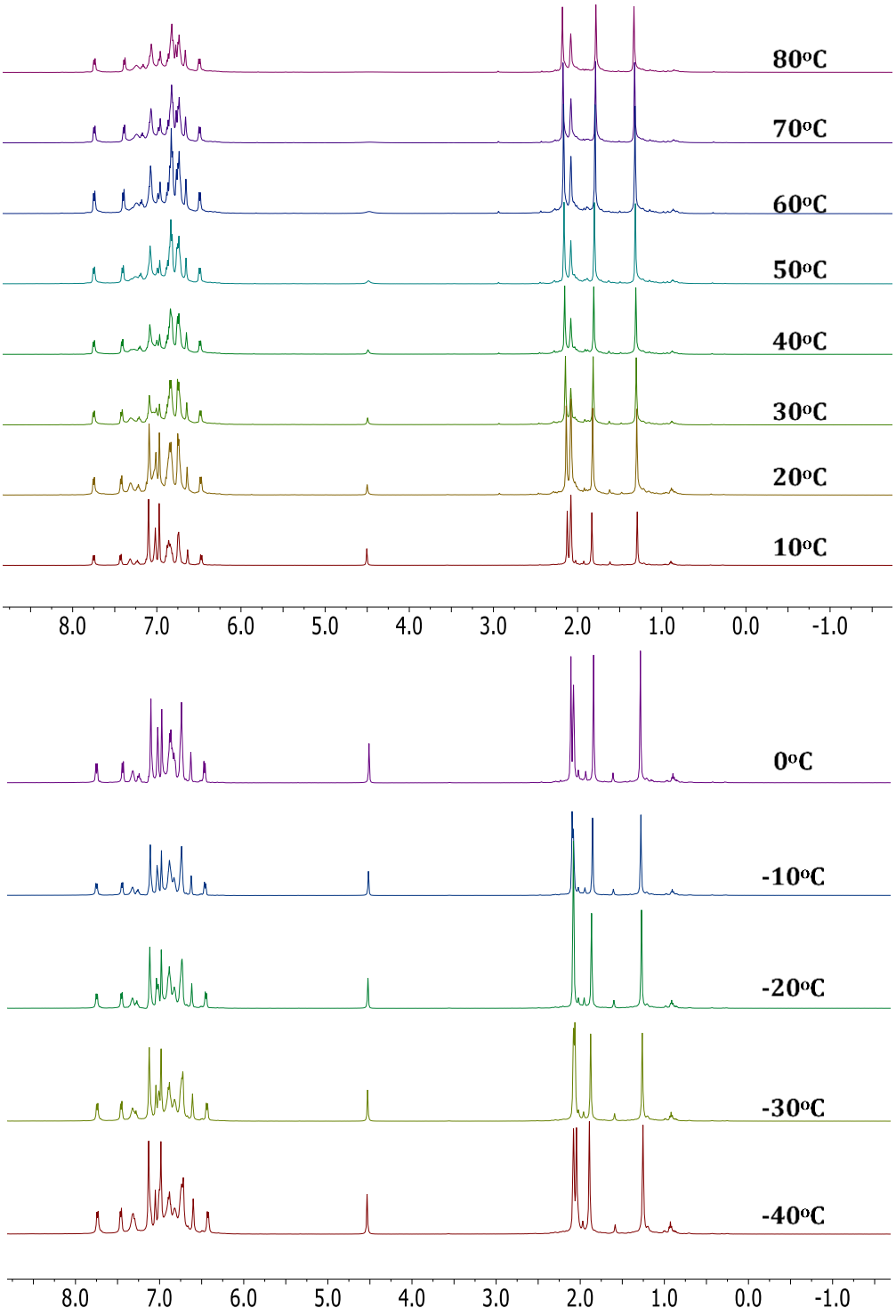

Figure 3.15 ^{1}H NMR spectrum showing the downfield region of **(^{Mes}CCC)Co(H$_2$)(PPh$_3$)** from 80°C to -40°C.

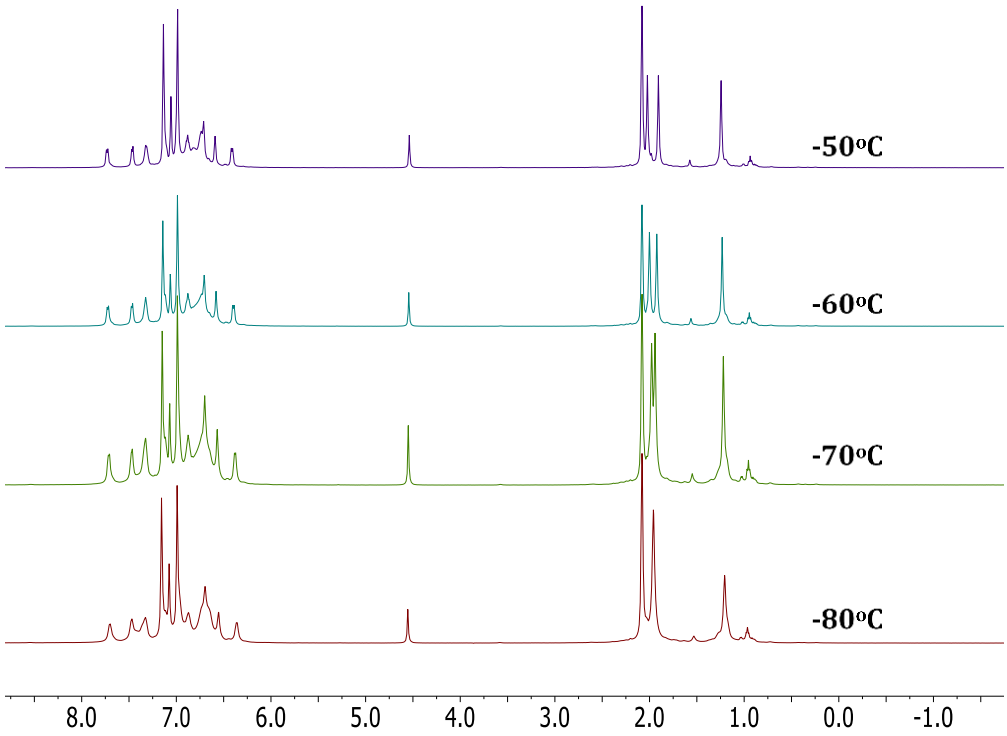

Figure 3.16 ^{1}H NMR spectrum showing the downfield region of **(^{Mes}CCC)Co(H$_2$)(PPh$_3$)** from -50°C to -80°C.

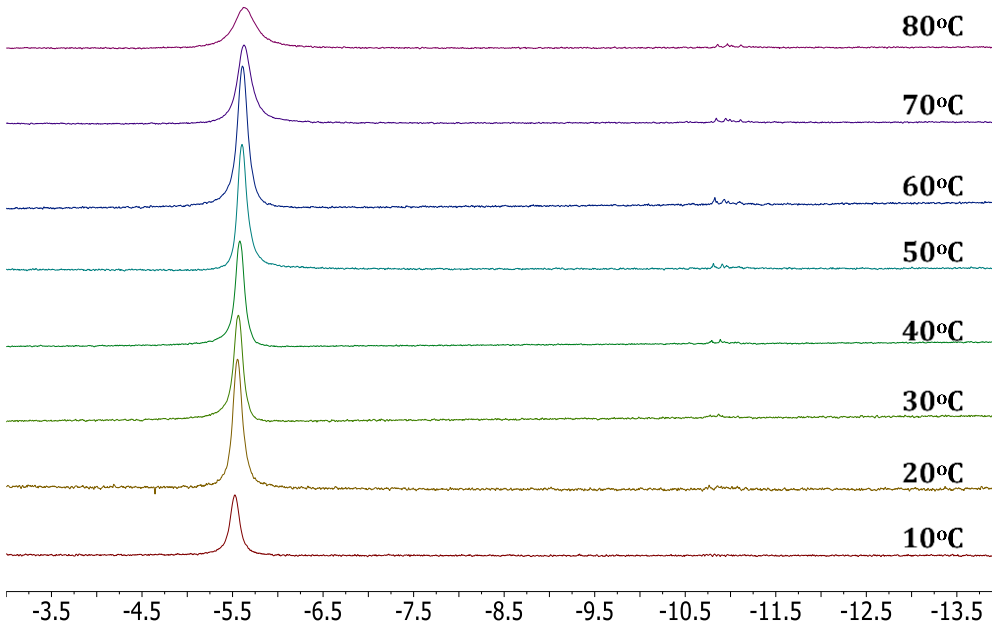

Figure 3.17 ^{1}H NMR spectrum showing the upfield region of **(^{Mes}CCC)Co(H$_2$)(PPh$_3$)** from 80°C to 10°C.

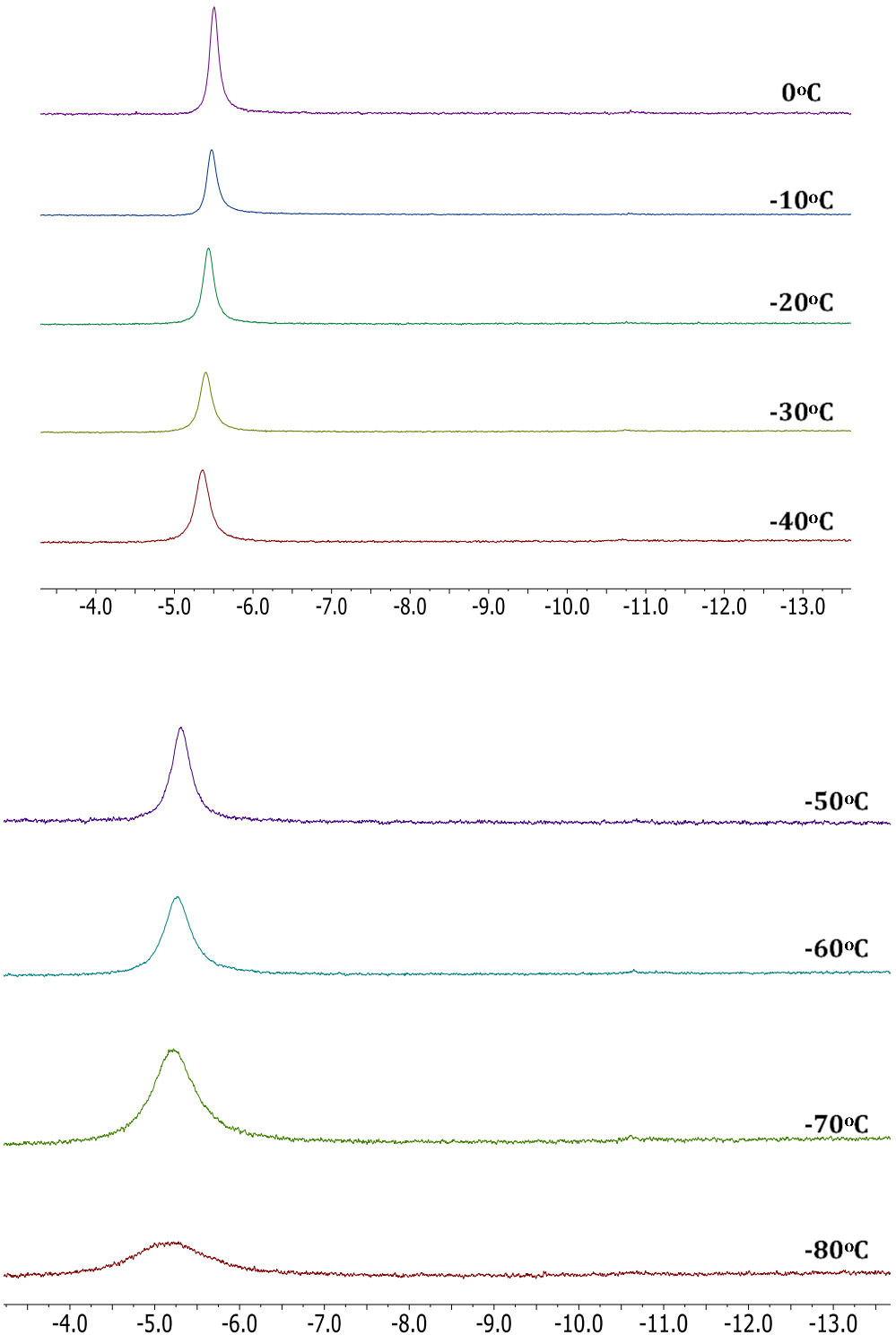

Figure 3.18 ^{1}H NMR spectrum showing the upfield region of **(^{Mes}CCC)Co(H_2)(PPh_3)** from 0°C to -80°C.

General procedure for olefin hydrogenation studies. A standard J. Young NMR tube was charged with a solution of olefin, 1,3,5-trimethylbenzene (internal standard) and **(^{Mes}CCC)Co(N_2)(PPh_3)** (2 mol%) in *ca.* ½ ml of benzene-d_6. The sample was subjected to two freeze-pump-thaw cycles and H_2 gas (1 atm) was added at 77K on a high-vacuum line. The sample was allowed to warm to ambient temperature, resulting in 4 atm of H_2 gas. The catalytic reaction was monitored by ^{1}H and ^{13}C NMR spectroscopy. Each catalytic experiment was reproduced. Control experiments were carried under similar catalytic conditions. Using **(^{Mes}CCC)CoCl_2py** (2 mol%) and styrene, no hydrogenation of the olefin was observed. The use of **(^{Mes}CCC)Co(N_2)(PPh_3)** (2 mol%) with one drop of Hg displayed similar results for the hydrogenation of styrene.

Hydrogenation with **(^{Mes}CCC)Co(H_2)(PPh_3)**.

A 50 mL schlenk flask charged with **(^{Mes}CCC)Co(N_2)(PPh_3)** (0.020 g, 0.0225 mmol) and 5 mL of benzene was subjected to three freeze pump thaw cycles and placed under 1 atm of H_2 gas. Styrene (0.127 mL, 1.105 mmol) was degassed using argon and transferred to the solution of **(^{Mes}CCC)Co(H_2)(PPh_3)** via an airtight syringe. The reaction was stirred at room temperature for 2 hours and complete conversion to ethylbenzene was determined using GC-MS.

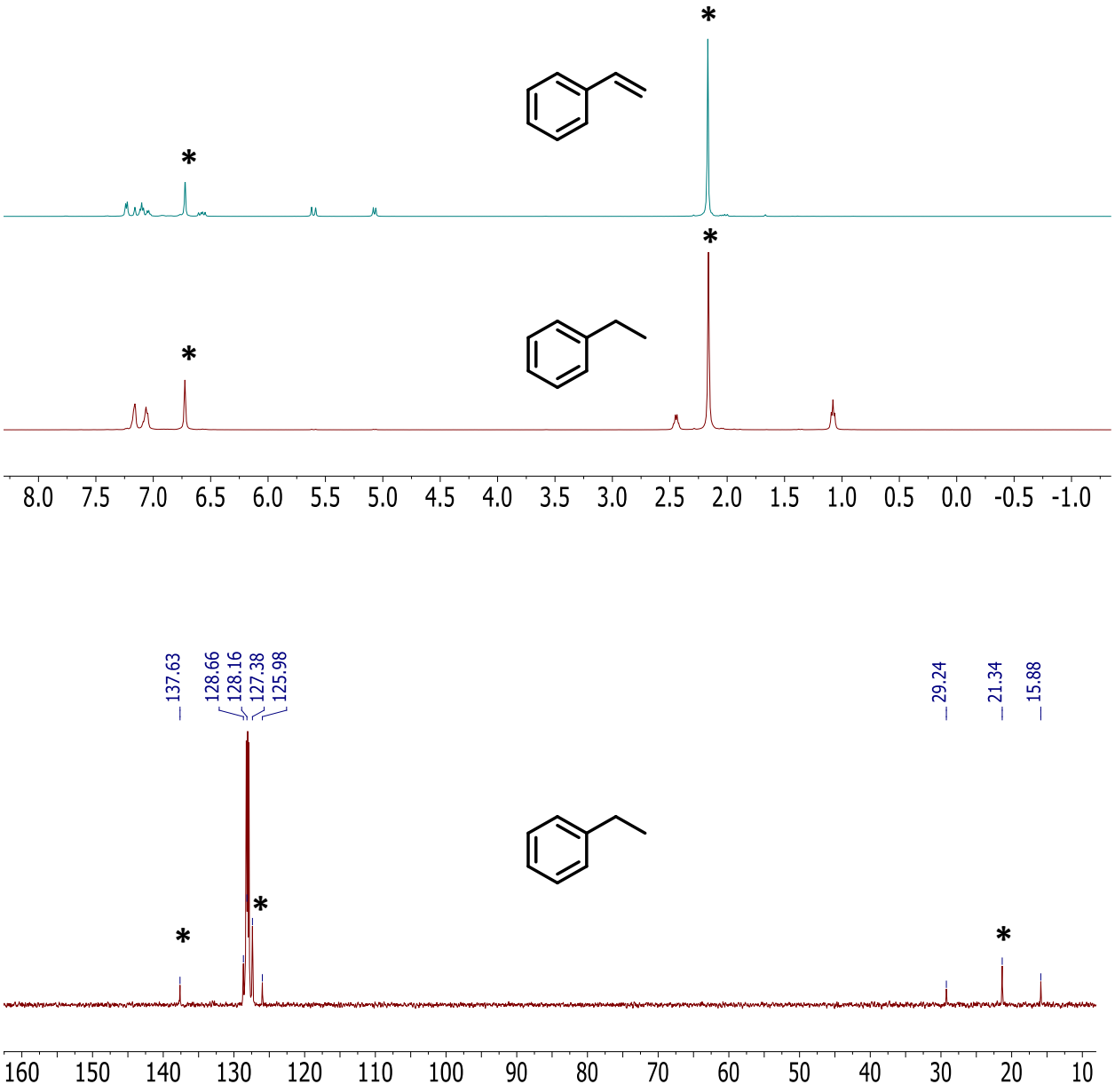

Figure 3.19 ^{1}H NMR (C_6D_6, 500 MHz) spectrum of **(^{Mes}CCC)Co(N_2)(PPh_3)** (2%), mesitylene (*) and styrene under N_2 (top). ^{1}H NMR spectrum of **(^{Mes}CCC)Co(N_2)(PPh_3)** (2%), mesitylene (*) and styrene under 4 atm of H_2 after 2 h (middle). ^{13}C NMR spectrum of **(^{Mes}CCC)Co(N_2)(PPh_3)** (2%), mesitylene (*) and styrene under 4 atm of H_2 after 2 h (bottom).

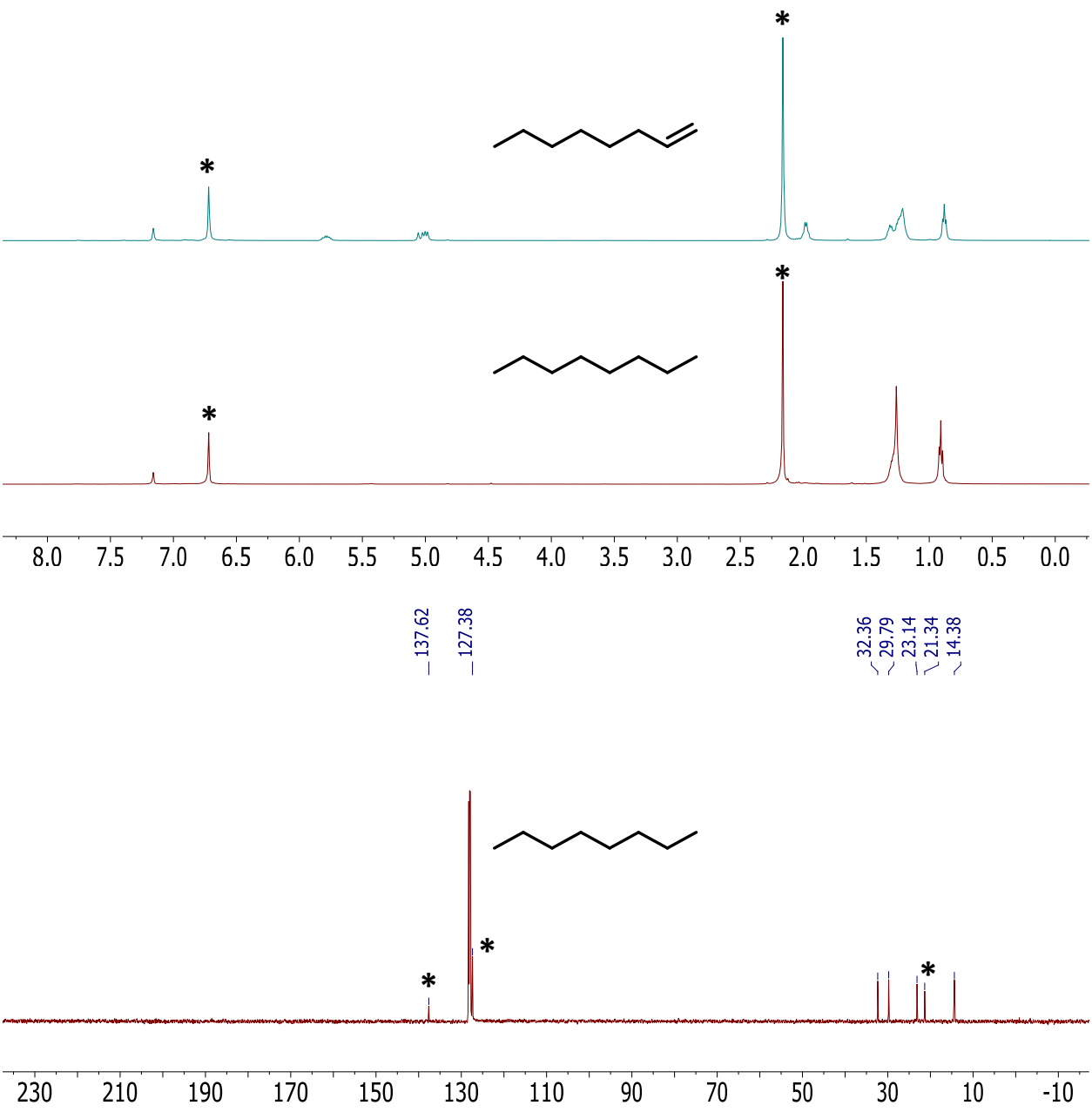

Figure 3.20 ^{1}H NMR (C_6D_6, 500 MHz) spectrum of **(^{Mes}CCC)Co(N_2)(PPh_3)** (2%), mesitylene (*) and 1-octene under N_2 (top). ^{1}H NMR spectrum of **(^{Mes}CCC)Co(N_2)(PPh_3)** (2%), mesitylene (*) and 1-octene under 4 atm of H_2 after 3 h (middle). ^{13}C NMR spectrum of **(^{Mes}CCC)Co(N_2)(PPh_3)** (2%), mesitylene (*) and 1-octene under 4 atm of H_2 after 3 h (bottom).

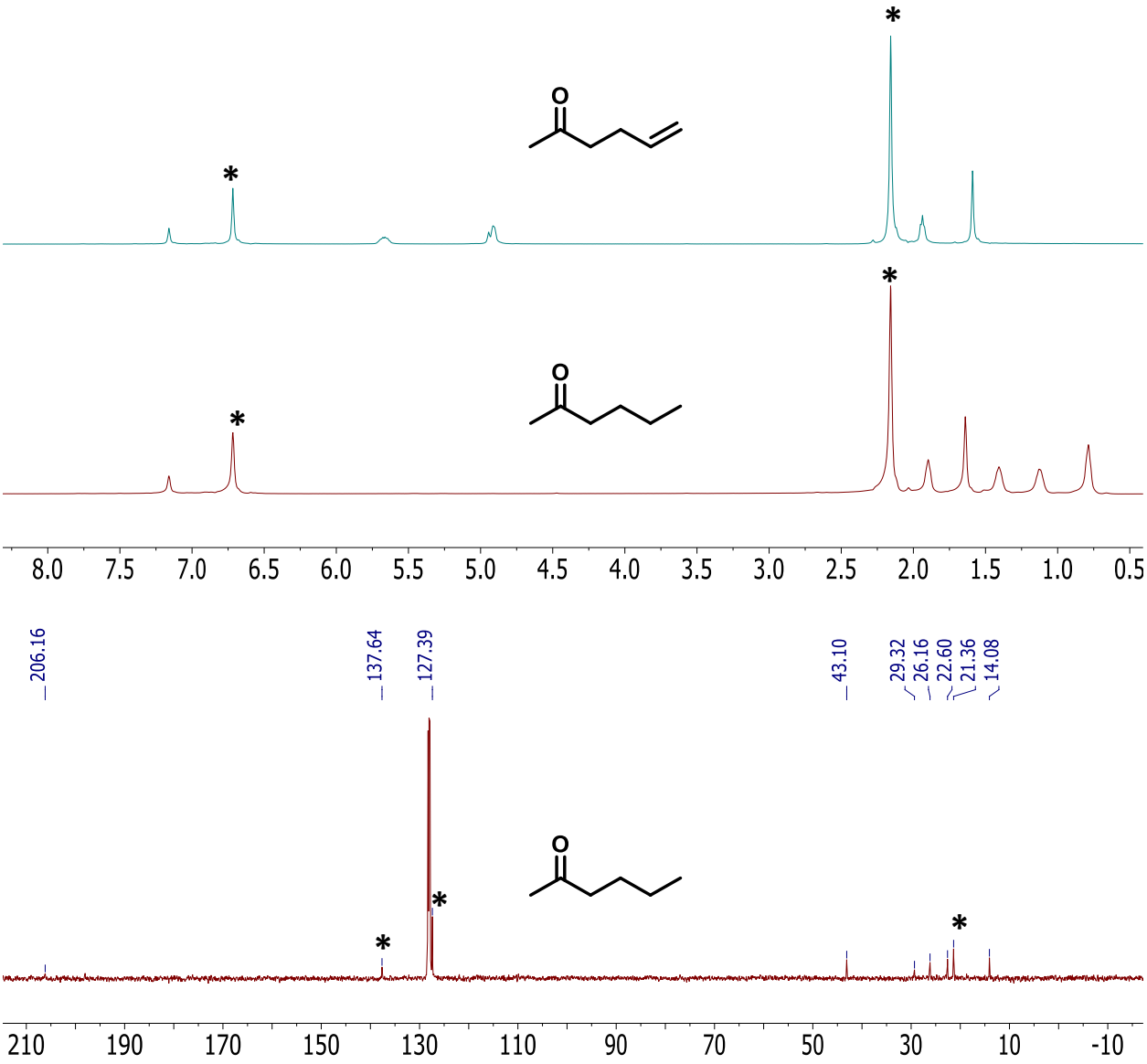

Figure 3.21 ^{1}H NMR (C_6D_6, 500 MHz) spectrum of **(^{Mes}CCC)Co(N_2)(PPh_3)** (2%), mesitylene (*) and hex-5-en-2-one under N_2 (top). ^{1}H NMR spectrum of **(^{Mes}CCC)Co(N_2)(PPh_3)** (2%), mesitylene (*) and hex-5-en-2-one under 4 atm of H_2 after 2 h (middle). ^{13}C NMR spectrum of **(^{Mes}CCC)Co(N_2)(PPh_3)** (2%), mesitylene (*) and hex-5-en-2-one under 4 atm of H_2 after 2 h (bottom).

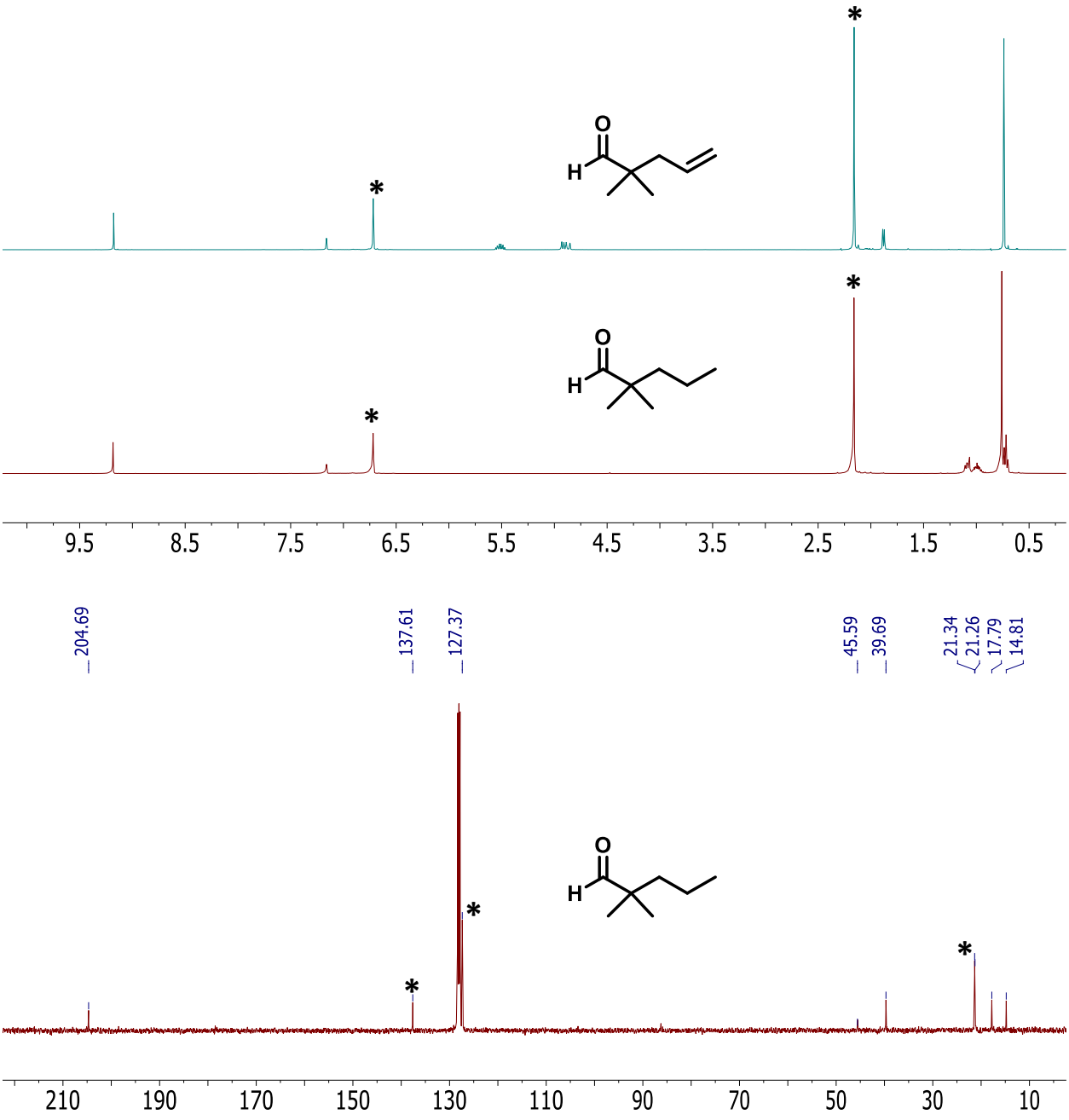

Figure 3.22. ^{1}H NMR (C_6D_6, 500 MHz) spectrum of **(^{Mes}CCC)Co(N_2)(PPh_3)** (2%), mesitylene (*) and 2,2-dimethylpent-4-enal under N_2 (top). ^{1}H NMR spectrum of **(^{Mes}CCC)Co(N_2)(PPh_3)** (2%), mesitylene (*) and 2,2-dimethylpent-4-enal under 4 atm of H_2 after 22 h (middle). ^{13}C NMR spectrum of **(^{Mes}CCC)Co(N_2)(PPh_3)** (2%), mesitylene (*) and 2,2-dimethylpent-4-enal under 4 atm of H_2 after 22 h (bottom).

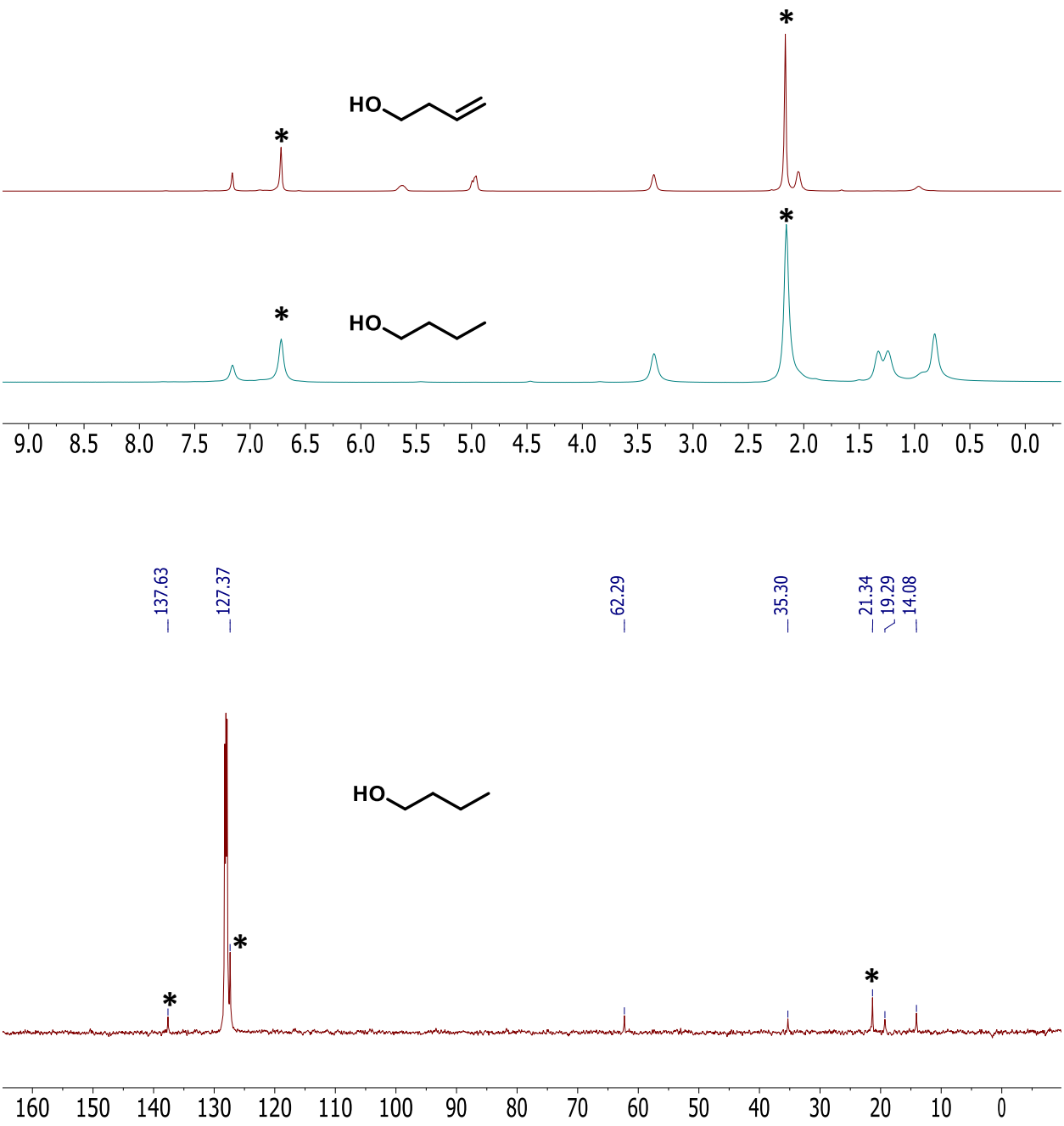

Figure 3.23 ^{1}H NMR (C_6D_6, 500 MHz) spectrum of **(^{Mes}CCC)Co(N_2)(PPh_3)** (2%), mesitylene (*) and but-3-en-1-ol under N_2 (top). ^{1}H NMR spectrum of **(^{Mes}CCC)Co(N_2)(PPh_3)** (2%), mesitylene (*) and but-3-en-1-ol under 4 atm of H_2 after 22 h (middle). ^{13}C NMR spectrum of **(^{Mes}CCC)Co(N_2)(PPh_3)** (2%), mesitylene (*) and but-3-en-1-ol under 4 atm of H_2 after 2 h (bottom).

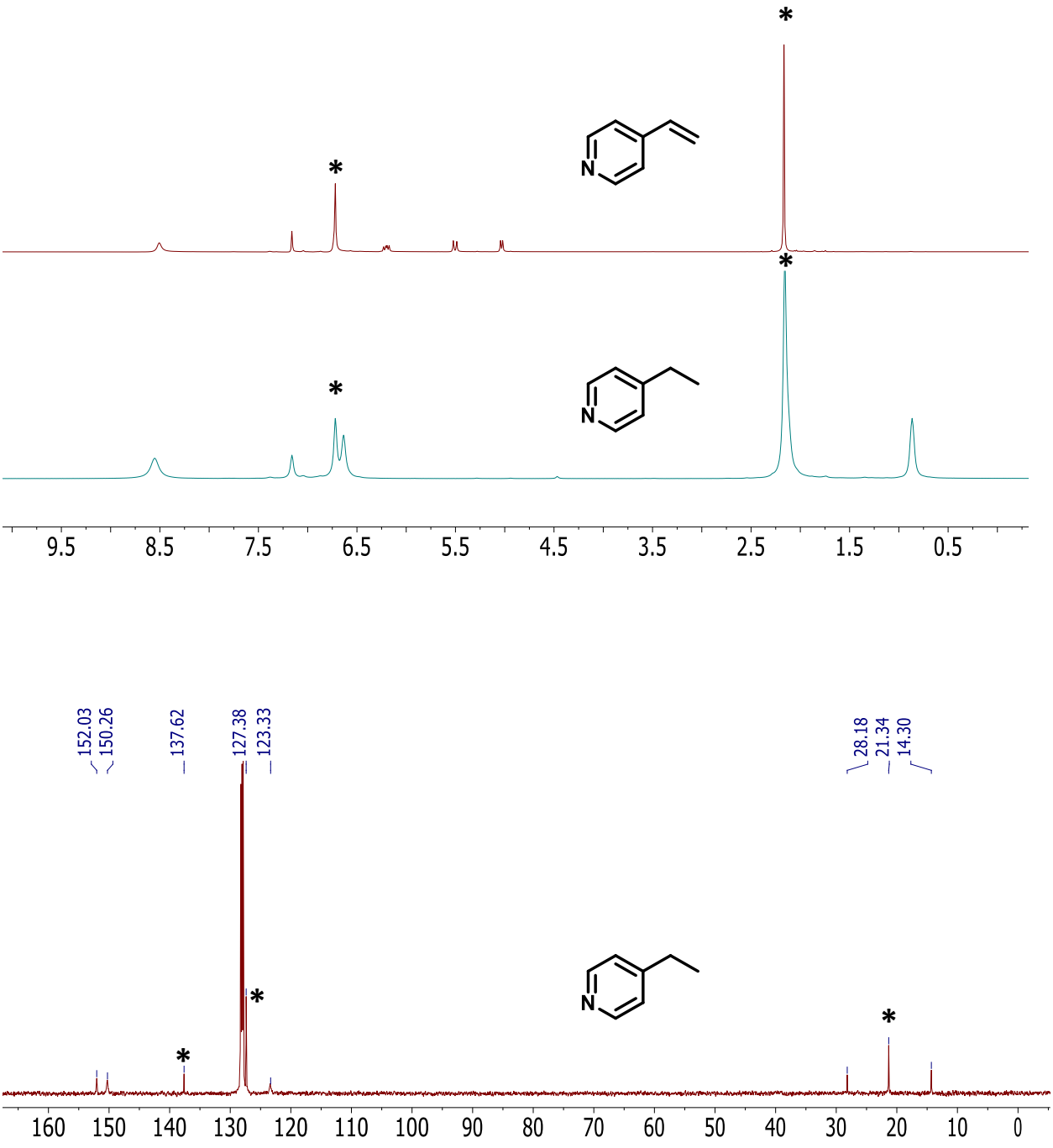

Figure 3.24 ^{1}H NMR (C_6D_6, 500 MHz) spectrum of **(^{Mes}CCC)Co(N_2)(PPh_3)** (2%), mesitylene (*) and 4-vinylpyridine under N_2 (top). ^{1}H NMR spectrum of **(^{Mes}CCC)Co(N_2)(PPh_3)** (2%), mesitylene (*) and 4-vinylpyridine under 4 atm of H_2 after 22 h (middle). ^{13}C NMR spectrum of **(^{Mes}CCC)Co(N_2)(PPh_3)** (2%), mesitylene (*) and 4-vinylpyridine under 4 atm of H_2 after 2 h (bottom).

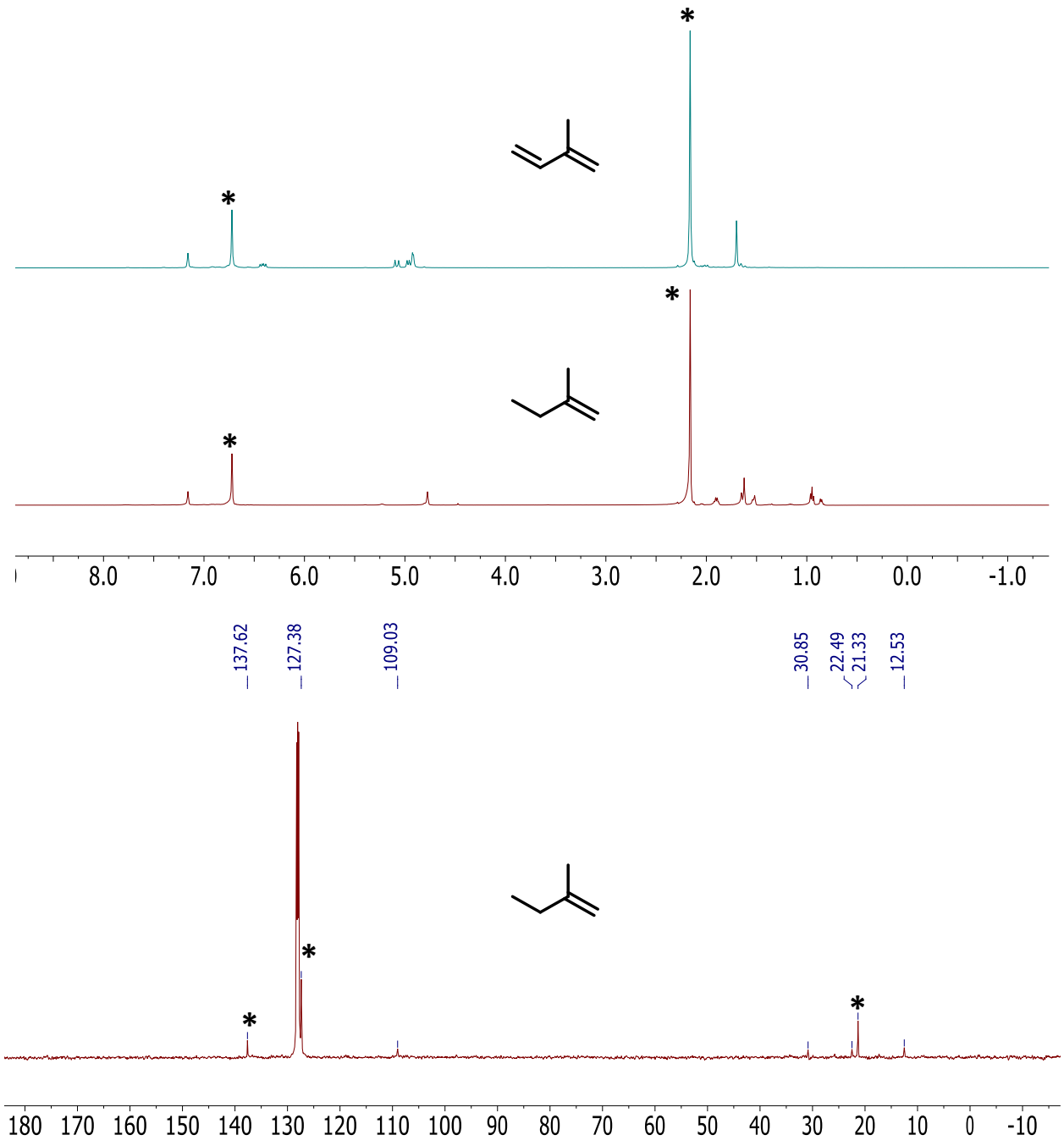

Figure 3.25 ^{1}H NMR (C_6D_6, 500 MHz) spectrum of **(^{Mes}CCC)Co(N_2)(PPh_3)** (2%), mesitylene (*) and isoprene under N_2 (top). ^{1}H NMR spectrum of **(^{Mes}CCC)Co(N_2)(PPh_3)** (2%), mesitylene (*) and isoprene under 4 atm of H_2 after 21 h (middle). ^{13}C NMR spectrum of **(^{Mes}CCC)Co(N_2)(PPh_3)** (2%), mesitylene (*) and isoprene under 4 atm of H_2 after21 h (bottom).

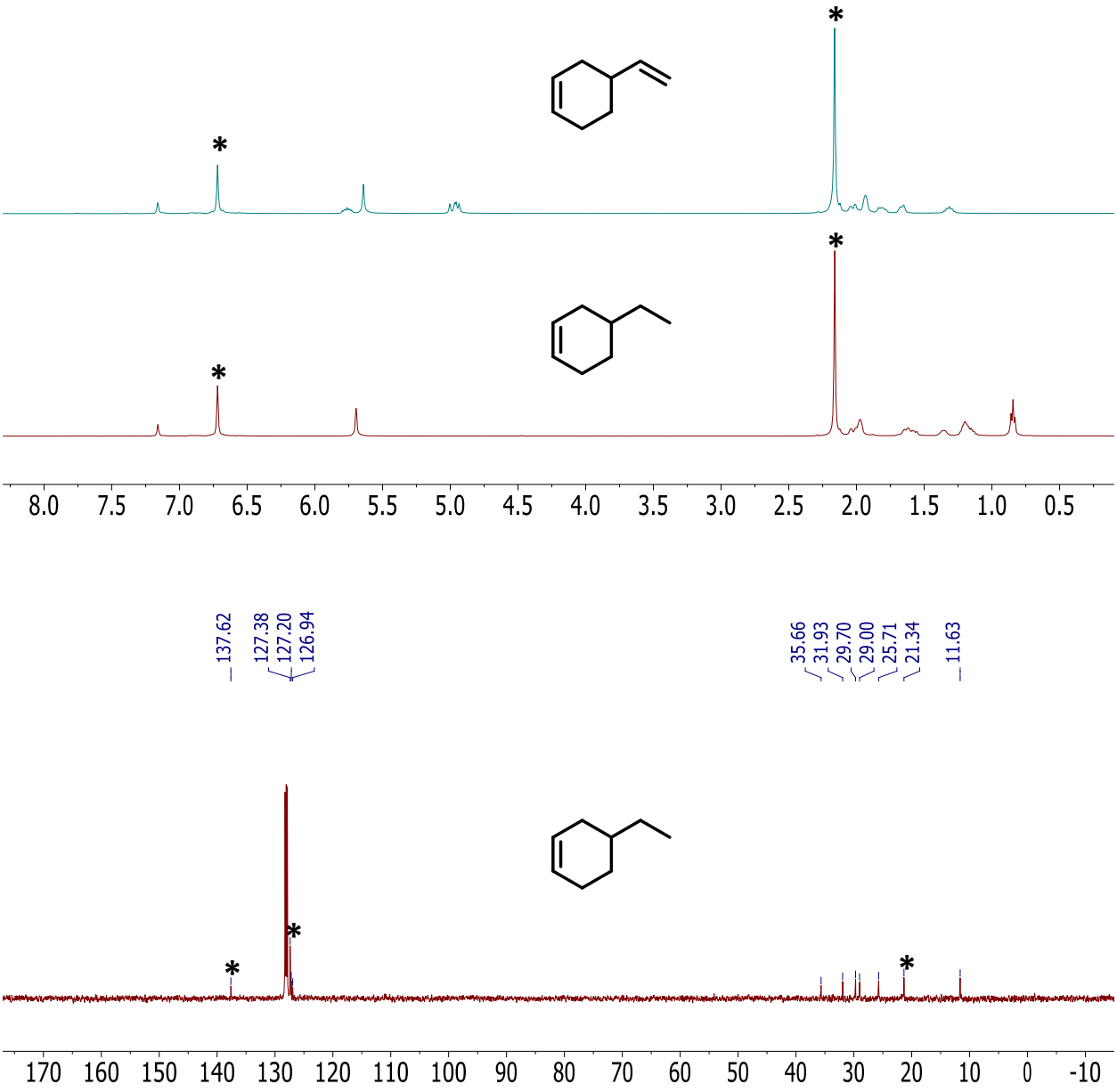

Figure 3.26 ^{1}H NMR (C_6D_6, 500 MHz) spectrum of **(^{Mes}CCC)Co(N_2)(PPh_3)** (2%), mesitylene (*) and 4-vinylcyclohexene under N_2 (top). ^{1}H NMR spectrum of **(^{Mes}CCC)Co(N_2)(PPh_3)** (2%), mesitylene (*) and 4-vinylcyclohexene under 4 atm of H_2 after 2 h (middle). ^{13}C NMR spectrum of **(^{Mes}CCC)Co(N_2)(PPh_3)** (2%), mesitylene (*) and 4-vinylcyclohexene under 4 atm of H_2 after 2 h (bottom).

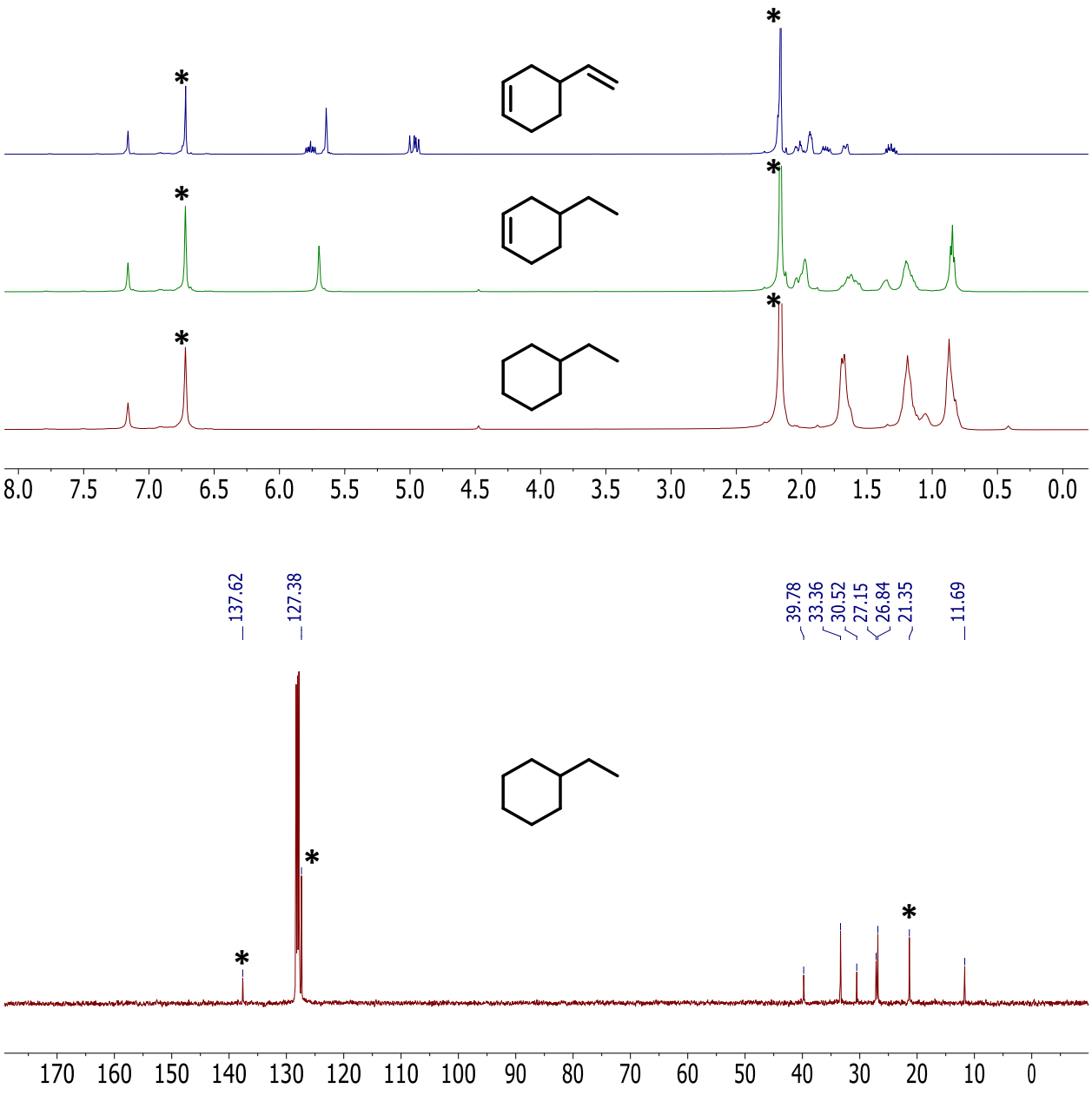

Figure 3.27. ^{1}H NMR (C_6D_6, 500 MHz) spectrum of **(^{Mes}CCC)Co(N_2)(PPh_3)** (2%), mesitylene (*) and 4-vinylcyclohexene under N_2 (top-blue). ^{1}H NMR spectrum of **(^{Mes}CCC)Co(N_2)(PPh_3)** (2%), mesitylene (*) and 4-vinylcyclohexene under 4 atm of H_2 after 2 h (top-green) at rt.). ^{1}H NMR spectrum of **(^{Mes}CCC)Co(N_2)(PPh_3)** (2%), mesitylene (*) and 4-vinylcyclohexene under 4 atm of H_2 after 19 h (top-red) at 60°C. ^{13}C NMR spectrum of **(^{Mes}CCC)Co(N_2)(PPh_3)** (2%), mesitylene (*) and 4-vinylcyclohexene under 4 atm of H_2 after 19 h at 60°C (bottom).

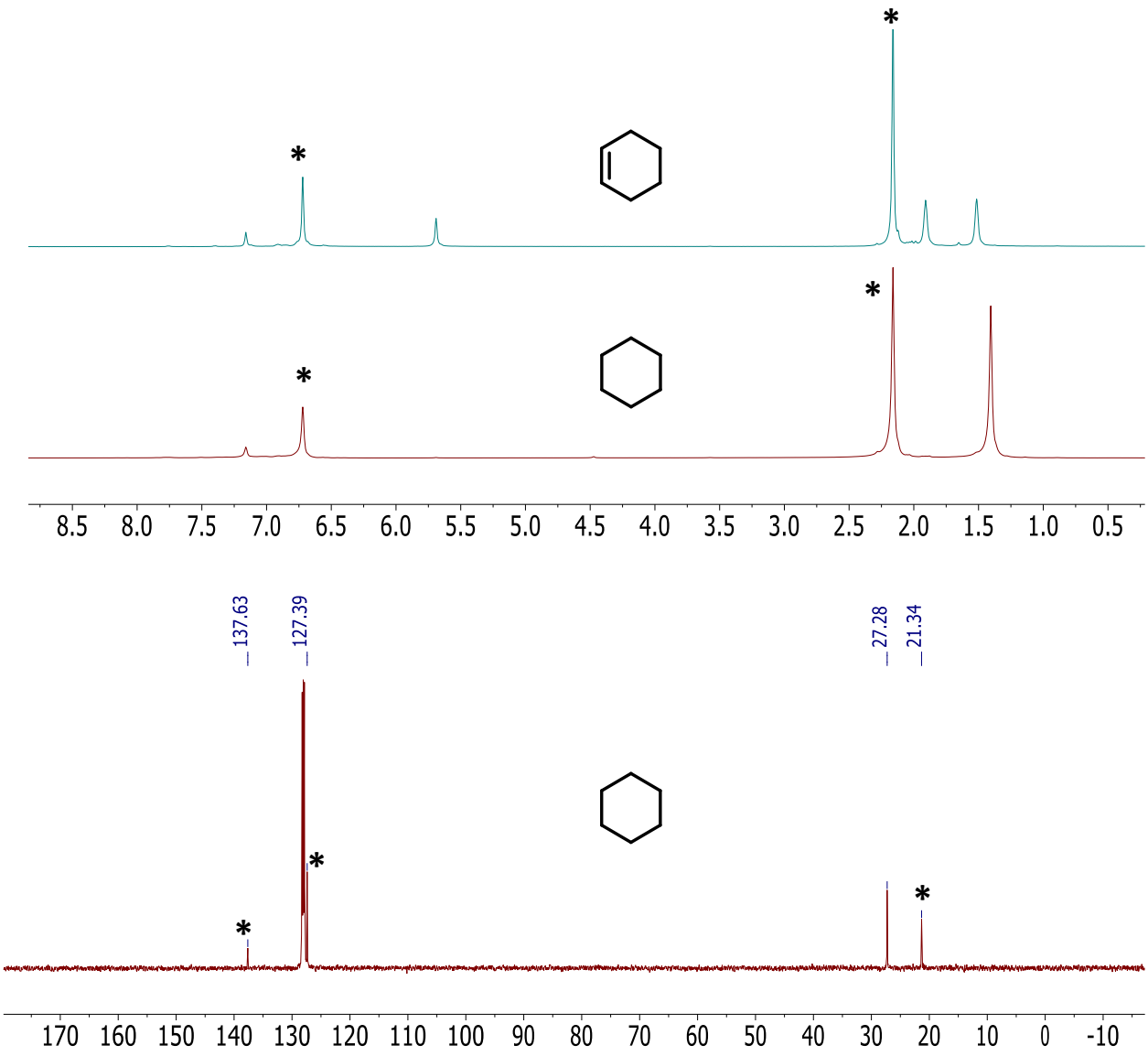

Figure 3.28 ^{1}H NMR (C_6D_6, 500 MHz) spectrum of **(^{Mes}CCC)Co(N_2)(PPh_3)** (2%), mesitylene (*) and cyclohexene under N_2 (top). ^{1}H NMR spectrum **(^{Mes}CCC)Co(N_2)(PPh_3)** (2%), mesitylene (*) and cyclohexene under 4 atm of H_2 after 24 h at 60°C (middle). ^{13}C NMR spectrum of **(^{Mes}CCC)Co(N_2)(PPh_3)** (2%), mesitylene (*) and cyclohexene under 4 atm of H_2 after 24 h at 60°C (bottom).

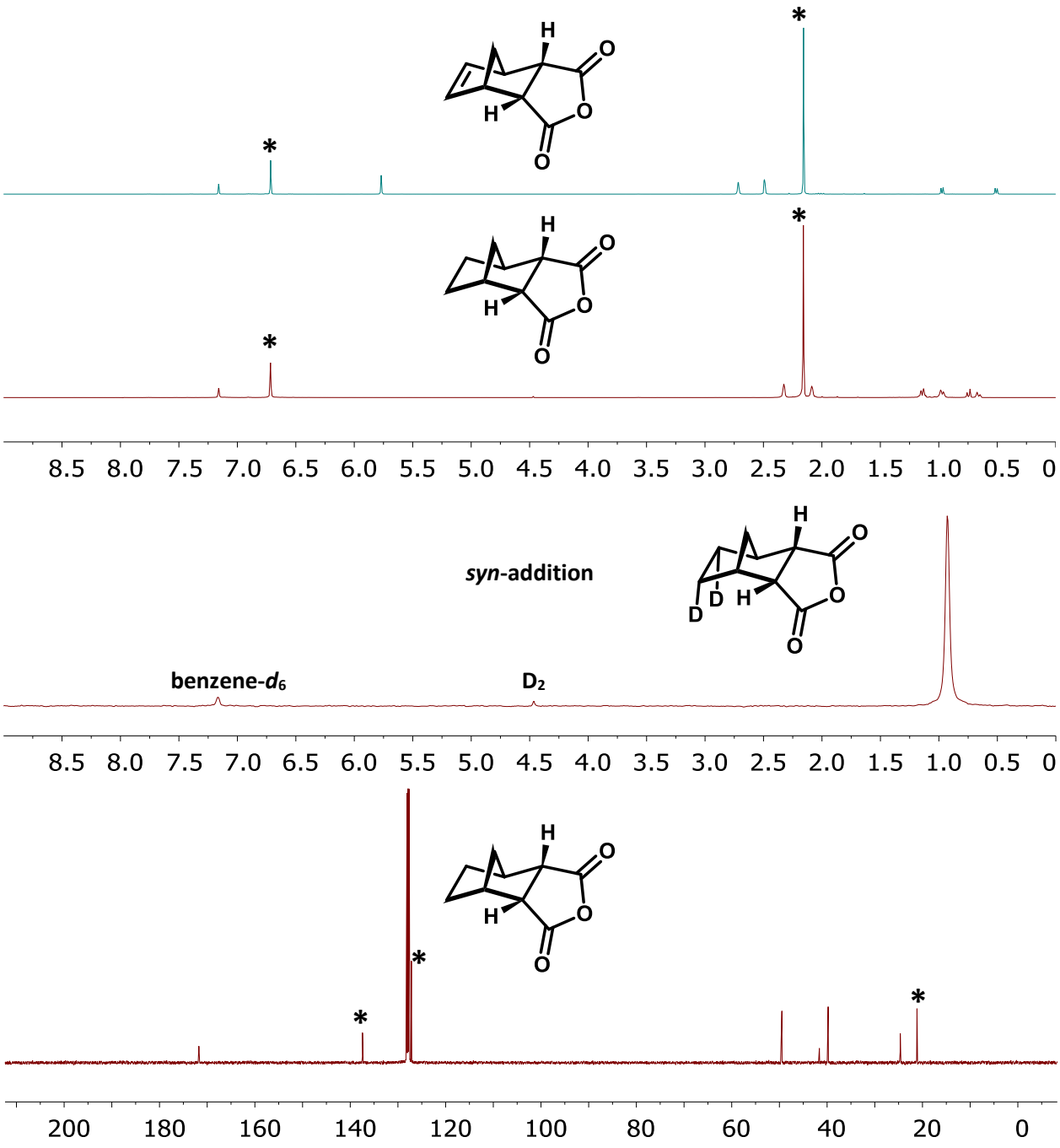

Figure 3.29 ^{1}H NMR (C_6D_6, 500 MHz) spectrum of **(^{Mes}CCC)Co(N_2)(PPh_3)** (2%), mesitylene (*) and *cis*-5-norbornene-*endo*-2,3-dicarboxylic anhydride under N_2 (top-teal). ^{1}H NMR spectrum **(^{Mes}CCC)Co(N_2)(PPh_3)** (2%), mesitylene (*) and *cis*-5-norbornene-*endo*-2,3-dicarboxylic anhydride under 4 atm of H_2 of after 17 h at 60°C (top-red). ^{2}H NMR (C_6H_6, 76.7 MHz) spectrum of **(^{Mes}CCC)Co(N_2)(PPh_3)** (2%), mesitylene (*) and *cis*-5-norbornene-*endo*-2,3-dicarboxylic anhydride under 4 atm of D_2 after 17 h at 60°C (top-red). ^{13}C NMR spectrum of **(^{Mes}CCC)Co(N_2)(PPh_3)** (2%), mesitylene (*) and *cis*-5-norbornene-*endo*-2,3-dicarboxylic anhydride under 4 atm of H_2 after 17h at 60°C (bottom).

Mechanistic studies

Styrene: A standard J. Young NMR tube was charged with a solution of styrene (12 µL, 0.112 mmol) and **(^{Mes}CCC)Co(N_2)(PPh_3)** (0.002 g, 0.0022 mmol) in *ca.* ½ ml of benzene-d_6. The sample was subjected to two freeze-pump-thaw cycles and D_2 gas (1 atm) was added at 77K on a high-vacuum line. The sample was allowed to warm to ambient temperature, resulting in 4 atm of D_2 gas. After letting sample sit at room temperature for 1 hour a ^{1}H NMR was taken (Figure 3.12). Another ^{1}H NMR was taken after 2 h at room temperature and is shown in Figure 3.13.

Cyclohexene: A standard J. Young NMR tube was charged with a solution of cyclohexene (11 µL, 0.112 mmol) and **(^{Mes}CCC)Co(N_2)(PPh_3)** (0.002 g, 0.0022 mmol) in *ca.* ½ ml of benzene-d_6. The sample was subjected to two freeze-pump-thaw cycles and D_2 gas (1 atm) was added at 77K on a high-vacuum line. The sample was allowed to warm to ambient temperature, resulting in 4 atm of D_2 gas. After letting sample sit at 60°C for 1 hour a ^{1}H NMR was taken (Figure 3.27, below-teal). Another ^{1}H NMR was taken after 48 h at 60°C and is shown below in maroon, Figure 3.27.

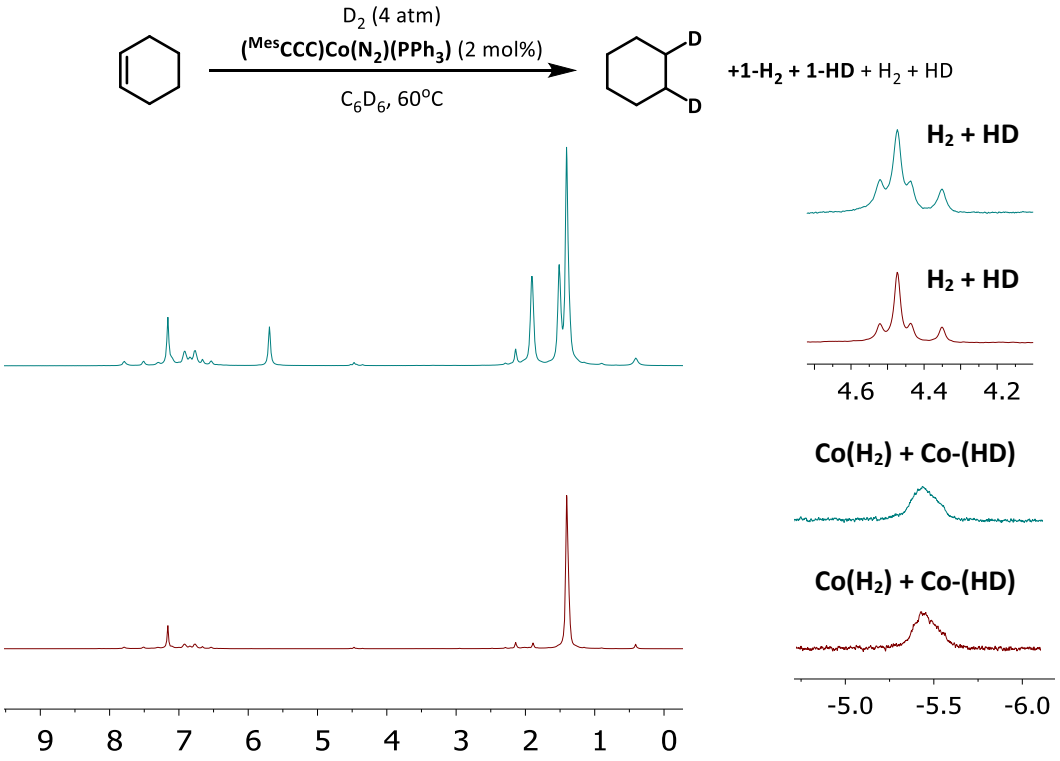

Figure 3.30 ^{1}H NMR (C_6D_6, 500 MHz) spectrum of **(^{Mes}CCC)Co(N_2)(PPh_3)** (2%) and cyclohexene under 4 atm of D_2 after 1 h at 60°C (top). ^{1}H NMR spectrum of **(^{Mes}CCC)Co(N_2)(PPh_3)** (2%) and cyclohexene under 4 atm of D_2 of after 48 h at 60°C (bottom).

A standard J. Young NMR tube was charged with a solution of cyclohexene (12 µL, 0.112 mmol) and **(^{Mes}CCC)Co(N$_2$)(PPh$_3$)** (0.002 g, 0.0022 mmol) in *ca.* ½ ml of benzene. The sample was subjected to two freeze-pump-thaw cycles and D_2 gas (1 atm) was added at 77K on a high-vacuum line. The sample was allowed to warm to ambient temperature, resulting in 4 atm of D_2 gas. After letting sample sit at 60°C for 1 hour a ^{2}H NMR was taken (below-teal). Another ^{2}H NMR was taken after 48 h at 60°C and is shown below in marron.

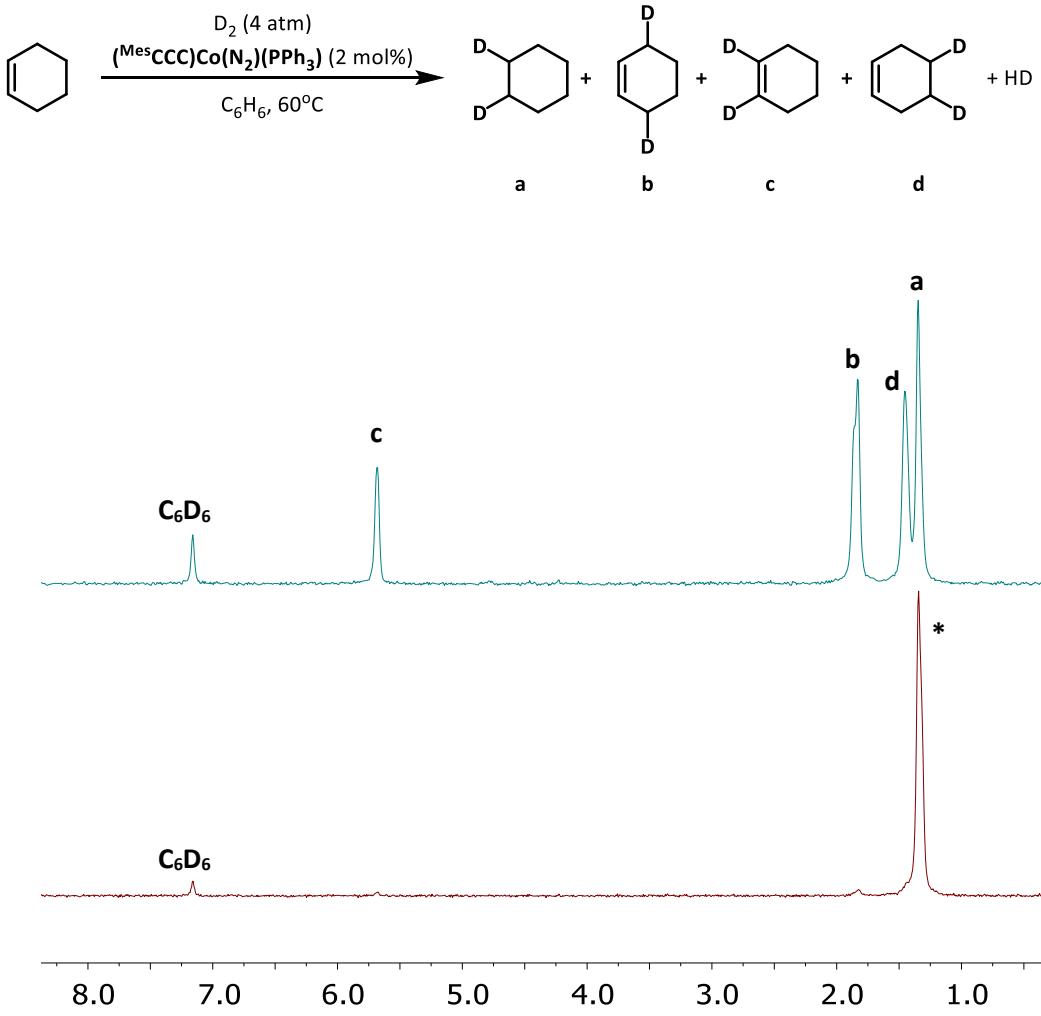

Figure 3.31 ^{1}H NMR (C_6H_6, 76.7 MHz) spectrum of **(^{Mes}CCC)Co(N$_2$)(PPh$_3$)** (2%) and cyclohexene under 4 atm of D_2 after 1 h at 60°C (top). ^{2}H NMR spectrum of **(^{Mes}CCC)Co(N$_2$)(PPh$_3$)** (2%) and cyclohexene under 4 atm of D_2 of after 48 h at 60°C (bottom). (* denotes partially deuterated cyclohexane).

***Para*hydrogen induced polarization NMR studies**

Sample Preparation. A standard J. Young NMR tube was charged with a solution of styrene (6 µL, 0.056 mmol) and **(^{Mes}CCC)Co(N_2)(PPh_3)** (0.001 g, 0.0011 mmol) in *ca.* ½ ml of benzene-d_6. The sample was subjected to two freeze-pump-thaw cycles and *p*-H_2 gas (1 atm) was added at 77K on a high-vacuum line. The sample was kept frozen in liquid nitrogen and warmed to ambient temperature and shaken immediately prior to interesting into the NMR spectrometer. The ALTADENA effect was thus observed. The spectra were collected at 20°C. Increasing the temperature of the probe to 75°C only prolonged the lifetime and intensity of the polarized signals.

NMR Spectrometer. All PHIP NMR data presented herein were collected on a Varian UNITY INOVA 500 NB High-Resolution NMR Console with a 5mm Varian $^1H\{^{13}C/^{15}N\}$ PFG Z probe. All spectra were collected in benzene-d_6 and the residual solvent resonance was referenced to 7.16 ppm. ^1H NMR spectra were recorded using 45° pulse angle. The spectral window of 30 ppm was used in both proton and ^1H-OPSY experiments. ^1H-OPSY NMR data was collected via a double quantum coherence pathway using the pulse sequence below (**Figure 3.32**). The OPSY spectra are anti-phase peaks, and they are generally displayed with absolute mode in the following spectra.[55,56]

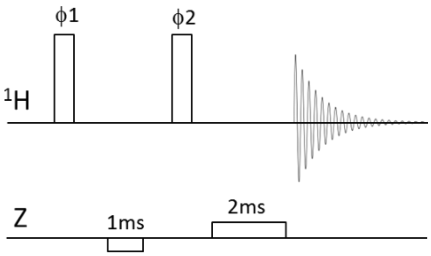

Figure 3.32 Double quantum OPSY pulse sequence (OPSY-d): the vertical bar at ^1H channel represents π/2 pulse. Phase cycle: ϕ1: $(y)_4(x)_4$, ϕ2: $(x)_4(y)_4$, rec: $(x)_4(y)_4$. Z Gradient: 50 G/cm rectangular gradient was used. First gradient was applied for 1ms in the opposite direction of the second gradient which was applied for 2ms. 0.5ms gradient recovery delays were used after each gradient. The acquisition time was 4 seconds and no delay between scans was used.

Generation of *para*-hydrogen. A parahydrogen converter was used to generate the *para*-H_2 enriched hydrogen gas. This consisted of copper tubing filled with a hydrous ferric oxide catalyst that was cooled to 15 K using a closed-cycle ^4He cryostat. A detailed description of the converter can be found in Tom *et al*., which was able to consistently convert naturally occurring hydrogen gas (3:1 *ortho*:*para*) to 99.99% *para*-H_2.[43]

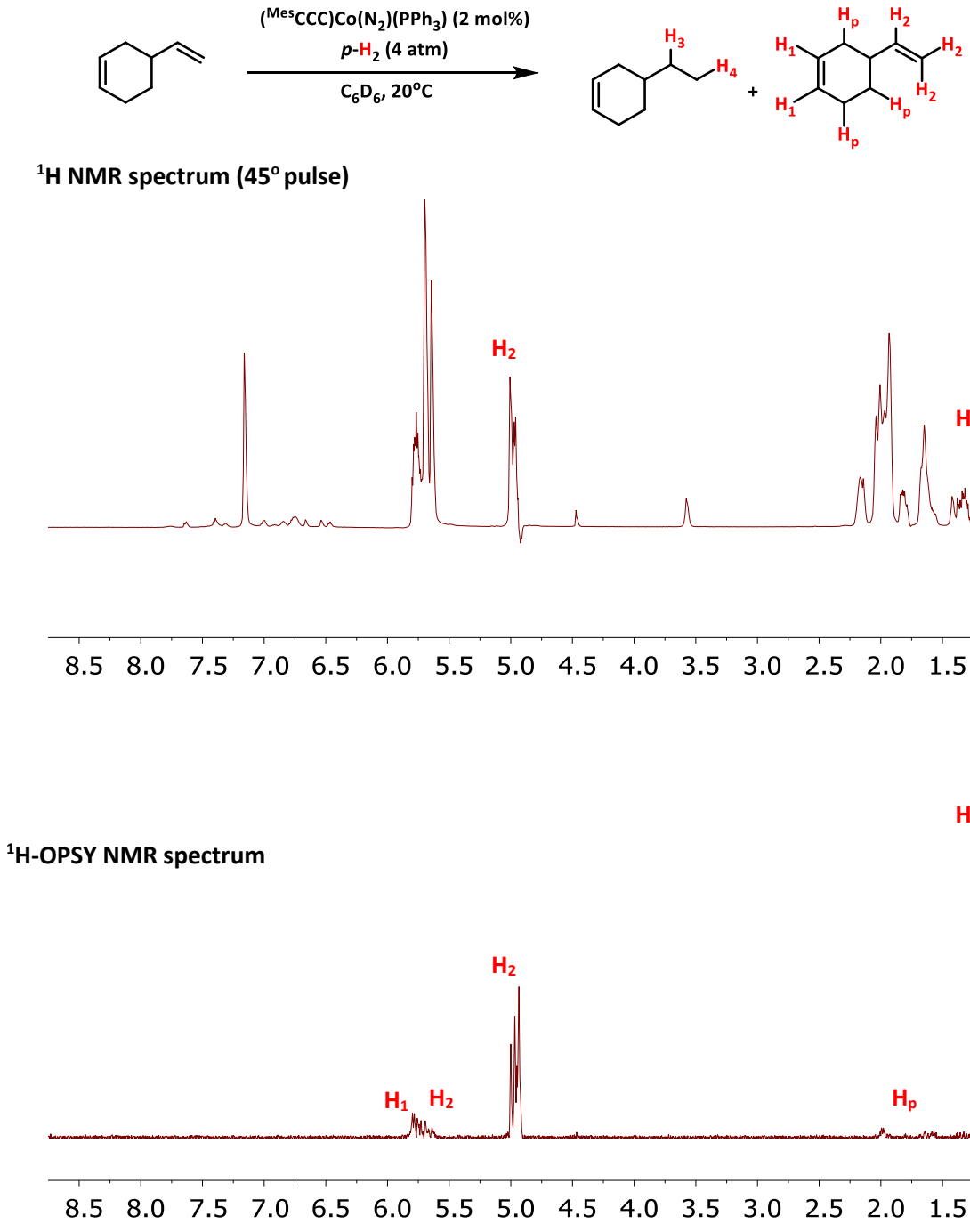

Figure 3.33 ^{1}H NMR (C_6D_6, 500 MHz, 45° pulse) spectrum of **(^{Mes}CCC)Co(N_2)(PPh_3)** (2 mol%) and 4-vinylcyclohexene under 4 atm of *p*-H_2 at 20°C (top). ^{1}H-OPSY NMR spectrum of **(^{Mes}CCC)Co(N_2)(PPh_3)** (2 mol%) and 4-vinylcyclohexene under 4 atm of *p*-H_2 at 20°C (bottom).

3.11 References

1. In Organotransition Metal Chemistry: From Bonding to Reactivity; Hartwig, J. F., Ed.; University Science Books: Sausalito, CA, 2010.
2. In Handbook of Homogenous Hydrogenation; de Vries, J. G., Elsevier, C. J., Eds. Wiley-VCH: New York, 2007.
3. Knijnenburg, Q.; Horton, A. D.; Heijden, H. V. D.; Kooistra, T.M.; Hetterscheid, D. G. H.; Smits, J. M. M.; Bruin, B.; Budzelaar, P. H. M.; Gal, A. W. Olefin hydrogenation using diimne pyridine complexes of Co and Rh. *J. Mol. Catal. A: Chem.* **2005**, *232*, 151−159.
4. Friedfeld, M. R.; Shevlin, M.; Margulieux, G. W.; Campeau, L.-C.; Chirik, P. J. Cobalt-Catalyzed Enantioselective Hydrogenation of Minimally Functionalized Alkenes: Isotopic Labeling Provides Insight into the Origin of Stereoselectivity and Alkene Preferences. *J. Am. Chem. Soc.* **2016**, *138*, 3314−3324.
5. Chirik, P. J. Iron- and Cobalt-Catalyzed Alkene Hydrogenation: Catalysis with Both Redox-Active and Strong Field Ligands. *Acc. Chem. Res.* **2015**, *48*, 1687−1695.
6. Jing, Y.; Chen, X.; Yang, X. Computational Mechanistic Study of the Hydrogenation and Dehydrogenation Reactions Catalyzed by Cobalt Pincer Complexes. *Organometallics* **2015**, *34*, 5716− 5722.
7. Zhang, G.; Vasudevan, K. V.; Scott, B. L.; Hanson, S. K. Understanding the Mechanisms of Cobalt-Catalyzed Hydrogenation and Dehydrogenation Reactions. *J. Am. Chem. Soc.* **2013**, *135*, 8668−8681.
8. Zhang, G.; Scott, B. L.; Hanson, S. K. Mild and Homogeneous Cobalt-Catalyzed Hydrogenation of C=C, C=O, and C=N Bonds. *Angew. Chem., Int. Ed.* **2012**, *51*, 12102−12106.
9. Lin, T.-P.; Peters, J. C. Boryl–Metal Bonds Facilitate Cobalt/Nickel-Catalyzed Olefin Hydrogenation. *J. Am. Chem. Soc.* **2014**, *136*, 13672− 13683.
10. Lin, T.-P.; Peters, J. C. Boryl-Mediated Reversible H_2 Activation at Cobalt: Catalytic Hydrogenation, Dehydrogenation, and Transfer Hydrogenation. *J. Am. Chem. Soc.* **2013**, *135*, 15310− 1531.
11. Friedfeld, M. R.; Margulieux, G. W.; Schaefer, B. A.; Chirik, P. J. Bis(phosphine)cobalt Dialkyl Complexes for Directed Catalytic Alkene Hydrogenation. *J. Am. Chem. Soc.* **2014**, *136*, 13178−13181.
12. Ingleson, M.; Fan, H.; Pink, M.; Tomaszewski, J.; Caulton, K. Three-Coordinate Co(I) Provides Access to Unsaturated Dihydrido-Co(III) and Seven-Coordinate Co(V). *J. Am. Chem. Soc.* **2006**, *128*, 1804−1805.

13. Bart, S. C.; Lobkovsky, E.; Chirik, P. J. Preparation and Molecular and Electronic Structures of Iron(0) Dinitrogen and Silane Complexes and Their Application to Catalytic Hydrogenation and Hydrosilation. *J. Am. Chem. Soc.* **2004**, *126*, 13794−13807.
14. Lee, Y.; Kinney, A. R.; Hoffman, B. M.; Peters, J. C. Characterization of a Non-classical Dihydrogen Adduct of an S = ½ Fe(I) Center. *J. Am. Chem. Soc.* **2011**, *133*, 16366−16369.
15. Fong, H.; Peters, J. C. Hydricity of an Fe-H Species and Catalytic CO_2 Hydrogenation. *Inorg. Chem.* **2015**, *54*, 5124−5135.
16. Liu, T.; Wang, X.; Hoffmann, C.; DuBois, D. L.; Bullock, R. M. Heterolytic Cleavage of Hydrogen by an Iron Hydrogenase Model: An Fe-H···H-N Dihydrogen Bond Characterized by Neutron Diffraction. *Angew. Chem., Int. Ed.* **2014**, *53*, 5300−5304
17. He, T.; Tsvetkov, N. P.; Andino, J. G.; Gao, X.; Fullmer, B. C.; Caulton, K. G. Mechanism of Heterolysis of H_2 by an Unsaturated d^8 Nickel Center: via Tetravalent Nickel? *J. Am. Chem. Soc.* **2010**, *132*, 910−911.
18. Harman, W. H.; Lin, T.-P.; Peters, J. C. A d^{10} Ni-(H_2) Adduct as an Intermediate in H-H Oxidative Addition across a Ni-B Bond. *Angew. Chem., Int. Ed.* **2014**, *53*, 1081−1086.
19. Crabtree, R. H. Dihydrogen Complexation. *Chem. Rev.* **2016**, *116*, 8750−8769.
20. Kubas, G. J. Catalytic Processes Involving Dihydrogen Complexes and Other Sigma-bond Complexes. *Catal. Lett.* **2005**, *104*,79−101.
21. Torrent, M.; Sola, M.; Frenking, G. Theoretical Studies of Some Transition-Metal-Mediated Reactions of Industrial and Synthetic Importance. *Chem. Rev.* **2000**, *100*, 439− 493.
22. Esteruelas, M. A.; Oro, L. A. Dihydrogen Complexes as Homogenous Reduction Catalysts. *Chem. Rev.* **1998**, *98*, 577−588.
23. Suess, D. L. M.; Tsay, C.; Peters, J. C. Dihydrogen Binding to Isostructural S = ½ and S = 0 Cobalt Complexes. *J. Am. Chem. Soc.* **2012**, *134*, 14158−14164.
24. Hebden, T. J.; St. John, A. J.; Gusev, D. G.; Kaminsky, W.; Goldberg, K. I.; Heinekey, D. M. Preparation of a dihydrogen complex of cobalt. *Angew. Chem.* **2011**, *123*, 1913− 1916.
25. Ramirez-Cuesta, A. J.; Mitchell, P. C. H.; Parker, S. F. An inelastic neutron scattering study of the interaction of dihydrogen with the cobalt site of a cobalt aluminophosphate catalyst: Two-dimensional quantum rotation of adsorbed dihydrogen. *J. Mol. Catal. A: Chem.* **2001**, *167*, 217−224.

26. Gadd, G. E.; Upmacis, R. K.; Poliakoff, M.; Turner, J. J. Complexes of iron and cobalt containing coordinated molecular dihydrogen: infrared evidence for $Fe(CO)(NO)_2(H_2)$ and $Co(CO)_2(NO)(H_2)$ in liquefied xenon solution. *J. Am. Chem. Soc.* **1986**, *108*, 2547−2552.
27. Solà, M.; Ziegler, T. Theoretical Study on Acetaldehyde and Ethanol Elimination from the Hydrogenation of $CH_3(O)CCo(CO)_3$. *Organometallics* **1996**, *15*, 2611−2618.
28. Versluis, L.; Ziegler, T. Theoretical study on H_2-induced acetaldehyde elimination from cobalt complex $CH_3(O)CCo(CO)_3$. Organometallics **1990**, *9*, 2985−2992.
29. Godard, C.; Duckett, S. B.; Polas, S.; Tooze, R.; Whitwood, A. C. An NMR study of cobalt-catalyzed hydroformylation using *para*-hydrogen induced polarization. *Dalton Trans.* **2009**, 2496−2509.
30. Godard, C.; Duckett, S. B.; Polas, S.; Tooze, R.; Whitwood, A. C. Detection of Intermediates in Cobalt-Catalyzed Hydroformylation Using *para*-Hydrogen-Induced Polarization. *J. Am. Chem. Soc.* **2005**, *127*, 4994−4995.
31. Ibrahim, A. D.; Tokmic, K.; Brennan, M. B.; Kim, D. Matson, E. M.; Nilges, M. J.; Bertke, J. A.; Fout, A. R. Monoanionic bis(carbene) pincer complexes featuring cobalt(I-III) oxidation states. *Dalton Trans.* **2016**, *45*, 9805-9811.
32. Ibrahim, A. D.; Entsminger, S. W.; Zhu, L.; Fout, A. R. A Highly Chemoselective Cobalt Catalyst for the Hydrosilylation of Alkenes using Tertiary Silanes and Hydrosiloxanes. *ACS Catal.* **2016**, *6*, 3589-3593.
33. Desrosiers, P. J.; Cai, L.; Richards, R.; Halpern, J.; Lin, Z. Assessment of the "T1 criterion" for distinguishing between classical and nonclassical transition-metal hydrides: hydride relaxation rates in tris(triarylphosphine)osmium tetrahydrides and related polyhydrides. *J. Am. Chem. Soc.* **1991**, *113*, 4173−4184.
34. Heinekey, D. M.; van Roon, M. Dihydride Complexes of the Cobalt and Iron Group Metals: An Investigation of Structure and Dynamic Behavior. *J. Am. Chem. Soc.* **1996**, *118*, 12134−12140.
35. Heinekey, D. M.; Liegeois, A.; van Roon, M. Cationic Dihydrogen Complexes of Rhodium and Cobalt: A Reinvestigation. *J. Am. Chem. Soc.* **1994**, *116*, 8388−8389.
36. Bianchini, C.; Mealli, C.; Peruzzini, M.; Zanobini, F. Reversible Uptake of Hydrogen and Nitrogen at Cobalt in the Solid State. Influence of the Counter Anion on the Formation of Classical Dihydride vs. Nonclassical η^2-Dihydrogen forms of $[(PP_3)CoH_2]+$. *J. Am. Chem. Soc.* **1992**, *114*, 5905−5906.
37. Bianchini, C.; Mealli, C.; Meli, A.; Peruzzini, M.; Zanobini, F. A Stable η^2-Dihydrogen Complex of Cobalt. Role of the Hydrogen-Hydrogen Interaction in Hydrogen Transfer from Metal to Alkene. *J. Am. Chem. Soc.* **1988**, *110*, 8725−8726.

38. Maltby, P. A.; Schlaf, M.; Steinbeck, M.; Lough, A. J.; Morris, R. H.; Klooster, W. T.; Koetzle, T. F.; Srivastava, R. C. Dihydrogen with Frequency of Motion Near the ^{1}H Larmor Frequency. Solid-State Structures and Solution NMR Spectroscopy of Osmium Complexes *trans*-$[Os(H\cdot\cdot H)X(PPh_2CH_2CH_2PPh_2)_2]+$ (X = Cl, Br). *J. Am. Chem. Soc.* **1996**, *118*, 5396−5407.
39. Doherty, M. D.; Grant, B.; White, P. S.; Brookhart, M. Reactions of H_2 and R_3SiH with Electrophilic Cobalt(III) Alkyl Complexes: Spectroscopic Characterization, Dynamics, and Chemistry of $[Cp^*Co(L)(H)(\eta^2\text{-}H_2)][B(Ar_F)_4]$ and $[Cp^*Co(L)(H)(\eta^2\text{-}HSiR_3)][B(Ar_F)_4]$. *Organometallics* **2007**, *26*, 5950−5960.
40. Heinekey, D. M.; Voges, M. H.; Barnhart, D. M. Rhenium Dihydrogen Complexes with Isonitrile Coligands: Novel Displacement of Chloride by Hydrogen. *J. Am. Chem. Soc.* **1996**, *118*, 10792−10802.
41. Addison, A. W.; Rao, T. N.; Reedijk, J.; Van Rijn, J.; Verschoor, G. C. Synthesis, structure, and spectroscopic properties of copper(II) compounds containing nitrogen–sulphur donor ligands; the crystal and molecular structure of aqua[1,7-bis(N-methylbenzimidazol-2'-yl)-2,6-dithiaheptane]copper(II) perchlorate. *J. Chem. Soc., Dalton Trans.* **1986**, 1349-1356.
42. Widegren, J. A.; Finke, R. G. A review of the problem of distinguishing true homogeneous catalysis from soluble or other metal-particle heterogeneous catalysis under reducing conditions. *J. Mol. Catal. A: Chem.* **2003**, *198*, 317−341
43. Tom, B. A.; Bhasker, S.; Miyamoto, Y.; Momose, T.; McCall, B. J. Producing and quantifying enriched *para*-H_2. *Rev. Sci. Instrum.* **2009**, *80*, 016108.
44. Duckett, S. B.; Mewis, R. E. Application of *Para*hydrogen Induced Polarization Techniques in NMR Spectroscopy and Imaging. *Acc. Chem. Res.* **2012**, *45*, 1247− 1257.
45. Leutzsch, M.; Wolf, L. M.; Gupta, P.; Fuchs, M.; Thiel, W.; Farès, C.; Fürstner, A. Formation of Ruthenium Carbenes by *gem*-Hydrogen Transfer to Internal Alkynes: Implications for Alkyne *trans*-Hydrogenation. *Angew. Chem., Int. Ed.* **2015**, *54*, 12431−12436.
46. Buljubasich, L.; Franzoni, M. B.; Münnemann, K. *para*hydrogen Induced Polarization by Homogeneous Catalysis: Theory and Applications. *Top. Curr. Chem.* **2013**, *338*, 33−74.
47. Aguilar, J. A.; Elliott, P. I. P.; López-Serrano, J.; Adams, R. W.; Duckett, S. D. Only *para*-hydrogen spectroscopy (OPSY), a technique for the selective observation of *para*-hydrogen enhanced NMR signals. *Chem. Commun.* **2007**, 1183−1185.
48. Pravica, M. G.; Weitekamp, D. P. Net NMR alignment by adiabatic transport of parahydrogen addition products to high magnetic field. *Chem. Phys. Lett.* **1988**, *145*, 255−258.

49. Adams, R. W.; Aguilar, J. A.; Atkinson, K. D.; Cowley, M. J.; Elliott, P. I. P.; Duckett, S. B.; Green, G. G. R.; Khazal, I. G.; López- Serrano, J.; Williamson, D. C. Reversible Interactions with para-Hydrogen Enhance NMR Sensitivity by Polarization Transfer. *Science* **2009**, *323*, 1708−1711.
50. Atkinson, K. D.; Cowley, M. J.; Elliott, P. I. P.; Duckett, S. B.; Green, G. G. R.; López-Serrano, J.; Whitwood, A. C. Spontaneous Transfer of Parahydrogen Derived Spin Order to Pyridine at Low Magnetic Field. *J. Am. Chem. Soc.* **2009**, *131*, 13362−13368.
51. Atkinson, K. D.; Cowley, M. J.; Duckett, S. D.; Elliott, P. I. P.; Green, G. G. R.; López-Serrano, J.; Khazal, I. G.; Whitwood, A. C. *Para*-Hydrogen Induced Polarization without Incorporation of *Para*-Hydrogen into the Analyte. *Inorg. Chem.* **2009**, *48*, 663−670.
52. Adams, R. W.; Duckett, S. B.; Green, R. A.; Williamson, D. C.; Green, G. G. R. A theoretical basis for spontaneous polarization transfer in non-hydrogenative *para*hydrogen-induced polarization. *J. Chem. Phys.* **2009**, *131*, 194505.
53. Pangborn, A.B.; Giardello, M.A.; Grubbs, R. H.; Rosen, R. K.; Timmers, F. J. Safe and Convenient Procedure for Solvent Purification. *Organometallics*, **1996**, *15*, 1518−1520.
54. Wietz, I. S.; Rabinovitz, M. The application of C_8K for organic synthesis: reduction of substituted naphthalenes. *J. Chem. Soc. Perkin Trans.* **1993**, *1*, 117-120.
55. Aguilar, J. A.; Adam, R. W.; Duckett, S. B.; Green, G. G. R.; Kandiah, R. Selective detection of hyperpolarized NMR signals derived from para-hydrogen using the Only Para-hydrogen SpectroscopY (OPSY) approach. *J. Magn. Reson.* **2011**, *208*, 49-57.
56. Duckett, S. B.; Green, G. G. R.; Cowley, M. J. Pulse sequencing with hyperpolarisable nuclei. US Patent 20,110,274,626, November 10, 2011.

CHAPTER 4: SEMIHYDROGENATION OF ALKYNES USING A WELL-DEFINED NONCLASSICAL COBALT-H_2 CATALYST: A *PARA*HYDROGEN INDUCED POLARIZATION NMR STUDY INTO THE ORIGIN OF *E*-SELECTIVITY[†]

4.1 Introduction

The semihydrogenation of alkynes to alkenes is a noteworthy transformation in the bulk and fine chemical industries.[1] Heterogeneous systems such as Lindlar's catalyst, Pb-poisoned Pd on $CaCO_3$,[2] are commonly utilized to accomplish this transformation, yielding the corresponding *Z*-alkene. Homogenous counterparts such as Wilkinson's catalyst[3] and the widely utilized cationic Schrock–Osborn rhodium system[4,5] are also capable of the semihydrogenation of alkynes to *Z*-alkenes. However, the formation of *E*-alkenes by means of hydrogenation is much more difficult. This is, in part, due to the nature of H_2 addition, favoring one side of the substrate and thereby adding in a *cis*-manner. Birch-type reductions, which dissolve metals in ammonia, circumvent this challenge by providing good *E*-selectivity; however, the conditions employed for this transformation are incompatible with highly functionalized alkynes. Increased functional group tolerance has been achieved with the use of chromium reagents,[6,7] and more recently, transition-metal systems featuring Ir,[8] Ru,[9] Pd,[10,11] and Co;[12] however, these processes are accompanied by stoichiometric amounts of waste.

Recently, Fürstner[13,14] and Bargon[15] reported *trans*-selective cationic Ru alkyne hydrogenation catalysts, through which direct *trans*-hydrogenation was operative. More commonly, *E*-selectivity is achieved by means of *Z* to *E* isomerization under the catalytic conditions employed. For example, Furukawa and Komatsu[16] reported a tandem heterogeneous catalytic system consisting of Pd_3Pb/SiO_2 for alkyne semihydrogenation and $RhSb/SiO_2$ for *trans*-isomerization yielding *E*-selective products in good yields; however, the need for two catalyst types coupled to the environmental concerns that arise with the use of lead make this process less desirable. A heterobimetallic silver–ruthenium system[17] and an iron pincer catalyst[18] have also been reported for the semihydrogenation of alkynes, with the *Z* to *E* isomerization occurring at elevated temperatures (≥90 °C). The use of atom-economical reagents,[19,20] as well as the reclusion of noble-metal complexes, are important considerations in developing environmentally benign catalytic system.[21,22]

[†] Portions of this chapter are reproduced from the following publications with permission from the authors. Tokmic, K.; Fout, A. R. Alkyne Semihydrogenation with a Well-Defined Nonclassical Co-H_2 Catalyst: A H_2 Spin on Isomerization and *E*-Selectivity. *J. Am. Chem. Soc.* **2016**, *138*, 13700-13705.

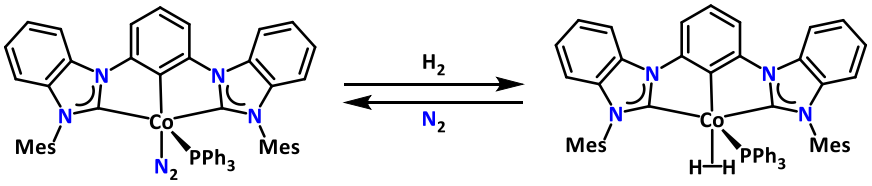

Scheme 4.1 Synthesis of **(^{Mes}CCC)Co(H_2)(PPh_3)** from **(^{Mes}CCC)Co(N_2)(PPh_3)**.

The initial interest in hydrogenation began with the discovery of a catalytically active cobalt dihydrogen complex **(^{Mes}CCC)Co(H_2)(PPh_3)**, (^{Mes}CCC = bis(mesityl-benzimidazol-2-ylidene)phenyl), that was generated from the addition of H_2 to **(^{Mes}CCC)Co(N_2)(PPh_3)**, (Scheme 4.1).[23] In these studies, **(^{Mes}CCC)Co(H_2)(PPh_3)** was demonstrated to be selective toward the hydrogenation of terminal olefins under ambient conditions, while the hydrogenation of internal olefins proceeded at higher temperatures. With the use of ^{1}H, ^{2}H and para-hydrogen (*p*-H_2) induced polarization (PHIP) transfer NMR spectroscopy, catalytically relevant intermediates were identified and the role of **(^{Mes}CCC)Co(H_2)(PPh_3)** in a Co(I)/Co(III) redox process was established. Interested in further examining the catalytic reactivity of the low-valent cobalt bis(carbene) complex using H_2 and informed by the mechanistic insights gleaned from the alkene hydrogenation, the semihydrogenation of alkynes was investigated. It was hypothesized that the catalytic hydrogenation of internal alkynes using **(^{Mes}CCC)Co(N_2)(PPh_3)** and H_2 would result in the formation of internal olefins; if this reaction could proceed at low temperatures then further reduction of the olefin by the cobalt catalyst would be limited.

In this chapter the utility of **(^{Mes}CCC)Co(N_2)(PPh_3)** toward the *E*-selective semihydrogenation of internal alkynes using H_2 under mild conditions is described. A detailed mechanistic understanding, informed by multinuclear and PHIP transfer NMR studies of this process, has elucidated that the formation of *E*-alkenes occurs first by *cis*-hydrogenation of the alkyne, followed by *trans*-isomerization.

4.2 Initial catalytic studies and optimization of reaction conditions

The initial experiments focused on investigating reaction conditions (catalyst loading, temperature, and solvent), as well as conducting appropriate control experiments, using diphenylacetylene as a model substrate (Table 4.1). The use of **(^{Mes}CCC)Co(N_2)(PPh_3)** (2 mol %) in THF at 30 °C and 4 atm of H_2 resulted in 80% conversion to the alkene with a high *E*/*Z* ratio (Table 4.1, entry 1). Lowering the catalyst loading to 1% resulted in increased conversion to the alkene (Table 4.1, entry 2) and changing the solvent to benzene did not affect the outcome of the reaction (Table 4.1, entry 3). Furthermore, increasing the temperature in increments of 10 °C only resulted in higher amounts of the alkane product, while the *E*/*Z* ratio of the

Table 4.1 Control experiments and optimization of the semihydrogenation of diphenylacetylene.

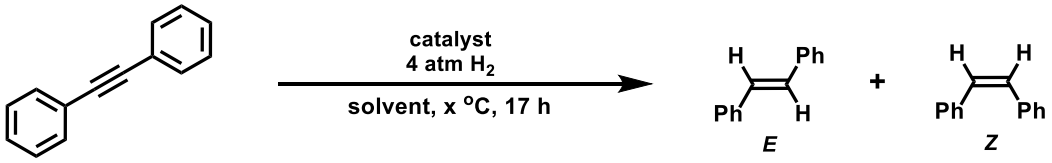

entry	catalyst	mol %	solvent	temp	alkene (conversion)[a]	*E/Z*
1	(^{Mes}CCC)Co(N_2)(PPh_3)	2	THF	30 °C	80%*	>99
2	(^{Mes}CCC)Co(N_2)(PPh_3)	1	THF	30 °C	82%*	>99
3	(^{Mes}CCC)Co(N_2)(PPh_3)	1	82%*	30 °C	82%*	>99
4	(^{Mes}CCC)Co(N_2)(PPh_3)	2	THF	40 °C	70%*	>99
5	(^{Mes}CCC)Co(N_2)(PPh_3)	2	THF	50 °C	60%*	>99
6[b]	(^{Mes}CCC)Co(N_2)(PPh_3)	1	THF	30 °C	82%*	>99
7	[H_3(^{Mes}CCC)]Cl_2	2	THF	30 °C	0%	N/A
8	(^{Mes}CCC)CoCl_2py	2	THF	30 °C	0%	N/A
9	(^{Mes}CCC)Co(N_2)(PPh_3) + PPh_3 (1 eq.)	2	THF	30 °C	40%	<1
10	(^{Mes}CCC)Co(N_2)(PPh_3) + PPh_3 (10 eq.)	2	THF	30 °C	0%	N/A
11	(^{Mes}CCC)Co(N_2)(PPh_3) + Hg	2	THF	30 °C	82%*	>99

(*remainder was alkane, [a]measured by GC-MS,[b]1 atm of H_2)

alkene product remained the same (Table 4.1, entries 4 and 5). Lowering the pressure of H_2 to 1 atmosphere did not change the yield of the reaction (Table 4.1, entry 6). In addition, the use of the imidazolium ligand precursor (Table 4.1, entry 7) or catalyst precursors (Table 4.1, entry 8) resulted in no product formation and only starting material was recovered.

To understand the role of phosphine in the catalytic sequence, the equivalents of PPh_3 were varied (Table 4.1, entries 9 and 10). Increasing the amounts of PPh_3 resulted in lower to no conversion of the alkyne to product, likely due to competiting binding of the phosphine and the alkyne to the metal center. Furthermore, to confirm that this reaction is homogeneous,[24] one drop of mercury was added under catalytic conditions, and no change in product outcome was observed (Table 4.1, entry 11).

4.3 Substrate scope

Encouraged by the preliminary studies and utilizing the optimized reaction conditions (THF as the solvent at 30 °C with 4 atm of H_2), the utility of **(^{Mes}CCC)Co(N_2)(PPh_3)** toward the semihydrogenation of an range of substrates bearing a variety of functional groups was investigated (Table 4.2). *Para*-substituted diphenylacetylenes featuring electron-donating and -withdrawing groups (**2b** and **2c**, respectively) proceeded with excellent *E*/*Z* selectivity and good yields. Additionally, an asymmetric *para*-substituted diphenylacetylene featuring a boronate ester and methoxy group (**2e**) was tolerated under these conditions, proceeding in good yields and *E*/*Z* selectivity. Dialkyl-substituted acetylene (**2d**) resulted in the

full conversion to the alkene products with lower selectivity for the *E* isomer; the over-reduced alkane byproducts, however, were not detected by GC-MS or ^{1}H NMR spectroscopy.

The catalytic activity of **(^{Mes}CCC)Co(N$_2$)(PPh$_3$)** toward the reduction of terminal alkynes was examined to understand the limitations of the catalytic system. The attempted hydrogenation of phenylacetylene resulted in catalyst decomposition, and no hydrogenation of the product was observed. Upon employing a protecting group (trimethylsilyl, TMS), **2f**, the reaction proceeded with good *E*/*Z* selectivity and the silyl group remained intact under these conditions, whereas acidic conditions employed in a Pd-catalyzed alkyne reduction[25] resulted in cleavage of the TMS group. The catalytic system was further extended to include methyl, methoxy, and bromo ortho-substituted derivatives (**2g**–**2i**) of **2f**. Interestingly, a derivative featuring an amine group did not proceed well (<1% conversion) under these conditions, likely because of binding of the amine to the metal center. A modification of the reaction conditions by increasing the temperature to 90 °C and lowering the H_2 pressure (1 atm) of the reaction successfully obviated this difficulty, resulting in reduction of the substrate, **2j**, to the *E* product in high yields. Similarly, a substrate bearing a hydroxyl functionality is tolerated, but proceeded with lower *E*/*Z* selectivity (**2k**) under standard reaction conditions. Furthermore, substrates featuring furanyl, thienyl, and imidazolyl groups (**2l**–**2n**) exhibited good yields and excellent *E*/*Z* selectivity under regular reaction conditions. Lastly, we examined the semihydrogenation of a substrate bearing two internal alkynes. Under

Table 4.2 Substrate scope

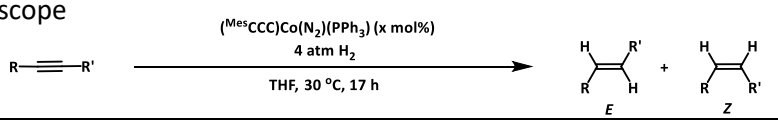

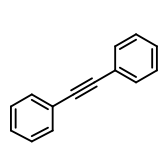

1 mol % (2a)
79% (82%), E:Z > 99

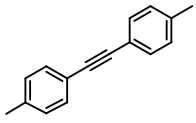

2 mol % (2b)
90% (96%), E:Z > 99

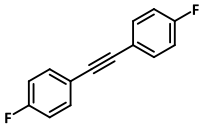

2 mol % (2c)
73% (75%), E:Z > 99

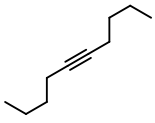

2 mol % (2d)
69% (>99%), E:Z > 81:19

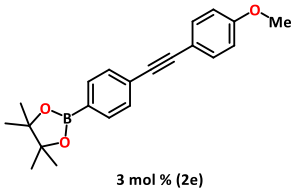

3 mol % (2e)
86% (89%), E:Z > 99

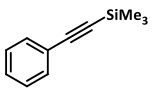

2 mol % (2f)
59% (89%), E:Z 99:1

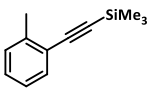

2 mol % (2g)
86% (97%), E:Z > 99

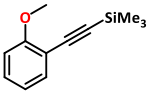

3 mol % (2h)
77% (85%), E:Z > 99

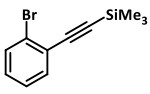

3 mol % (2i)
68% (70%), E:Z > 99

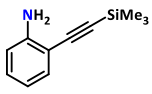

5 mol % (2j)[a]
96% (97%), E:Z 99:1

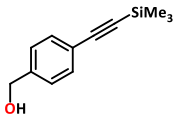

3 mol % (2k)
80% (96%), E:Z 90:10

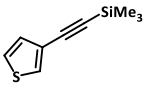

2 mol %(2l)
68% (78%), E:Z > 99

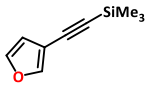

2 mol % (2m)
64% (87%), E:Z > 99

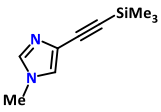

2 mol % (2n)
83% (92%), E:Z > 99

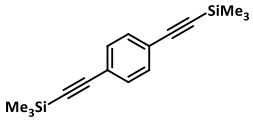

2 mol % (2o)
66% (95%), E,E:Z,Z > 99

Isolated yields are an avgerage of duplicate runs and conversion to alkene is listed in parentheses. [a]Heated to 90°C with 1 atm of H_2.

optimized catalytic conditions, the reduction of **2o** resulted in excellent *E*/*Z* selectivity of both C=C bonds in good yield.

These results clearly show the general applicability of this approach toward the semihydrogenation of a variety of alkynes using H_2 and **(^{Mes}CCC)Co(N_2)(PPh_3)** under ambient conditions. The retention of excellent *E*/*Z* selectivity and yield upon a half-gram scale for the semihydrogenation of diphenylacetylene demonstrates the potential of this system in organic synthesis. However, in some cases less than ideal *E*/*Z* selectivity and over-reduction of the alkenes were also observed. To envision the full potential of this system, mechanistic studies of this process were undertaken, as such studies would promote further progress in limiting over-reduction to alkanes and increasing *E*-selectivity.

4.4 Mechanistic studies – hydrogenation

Fürstner and co-workers[13] reported a ruthenium system that was competent toward the semi-hydrogenation of alkynes to *E*-alkenes. A follow-up NMR study employing PHIP transfer, supplemented by computational work[14] and earlier studies of ionic ruthenium platforms by Bargon and co-workers,[15] provided unambiguous evidence of direct *trans*-hydrogenation of alkynes. Accordingly, to gain insight into the observed semihydrogenation activity of **(^{Mes}CCC)Co(N_2)(PPh_3)** with H_2, multinuclear and PHIP transfer NMR studies were performed. If the *p*-H_2 molecules are transferred in a pairwise manner to magnetically distinctive positions on a substrate while remaining mutually coupled and occur faster than the relaxation rate of the protons, then a characteristic hyperpolarized emission and absorption signals should be observed in the ^{1}H NMR spectrum.[26] This technique would provide direct evidence for *cis*- or *trans*-hydrogenation since the resulting spectrum would provide unequivocal information on the initial addition of the hydrogen atoms to the substrate. In the mechanistic studies, a 45° pulse and a double quantum OPSY[27] (Only Parahydrogen Spectroscopy) filter in the ^{1}H NMR experiment were employed following introduction of *p*-H_2 at low-field (ALTADENA[28] conditions; see chapter 1 for description).

A set of representative alkynes (**2e**, **2f**, **2h**, **2i**, and **2l**) was investigated to examine if *cis*- or *trans*-hydrogenation is operative. The addition of *p*-H_2 (4 atm) to a benzene-d_6 solution containing **(^{Mes}CCC)Co(N_2)(PPh_3)** (2 mol %) and **2f** (Figures 4.1), **2e**, **2h**, **2i**,or **2l** (Figures 4.10−4.13) at 30 and 75 °C[29] each resulted in the enhancement of the resulting alkene product resonances in the ^{1}H NMR spectrum. Based on the coupling constant of the resulting hyperpolarized alkene product of **2f** ($^3J_{HH}$ = 14.4 and 14.0 Hz), it was determined that *cis*-addition occurs under catalytic conditions. Furthermore, **2e**, **2h**, **2i**, and **2l** all displayed alkene coupling constants consistent with cis-addition and no signals corresponding to the *trans*-alkene products were observed by the PHIP transfer NMR experiments in this set of alkynes. In

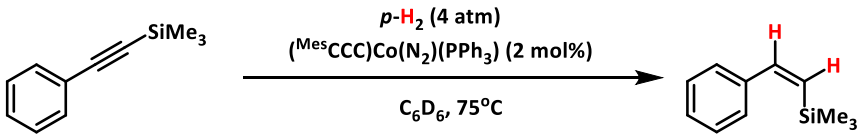

^{1}H-OPSY NMR spectrum – C_6D_6

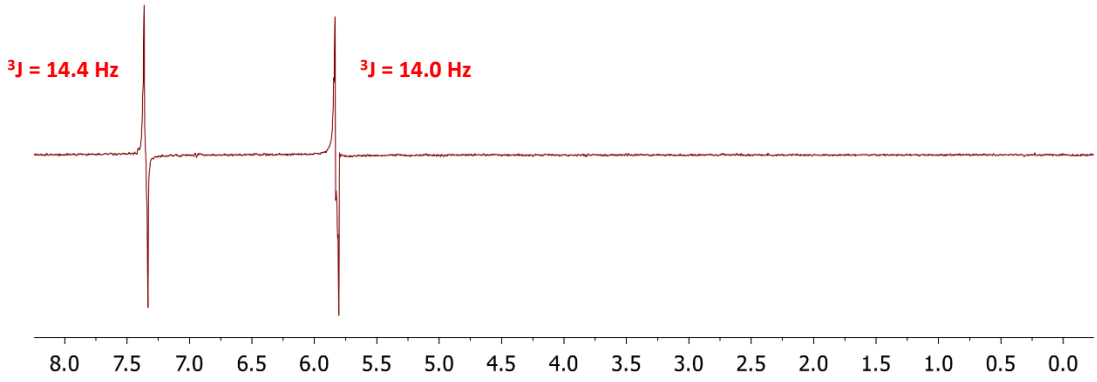

^{1}H-45° NMR spectrum – C_6D_6

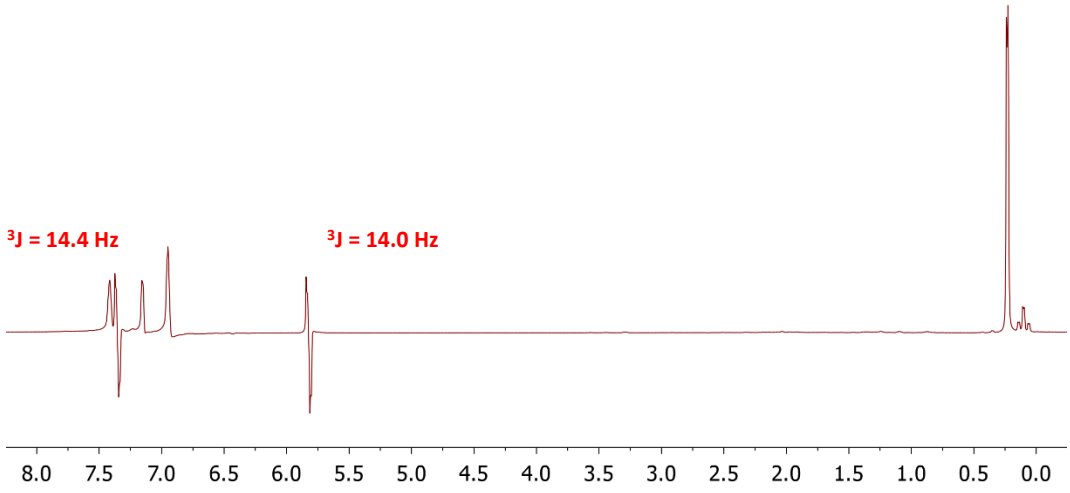

Figure 4.1 ^{1}H-OPSY (top) and ^{1}H NMR using a 45° pulse (C_6D_6) spectra of **(^{Mes}CCC)Co(N_2)(PPh_3)** (2 mol%) and **2f** under 4 atm of *p*-H_2 at 75 °C.

addition, these data also demonstrate that both H atoms of *p*-H_2 add to the alkyne in a concerted fashion, similar to our previously reported olefin hydrogenation with **(^{Mes}CCC)Co(N_2)(PPh_3)**.[23] Since *trans*-hydrogenation is not operative in the catalytic process and the more thermodynamically stable *E*-alkene products are formed throughout, we hypothesized that the generated *cis*-alkenes are converted to *trans*-alkenes via a cobalt-mediated isomerization process. Even though the *Z* to *E* isomerization is thermodynamically favorable, examples of cobalt-mediated systems capable of such processes are rare.[12,30]

4.5 Mechanistic studies – isomerization

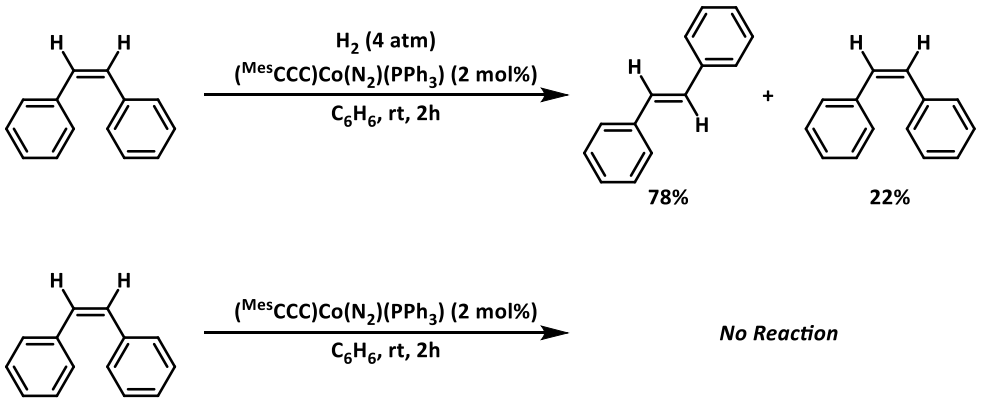

Figure 4.2 *Cis*-stilbene with **(^{Mes}CCC)Co(N_2)(PPh_3)** (2 mol%) under 4 atm of H_2 (top) and *cis*-stilbene with **(^{Mes}CCC)Co(N_2)(PPh_3)** (2 mol%) in the absence of 4 atm of H_2 (bottom).

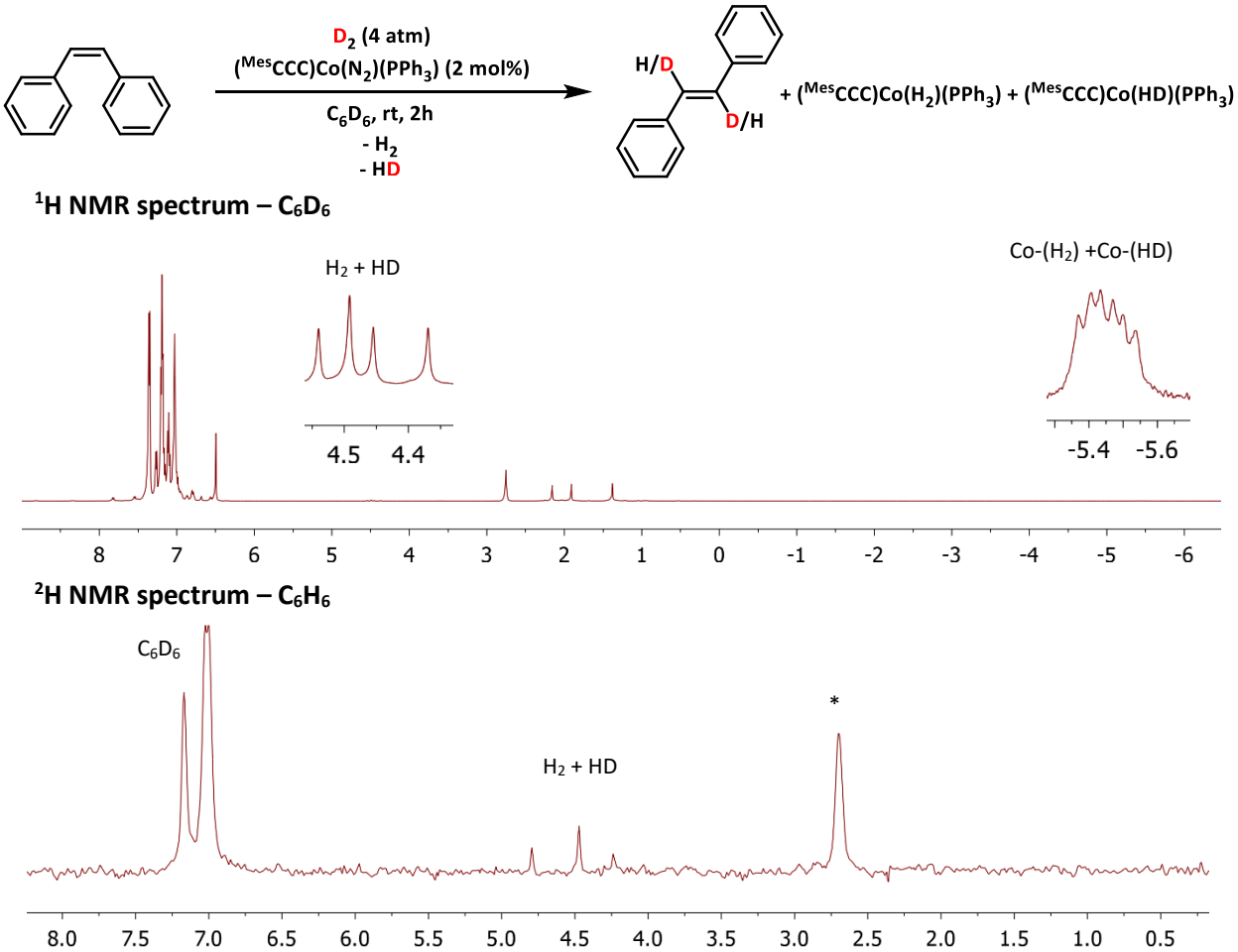

Figure 4.3 ^{1}H NMR spectrum of **(^{Mes}CCC)Co(H_2)(PPh_3)** and *cis*-stilbene under D_2 (4 atm) after 2 h at room temperature (top). ^{2}H NMR spectrum of **(^{Mes}CCC)Co(H_2)(PPh_3)** and *cis*-stilbene under D_2 (4 atm) after 2 h at room temperature (bottom). (* denotes alkane (sp^3-CD_2) protons).

To test our hypothesis, a solution consisting of *cis*-stilbene and **(^{Mes}CCC)Co(N$_2$)(PPh$_3$)** (2 mol %) was stirred at room temperature under 4 atm of H_2 for 2 h (Figure 4.2). The formation of *trans*-stilbene (78%) from *cis*-stilbene was detected by GC-MS (Figure 4.2). When H_2 gas was omitted, no isomerization occurred at 30 °C, but 30% isomerization to *trans*-stilbene was observed after heating the reaction to 80 °C for 18 h. Nevertheless, under catalytic conditions, the involvement of **(^{Mes}CCC)Co(H$_2$)(PPh$_3$)** is clearly evident (*vide infra*) in the formation of *trans*-alkenes.

To understand if β-hydride elimination of a Co(III)-alkyl intermediate may be involved in the isomerization process, isotopic labeling experiments were performed. A solution of **(^{Mes}CCC)Co(N$_2$)(PPh$_3$)** (2 mol %) and *cis*-stilbene under 4 atm of D_2 at room temperature was monitored by ^{1}H and ^{2}H NMR spectroscopy (Figure 4.3). From the ^{2}H NMR spectrum, the incorporation of deuterium into *trans*-stilbene and 1,2-diphenylethane was observed, in addition to the formation of HD gas (Figure 4.3). The ^{1}H NMR spectrum also revealed the formation of H_2 and HD, as well as **(^{Mes}CCC)Co(H$_2$)(PPh$_3$)** and **(^{Mes}CCC)Co(HD)(PPh$_3$)** (Figure 4.3). Furthermore, comparable results were observed when using *cis*-4-octene and 55% deuterium incorporation only into the olefinic region of *trans*-4-octene was observed after 5 h (Figure 4.9). These results support β-hydride elimination from a Co(III)-alkyl intermediate and is the basis for the observed *E*-selectivity in the semihydrogenation of alkynes.

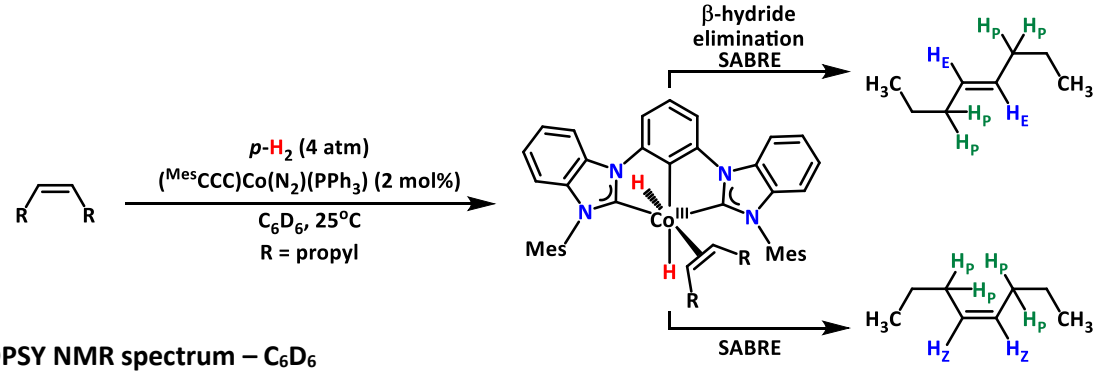

^{1}H-OPSY NMR spectrum – C$_6$D$_6$

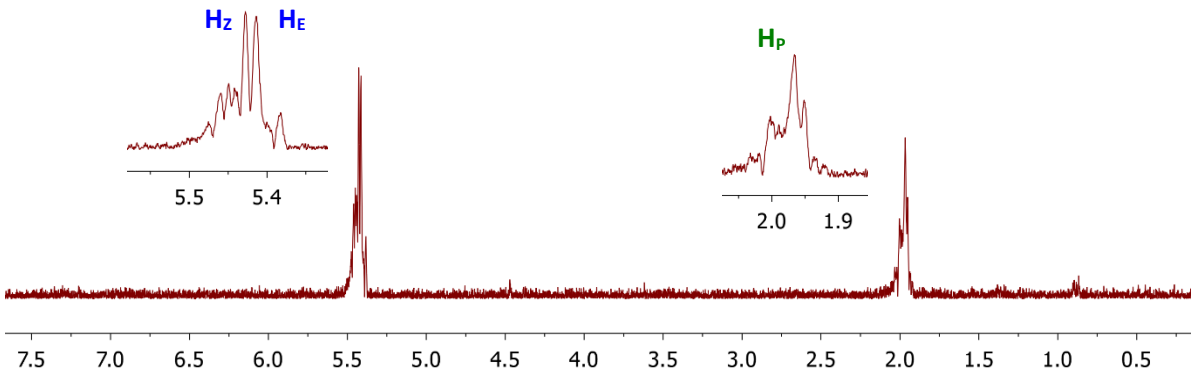

Figure 4.4 ^{1}H-OPSY NMR (C$_6$D$_6$, 500 MHz) spectrum of (^{Mes}CCC)Co(N$_2$)(PPh$_3$) (2 mol %) and *cis*-4-octene under 4 atm of *p*-H_2 at 25 °C.

In an effort to gain further insight into the catalytic reaction, a solution consisting of **(^{Mes}CCC)Co(N_2)(PPh_3)** (2 mol %) and *cis*-4-octene under 4 atm of *p*-H_2 in benzene-d_6 was monitored by ^{1}H-OPSY NMR spectroscopy (Figures 4.4). Polarization of the olefinic and the α-carbon protons of *cis*-4-octene, as well as the isomerized *trans*-4-octene, were observed. Akin to the deuterium studies, reduction of the substrate did not occur. This polarization is due to a SABRE (Signal Amplification By Reversible Exchange) effect.[31-33] This effect polarizes the ^{1}H NMR resonances of the substrate using *p*-H_2 without a chemical modification to the substrate. Duckett and co-workers[31] cited the importance of reversible binding of a substrate for this effect and provided a theoretical rationale for this process.[34]

4.6 Proposed mechanism

Based on the ^{1}H, ^{2}H, and PHIP transfer NMR studies, a comprehensive mechanistic pathway for the catalytic semihydrogenation alkynes using **(^{Mes}CCC)Co(N_2)(PPh_3)** is presented in Figures 4.5. The formation of **(^{Mes}CCC)Co(H_2)(PPh_3)** from **(^{Mes}CCC)Co(N_2)(PPh_3)** results under a H_2 atmosphere, as well as the reverse reaction under a N_2 atmosphere.[23] Inhibition of hydrogenation by the addition of excess PPh_3 supports ligand-substrate exchange between **(^{Mes}CCC)Co(H_2)(PPh_3)** and ***I-1***. The alkyne dihydrogen complex, ***I-1***, is generated in the presence of alkyne and, upon oxidative addition of H_2 onto the metal center,

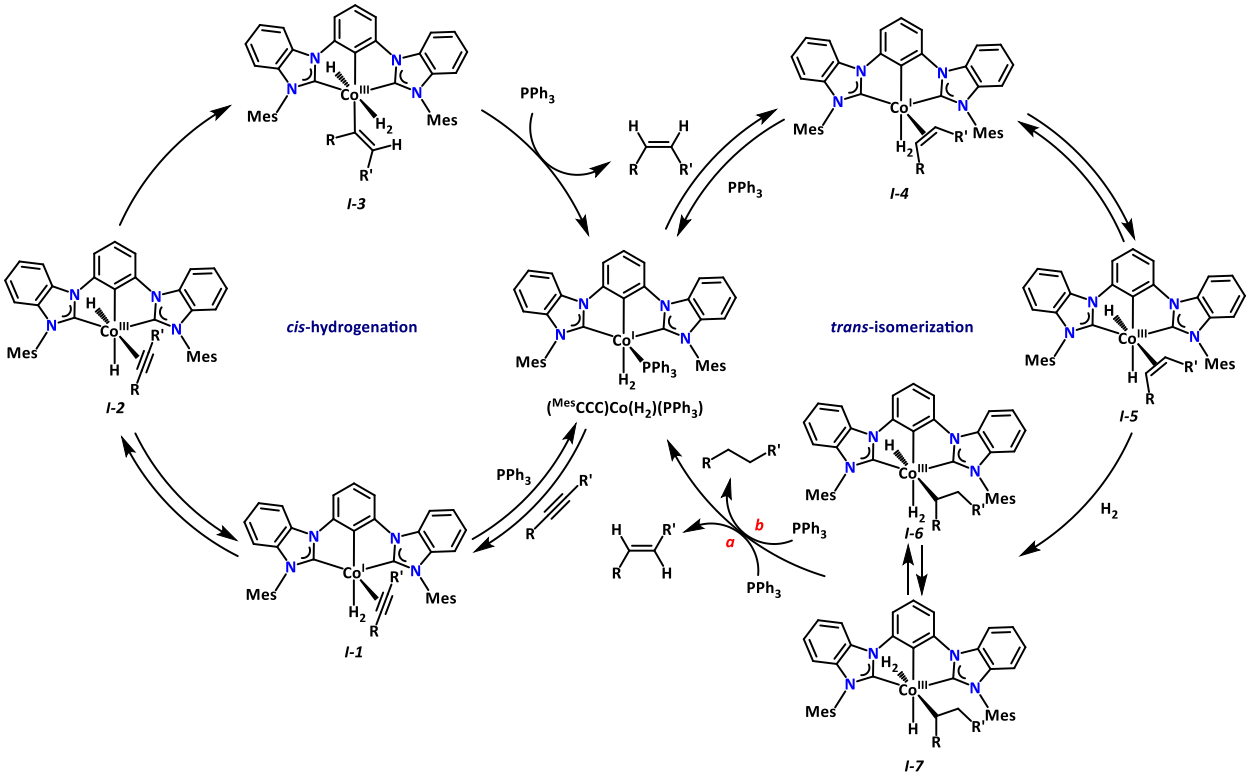

Figure 4.5 Proposed catalytic cycle for the *cis*-hydrogenation of internal alkynes, followed by *trans*-isomerization using **(^{Mes}CCC)Co(N_2)(PPh_3)** (2 mol %) and H_2.

intermediate ***I-2*** results. The observation of the PHIP enhanced *cis*-alkene product requires the formation of intermediate ***I-2***. Next, migratory insertion of the alkyne forms a Co(III)-(η^1-vinyl) hydride/dihydrogen species, ***I-3***. Finally, reductive elimination of the *cis*-alkene and coordination of PPh_3 regenerates the active species, **(^{Mes}CCC)Co(H_2)(PPh_3)**.

Isomerization to the *trans*-alkene product (Figure 4.5, *trans*-isomerization) commences with the coordination of the *cis*-olefin to **(^{Mes}CCC)Co(H_2)(PPh_3)** by phosphine displacement, resulting in ***I-4***. The polarization of 4-octene through the SABRE effect indicates ***I-4*** and ***I-5*** are reversible. Following oxidative addition of H_2 onto the cobalt center, migratory insertion results in the Co(III)-alkyl dihydrogen/hydride species (***I-6*** and ***I-7***). The formation of HD and H_2 established from deuterium studies is a result of the exchange between ***I-6*** and ***I- 7*** and confirms that β-hydride elimination is operative in the isomerization of *cis*-alkene to *trans*-alkene (Figure 4.5, pathway a). This is further supported by deuterium incorporation into the *trans*-olefin exclusively upon *cis*-olefin isomerization using D_2. Therefore, formation of ***I-5*** from ***I-6*** or ***I-7*** does not occur. In competition with β-hydride elimination, reductive elimination of the alkane product (Figure 4.5, pathway b), albeit kinetically slower, is also operative.

4.7 Conclusion

In conclusion, the catalytic utility of **(^{Mes}CCC)Co(N_2)(PPh_3)** was extended toward the semihydrogenation of a broad scope of internal alkynes with excellent selectivity toward *E*-alkenes. Spectroscopic ^{1}H, ^{2}H, and PHIP transfer NMR studies enabled the identification of key reaction intermediates and established that *cis*-hydrogenation occurs first, followed by *trans*-isomerization under a H_2 atmosphere to yield the corresponding *E*-alkenes. Lastly, this system signifies an atom-economical route toward the preparation of a wide variety of *E*-alkenes from alkynes under relatively mild conditions and mechanistic investigations of this process have the potential to further guide development in this area of study.

4.8 Experimental section

General considerations. All manipulations of air- and moisture-sensitive compounds were carried out in the absence of water and dioxygen in an MBraun inert atmosphere drybox under a dinitrogen atmosphere except where specified otherwise. All glassware was oven dried for a minimum of 8 h and cooled in an evacuated antechamber prior to use in the drybox. Solvents for sensitive manipulations were dried and deoxygenated on a Glass Contour System (SG Water USA, Nashua, NH) and stored over 4 Å molecular sieves purchased from Strem following a literature procedure prior to use.[35] Chloroform-*d*, and

benzene-d_6 were purchased from Cambridge Isotope Labs and were degassed and stored over 4 Å molecular sieves prior to use. Lithium hexamethyldisilazane was purchased from Sigma-Aldrich and recrystallized from toluene under an inert atmosphere prior to use. Celite® 545 (J. T. Baker) was dried in a Schlenk flask for 24 h under dynamic vacuum while heating to at least 150˚C prior to use in a glovebox. NMR Spectra were recorded at room temperature on a Varian spectrometer operating at 500 MHz (^{1}H NMR) and 126 MHz (^{13}C NMR) (U500, VXR500, UI500NB) and referenced to the residual $CHCl_3$ and C_6D_5H resonance (δ in parts per million, and *J* in Hz). Potassium graphite (KC_8),[36] **(^{Mes}CCC)CoCl$_2$py**[37] and **(^{Mes}CCC)Co(N$_2$)(PPh$_3$)**[37] were prepared according to literature procedures.

General procedure for alkyne hydrogenation studies. A 50 mL storage vessel charged with **(^{Mes}CCC)Co(N$_2$)(PPh$_3$)** (0.020 g, 0.0225 mmol), alkyne and 4 mL of THF was subjected to two freeze pump thaw cycles and placed under 1 atm of H_2 gas at 77K. The mixture was allowed to warm to room temperature, resulting in 4 atm of H_2 gas. In the case of where 1 atm of H_2 was utilized, upon degassing after 2 freeze pump thaw cycle, the reaction vessel was allowed to warm to room temperature for 30 min, then 1 atm of H_2 gas introduced. The flask was placed in a 30 ^{o}C oil bath to ensure a consistent temperature was used in all catalytic runs. After 17h, the reaction was removed from the oil bath, the H_2 gas was vented and the reaction was analyzed by GCMS to determine conversion. In all cases (**2a** to **2o**), alkyne starting material was not detected by GCMS after the completion of the reaction. Alkene conversion is listed below accompanied by alkane in parenthesis. The THF was removed under reduced pressure and the crude mixture was purified by through a silica plug, eluting with the corresponding solvent (*vide infra*). Selectivity was determined by NMR spectroscopy. 1,2-di-*p*-tolyethyne and 1,2-bis(4-fluorophenyl)ethyne were prepared according to literature procedures.[38] 4-[(Trimethylsilyl)ethynyl]-phenylboronic acid pinacol ester, 3-[(trimethylsilyl)ethynyl]thiophene and *cis*-4-octene were purchased from Alfa Aesar. The remainder of the alkyne substrates and *trans*-4-octene were purchased from Sigma-Aldrich.

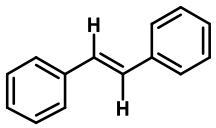

(E)-1,2-diphenylethene: (2a)[39] NMR data (in $CDCl_3$, 25 °C, 500 MHz): ^1H: δ = 7.53 (d, J = 8.0, 4H), 7.37 (t, J = 7.3, 4H), 7.23-7.29 (m, 2H), 7.12 (s, 2H). ^{13}C δ = 137.4, 128.8, 127.8, 126.6. Conversion to alkene was 82% (18). Isolated Yield: (16.0 mg, 0.0888 mmol, 79%) E:Z (>99). **(^{Mes}CCC)Co(N_2)(PPh_3)** (0.001 g, 0.0011 mmol) loading was 1%. Final product was purified by filtering the crude mixture over silica gel and eluting with hexanes. Increased scale: **(^{Mes}CCC)Co(N_2)(PPh_3)** (27 mg, 0.0302 mmol), diphenylacetylene (0.540g, 3.030 mmol) and 108 mL of THF were used. After standard workup, **2a** (435.4 mg, 2.415 mmol, 80 %) was isolated.

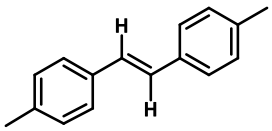

(E)-1,2-di-*p*-tolylethene: (2b)[40] NMR data (in $CDCl_3$, 25 °C, 500 MHz): ^1H: δ = 7.40 (d, J = 8.0, 4H), 7.16 (d, J = 8, 4H), 7.04 (s, 2H), 2.36 (s, 6H). ^{13}C δ = 129.5, 127.7, 126.4, 21.4. Conversion to alkene was 96% (4). Isolated Yield: (10.5 mg, 0.0504 mmol, 90%) E:Z (>99). **(^{Mes}CCC)Co(N_2)(PPh_3)** loading was 2%. Final product was purified by filtering the crude mixture over silica gel and eluting with hexanes.

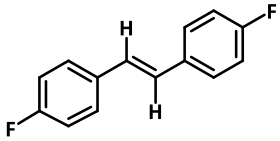

(E)-1,2-bis(4-fluorophenyl)ethene: (2c)[40] NMR data (in $CDCl_3$, 25 °C, 500 MHz): ^1H: δ = 7.44-7.48 (m, 4H), 7.02-7.09 (m, 4H), 6.98 (s, 2H). ^{13}C δ = 128.1, 128.0, 127.4, 115.9, 115.7. ^{19}F δ = -114.63. Conversion to alkene was 75% (25). Isolated Yield: (8.9 mg, 0.0560 mmol, 73%) E:Z (>99). **(^{Mes}CCC)Co(N_2)(PPh_3)** loading was 2%. Final product was purified by filtering the crude mixture over silica gel and eluting with hexanes.

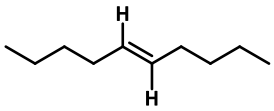

(E)-dec-5-ene: (2d) NMR data (in $CDCl_3$, 25 °C, 500 MHz): ^1H: δ =5.41-5.37 (m, 2H), 2.01-1.94 (m, 4H), 1.37-1.27 (m, 8H), 0.95-0.86 (m, 6H). ^{13}C δ = 130.5, 32.5, 32.0, 22.4, 14.1. Conversion to alkene was 100%. Isolated Yield: (21.7 mg, 0.155 mmol, 69%) E:Z (81:19). **(^{Mes}CCC)Co(N_2)(PPh_3)** loading was 2%. Final product was isolated by filtering the crude mixture over silica gel and eluting with hexanes.

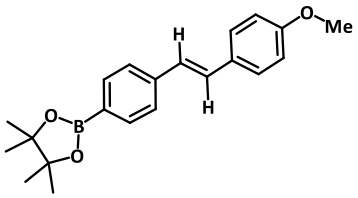

(E)-2-(4-(4-methoxystyryl)phenyl)-4,4,5,5-tetramethyl-1,3,2-dioxaborolane: (2e) NMR data (in $CDCl_3$, 25 °C, 500 MHz): ^{1}H: δ = 7.79 (d, J = 7.5, 2H), 7.52-7.45 (m, 4H), 7.14 (d, J = 16.5, 1 H), 6.99 (d, J = 16. 1 H), 6.91 (d, J = 8.5, 2 H), 3.84 (s, 3 H),1.36 (s, 12 H). ^{13}C δ = 140.5, 135.3, 134.8, 130.3, 129.3, 128.3, 128.0, 126.6, 125.7, 113.7, 83.9, 55.5, 25.0. Conversion to alkene was 89% (11). Isolated Yield: (21.6 mg, 0.0642 mmol, 86%) E:Z (>99). HRMS (ESI), calc. for $C_{21}H_{26}O_3B$ $(M)^+$: calculated 337.1975; found 337.1971. **(^{Mes}CCC)Co(N_2)(PPh_3)** loading was 3%. Final product was purified by filtering the crude mixture over silica gel and eluting with ethyl acetate.

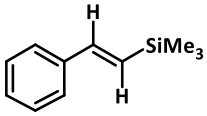

(E)-trimethyl(styryl)silane: (2f)[41] NMR data (in $CDCl_3$, 25 °C, 400 MHz): ^{1}H: δ = 7.45 (d, J = 7.5, 2H), 7.34 (t, J = 7.5, 2H), 7.26 (m, 1H), 6.89 (d, J = 19.0, 1H), 6.50 (d, J = 19.5, 1H), 0.17 (s, 9H). ^{13}C δ = 143.7, 138.4, 129.6, 128.6, 128.1, 126.5, -1.1. Conversion to alkene was 89% (11). Isolated Yield: (11.7 mg, 0.0664 mmol, 59%) E:Z (99:1). **(^{Mes}CCC)Co(N_2)(PPh_3)** loading was 2%. Final product was purified by filtering the crude mixture over silica gel and eluting with hexanes.

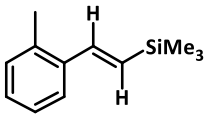

(E)-trimethyl(2-methylstyryl)silane: (2g)[42] NMR data (in $CDCl_3$, 25 °C, 500 MHz): ^{1}H: δ = 7.52 (d, J = 8.5, 1H), 7.11-7.21 (m, 4H), 6.39 (d, J = 19, 1H), 2.39 (s, 3H), 0.18 (s, 9H). ^{13}C δ = 141.4, 137.7, 135.4, 131.5, 130.4, 127.8, 126.2, 125.4, 19.8, -1.02. Conversion to alkene was 97% (3). Isolated yield: (18.24 mg, 0.0958 mmol, 86%) E:Z (>99). **(^{Mes}CCC)Co(N_2)(PPh_3)** loading was 2%. Final product was purified by filtering the crude mixture over silica gel and eluting with hexanes.

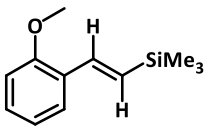

(E)-(2-methoxystyryl)trimethylsilane: (2h)[43] NMR data (in $CDCl_3$, 25 °C, 500 MHz): ^{1}H: δ = 7.54 (d, J = 8.5, 1H), 7.29 (d, J = 19.0, 1H), 7.23 (t, J = 8.5, 1H), 6.94 (t, J = 7.5, 1H), 6.87 (d, J = 8. 1H), 6.46 (d, J = 19.5, 1H), 3.86 (s, 3H), 0.17 (s, 9H). ^{13}C δ = 142.2, 137.9, 130.1, 129.1, 126.3, 120.7, 111.0, 55.6, 0.98. Conversion to alkene was 85% (15). Isolated yield: (13.0 mg, 0.0630 mmol, 85%) E:Z (>99). **(^{Mes}CCC)Co(N_2)(PPh_3)** loading was 3%. Final

product was purified by filtering the crude mixture over silica gel and eluting with hexanes.

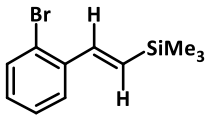

(E)-(2-bromostyryl)trimethylsilane: (2i)[44] NMR data (in $CDCl_3$, 25 °C, 500 MHz): ^{1}H: δ = 7.58 (d, J = 7.5, 1H), 7.54 (d, J = 8.0, 1H), 7.21-7.29 (m, 3H), 7.10 (t, J = 8.5, 1H), 6.45 (d, J = 19, 1H), 0.18 (s, 9H). ^{13}C δ = 142.2, 133.5, 133.0, 129.2, 127.6, 1273,127.0, -1.1. Conversion to alkene was 70% (30). Isolated yield: (9.23 mg, 0.0361 mmol, 68%) E:Z (>99). **(^{Mes}CCC)Co(N_2)(PPh_3)** loading was 3%. Final product was purified by filtering the crude mixture over silica gel and eluting with hexanes.

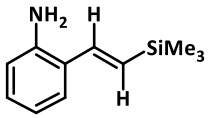

(E)-2-(2-(trimethylsilyl)vinyl)aniline: (2j) NMR data (in $CDCl_3$, 25 °C, 500 MHz): ^{1}H: δ = 7.32 (d, J = 9.0, 2H), 7.07 (t, J = 7.5, 1H), 6.95 (d, J = 19.0, 1H), 6.77 (t, J = 7.3, 1H), 6.67 (d, J = 8.0, 1H), 6.35 (d, J = 19.0, 1H), 3.77 (s, 2H), 0.16 (s, 9H). NMR data (in $CDCl_3$, 25 °C, 400 MHz): ^{13}C δ = 142.2, 139.0, 131.7, 128.8, 127.2, 119.2, 116.4,-1.0. Conversion to alkene was 97% (3). Isolated Yield: (8.74 mg, 0.0457 mmol, 96%) E:Z (>99). **(^{Mes}CCC)Co(N_2)(PPh_3)** loading was 5%. HRMS (ESI), calc. for $C_{11}H_{18}NSi$ $(M)^+$: calculated 192.1209; found 192.1215. Final product was purified by filtering the crude mixture over silica gel and eluting with a ethyl acetate and hexanes mixture (10:90). Reaction was heated to 90^{o}C under 1 atm of H_2 for 17h.

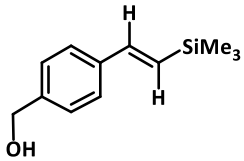

(E)-(4-(2-(trimethylsilyl)vinyl)phenyl)methanol: (2k) NMR data (in $CDCl_3$, 25 °C, 500 MHz): ^{1}H: δ = 7.44 (d, J = 8, 2H), 7.33 (d, J = 8, 1H), 6.87 (d, J = 19.2, 1H), 6.48 (d, J = 19.2, 1H), 4.69 (s, 1H), 4.68 (s, 1H), 0.16 (s, 9H). ^{13}C δ = 143.3, 127.3, 126.7, 65.3, -1.08. Conversion to alkene was 96% (4). Isolated Yield: (12.2 mg, 0.0593 mmol, 80%) E:Z (90:10). HRMS (ESI), calc. for $C_{12}H_{18}OSi$ $(M)^+$: calculated 206.1127; found 206.1126. **(^{Mes}CCC)Co(N_2)(PPh_3)** loading was 3%. The crude product was dissolved in DCM and let stand over molecular sieves in the drybox for 24 h, then the mixture was filtered over silica gel, eluting with DCM.

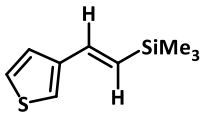

(E)-trimethyl(2-(thiophen-3-yl)vinyl)silane: (2l)[43] NMR data (in $CDCl_3$, 25 °C, 500 MHz): ^{1}H: δ =7.30-7.21 (m, 2H), 7.20 (s, 1H), 6.88 (d, J = 19.2, 1H), 6.26 (d, J = 20.8, 1H), 0.15 (s, 9H).^{13}C δ = 137.5, 129.3, 126.0, 125.0, 122.6, -1.10. Conversion to alkene was 78% (22). Isolated Yield: (13.9 mg, 0.0764 mmol, 68%) E:Z (>99). **(^{Mes}CCC)Co(N_2)(PPh_3)** loading was 2%. Final product was isolated by filtering the crude mixture over silica gel and eluting with hexanes.

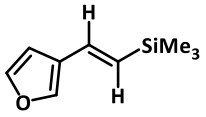

(E)-(2-(furan-3-yl)vinyl)trimethylsilane: (2m)[43] NMR data (in $CDCl_3$, 25 °C, 500 MHz): ^{1}H: δ = 7.44 (s, 1H), 7.36 (s, 1H), 6.75 (d, J = 19.2, 1H), 6.59 (s, 1H), 6.12 (d, J = 18.8, 1H), 0.13 (s, 9H). ^{13}C δ = 143.7, 140.8, 133.3, 129.2, 107.4, -1.11. Conversion to alkene was 87% (13). Isolated Yield: (11.9 mg, 0.0714 mmol, 64%) E:Z (>99). **(^{Mes}CCC)Co(N_2)(PPh_3)** loading was 2%. Final product was purified by filtering the crude mixture over silica gel and eluting with hexanes.

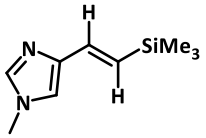

(E)-1-methyl-5-(2-(trimethylsilyl)vinyl)-1H-imidazole: (2n) NMR data (in $CDCl_3$, 25 °C, 500 MHz): ^{1}H: zδ = 7.39 (s, 1H), 7.25 (s, 1H), 6.67 (d, J = 19.0, 1H), 6.30 (d, J = 19, 1H), 3.68 (s, 3H), 0.18 (s, 9H). ^{13}C δ = 138.8, 130.0, 129.0, 128.1, 32.1, -1.2. Conversion to alkene was 92% (8). Isolated Yield: (16.8 mg, 0.0930 mmol, 83%) E:Z (>99). HRMS (ESI), calc. for $C_9H_{17}NSi$ $(M)^+$: calculated 181.1161; found 181.1161. **(^{Mes}CCC)Co(N_2)(PPh_3)** loading was 2%. Final product was purified by filtering the crude mixture over silica gel and eluting with acetone.

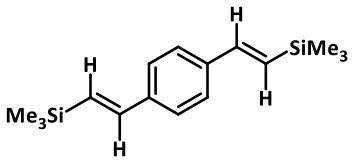

1,4-bis((E)-2-(trimethylsilyl)vinyl)benzene: (2o)[42] NMR data (in $CDCl_3$, 25 °C, 500 MHz): ^{1}H: δ = 7.40 (s, 4H), 6.86 (d, J = 19, 2H), 6.49 (d, J = 19. 2 H), 0.17 (s, 18H). ^{13}C δ = 143.3, 138.1, 129.7, 126.7, -1.07. Conversion to alkene 55% and alkene:alkane mixture was 40% (5). Isolated Yield of both compounds: (20.0 mg, 0.0739 mmol, 66%) E:Z (>99). **(^{Mes}CCC)Co(N_2)(PPh_3)** loading was 2%. Final product was purified by filtering the crude mixture over silica gel and eluting with hexanes.

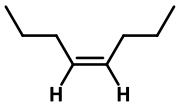

***cis*-4-octene:** NMR data (in C_6D_6, 25 °C, 500 MHz): ^{1}H: δ = 5.44 (t, J = 5.1, 2H), 2.01 (q, J = 6.6, 4H), 1.35 (sext, J = 7.3. 4 H), 0.89 (t, J = 7.4, 6H).

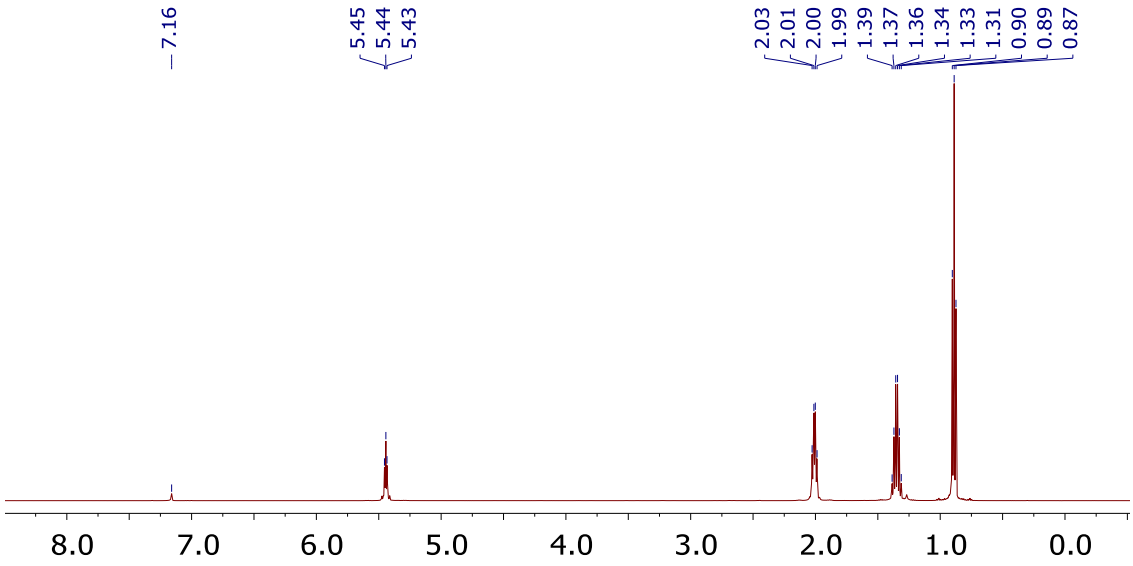

Figure 4.6 ^{1}H NMR (C_6D_6, 500 MHz, 25°C) spectrum of *cis*-4-octene.

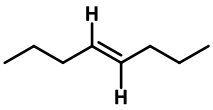

***trans*-4-octene:** NMR data (in C_6D_6, 25 °C, 500 MHz): ^{1}H: δ = 5.42 (t, J = 5.0, 2H), 1.97 (q, J = 6.2, 6H), 1.36 (sext, J = 7.3. 6 H), 0.89 (t, J = 7.4, 9H).

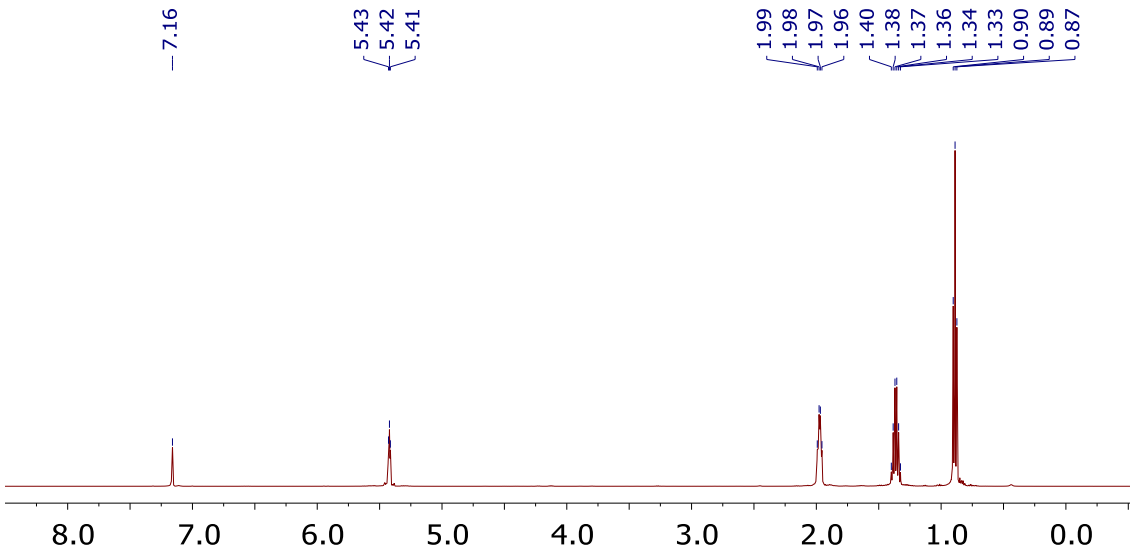

Figure 4.7 ^{1}H NMR (C_6D_6, 500 MHz, 25°C) spectrum of *trans*-4-octene.

Mechanistic studies

Deuterium NMR studies using *cis*-stilbene.

A standard J. Young NMR tube was charged with a solution of *cis*-stilbene (20 µL, 0.112 mmol) and **(^{Mes}CCC)Co(N_2)(PPh_3)** (0.002 g, 0.0022 mmol) in *ca.* ½ ml of benzene-d_6. The sample was subjected to two freeze-pump-thaw cycles and D_2 gas (1 atm) was added at 77K on a high-vacuum line. The sample was warmed to ambient temperature, resulting in 4 atm of D_2 gas. After letting sample sit at room temperature for 2 hours a ^{1}H NMR was taken. The ^{1}H NMR spectrum is shown in Figure 4.3.

A standard J. Young NMR tube was charged with a solution of *cis*-stilbene (20 µL, 0.112 mmol) and **(^{Mes}CCC)Co(N_2)(PPh_3)** (0.002 g, 0.0022 mmol) in *ca.* ½ ml of benzene. The sample was subjected to two freeze-pump-thaw cycles and D_2 gas (1 atm) was added at 77K on a high-vacuum line. The sample was warmed to ambient temperature, resulting in 4 atm of D_2 gas. After letting sample sit at room temperature for 2 hours a ^{2}H NMR was taken. The ^{2}H NMR spectrum is shown in Figure 4.3.

Cis-4-octene

A standard J. Young NMR tube was charged with a solution of *cis*-4-octene (17 µL, 0.112 mmol), mesitylene (15.5 µL, 0.112 mmol) and **(^{Mes}CCC)Co(N$_2$)(PPh$_3$)** (0.002 g, 0.0022 mmol) in *ca.* ½ ml of benzene-d_6. The sample was subjected to two freeze-pump-thaw cycles and D_2 gas (1 atm) was added at 77K on a high-vacuum line. The sample was warmed to ambient temperature, resulting in 4 atm of D_2 gas. After letting sample sit at room temperature for 5 hours a ^{1}H NMR was taken (Figure 4.8). Deuterium incorporation into *trans*-4-octene was determined by use of mesitylene as internal standard. Found 55% deuterium incorporation into *trans*-4-octene.

***Para*hydrogen induced polarization NMR studies**

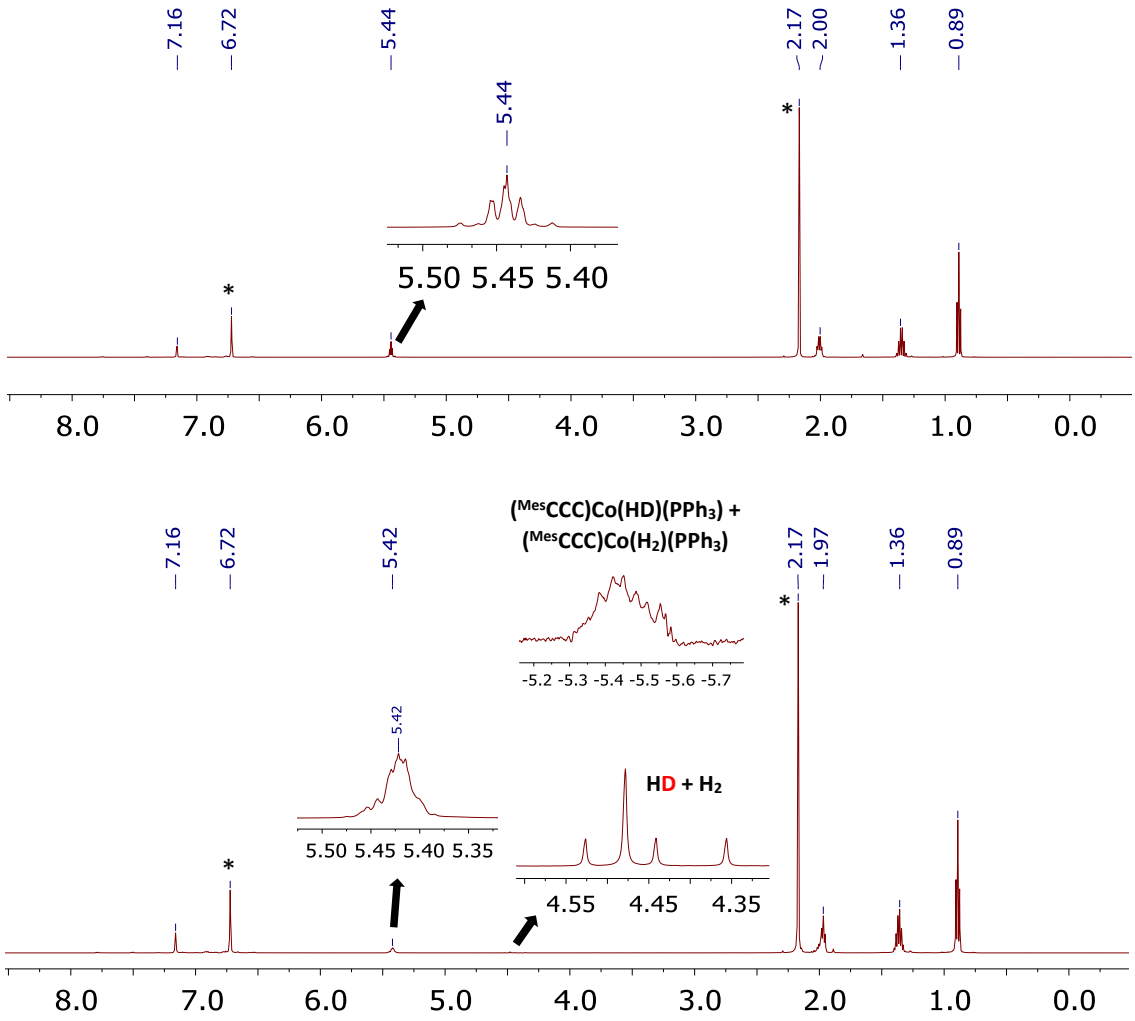

Figure 4.8 ^{1}H NMR (C_6D_6, 500 MHz) spectrum of **(^{Mes}CCC)Co(N$_2$)(PPh$_3$)** (2 mol%) and *cis*-4-octene under 4 atm of D_2 after 5 h at room temperature (bottom). (Top denotes starting **(^{Mes}CCC)Co(N$_2$)(PPh$_3$)** and *cis*-4-octene). (*denotes mesitylene.)

Sample preparation. A standard J. Young NMR tube was charged with a solution of alkyne and **(^{Mes}CCC)Co(N_2)(PPh_3)** (0.001 g, 0.0011 mmol, 2 mol%) in *ca.* ½ mL of benzene-d_6. The sample was subjected to two freeze-pump-thaw cycles and *p*-H_2 gas (1 atm) was added at 77K on a high-vacuum line. The sample was kept frozen in liquid nitrogen and warmed to ambient temperature and shaken immediately prior to interesting into the NMR spectrometer. The ALTADENA effect was thus observed. The spectra were collected at 30°C. Increasing the temperature of the probe to 75°C only prolonged the lifetime and intensity of the polarized signals. Upon signal decay from *p*-H_2 being consumed in solution, the signal from PHIP was regained by removing, shaking, and inserting the J. Young NMR tube from the NMR spectrometer. PASADENA effect was observed while using trimethyl(phenylethynyl)silane as a substrate.

NMR spectrometer. All PHIP NMR data presented herein were collected on a Varian UNITY INOVA 500 NB High-Resolution NMR Console with a 5mm Varian $^1H\{^{13}C/^{15}N\}$ PFG Z probe. All spectra were collected in benzene-d_6 and the residual solvent resonance was referenced to 7.16 ppm. ^1H NMR spectra were recorded using 45° pulse angle. The spectral window of 30 ppm was used in both proton and ^1H-OPSY experiments. ^1H-OPSY NMR data was collected via a double quantum coherence pathway using the pulse sequence below (**Figure 4.9**). The OPSY spectra are anti-phase peaks, and they are generally displayed with absolute mode in the following spectra.[45,46]

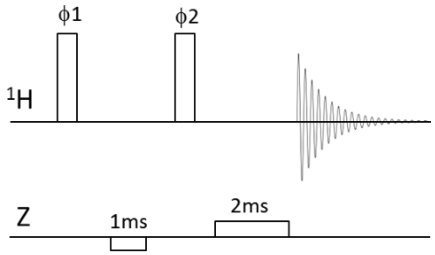

Figure 4.9 Double quantum OPSY pulse sequence (OPSY-d): the vertical bar at ^1H channel represents $\pi/2$ pulse. Phase cycle: $\phi1$: $(y)_4(x)_4$, $\phi2$: $(x)_4(y)_4$, rec: $(x)_4(y)_4$. Z Gradient: 50 G/cm rectangular gradient was used. First gradient was applied for 1ms in the opposite direction of the second gradient which was applied for 2ms. 0.5ms gradient recovery delays were used after each gradient. The acquisition time was 4 seconds and no delay between scans was used.

Generation of *para*-hydrogen. A parahydrogen converter was used to generate the *para*-H_2 enriched hydrogen gas. This consisted of copper tubing filled with a hydrous ferric oxide catalyst that was cooled to 15 K using a closed-cycle ^{4}He cryostat. A detailed description of the converter can be found in Tom *et al*., which was able to consistently convert naturally occurring hydrogen gas (3:1 *ortho*:*para*) to 99.99% *para*-H_2.[47]

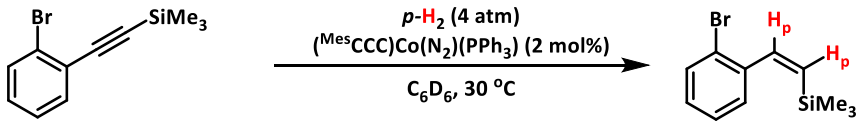

^{1}H-OPSY NMR spectrum (displayed in absolute mode)

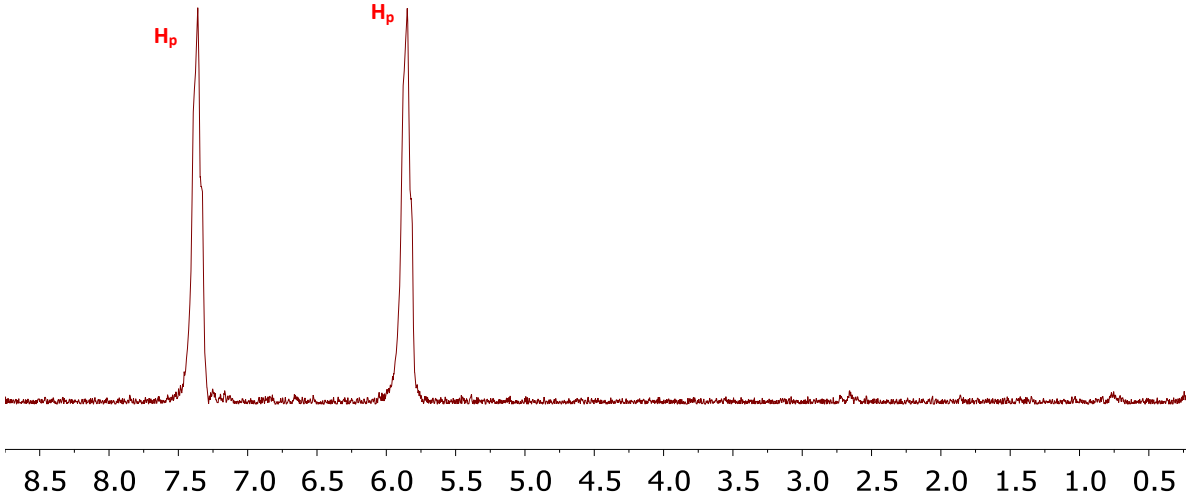

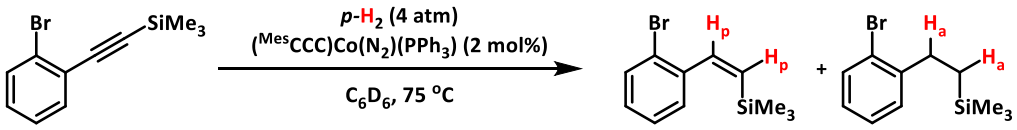

^{1}H-OPSY NMR spectrum (displayed in absolute mode)

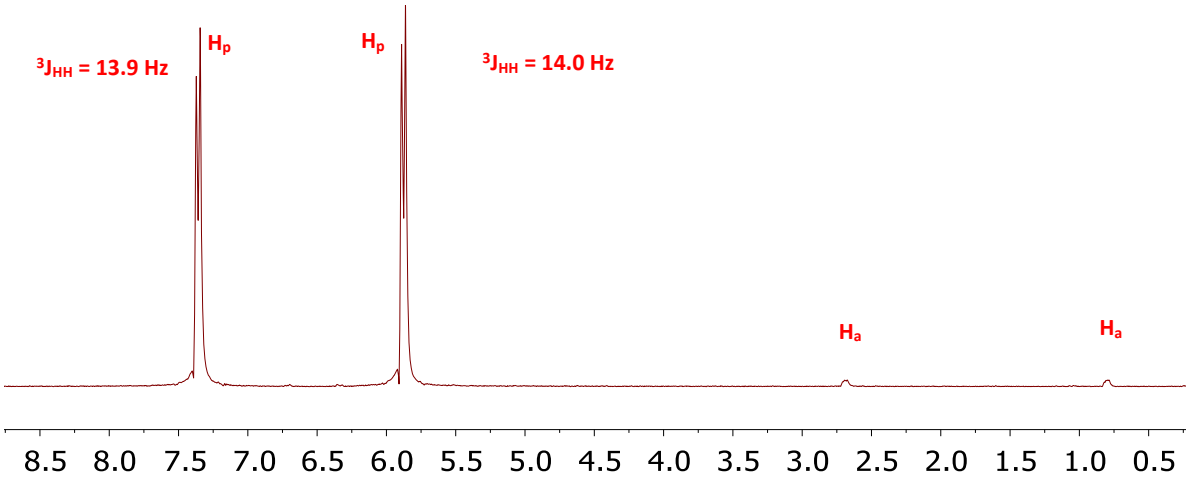

Figure 4.10 ^{1}H-OPSY NMR (C_6D_6, 500 MHz) spectrum of **(^{Mes}CCC)Co(N_2)(PPh_3)** (2 mol%) and ((2-bromophenyl)ethynyl)trimethylsilane under 4 atm of *p*-H_2 at 30 °C (top). ^{1}H-OPSY NMR spectrum of **(^{Mes}CCC)Co(N_2)(PPh_3)** (2 mol%) and ((2-bromophenyl)ethynyl)trimethylsilane under 4 atm of *p*-H_2 at 75 °C (bottom).

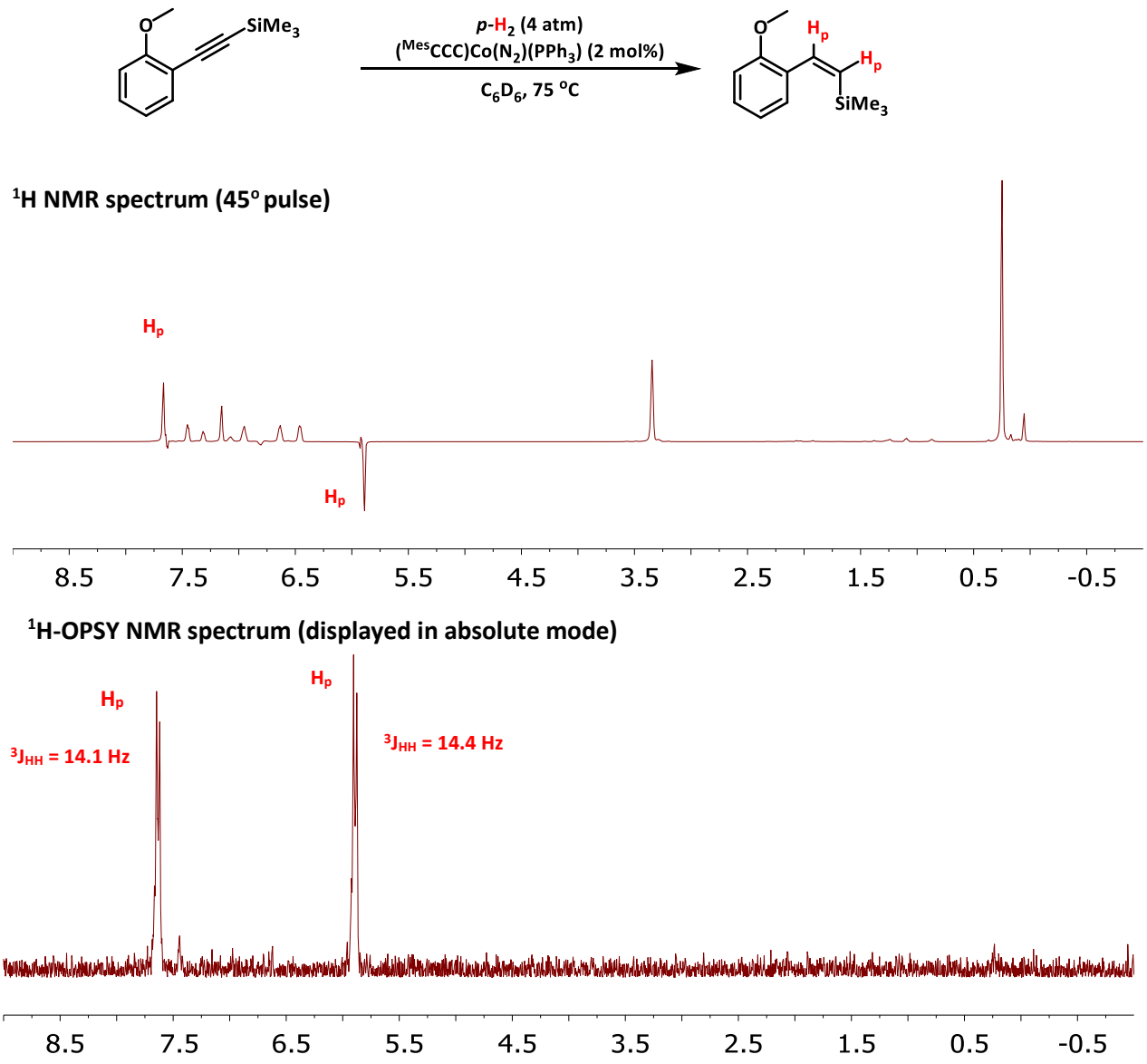

Figure 4.11 ^{1}H NMR (C_6D_6, 500 MHz, 45° pulse) spectrum of **(^{Mes}CCC)Co(N_2)(PPh_3)** (2 mol%) and ((2-methoxyphenyl)ethynyl)trimethylsilane under 4 atm of *p*-H_2 at 75 °C (top). ^{1}H-OPSY NMR (C_6D_6, 500 MHz) spectrum of **(^{Mes}CCC)Co(N_2)(PPh_3)** (2 mol%) and ((2-methoxyphenyl)ethynyl)trimethylsilane under 4 atm of *p*-H_2 at 75 °C (bottom).

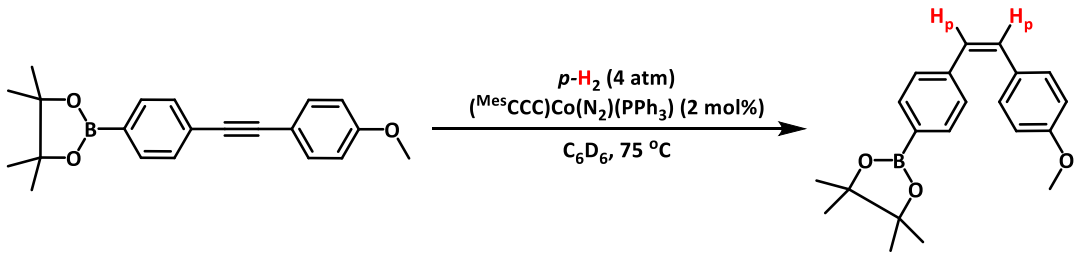

^{1}H NMR spectrum (45° pulse)

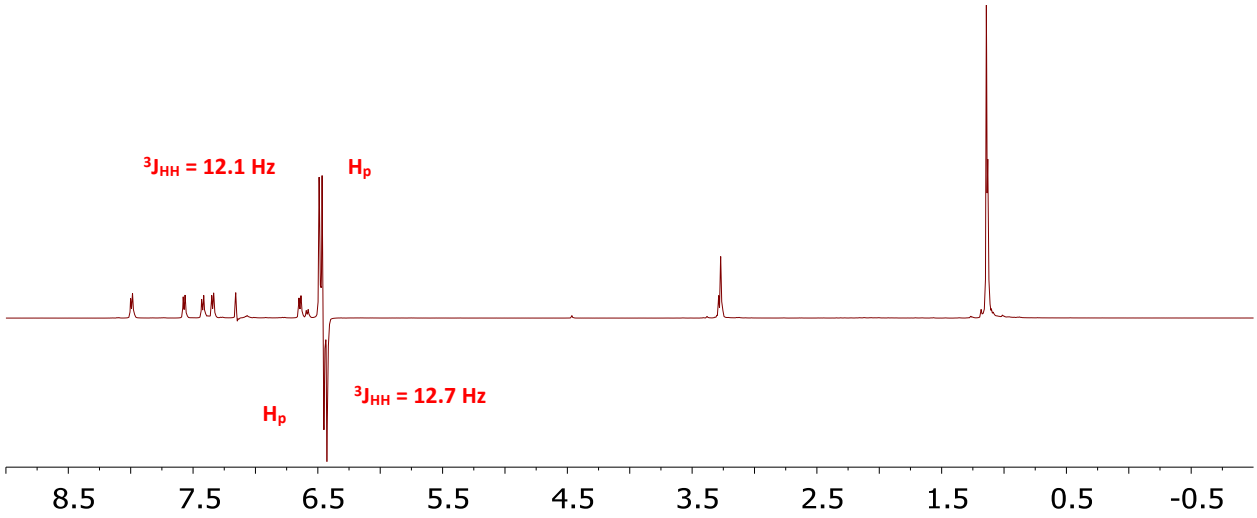

^{1}H-OPSY NMR spectrum (displayed in absolute mode)

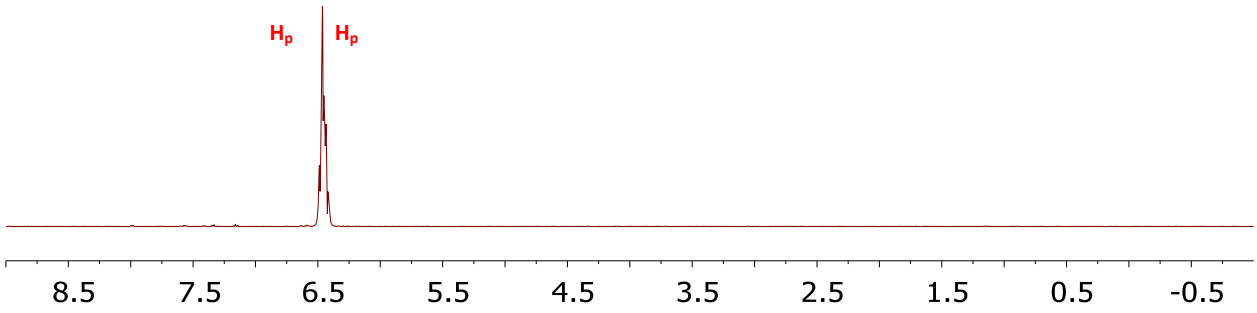

Figure 4.12 ^{1}H NMR (C_6D_6, 500 MHz, 45° pulse) spectrum of **(^{Mes}CCC)Co(N_2)(PPh_3)** (2 mol%) and 2-(4-((4-methoxyphenyl)ethynyl)phenyl)-4,4,5,5-tetramethyl-1,3,2-dioxaborolane under 4 atm of *p*-H_2 at 75 °C (top). ^{1}H-OPSY NMR (C_6D_6, 500 MHz) spectrum of **(^{Mes}CCC)Co(N_2)(PPh_3)** (2 mol%) and 2-(4-((4-methoxyphenyl)ethynyl)phenyl)-4,4,5,5-tetramethyl-1,3,2-dioxaborolane under 4 atm of *p*-H_2 at 75 °C (bottom).

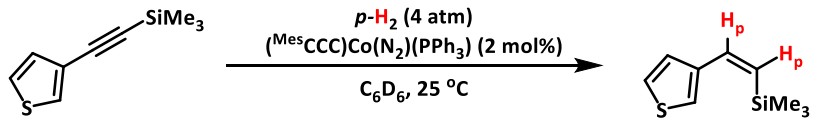

^{1}H NMR spectrum (45° pulse)

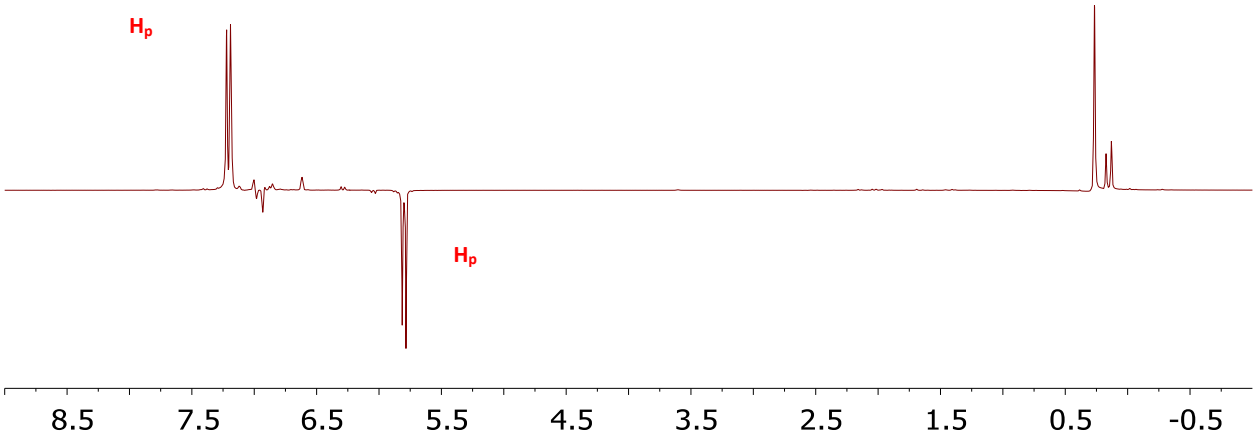

^{1}H-OPSY NMR spectrum (displayed in absolute mode)

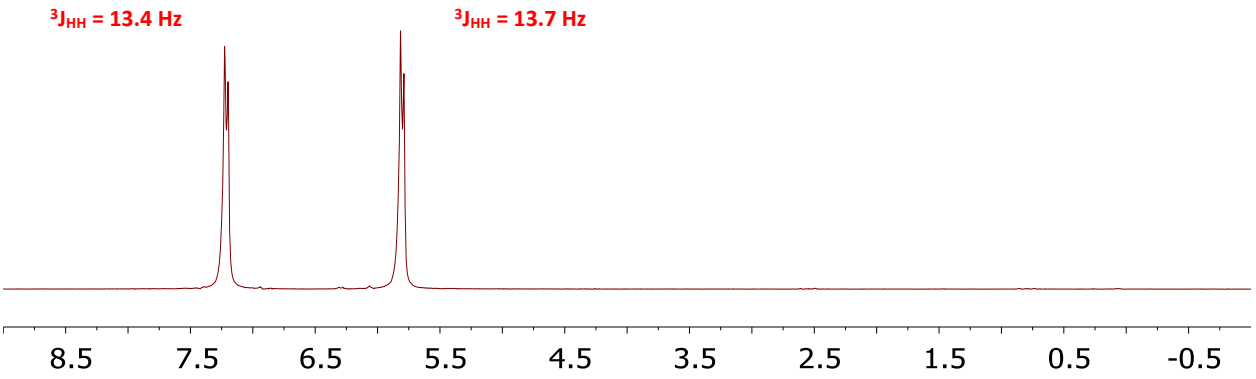

Figure 4.13 ^{1}H NMR (C_6D_6, 500 MHz, 45° pulse) spectrum of **(^{Mes}CCC)Co(N_2)(PPh_3)** (2 mol%) and trimethyl-(thiophen-3-ylethynyl)silane under 4 atm of *p*-H_2 at 25 °C (top). ^{1}H-OPSY NMR (C_6D_6, 500 MHz) spectrum of **(^{Mes}CCC)Co(N_2)(PPh_3)** (2 mol%) and trimethyl(thiophen-3-ylethynyl)silane under 4 atm of *p*-H_2 at 25 °C (bottom).

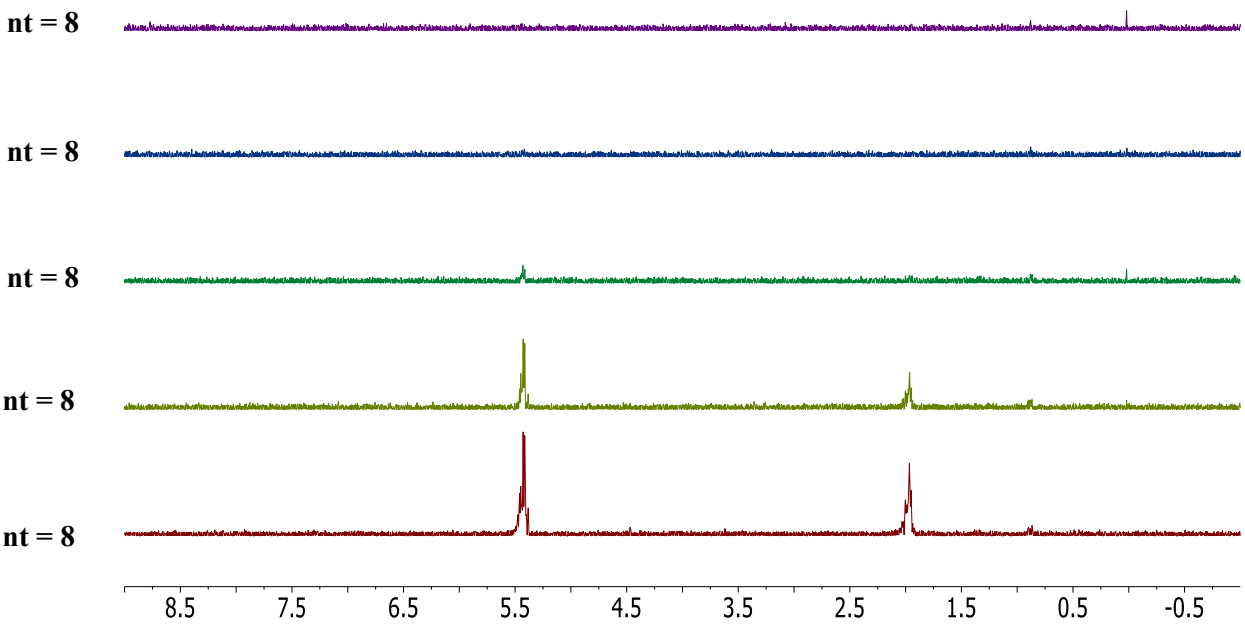

Figure 4.14 ^{1}H-OPSY NMR (C_6D_6, 500 MHz, 25°C) array spectrum of **(^{Mes}CCC)Co(N_2)(PPh_3)** (2 mg, 0.0022 mmol, 2 mol%) and *cis*-4-octene (17 µL, 0.112 mmol) under 4 atm of *p*-H_2 at 25°C in ½ mL of C_6D_6. 8 transients (nt) for each spectrum shown with total time of 2 min and 50 sec (nt = 8,8,8,8,8). Bottom spectrum was collected first (red), showing the decay of polarization with each subsequent set of scans going towards the top (purple).

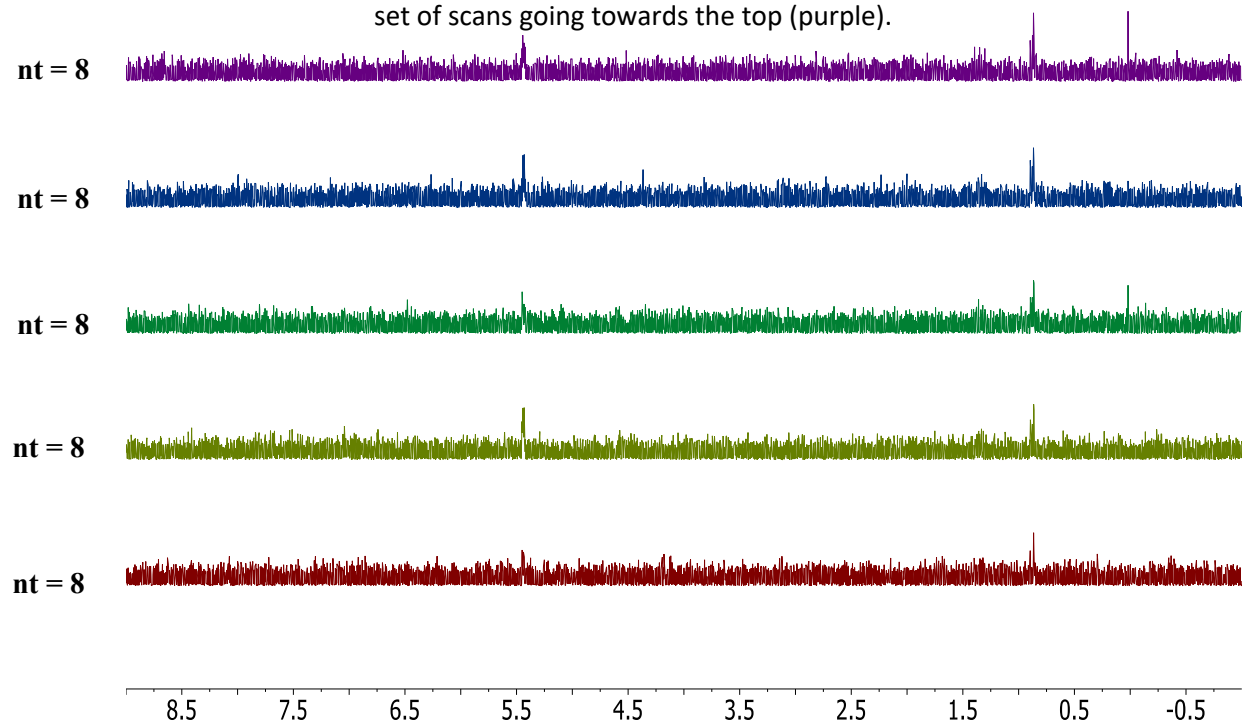

Figure 4.15 ^{1}H-OPSY NMR (C_6D_6, 500 MHz, 25°C) array spectrum of **(^{Mes}CCC)Co(N_2)(PPh_3)** (2 mg, 0.0022 mmol, 2 mol%) and *cis*-4-octene (17 µL, 0.112 mmol) under 4 atm of *p*-H_2 at 25°C in ½ mL of C_6D_6 from above (Figure S14). The J-young NMR tube was opened and exposed to ambient atmosphere, shaken and NMR data was collected. 8 transients (nt) for each spectrum shown with total time of 2 min and 50 sec (nt = 8,8,8,8,8). Bottom spectrum was collected first (red), showing the residual signal breakthrough in each scan upon fitting to highest peak for resonances at 5.44 and 0.89 ppm.

4.9 References

1. Crespo-Quesada, M.; Cardenas-Lizana, F.; Dessimoz, A.-L.; Kiwi- Minsker, L. Modern Trends in Catalyst and Process Design for Alkyne Hydrogenations. *ACS Catal.* **2012**, *2*, 1773−1786.
2. Lindlar, H.; Dubuis, R. PALLADIUM CATALYST FOR PARTIAL REDUCTION OF ACETYLENES. *Org. Synth.* **1966**, *46*, 89.
3. Osborn, J. A.; Jardine, F. H.; Young, J. F.; Wilkinson, G. The preparation and properties of tris(triphenylphosphine)halogenorhodium(I) and some reactions thereof including catalytic homogeneous hydrogenation of olefins and acetylenes and their derivatives. *J. Chem. Soc. A* **1966**, 1711−1732.
4. *Organotransition Metal Chemistry: From Bonding to Reactivity*; Hartwig, J. F., Eds.; University Science Books: Sausalito, CA, 2010; p 640.
5. Schrock, R. R.; Osborn, J. A. Catalytic hydrogenation using cationic rhodium complexes. 3. The selective hydrogenation of dienes to monoenes. *J. Am. Chem. Soc.* **1976**, *98*, 2143− 2147.
6. Castro, C. E.; Stephens, R. D. The Reduction of Multiple Bonds by Low-Valent Transition Metal Ions. The Homogeneous Reduction of Acetylenes by Chromous Sulfate. *J. Am. Chem. Soc.* **1964**, *86*, 4358− 4363.
7. Smith, A. B., III; Levenberg, P. A.; Suits, J. Z. Chromium (II) Reagents; 1. Reduction of α-Acetylenic Ketones to *trans*-Enones. *Synthesis* **1986**, *1986*, 184−189.
8. Tani, K.; Iseki, A.; Yamagata, T. Efficient transfer hydrogenation of alkynes and alkenes with methanol catalysed by hydrido(methoxo)iridium(III) complexes. *Chem. Commun.* **1999**, 1821−1822.
9. Trost, B. M.; Ball, Z. T.; Jöge, T. A Chemoselective Reduction of Alkynes to (*E*)-Alkenes. *J. Am. Chem. Soc.* **2002**, *124*, 7922−7923.
10. Shirakawa, E.; Otsuka, H.; Hayashi, T. Reduction of alkynes into 1,2-dideuterioalkenes with hexamethyldisilane and deuterium oxide in the presence of a palladium catalyst. *Chem. Commun.* **2005**, 5885−5886.
11. Shen, R.; Chen, T.; Zhao, Y.; Qiu, R.; Zhou, Y.; Yin, S.; Wang, X.; Goto, M.; Han, L. Facile Regio- and Stereoselective Hydrometalation of Alkynes with a Combination of Carboxylic Acids and Group 10 Transition Metal Complexes: Selective Hydrogenation of Alkynes with Formic Acid. *J. Am. Chem. Soc.* **2011**, *133*, 17037−17044.

12. Fu, S.; Chen, N.; Liu, X.; Shao, Z.; Luo, S.; Liu, Q. Ligand-Controlled Cobalt-Catalyzed Transfer Hydrogenation of Alkynes: Stereodivergent Synthesis of *Z*- and *E*-Alkenes. *J. Am. Chem. Soc.* **2016**, *138*, 8588−8594.
13. Radkowski, K.; Sundararaju, B.; Fürstner, A. A Functional-Group-Tolerant Catalytic *trans* Hydrogenation of Alkynes. *Angew. Chem., Int. Ed.* **2013**, *52*, 355−360.
14. Leutzsch, M.; Wolf, M. L.; Gupta, P.; Fuchs, M.; Thiel, W.; Farès, C.; Fürstner, A. Formation of Ruthenium Carbenes by *gem*-Hydrogen Transfer to Internal Alkynes: Implications for Alkyne *trans*-Hydrogenation. *Angew. Chem., Int. Ed.* **2015**, *54*, 12431−12436.
15. Schleyer, D.; Niessen, H. G.; Bargon, J. *In situ* ^{1}H-PHIP-NMR studies of the stereoselective hydrogenation of alkynes to (*E*)-alkenes catalyzed by a homogeneous [Cp*Ru]$^{+}$ catalyst. *New J. Chem.* **2001**, *25*, 423−426.
16. Furukawa, S.; Komatsu, T. Selective Hydrogenation of Functionalized Alkynes to (E)-Alkenes, Using Ordered Alloys as Catalysts. *ACS Catal.* **2016**, *6*, 2121-2125.
17. Karunananda, M. K.; Mankad, N. P. *E*-Selective Semi-Hydrogenation of Alkynes by Heterobimetallic Catalysis. *J. Am. Chem. Soc.* **2015**, *137*, 14598−14601.
18. Srimani, D.; Diskin-Posner, Y.; Ben-David, Y.; Milstein, D. Iron Pincer Complex Catalyzed, Environmentally Benign, *E*-Selective Semi-Hydrogenation of Alkynes. *Angew. Chem., Int. Ed.* **2013**, *52*, 14131−14134.
19. Trost, B. M. On Inventing Reactions for Atom Economy. *Acc. Chem. Res.* **2002**, *35*, 695−705.
20. Sheldon, R. A. Fundamentals of green chemistry: efficiency in reaction design. *Chem. Soc. Rev.* **2012**, *41*, 1437−1451.
21. Baker, R. T.; Tumas, W. Toward Greener Chemistry. *Science* **1999**, *284*, 1477−1479.
22. Anastas, P. T.; Kirchhoff, M. M. Origins, Current Status, and Future Challenges of Green Chemistry. *Acc. Chem. Res.* **2002**, *35*, 686− 694.
23. Tokmic, K.; Markus, C. R.; Zhu, L.; Fout, A. R. Well-Defined Cobalt(I) Dihydrogen Catalyst: Experimental Evidence for a Co(I)/Co(III) Redox Process in Olefin Hydrogenation. *J. Am. Chem. Soc.* **2016**, *138*, 11907-11913.
24. Widegren, J. A.; Finke, R. G. A review of the problem of distinguishing true homogeneous catalysis from soluble or other metal-particle heterogeneous catalysis under reducing conditions. *J. Mol. Catal. A: Chem.* **2003**, *198*, 317−341.
25. Shen, R.; Chen, T.; Zhao, Y.; Qiu, R.; Zhou, Y.; Yin, S.; Wang, X.; Goto, M.; Han, L. Facile Regio- and Stereoselective Hydrometalation of Alkynes with a Combination of Carboxylic Acids and Group 10

Transition Metal Complexes: Selective Hydrogenation of Alkynes with Formic Acid. *J. Am. Chem. Soc.* **2011**, *133*, 17037−17044.

26. Duckett, S. B.; Mewis, R. E. Application of *Para*hydrogen Induced Polarization Techniques in NMR Spectroscopy and Imaging. *Acc. Chem. Res.* **2012**, *45*, 1247− 1257
27. Aguilar, J. A.; Elliott, P. I. P.; López-Serrano, J.; Adams, R. W.; Duckett, S. D. Only *para*-hydrogen spectroscopy (OPSY), a technique for the selective observation of *para*-hydrogen enhanced NMR signals. *Chem. Commun.* **2007**, 1183−1185.
28. Pravica, M. G.; Weitekamp, D. P. Net NMR alignment by adiabatic transport of parahydrogen addition products to high magnetic field. *Chem. Phys. Lett.* **1988**, *145*, 255−258.
29. Collecting the NMR data at 30 and 75 °C resulted in the same enhanced signals. However, at higher temperatures the enhancement was longer lived due to increased *p*-H_2 exchange within the sample, which allowed for more resolved spectra to be collected. **2l** was collected at 25 °C.
30. Bianchini, C.; Mealli, C.; Meli, A.; Peruzzini, M.; Zanobini, F. *J. Am. Chem. Soc.* **1988**, *110*, 8725−8726.
31. Adams, R. W.; Aguilar, J. A.; Atkinson, K. D.; Cowley, M. J.; Elliott, P. I. P.; Duckett, S. B.; Green, G. G. R.; Khazal, I. G.; López- Serrano, J.; Williamson, D. C. Reversible Interactions with para-Hydrogen Enhance NMR Sensitivity by Polarization Transfer. *Science* **2009**, *323*, 1708−1711.
32. Atkinson, K. D.; Cowley, M. J.; Elliott, P. I. P.; Duckett, S. B.; Green, G. G. R.; López-Serrano, J.; Whitwood, A. C. Spontaneous Transfer of Parahydrogen Derived Spin Order to Pyridine at Low Magnetic Field. *J. Am. Chem. Soc.* **2009**, *131*, 13362−13368.
33. Atkinson, K. D.; Cowley, M. J.; Duckett, S. D.; Elliott, P. I. P.; Green, G. G. R.; López-Serrano, J.; Khazal, I. G.; Whitwood, A. C. *Para*-Hydrogen Induced Polarization without Incorporation of *Para*-Hydrogen into the Analyte. *Inorg. Chem.* **2009**, *48*, 663−670.
34. Adams, R. W.; Duckett, S. B.; Green, R. A.; Williamson, D. C.; Green, G. G. R. A theoretical basis for spontaneous polarization transfer in non-hydrogenative *para*hydrogen-induced polarization. *J. Chem. Phys.* **2009**, *131*, 194505.
35. Pangborn, A.B.; Giardello, M.A.; Grubbs, R. H.; Rosen, R. K.; Timmers, F. J. Safe and Convenient Procedure for Solvent Purification. *Organometallics*, **1996**, *15*, 1518−1520.
36. Wietz, I. S.; Rabinovitz, M. The application of C_8K for organic synthesis: reduction of substituted naphthalenes. *J. Chem. Soc. Perkin Trans.* **1993**, *1*, 117-120.

37. Ibrahim, A. D.; Tokmic, K.; Brennan, M. B.; Kim, D. Matson, E. M.; Nilges, M. J.; Bertke, J. A.; Fout, A. R. Monoanionic bis(carbene) pincer complexes featuring cobalt(I-III) oxidation states. Dalton Trans. 2016, 45, 9805-9811.
38. Mio, M. J.; Kopel, L. C.; Braun, J. B.; Gadzikwa, T. L.; Hull, K. L.; Brisbois, R. G.; Markworth, C. J.; Grieco, P. A. One-Pot Synthesis of Symmetrical and Unsymmetrical Bisarylethynes by a Modification of the Sonogashira Coupling Reaction. *Org. Lett*. **2002**, *4*, 3199-3202.
39. Mahesh, M.; Mursphy, J. A.; Wessel, H. P. Novel Deoxygenation Reaction of Epoxides by Indium. *J. Org. Chem.* **2005**, *70*, 4118-4123.
40. Zhao, F.; Luo, J.; Liao, Y.; Peng, S.; Deng, G. Sodium Sulfinate-Mediated *trans*-Stilbene Formation from Benzylic Halides. *Adv. Synth. Catal.* **2012**, *354*, 1914-1918.
41. Krasovskiy, A.; Lipshutz, B. H. Ligand Effects on Negishi Couplings of Alkenyl Halides. *Org. Lett.* **2011**, *13*, 3818-3821.
42. Ni, Z.; Yang, P.; Ng, D. K. P.; Tzeng, Y.; Luh, T. Transition metal promoted reaction. Unified synthesis of vinylsilanes and silylated butadienes. Nickel-catalyzed olefination and silylolefination of dithioacetals. *J. Am. Chem. Soc.* **1990**, *112*, 9356-9364.
43. Karabelas, K.; Hallberg, A. Synthesis of (*E*)-(2-arylethenyl)silanes by palladium-catalyzed arylation of vinylsilanes in the presence of silver nitrate. *J. Org. Chem.* **1986**, *51*, 5286-5290.
44. Maercker, A.; Reider, K.; Girreser, U. The Reaction of Substituted Vinylsilanes with Lithium Metal. *Eur. J. Org. Chem.* **1998**, 1455-1465.
45. Aguilar, J. A.; Adam, R. W.; Duckett, S. B.; Green, G. G. R.; Kandiah, R. Selective detection of hyperpolarized NMR signals derived from para-hydrogen using the Only Para-hydrogen SpectroscopY (OPSY) approach. *J. Magn. Reson.* **2011**, *208*, 49-57.
46. Duckett, S. B.; Green, G. G. R.; Cowley, M. J. Pulse sequencing with hyperpolarisable nuclei. US Patent 20,110,274,626, November 10, 2011.
47. Tom, B. A.; Bhasker, S.; Miyamoto, Y.; Momose, T.; McCall, B. J. Producing and quantifying enriched *para*-H_2. *Rev. Sci. Instrum.* **2009**, *80*, 016108.

CHAPTER 5: MECHANISTIC INSIGHTS INTO THE COBALT-CATALYZED LEWIS ACID-ASSITED NITRILE HYDROGENATION TO PRIMARY AMINES: A *PARA*HYDROGEN INDUCED POLARIZATION NMR STUDY [†]

5.1 Introduction

The catalytic hydrogenation of unsaturated functionalities is one of the most atom-economical transformations within organic chemistry. The majority of these transformations are mediated by transition metal catalysts involving metal-hydride intermediates through the homolytic activation of H_2.[1,2] Wilkinson's catalyst, $Rh(PPh_3)_3Cl$, adheres to the metal-hydride route and readily hydrogenates carbon-carbon multiple bonds.[3] More demanding unsaturated polar functionalities featuring C=O, C=N or C≡N bonds, however, are more commonly hydrogenated using alternative strategies. Such strategies involve catalytic systems manifesting the heterolytic cleavage of H_2, as commonly observed in metal-ligand cooperative platforms pioneered by the Nobel Prize winning work of Noyori.[4] These routes are distinct from the classical oxidative addition, insertion and reductive elimination pathways generally recognized for the hydrogenation of unsaturated organic compounds,[5] but instead involve the formation of metal-hydride and ligand-proton features, in which the catalytic system is then well suited for the reduction of the polar groups.

Developments for the selective formation of primary amines have continued to attract interest because of their importance in the bulk and fine chemical industries. Reduction of nitriles to primary amines is commonly accomplished using heterogeneous hydrogenation processes;[6-8] however, stoichiometric amounts of promiscuous metal-hydride sources[9,10]can also be employed. In these cases, the functional group tolerance is limited due to the harsh conditions typically used, and the selectivity

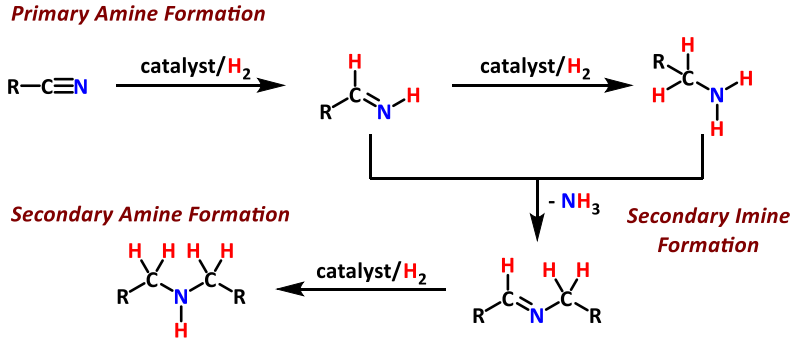

Scheme 5.1 Primary amine, secondary imine and secondary amine formation during nitrile hydrogenation.

[†] Portions of this chapter are reproduced from the following publications with permission from the authors. Tokmic, K.; Jackson, B. J.; Salazar, A.; Woods, T. J.; Fout, A. R. Cobalt-Catalyzed and Lewis Acid-Assisted Nitrile Hydrogenation to Primary Amines: A Combined Effort. *J. Am. Chem. Soc.* **2017**, *139*, 13554-13561.

toward the formation of primary amines decreases due to side reactions (Scheme 5.1). Among the synthetic methodologies for the formation of primary amines, the selective and catalytic reduction of nitriles using H_2 represents the most atom-economical route.

Homogeneous counterparts are often more selective for primary amines and operate under milder conditions. Catalytic systems based on rhenium,[11] ruthenium,[12-19] and rhodium[20,21] complexes have been shown to effectively mediate the hydrogenation of nitriles to primary amines. Although these catalytic systems present good activity and selectivity, cost and environmental implications have motivated investigations into more sustainable systems. Due to the inherent abundance and relatively lower cost, late first-row transition metals present themselves as promising alternatives to their second- and third-row congeners.[22,23]

Recent work by Beller demonstrates the utility of incorporating bifunctional motifs into manganese- and iron-based nitrile hydrogenation systems.[24-26] Iron and cobalt catalysts developed by Milstein and coworkers also carry out this transformation, citing metal-hydride intermediates for the observed reactivity.[27,28] Very recently, a cobalt catalyst solely featuring phosphine ligands was reported to carry out this transformation; however, the operative mechanism has not yet been elucidated.[29] Exclusively metal-centered nitrile hydrogenation using first-row transition metals has remained elusive, and experimental investigations into this approach would further advance the potential of such strategies.

The cobalt complex, **(^{Mes}CCC)Co(H_2)(PPh_3)** (^{Mes}CCC = bis(mesityl-benzimidazol-2-ylidene)phenyl), which was active for the hydrogenation of terminal olefins and the *E*-selective semihydrogenation of internal alkynes has been previously described.[30,31] Mechanistic insights from ^{1}H NMR spectroscopy and *para*-hydrogen (*p*-H_2) induced polarization (PHIP) transfer NMR studies revealed a metal-centered Co(I/III) redox process was operative. Reasoning that the multielectron redox process with cobalt is a direct result of incorporating the strong-field bis(carbene) pincer ligand as part of the catalytic system, the competency of these cobalt complexes in the hydrogenation of nitriles was investigated.

Investigations using low-valent late first-row transition metal complexes for catalytic transformations face a significant limitation from their greater sensitivity to air and moisture compared to their platinum group congeners. To overcome this challenge, the *in situ* activation of stable precursors, generally higher oxidation state metal sources, is accomplished by employing readily available Grignard or metal hydride reagents,[32-36] or metal alkoxides, as recently demonstrated by Thomas and coworkers.[37] Naturally, **(^{Mes}CCC)Co(H_2)(PPh_3)** oxidizes upon exposure to air, so we sought to determine the feasibility of a bench-stable Co(III) analogue, **(^{Mes}CCC)$CoCl_2$py**, for the hydrogenation of nitriles.[38] Encouraged by our previous

studies demonstrating that lower oxidation states of cobalt can be accessed using a hydride source,[30] the use of a commercially available source, $NaHBEt_3$, was used as an *in situ* activator.

Herein the selective hydrogenation of nitriles to primary amines using a bench-stable catalyst precursor, **(^{Mes}CCC)CoCl$_2$py** (py = pyridine), under 4 atm of H_2 pressure is discussed. The mechanistic insights stemming from PHIP transfer NMR studies as well as stoichiometric reactions demonstrate the dual role of $NaHBEt_3$ in the observed catalysis: (1) reduction of the Co(III) precursor to the active Co(I) catalyst and (2) hydrogenation of the nitrile functionality induced by the resulting Lewis acid, BEt_3.

5.2 Optimization of reaction conditions and catalytic activity

The reaction conditions were optimized following previously reported systems[27,28] using benzonitrile as a model substrate. The use of **(^{Mes}CCC)CoCl$_2$py** (2 mol%), KO^{t}Bu (6 mol%), and $NaHBEt_3$ (4 mol%) in toluene at 115 °C under 4 atm of H_2 for 8 h resulted in complete conversion of the nitrile with excellent selectivity to the primary amine.[39] Furthermore, the catalytic utility of **(^{Mes}CCC)CoCl$_2$py** was extended to hydrogenate both aliphatic and aromatic nitriles and is tolerant of amines, esters, and halides (Scheme 5.2).[39] These results, demonstrate the utility of this system in hydrogenating nitriles under low hydrogen pressure and moderate temperatures using a bench-stable cobalt precatalyst. However, to fully understand the nuances of the catalytic system, detailed mechanistic studies examining the nature of H_2 addition and the active species were needed. Such studies would delineate the metal-centered reactivity from bifunctional motifs and resemble the multielectron catalytic processes observed in similar cobalt bis(carbene) complexes.[30,31]

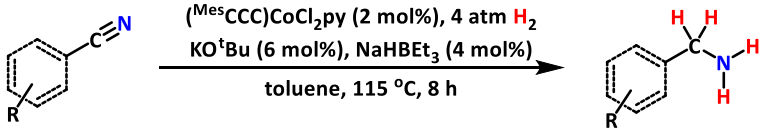

Scheme 5.2 Nitrile hydrogenation using **(^{Mes}CCC)CoCl$_2$py**, H_2 gas, KO^{t}Bu and $NaHBEt_3$ to primary amines.

5.3 Mechanistic studies using PHIP

In the interest of probing the reaction mechanism, *in situ* ^{1}H NMR studies of the catalytic nitrile hydrogenation were investigated. Previously, PHIP transfer NMR studies were carried out of a related Co(η^2-H_2) bis(carbene) pincer catalyst for the pairwise hydrogenation of carbon−carbon multiple bonds.[31,31] Accordingly, a PHIP transfer NMR study of the hydrogenation of nitriles under catalytic conditions with *p*-H_2 was employed to provide mechanistic insights (*vide infra*) due to the intrinsic properties associated with PHIP.

PHIP NMR spectroscopy has been demonstrated as an effective analytical method to study heterogeneous[40-44] and homogeneous[45-49] hydrogenation reactions, H_2 reactivity with metal complexes, and, in rare instances, even metal-free compounds.[50,51] The hyperpolarization of ^{1}H NMR signals resulting from PHIP are an indication of the pairwise addition of the H atoms of *p*-H_2 to magnetically distinct positions on a substrate. Moreover, the characteristic emission and absorption signals are observed *in situ* via ^{1}H NMR spectroscopy when the addition of *p*-H_2 occurs faster than the relaxation rate of the corresponding nuclei, and the spin−spin coupling of the added *p*-H_2 in the hydrogenated product is

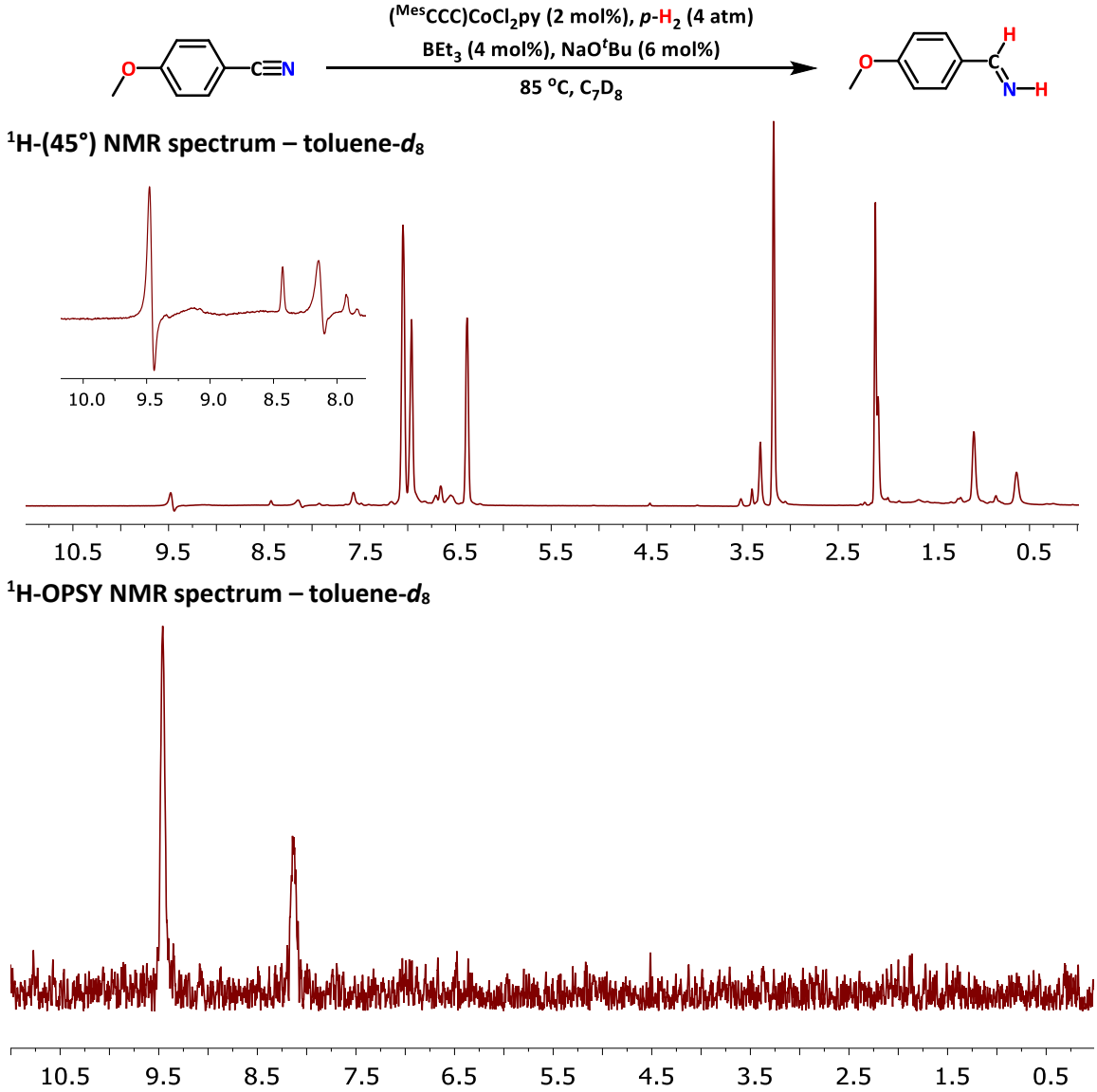

Figure 5.1 ^{1}H NMR (C_7D_8, 600 MHz) spectrum of **(^{Mes}CCC)CoCl$_2$py** (2 mol %), $NaHBEt_3$ (4 mol %), KO^tBu (6 mol %), and 4-methoxybenzonitrile under 4 atm of *p*-H_2 at 85 °C collected using a 45° pulse (top) and ^{1}H-OPSY pulse (bottom).

retained. In the studies presented herein, a 45° pulse and a double quantum OPSY (only para-hydrogen spectroscopy) filter in the ^{1}H NMR experiment were used following the addition of *p*-H_2.

For the ^{1}H NMR mechanistic studies, 4-methoxybenzonitrile was chosen because the methoxy group (R-OCH_3) provides a discernible ^{1}H NMR resonance in the nitrile and hydrogenation products (imine and amine). The addition of *p*-H_2 to a toluene-d_6 solution consisting of 4-methoxybenzonitrile, **(^{Mes}CCC)CoCl$_2$py** (2 mol%), $NaHBEt_3$ (4 mol%) and KO^tBu (6 mol%) did not result in the observation of hyperpolarized resonances at 30 or 60 °C. Polarization of the imine moiety (R-HC=NH) was seen (Figure 5.1) when the solution was heated to 85 °C. Although the *p*-H_2 was added outside the NMR spectrometer (low-field) and at room temperature before being inserted into the spectrometer, the PASADENA (*para*-hydrogen and synthesis allow dramatically enhanced nuclear alignment) effect was observed. In this case, the transfer of *p*-H_2 occurred inside (high-field) the NMR spectrometer at 85 °C with the retention of the spin-spin coupling between the H-H atoms. The use of a double-quantum OPSY pulse sequence further corroborated the pairwise hydrogenation of the nitrile group (Figure 5.1, bottom). The hyperpolarization resulting from the hydrogenation of a nitrile, imine, or other polar functionalities with *p*-H_2 has not been demonstrated thus far, with only non-hydrogenative means having been observed.[53-59] The PASADENA effect was also observed when using 4-(trifluoromethyl)benzonitrile (Figure 5.14).

Although the formation of the primary amine product was also observed in the ^{1}H NMR spectrum, a PHIP effect was not seen for the corresponding protons (R−CH_2−NH_2), suggesting a different mechanism may be operative for the hydrogenation of the imine. One possible mechanism for imine hydrogenation involves a non-pairwise transfer of H_2 by an inner-sphere hydride-transfer mechanism.[60,61] However, if the hydrogenation of the imine proceeds too slowly,[62,63] or the protons of the amine readily exchange with protic functionalities, then the PHIP effect would also be quenched.

5.4 Stoichiometric reactions

Intrigued by the PHIP data, additional mechanistic and stoichiometric studies were performed to describe the active catalytic species. To this end, the reactivity between **(^{Mes}CCC)CoCl$_2$py** and $NaHBEt_3$ was investigated next. It was hypothesized that the treatment of **(^{Mes}CCC)CoCl$_2$py** with $NaHBEt_3$ would reduce the precatalyst to an active cobalt(I) species proceeding through a (^{Mes}CCC)Co−$(H)_2$ intermediate, followed by reductive coupling of H_2. Accordingly, treatment of a solution of **(^{Mes}CCC)CoCl$_2$py** in benzene-d_6 with 2 equiv of $NaHBEt_3$ in a J. Young NMR tube resulted in the formation of a brown solution. Monitoring by ^{1}H NMR spectroscopy revealed broadened downfield resonances corresponding to the aryl protons, while the retention of a C_2-symmetric complex was discerned by the corresponding mesityl-CH_3

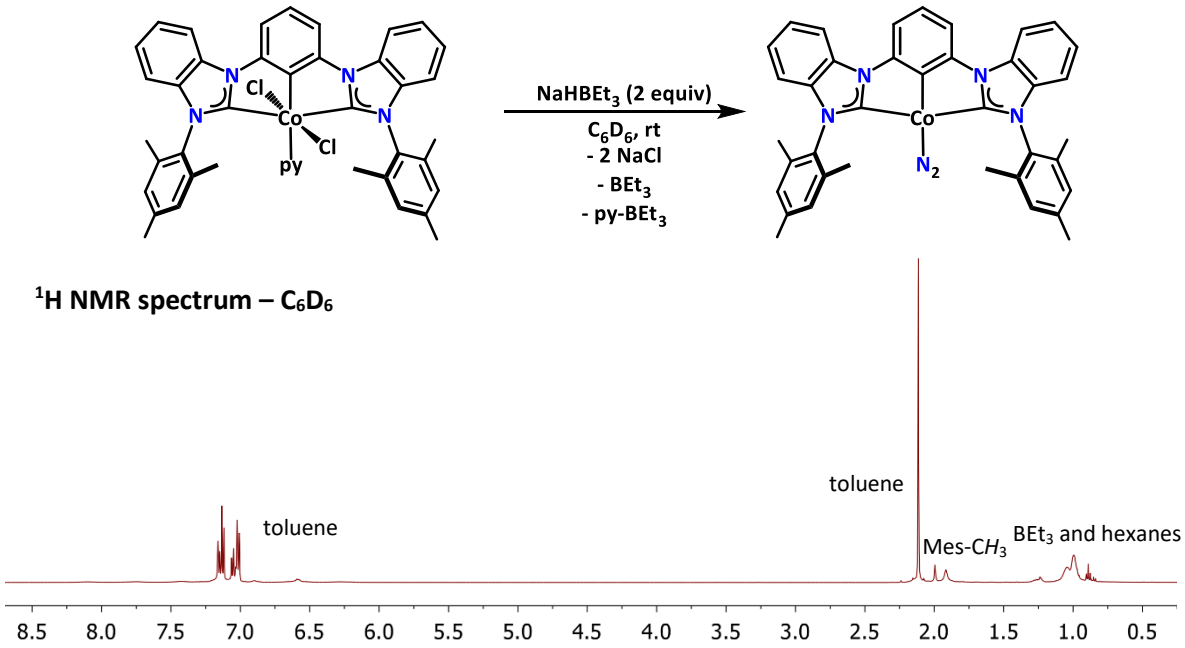

Figure 5.2 ^{1}H NMR (C_6D_6, 500 MHz) spectrum of **(^{Mes}CCC)CoCl$_2$py** and 2 equiv of $NaHBEt_3$.

resonances at 1.99 and 1.92 ppm (Figure 5.2). Interrogation of the newly formed species by IR spectroscopy revealed an intense absorption at 2082 cm^{-1}, which was tentatively assigned to the vibration mode of a bound dinitrogen ligand.

Even though loss H_2 was not observed in the ^{1}H NMR spectrum (Figure 5.2), the addition of styrene to the previous reaction resulted in the formation of ethylbenzene, indicative of the formation of (^{Mes}CCC)Co-

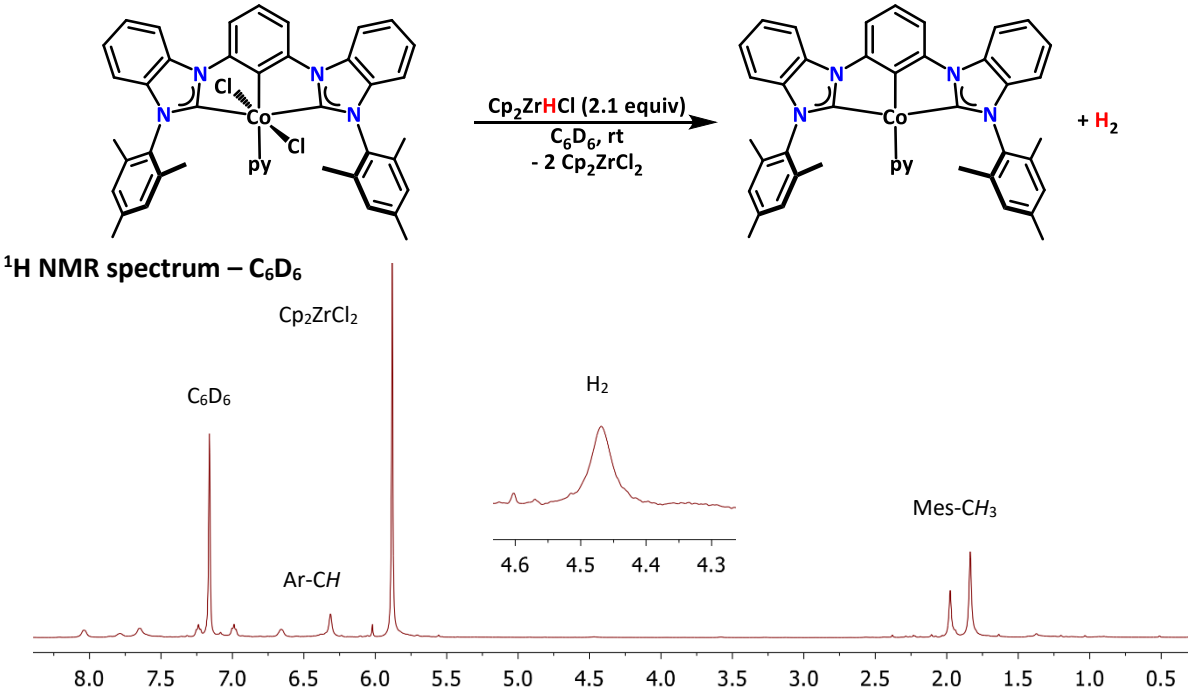

Figure 5.3 ^{1}H NMR (C_6D_6, 500 MHz) spectrum of **(^{Mes}CCC)CoCl$_2$py** and 2.1 equiv of Cp_2ZrHCl.

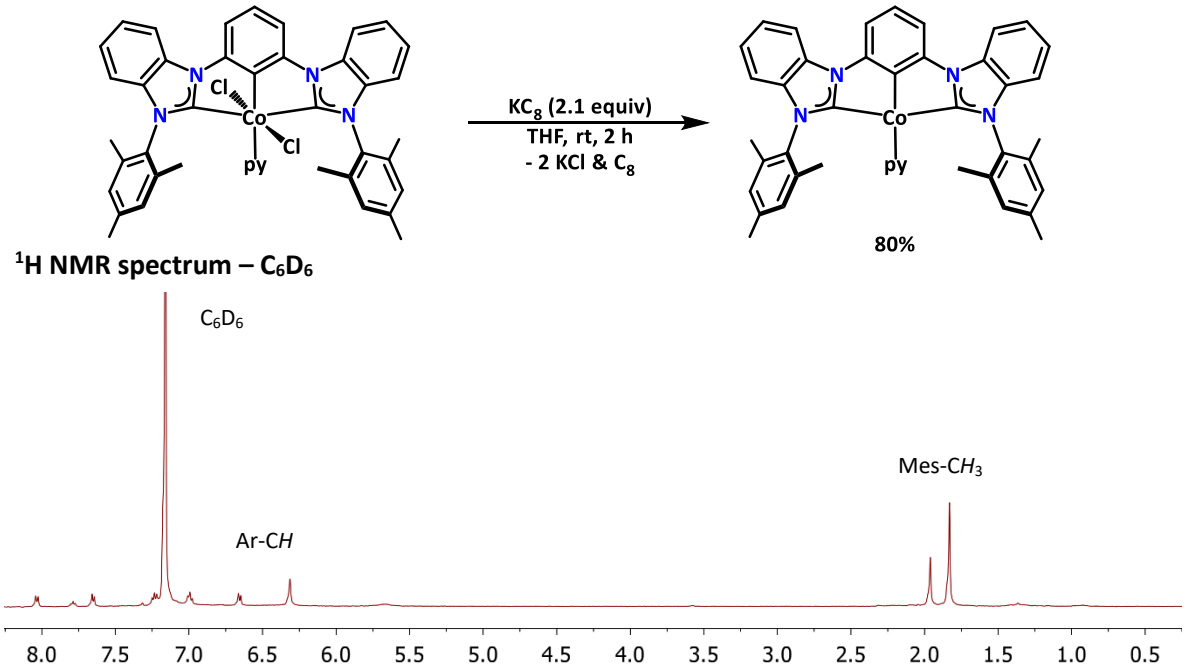

Figure 5.4 ^{1}H NMR (C_6D_6, 500 MHz) spectrum of **(^{Mes}CCC)Co-py**.

$(H)_2$ *in situ*. Alternatively, using Cp_2ZrHCl (Cp = cyclopentadienyl) as the hydride source resulted in a new complex, **(^{Mes}CCC)Co-py** (*vide infra*) with concomitant formation of H_2 (Figure 5.3). Furthermore, the IR spectrum did not contain a dinitrogen stretch, indicating that a Co−N_2 complex was not present. After unsuccessful attempts to isolate the reduced species from the corresponding byproducts, an alternative route was used for the preparation of **(^{Mes}CCC)Co-py**.

The reduction of **(^{Mes}CCC)CoCl$_2$py** with 2 equiv of KC_8 furnished **(^{Mes}CCC)Co-py** in 80% yield (Figure 5.4). Characterization of **(^{Mes}CCC)Co-py** by ^{1}H NMR spectroscopy (Figure 5.4) displayed a diamagnetic species that matched the product formed from the addition of Cp_2ZrHCl to **(^{Mes}CCC)CoCl$_2$py** (Figure 5.3). A C_2-symmetric complex was present in solution, as indicated by the two mesityl-C*H*$_3$ resonances of **(^{Mes}CCC)Co-py** at 1.96 and 1.84 ppm. Integration of the corresponding resonances in the ^{1}H NMR spectrum revealed the retention of the pyridine ligand in the reduced species. In contrast, the CCC ligand derivative featuring 2,6-diisopropylphenyl flanking groups loses pyridine upon reduction and yields a 16-electron Co(I)-N_2 complex.[38] Probing **(^{Mes}CCC)Co-py** by IR spectroscopy revealed the absence of a Co-N_2 moiety, further confirming the assignment of the complex by ^{1}H NMR spectroscopy. To unambiguously determine the molecular structure of **(^{Mes}CCC)Co-py**, single crystals suitable for X-ray diffraction studies were grown from a concentrated solution of the target complex in diethyl ether. The four-coordinate cobalt center adopts a square planar geometry, with the pyridine ligand *trans* to the Co-C_{aryl} bond (Figure 5.5, Table 5.1 and 5.2).

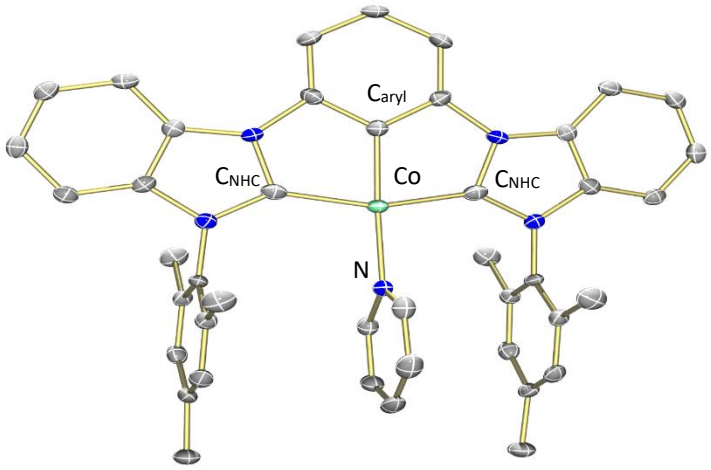

Figure 5.5 Molecular structure of **(MesCCC)Co-py** with 50% probability ellipsoids. Solvent and H atoms have been omitted for clarity.

After successfully isolating the reduced species, **(MesCCC)Co-py**, the coordination of the nitrile to the metal center was investigated since PHIP studies suggests that this process transpires throughout catalysis. Accordingly, that addition 1 equiv 4-methoxybenzonitrile to a freshly prepared solution of **(MesCCC)Co-py** in THF furnished **(MesCCC)Co(*p*-NCC$_6$H$_4$–OCH$_3$)** in 79% yield after workup. Characterization by ^{1}H NMR spectroscopy revealed a similar coordination environment to that of **(MesCCC)Co-py** (Figure

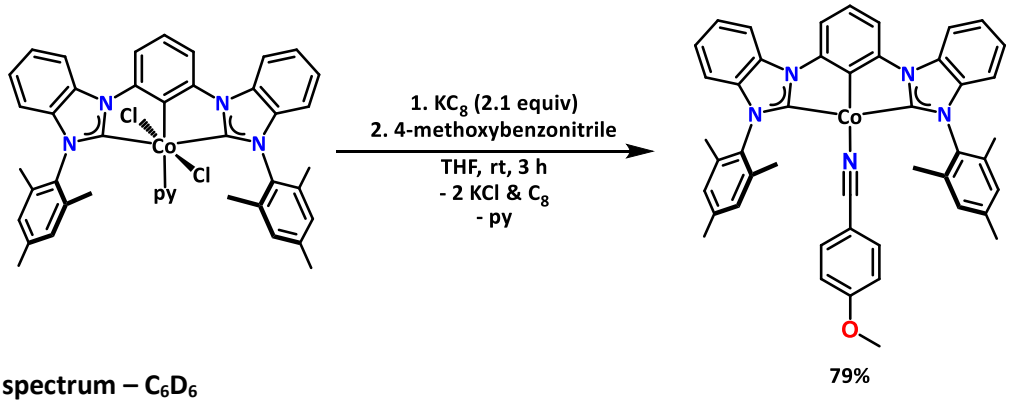

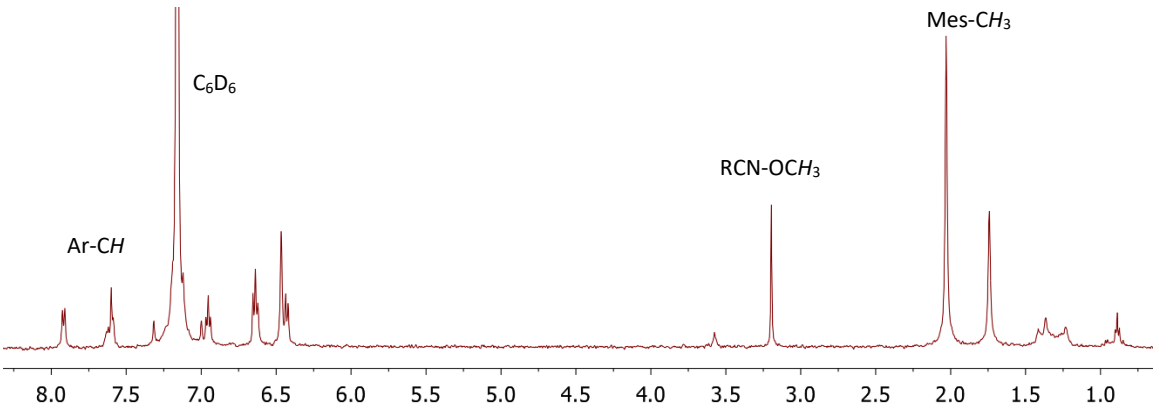

Figure 5.6 ^{1}H NMR (C_6D_6, 500 MHz) spectrum of **(MesCCC)Co(*p*-NCC$_6$H$_4$–OCH$_3$)**.

5.4), indicating that new species is also square planar. Furthermore, the integration of the ^{1}H NMR spectrum suggests the coordination of one nitrile ligand (Figure 5.6). Additionally, an examination of this species by IR spectroscopy revealed an intense absorption at 2184 cm^{-1}, which is red-shifted by 32 cm^{-1} from the free nitrile (ν_{CN} = 2216 cm^{-1}) and is consistent with an end-on coordination mode of the nitrile ligand.[64]

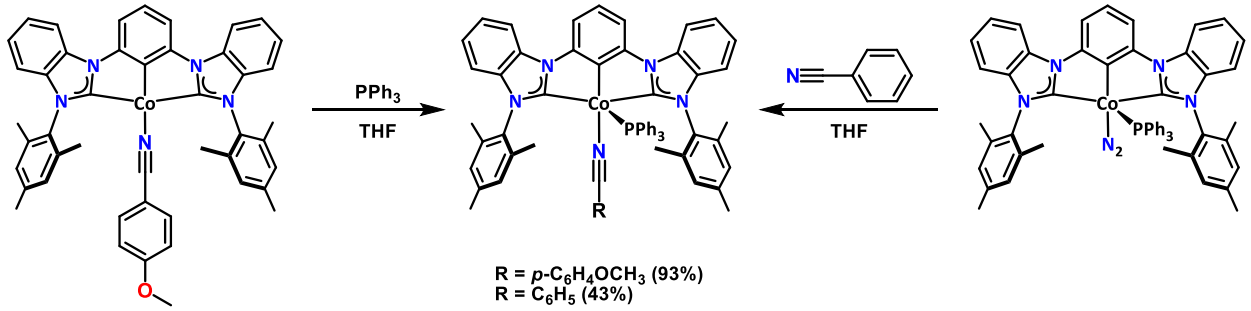

Scheme 5.3 Synthesis of **(^{Mes}CCC)Co(NCC$_6$H$_5$)(PPh$_3$)** and **(^{Mes}CCC)Co(*p*-NCC$_6$H$_4$–OCH$_3$)(PPh$_3$)**.

Attempts to grow single crystals of **(^{Mes}CCC)Co(*p*-NCC$_6$H$_4$–OCH$_3$)** suitable for X-ray structural determination studies proved unsuccessful. However, with the addition of 1 equiv of PPh$_3$ to **(^{Mes}CCC)Co(*p*-NCC$_6$H$_4$–OCH$_3$)**, single crystals suitable for X-ray diffraction studies of **(^{Mes}CCC)Co(*p*-NCC$_6$H$_4$–OCH$_3$)(PPh$_3$)** were obtained (Scheme 5.3). Alternatively, the addition of benzonitrile to the previously discussed **(^{Mes}CCC)Co(N$_2$)(PPh$_3$)** complex[38] furnishes **(^{Mes}CCC)Co(NCC$_6$H$_5$)(PPh$_3$)** (Figure 5.7). The cobalt centers in **(^{Mes}CCC)Co(*p*-NCC$_6$H$_4$–OCH$_3$)(PPh$_3$)** and **(^{Mes}CCC)Co(NCC$_6$H$_5$)(PPh$_3$)** adopt a square pyramidal geometry (τ = 0.25 and 0.19, respectively)[65] with the nitrile bound *trans* to the Co–C$_{aryl}$ bond. The C≡N bond distances in **(^{Mes}CCC)Co(*p*-NCC$_6$H$_4$–OCH$_3$)(PPh$_3$)** and **(^{Mes}CCC)Co(NCC$_6$H$_5$)(PPh$_3$)** (1.165(7) Å

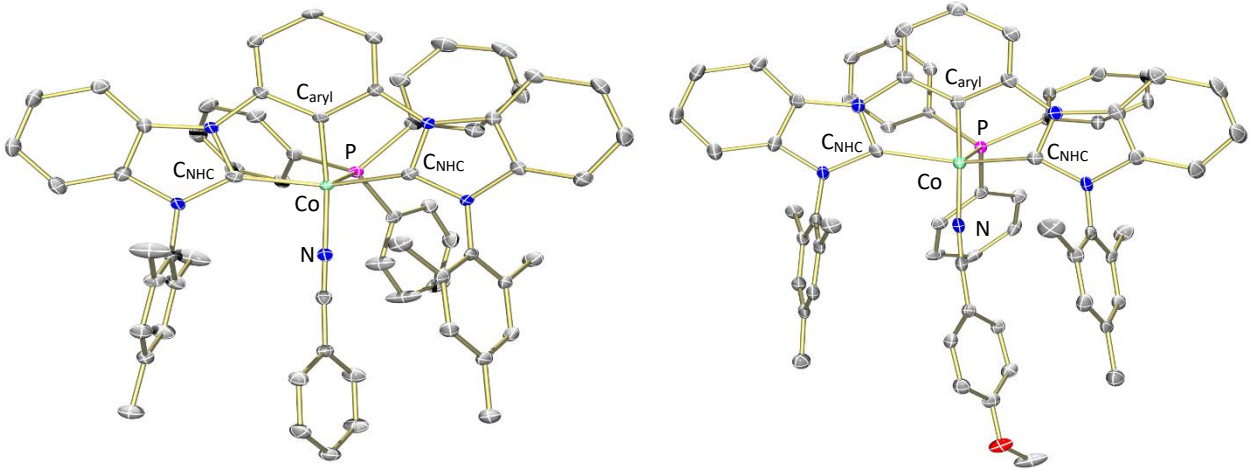

(^{Mes}CCC)Co(NCC$_6$H$_5$)(PPh$_3$) **(^{Mes}CCC)Co(*p*-NCC$_6$H$_4$–OCH$_3$)(PPh$_3$)**

Figure 5.7 Molecular structure of **(^{Mes}CCC)Co(NCC$_6$H$_5$)(PPh$_3$)** (left) with 50% probability ellipsoids and **(^{Mes}CCC)Co(*p*-NCC$_6$H$_4$–OCH$_3$)(PPh$_3$)** (right) with 30% probability ellipsoids. Solvent and H atoms have been omitted for clarity.

and 1.157(3) Å, respectively) are within error of the free molecules (1.1516(16) Å and 1.16 Å, respectively)[66,67] (Table 5.1 and 5.2). Additionally, vibrational modes in the IR spectrum corresponding to the bound nitriles are observed at 2202 and 2191 cm^{-1} for (**^{Mes}CCC)Co(*p*-NCC$_6$H$_4$–OCH$_3$)(PPh$_3$)** and **(^{Mes}CCC)Co(NCC$_6$H$_5$)(PPh$_3$)**, respectively. These are red-shifted form the free nitriles by 14 and 41 cm^{-1}, respectively, and support the end-on coordination mode of the nitrile to the metal center.

5.5 Mechanistic studies – catalytic reactions

Having established that the nitrile coordinates to the reduced cobalt species in an end-on fashion, the competency of **(^{Mes}CCC)Co-py** and **(^{Mes}CCC)Co(*p*-NCC$_6$H$_4$–OCH$_3$)** for nitrile hydrogenation were next explored. Using **(^{Mes}CCC)Co-py** (2 mol%), KO^{t}Bu (6 mol%) and 4 atm of H_2, the hydrogenation of 4-methylbenzonitrile did not proceed and starting material was recovered.[39] Under optimized conditions, 2 equiv of BEt_3 is generated upon the *in situ* reduction of the precatalyst, **(^{Mes}CCC)CoCl$_2$py**, with 2 equiv of $NaHBEt_3$. Surprisingly, the addition of 2 equiv of BEt_3 (4 mol%) to the catalytic reaction using **(^{Mes}CCC)Co-py** enabled hydrogenation to proceed.[39] This suggest the borane is acting as a Lewis acid and is involved in the catalysis. Furthermore, BPh_3, LiOTf, and $Ca(OTf)_2$ all proved effective Lewis acids for the catalytic reaction.[39] The use of **(^{Mes}CCC)Co(*p*-NCC$_6$H$_4$–OCH$_3$)** as the catalyst with the addition of Lewis acid was effective in the hydrogenation of 4-methoxybenzonitrile, indicating pyridine is not involved in the catalytic reaction.[39]

5.6 Mechanistic studies – catalytic reaction profile

To gain further mechanistic insights and selectivity into the observed Lewis acid-assisted catalysis, the reaction profile of a catalytic run was monitored. Even though mixtures were not observed when isolating each amine, the detection of side-products throughout the catalytic process would provide insights into the observed selectivity. Accordingly, the concentrations of the reaction components of a catalytic run were monitored to probe the reaction progress using GC−MS analysis. During these studies, the primary imine intermediate was not observed due to its reactive nature. Instead, the reaction profile was monitored *in situ* using ^{1}H NMR spectroscopy (Figure 5.15) to obtain a more accurate representation of the reaction components (Figure 5.8).

The plot shows the decrease of the nitrile and initial increase of the primary imine concentration, followed by consumption of the primary imine and the steady increase in the primary amine product. Notably, the formation of the secondary imine is limited, suggesting that the primary imine is favored over the secondary imine throughout the course of catalysis. The addition of 1 equiv of the corresponding

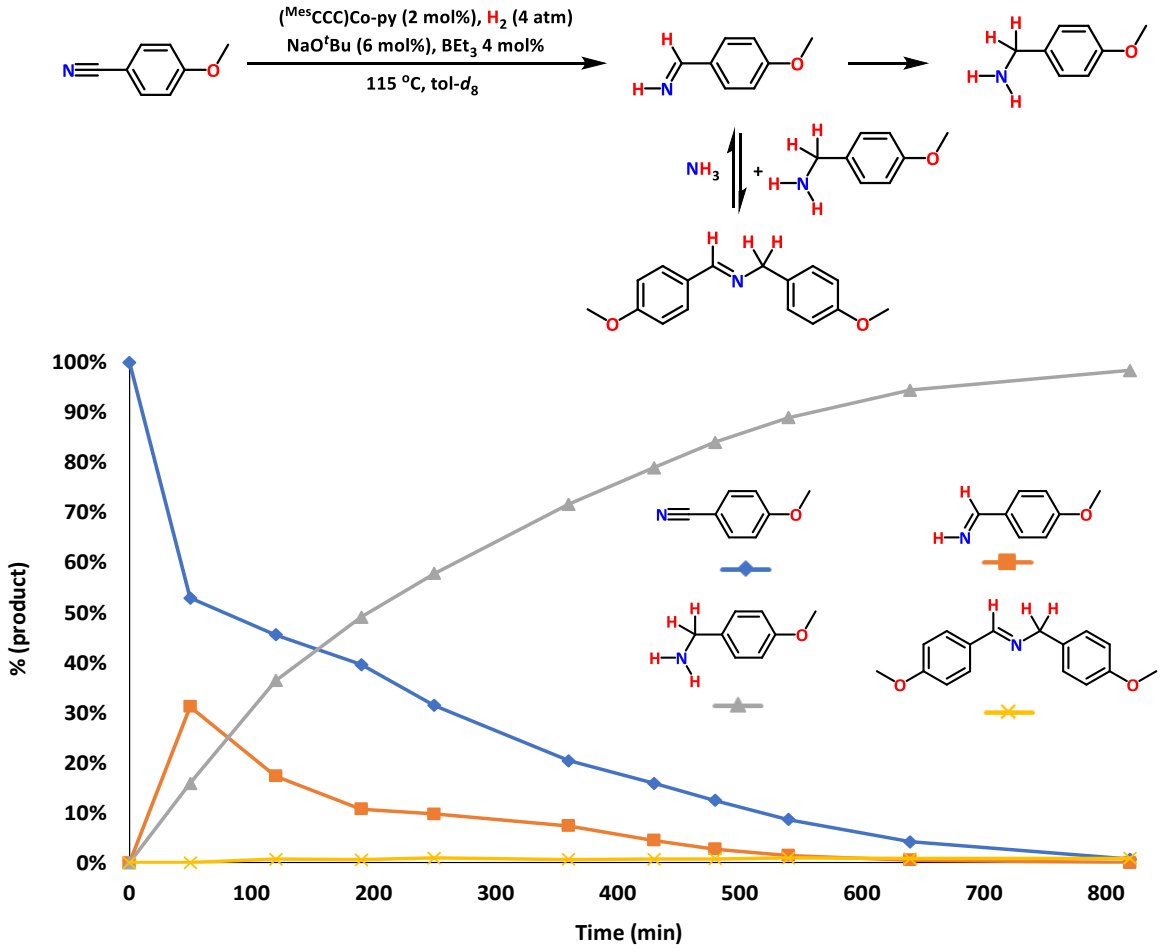

Figure 5.8 Reaction profile of the hydrogenation of 4-methoxybenzonitrile with **(^{Mes}CCC)Co-py** (2 mol%), BEt_3 (4 mol%), and NaO^{t}Bu (6 mol%) in toluene-d_8 under 4 atm of H_2.

amine (with respect to the nitrile) did not change the time required for the reaction to reach completion, indicating an increased amine concentration does not inhibit catalytic activity.

Based on these insights, additional experiments were performed to understand if the presence of a Lewis acid was necessary for the hydrogenation of the imine to proceed. Use of a primary imine surrogate, N-benzylidenebenzylamine, in the absence of Lewis acid yielded 10% conversion of the starting material to the secondary amine as observed by GC−MS. In contrast, the addition of BEt_3 (4 mol %) resulted in 90% conversion to the amine. Therefore, the Lewis acid also facilitates this second hydrogenation step but is not necessary for the reaction to occur.

5.7 Nitrile hydrogenation with ketone functionality

In view of these findings, the hydrogenation of 4-acetylbenzonitrile, a substrate that proved unamenable toward hydrogenation using previous reaction conditions was re-examined (vide supra). Recognizing that the Lewis acid is necessary for the hydrogenation of nitriles to proceed, the potential

interaction of the ketone functionality with the Lewis acid was hypothesized to inhibit the hydrogenation of the nitrile functionality. Accordingly, the addition of excess Lewis acid, 1.04 equiv with respect to substrate, during a catalytic run furnished the primary amine product in 95% yield.[39] Notably, the ketone functionality was not reduced under these conditions, which is a distinct difference from the hydrogenation catalysis with iron,[25] ruthenium[68,69] and palladium[70] systems.

5.8 Mechanistic studies – stoichiometric studies

To further understand the role of the Lewis acid, the stoichiometric reactivity between BEt_3 and the cobalt complexes, **(^{Mes}CCC)Co-py** and **(^{Mes}CCC)Co(*p*-NCC$_6$H$_4$–OCH$_3$)** was studied. Upon the addition of 1 equiv of BEt_3 to a solution of **(^{Mes}CCC)Co-py** in benzene-d_6, the formation of a C_2-symmetric species, **(^{Mes}CCC)Co–N$_2$**, was observed by ^{1}H NMR spectroscopy (Figure 5.9), akin to the reaction between **(^{Mes}CCC)CoCl$_2$py** and 2 equiv of $NaHBEt_3$ (Figure 5.2).

Computational modeling and experimental data have shown that reactivity of Lewis acidic boranes (BF_3 and $B(C_6F_5)_3$) with nitriles results in an electrostatic interaction in the subsequent adduct formation.[71,72] Interested in understanding if a nitrile···borane interaction was present, a solution of **(^{Mes}CCC)Co(*p*-NCC$_6$H$_4$–OCH$_3$)** was treated with BEt_3, and the mixture was monitored by ^{1}H NMR spectroscopy. Unfortunately, there was no change in the ^{1}H NMR in benzene-d_6 nor when monitoring the

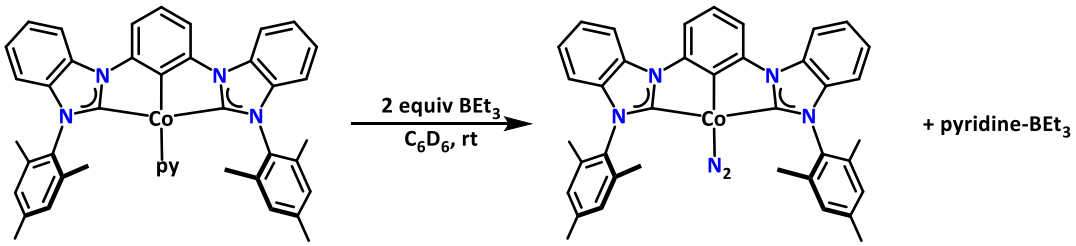

^{1}H NMR spectrum – C$_6$D$_6$

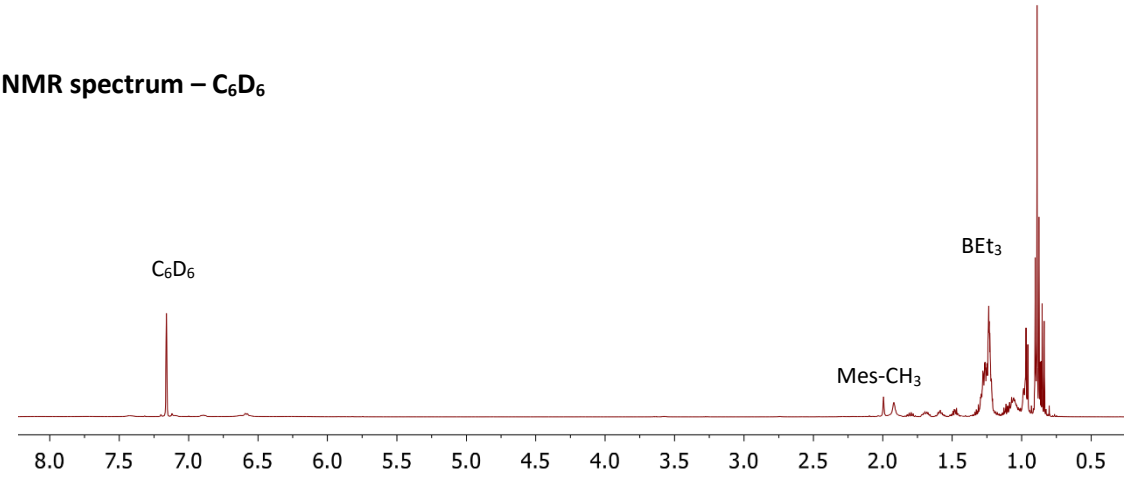

Figure 5.9 ^{1}H NMR spectrum (C_6D_6, 500 MHz) of the reaction **(^{Mes}CCC)Co-py** with 2 equiv of BEt_3 in benzene-d_6.

reaction in toluene-d_8 at 100 °C. Likewise, examining the reaction by IR spectroscopy revealed no change in the C≡N stretch, and the coordination of N_2 was not observed.

5.9 Mechanistic studies – PHIP studies using (^{Mes}CCC)Co-py

The PHIP transfer NMR studies were re-examined using **(^{Mes}CCC)Co-py** and BEt_3 to probe the importance of the Lewis acid in the pairwise process. Upon the addition of *p*-H_2 to a toluene-d_8 solution containing 4-(trifluoromethyl)benzonitrile, **(^{Mes}CCC)Co-py** (2mol %), NaO^{t}Bu (6 mol %), and BEt_3 (4 mol %)

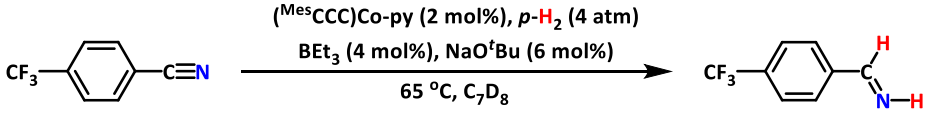

^{1}H NMR-(45°) spectrum – toluene-d_8

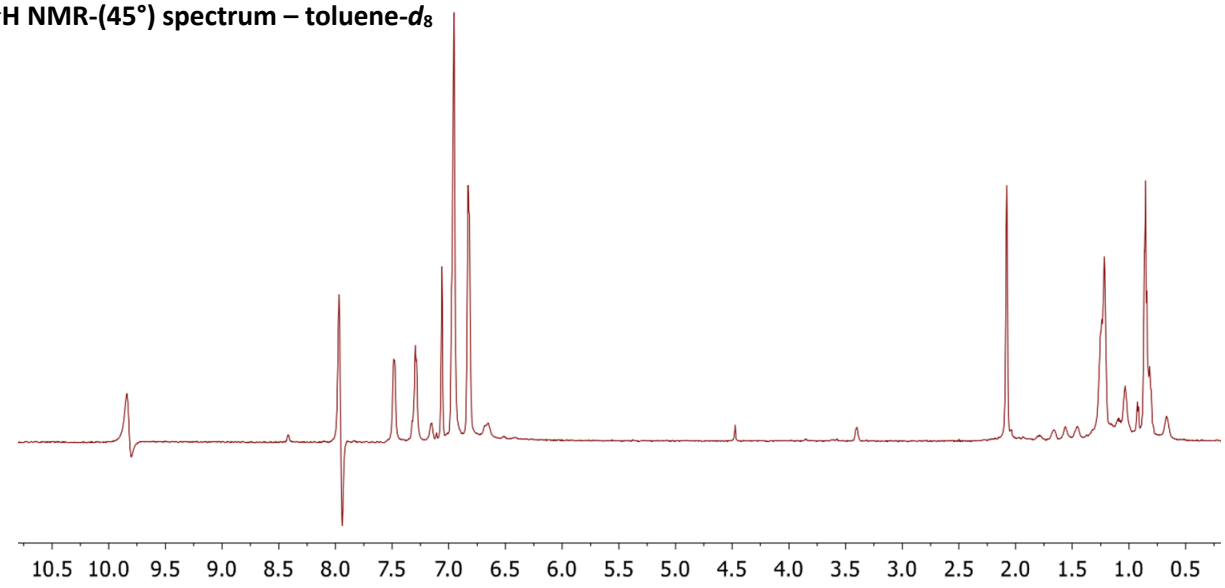

^{1}H NMR-OPSY spectrum – toluene-d_8

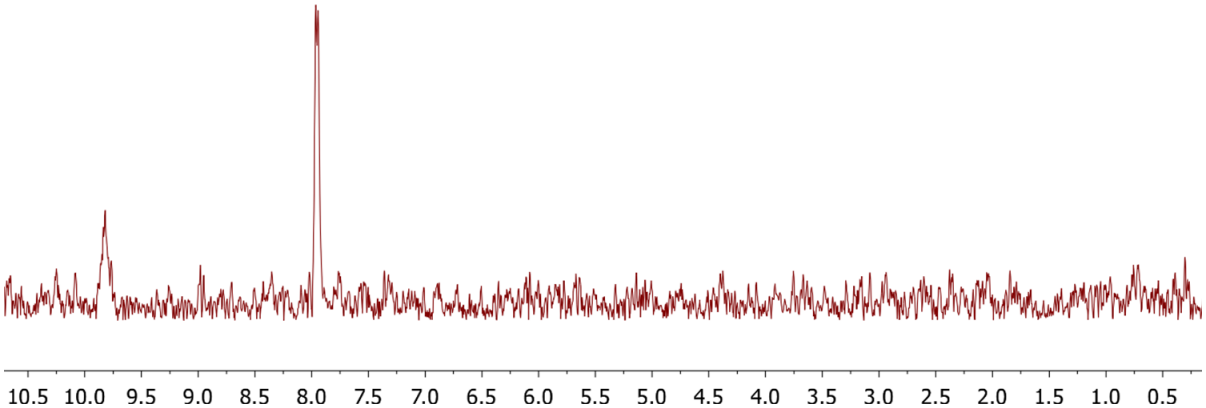

Figure 5.10 ^{1}H NMR (C_7D_8, 600 MHz) spectrum of **(^{Mes}CCC)Co-py (2 mol %)**, BEt_3 (4 mol %), KO^{t}Bu (6 mol %), and 4-(trifluoromethyl)benzonitrile under 4 atm of *p*-H_2 at 65 °C collected using a 45° pulse (top) and ^{1}H-OPSY pulse (bottom).

at 25 °C, hyperpolarization was not observed. When the solution was heated to 65 °C, the PASADENA effect of the primary imine group was observed in the ^{1}H NMR spectrum using a 45° and OPSY pulse (Figure 5.10). These results are comparable with the PHIP transfer NMR data using **(^{Mes}CCC)CoCl$_2$py** and NaHBEt$_3$, demonstrating that the Co(I)-species along with BEt$_3$ affords the same PHIP effect, albeit at lower temperatures. Additionally, similar effects were observed using 4-methoxybenzonitrile as the substrate (Figure 5.14). On the basis of the PHIP transfer NMR data, the first step in the hydrogenation of nitriles conforms with the concerted nature of H_2 addition, which is consistent with our previous studies of the cobalt-catalyzed hydrogenation of carbon−carbon multiple bonds using the same ligand platform.[30,31]

5.10 Proposed catalytic intermediate

Although the nitrile was found to coordinate to the cobalt center end-on at ambient temperatures, under catalytic conditions, the coordination mode changes to accommodate the pairwise addition of H_2 onto the metal center as indicated by the PHIP NMR data. One possibility involves a side-on coordination mode of the nitrile through the C≡N π-orbital proceeding through a three-center bonding environment. In the side-on coordination mode, the C≡N bond would be more amenable toward functionalization, and the nitrogen lone pair would be available to interact with a Lewis acid in a similar fashion as observed in bisphosphine nickel(0) complexes.[67,73,74] A computational study by Jiao and co-workers reported that the energy difference decreases between end-on and side-on coordination modes of acetonitrile in cobalt complexes with increasing electron-donating ability of the ligands, and therefore, the nitrile group becomes more negatively charged.[75] On the basis of these studies and those presented herein, the most viable role of the Lewis acid in the observed catalysis is depicted in Figure 5.11.

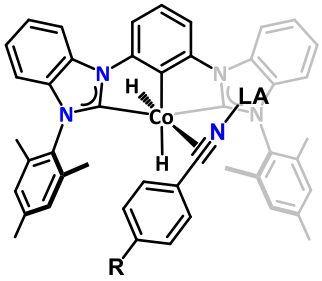

Figure 5.11 Proposed coordination of the Lewis acid to the cobalt-bound nitrile.

5.11 Conclusion

In conclusion, the catalytic activity of a cobalt bis(carbene) pincer system was extended toward the hydrogenation of a broad scope of nitriles with excellent selectivity toward the primary amines. Through the course of the studies, it was determined that the hydrogenation does not proceed without the

addition of catalytic amounts of a Lewis acid. Based on the mechanistic studies herein and corroborating literature precedents, the nature of the Lewis acid is proposed to facilitate a side-on coordination of the nitrile to the cobalt center, permitting a pairwise transfer of H_2 through a Co(I/III) redox process. Furthermore, supplemented by insights gleaned from the mechanistic studies, a nitrile featuring a ketone functionality was amenable toward the selective hydrogenation of only the nitrile, with the addition of superstoichiometric amounts of Lewis acid. Finally, in our approach investigating a bench-stable hydrogenation precatalyst accompanied by in situ activation by $NaHBEt_3$, the presumed innocence of the Lewis acid byproduct was contested, and it proved to hold a substantial role in the observed catalysis.

5.12 Experimental section

General considerations. All manipulations of air- and moisture-sensitive compounds were carried out in the absence of water and dioxygen in an MBraun inert atmosphere drybox under a dinitrogen atmosphere except where specified otherwise. All glassware was oven dried for a minimum of 8 h and cooled in an evacuated antechamber prior to use in the drybox. Solvents for sensitive manipulations were dried and deoxygenated on a Glass Contour System (SG Water USA, Nashua, NH) and stored over 4 Å molecular sieves purchased from Strem following a literature procedure prior to use.[76] Toluene-d_8 and benzene-d_6 were purchased from Cambridge Isotope Labs and were degassed and stored over 4 Å molecular sieves prior to use. Sodium triethylborohydride solution (1.0 M in toluene), triethylborane solution (1.0 M in hexanes), BPh_3, LiOTf, and $Ca(OTf)_2$ were purchased from Sigma-Aldrich. Celite® 545 (J. T. Baker) was dried in a Schlenk flask for 24 h under dynamic vacuum while heating to at least 150˚C prior to use in a glovebox. NMR Spectra were recorded at room temperature on a Varian spectrometer operating at 500 MHz (^{1}H NMR) and 126 MHz (^{13}C NMR) (U500, VXR500, UI500NB) and referenced to the residual C_7D_6H, $CHCl_3$ and C_6D_5H resonance (δ in parts per million, and *J* in Hz). Potassium graphite (KC_8),[77] Schwartz's reagent (Cp_2ZrHCl (Cp = cyclopentadienyl)[78], **(^{Mes}CCC)CoCl$_2$py**[38] and **(^{Mes}CCC)Co(N$_2$)(PPh$_3$)**[38] were prepared according to literature procedures.

Synthesis of cobalt(I) complexes

Preparation of (^{Mes}CCC)Co-py: A 20 mL scintillation vial was charged with **(^{Mes}CCC)CoCl$_2$py** (0.100 g, 0.133 mmol) and THF (10 mL). A suspension of KC_8 (0.038 g, 0.281 mmol) in THF (5 mL) was added to the mixture. After stirring for 2 hours, the dark brown suspension was filtered over Celite and concentrated to a dark solid under reduced pressure. The product was then extracted into benzene (3 x 5 mL), filtered over Celite, and lyophilized under reduced pressure to a dark brown solid (0.072 g, 0.105 mmol, 80%).

NMR data (in benzene-d_6, 25 °C): ^{1}H δ = 8.03 (d, J = 5.4, 2H), 7.79 (t, J = 7.4, 1H), 7.65 (d, J = 7.6, 2H), 7.23 (t, J = 7.8, 3H), 7.00 (t, J = 7.5, 3H), 6.66 (d, J = 7.8, 4H), 6.31 (s, 5H), 1.96 (s, 6H), 1.83 (s, 12H). ^{13}C δ = 147.4, 139.7, 137.1, 136.1, 135.1, 133.1, 129.1, 128.6, 127.5, 122.3, 122.2, 110.0, 108.5, 105.9, 20.9, 17.8. HRMS (ESI), calc. for $C_{43}H_{39}CoN_5$ $(M + H)^+$: calculated 684.2537; found 684.2543.

Preparation of (^{Mes}CCC)Co(*p*-NCC$_6$H$_4$OCH$_3$): A 20 mL scintillation vial was charged with **(^{Mes}CCC)CoCl$_2$py** (0.072 g, 0.095 mmol) and THF (10 mL). A suspension of KC_8 (0.026 g, 0.194 mmol) in THF (5 mL) was added to the mixture. After stirring for 2 hours, the dark brown suspension, **(^{Mes}CCC)Co-py**, was filtered over Celite and a solution of 3h3 (0.013 g, 0.095 mmol) was added. After stirring the mixture for 1 h, the solution was concentrated to a solid under reduced pressure. The product was then extracted into benzene (3 x 5 mL), filtered over Celite, and lyophilized under reduced pressure to a brown solid (0.055g, 0.074 mmol, 79%). Alternatively, **(^{Mes}CCC)Co(*p*-NCC$_6$H$_4$OCH$_3$)** can also be prepared by the addition of 1 equiv of 4-methoxybenzonitrile to **(^{Mes}CCC)Co-py** following the same work up procedure. NMR data (in benzene-d_6, 25 °C): ^{1}H δ = 7.92 (d, J = 8.0, 2H), 7.65-7.57 (m, 3H), 7.32 (s, 1H), 7.00 (s, 1H), 6.95 (t, J = 7.6, 2H), 6.64 (t, J = 8.1, 4H), 6.47 (s, 4H), 6.43 (d, J = 8.5, 2H), 3.20 (s, 3H), 2.03 (s, 12H), 1.74 (s, 6H). The low solubility of **(^{Mes}CCC)Co(*p*-NCC$_6$H$_4$OCH$_3$)** in benzene precluded the collection of ^{13}C NMR data. HRMS (ESI), calc. for $C_{46}H_{40}CoN_5O$ $(M)^+$: calculated 737.2565; found 737.2583. ATR-IR: 2184 cm^{-1} (Co-**N**≡**C**R).

Preparation of (^{Mes}CCC)Co(*p*-NCC$_6$H$_4$OCH$_3$)(PPh$_3$): A 20 mL scintillation vial was charged with **(^{Mes}CCC)Co(*p*-NCC$_6$H$_4$OCH$_3$)** (0.0300 g, 0.0413 mmol) and THF (10 mL). A solution of PPh_3 (0.010 g, 0.0413 mmol) in THF (5 mL) was added. After stirring the reaction mixture for 2h, the THF was removed under reduced pressure. The solid was triturated with hexanes (5 mL) and the volatiles were removed under reduced pressure to yield a dark purple solid (0.0381 g, 0.0385 mmol, 93%). NMR data (in benzene-d_6, 25 °C): ^{1}H δ = 7.81 (d, J = 8.0, 2H), 7.52 (d, J = 7.4, 2H), 7.33 (t, J = 7.8, 1H), 7.12 (t, J = 7.8, 3H), 7.02 (t, J = 7.8, 6H), 6.91 (t, J = 7.8, 6H), 6.87-6.83 (m, 5H), 6.51 (t, J = 8.0, 4H), 6.42-6.38 (m, 2H), 3.27 (s, 3H), 2.12 (s, 6H), 1.89 (s, 6H), 1.66 (s, 6H). ^{13}C δ = 207.2, 160.8, 139.2, 138.0, 137.4, 137.3, 136.8, 136.2, 135.6, 133.9, 133.6, 133.4, 133.3, 133.0, 130.1, 128.7, 121.5, 120.9, 118.3, 114.7, 113.1, 109.3, 107.6, 105.2, 55.0, 20.8, 18.7, 18.6. HRMS (ESI), calc. for $C_{56}H_{48}CoN_4P$ $(M - p\text{-}NCC_6H_4OCH_3)^+$: calculated 866.2949; found 866.2963. ATR-IR: 2202 cm^{-1} (Co-**N**≡**C**R).

Preparation of (^{Mes}CCC)Co(NCC$_6$H$_5$)(PPh$_3$): A 20 mL scintillation vial was charged with **(^{Mes}CCC)Co(N$_2$)(PPh$_3$)** (0.0645 g, 0.0727 mmol), THF (5 mL) and benzonitrile (7.4 uL, 0.0727 mmol). After

stirring the reaction for 1 h at room temperature, the THF was removed under a reduced pressure. The product was then washed with hexanes (2 x 5 mL) and extracted into benzene (3 x 5 mL), filtered over Celite, and the solvent was removed under reduced pressure. A dark purple powder was obtained (0.030 g, 0.031 mmol, 43%) after triturating hexanes (2x 5 mL). NMR data (in benzene-d_6, 25 °C): ^{1}H δ = 7.80 (d, J = 7.9, 2H), 7.52 (d, J = 7.7, 2H), 7.33 (t, J = 7.8, 1H), 7.12 (t, J = 7.7, 2H), 7.00 (t, J = 7.2, 6H), 6.92-6.87 (m, 6H), 6.86-6.81 (m, 6H), 6.80-6.75 (m, 2H), 6.57 (d, J = 7.4, 2H), 6.49 (d, J = 7.8, 2H), 6.40 (s, 4H), 2.10 (s, 6H), 1.86 (s, 6H), 1.58 (s, 6H). ^{13}C δ = 144.1, 139.2, 137.9, 137.3, 137.1, 137.1, 136.2, 135.5, 133.4, 133.3, 132.9, 132.0, 131.8, 131.7, 130.1, 129.5, 128.9, 128.7, 128.6, 128.4, 121.5, 121.0, 118.4, 109.3, 107.7, 105.3, 20.8, 18.7, 18.6. HRMS (ESI), calc. for $C_{56}H_{48}CoN_4P$ (M – NCPh)$^{+}$: calculated 866.2949; found 866.2946. ATR-IR: 2191 cm^{-1} (Co-**N**≡**C**R).

***In situ* stoichiometric reactivity studies**

Treatment of (^{Mes}CCC)CoCl$_2$py with 2.1 equivalents of Cp$_2$ZrHCl

Cp_2ZrHCl (0.003 g, 0.0123 mmol) was added to a J. Young NMR tube containing a saturated solution of **(^{Mes}CCC)CoCl$_2$py** (0.004 g, 0.0053 mmol) C_6D_6 (*ca.* 1/2 mL). Within 1 min, the color of the solution changed from green to red-brown and the resulting ^{1}H NMR spectrum displayed resonances corresponding to the formation of H_2 gas, Cp_2ZrCl_2 and **(^{Mes}CCC)Co-py**. (See Figure 5.3)

Treatment of (^{Mes}CCC)CoCl$_2$py with 2 equiv of NaHBEt$_3$

A 4 mL scintillation vial was charged with **(^{Mes}CCC)CoCl$_2$py** (0.004 g, 0.006 mmol), $NaHBEt_3$ (1.0 M in toluene, 12 µL, 0.011 mmol) and toluene (2 mL). Solution IR (C_7H_8): 2082 cm^{-1} (Co-**N$_2$**). (See Figure 5.2)

Table 5.1 Crystallographic parameters for **(^{Mes}CCC)Co-py**, **(^{Mes}CCC)Co(NCPh)(PPh_3)**, and **(^{Mes}CCC)Co(NCPh-*p*-OMe)(PPh_3).**

	(^{Mes}CCC)Co-py cd63zsa	**(^{Mes}CCC)Co(NCPh)(PPh_3)** cm72zsa	**(^{Mes}CCC)Co(NCPh-*p*-OMe)(PPh_3)** 483_2SA
Empirical Formula	C47 H48 Co N5 O	C67 H63 Co N5 O P	C64 H55 Co N5 O P
Formula Weight	757.83	1044.12	1000.03
Temperature	100(2) K	100(2) K	173(2) K
Wavelength	0.71073 Å	0.71073 Å	0.71073 Å
Crystal system	Orthorhombic	Monoclinic	Orthorhombic
Space group	Pnma	P 21/n	P $2_12_12_1$
Unit Cell Dimensions	a = 24.6141(9)Å b = 19.4717(7) Å c = 8.0534(3) Å α= 90° β= 90° γ = 90°	a =17.9017(10) Å b = 16.1949(10) Å c = 18.5938(12) Å α = 90° β = 93.322(3)° γ = 90°	a = 13.1921(10) Å b = 18.4856(16) Å c = 20.7607(14) Å α = 90° β = 90° γ = 90°
Volume	3859.8(2) $Å^3$	5381.6(6) $Å^3$	5062.8(7) $Å^3$
Z	8	4	4
Reflections collected	26577	128137	47750
Independent reflections	2378	9921	9271
Goodness-of-fit on F2	1.090	1.068	1.013
Final R indices [I>sigma(I)]	R1 = 0.0394 wR2 = 0.0963	R1 = 0.0378 wR2 = 0.0890	R1 = 0.0539 wR2 = 0.1011

Table 5.2 Selected bond lengths and angles for **(^{Mes}CCC)Co-py**, **(^{Mes}CCC)Co(NCPh)(PPh_3)**, and **(^{Mes}CCC)Co(NCPh-*p*-OMe)(PPh_3).**

	(^{Mes}CCC)Co-py	(^{Mes}CCC)Co(NCPh)(PPh_3)	(^{Mes}CCC)Co(NCPh-*p*-OMe)(PPh_3)
Bond Distances (Å)			
Co – C_{NHC}	1.901(3)	1.893(2)	1.892(6)
Co – C_{aryl}	1.855(4)	1.867(2)	1.870(5)
Co – C_{NHC}	1.901(3)	1.892(2)	1.908(5)
Co – N	1.962(2)	1.8927(19)	1.892(5)
Co – P	N/A	2.2399(7)	2.2213(15)
C≡N	N/A	1.157(3)	1.165(7)
Bond Angles (°)			
C_{aryl}-Co-$N_{py/N\equiv C}$	170.78(17)	161.71(9)	165.3(2)
C_{NHC}-Co-$N_{py/N\equiv C}$	100.65(9)	96.48(9)	95.5(2)
C_{NHC}-Co-C_{NHC}	158.34(18)	150.42(10)	150.5(2)
C_{NHC}-Co-C_{aryl}	79.80(9)	79.22(9)	79.7(3)
C_{aryl}-Co-P	N/A	91.85(7)	93.70(16)
C_{NHC}-Co-P	N/A	102.33(7)	102.43(17)
$N_{N\equiv C}$ -Co-P	N/A	106.43(6)	100.90(15)

Mechanistic studies

***Para*-hydrogen induced polarization NMR studies**

Sample preparation using (^{Mes}CCC)CoCl$_2$py. A standard J. Young NMR tube was charged with 4-methoxybenzonitrile (17.6. mg, 0.133 mmol), KO^{t}Bu (1.0 mg, 0.0089 mmol) and **(^{Mes}CCC)CoCl$_2$py** (2.0 mg, 0.0027 mmol) in *ca.* ½ ml of toluene-d_8. A solution of NaHBEt$_3$ (1.0 M in toluene, 5.3 µL, 0.0053 mmol) was added and the color the solution turned brown. The sample was subjected to two freeze-pump-thaw cycles and *p*-H$_2$ gas (1 atm) was added at 77K on a high-vacuum line. The sample was kept frozen in liquid nitrogen and warmed to ambient temperature and shaken immediately prior to inserting into the NMR spectrometer (Following ALTADENA conditions). No polarization was observed at 30 °C and 60 °C. Upon warming the probe temperature to 85 °C, polarization of the imine functionality was observed (see Figure 5.1). In the case of 4-(trifluoromethyl)benzonitrile, polarization of the imine functionality was observed upon warming the probe temperature to 80 °C (see Figure 5.13).

Sample preparation using (^{Mes}CCC)Co-py. A standard J. Young NMR tube was charged with 4-methoxybenzonitrile (9.7 mg, 0.0731 mmol), NaO^{t}Bu (0.4 mg, 0.0416 mmol), **(^{Mes}CCC)Co-py** (1.0 mg, 0.00146 mmol) and BEt$_3$ (1.0 M in hexane, 3.0 µL, 0.003 mmol) in *ca.* 1 ml of toluene-d_8. The sample was subjected to two freeze-pump-thaw cycles and *p*-H$_2$ gas (1 atm) was added at 77K on a high-vacuum line. The sample was kept frozen in liquid nitrogen and warmed to ambient temperature and shaken immediately prior to inserting into the NMR spectrometer. No polarization was observed at 25 °C. Upon warming the probe temperature to 65 °C, 70 °C and 75 °C, polarization of the H atoms of the imine functionality were observed (at 75 °C, the signals were more pronounced and are depicted in Figure 5.14). In the case of 4-(trifluoromethyl)benzonitrile, polarization of the imine functionality was observed upon warming the probe temperature to 55 °C and 65 °C. At 65 °C the imine signals were more pronounced and are depicted in Figure 5.10.

NMR spectrometer. All PHIP NMR data presented herein were collected on a Varian UNITY INOVA 500 NB High-Resolution NMR Console with a 5mm Varian ^{1}H{^{13}C/^{15}N} PFG Z probe. All spectra were collected in benzene-d_6 and the residual solvent resonance was referenced to 7.16 ppm. ^{1}H NMR spectra were recorded using 45° pulse angle. The spectral window of 30 ppm was used in both proton and ^{1}H-OPSY experiments. ^{1}H-OPSY NMR data was collected via a double quantum coherence pathway using the pulse sequence below (**Figure 5.12**). The OPSY spectra are anti-phase peaks, and they are generally displayed with absolute mode in the following spectra.[79,80]

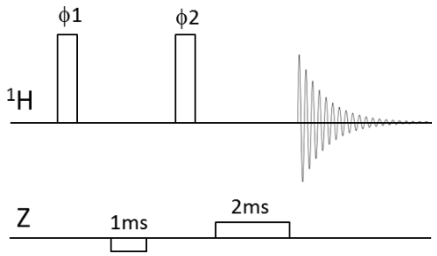

Figure 5.12 Double quantum OPSY pulse sequence (OPSY-d): the vertical bar at ^{1}H channel represents $\pi/2$ pulse. Phase cycle: $\phi1$: $(y)_4(x)_4$, $\phi2$: $(x)_4(y)_4$, rec: $(x)_4(y)_4$. Z Gradient: 50 G/cm rectangular gradient was used. First gradient was applied for 1ms in the opposite direction of the second gradient which was applied for 2ms. 0.5ms gradient recovery delays were used after each gradient. The acquisition time was 4 seconds and no delay between scans was used.

Generation of *para*-hydrogen. A parahydrogen converter was used to generate the *para*-H_2 enriched hydrogen gas. This consisted of copper tubing filled with a hydrous ferric oxide catalyst that was cooled to 15 K using a closed-cycle ^{4}He cryostat. A detailed description of the converter can be found in Tom *et al.*, which was able to consistently convert naturally occurring hydrogen gas (3:1 *ortho*:*para*) to 99.99% *para*-H_2.[81]

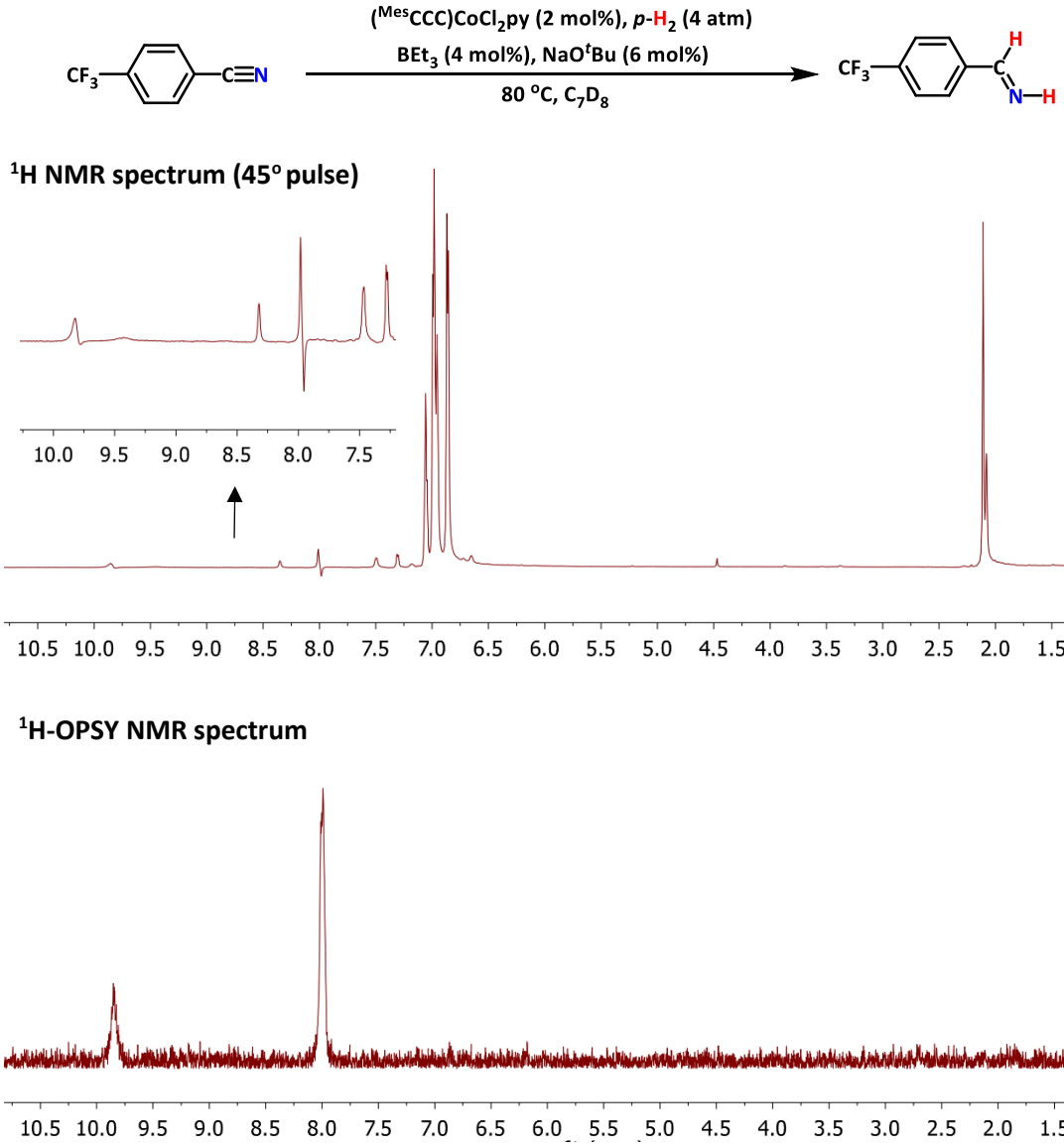

Figure 5.13 ^{1}H NMR (C_7D_8, 600 MHz, 45° pulse) spectrum of **(^{Mes}CCC)CoCl$_2$py** (2 mol%), NaHBEt$_3$ (4 mol%), KO^{t}Bu (6 mol%) and 4-(trifluoromethyl)benzonitrile under 4 atm of *p*-H_2 at 80 °C (top). ^{1}H-OPSY NMR (C_7D_8, 600 MHz) spectrum of (^{Mes}CCC)CoCl$_2$py (2 mol%), NaHBEt$_3$ (4 mol%), KO^{t}Bu (6 mol%) and 4-(trifluoromethyl)benzonitrile under 4 atm of *p*-H_2 at 80 °C (bottom).

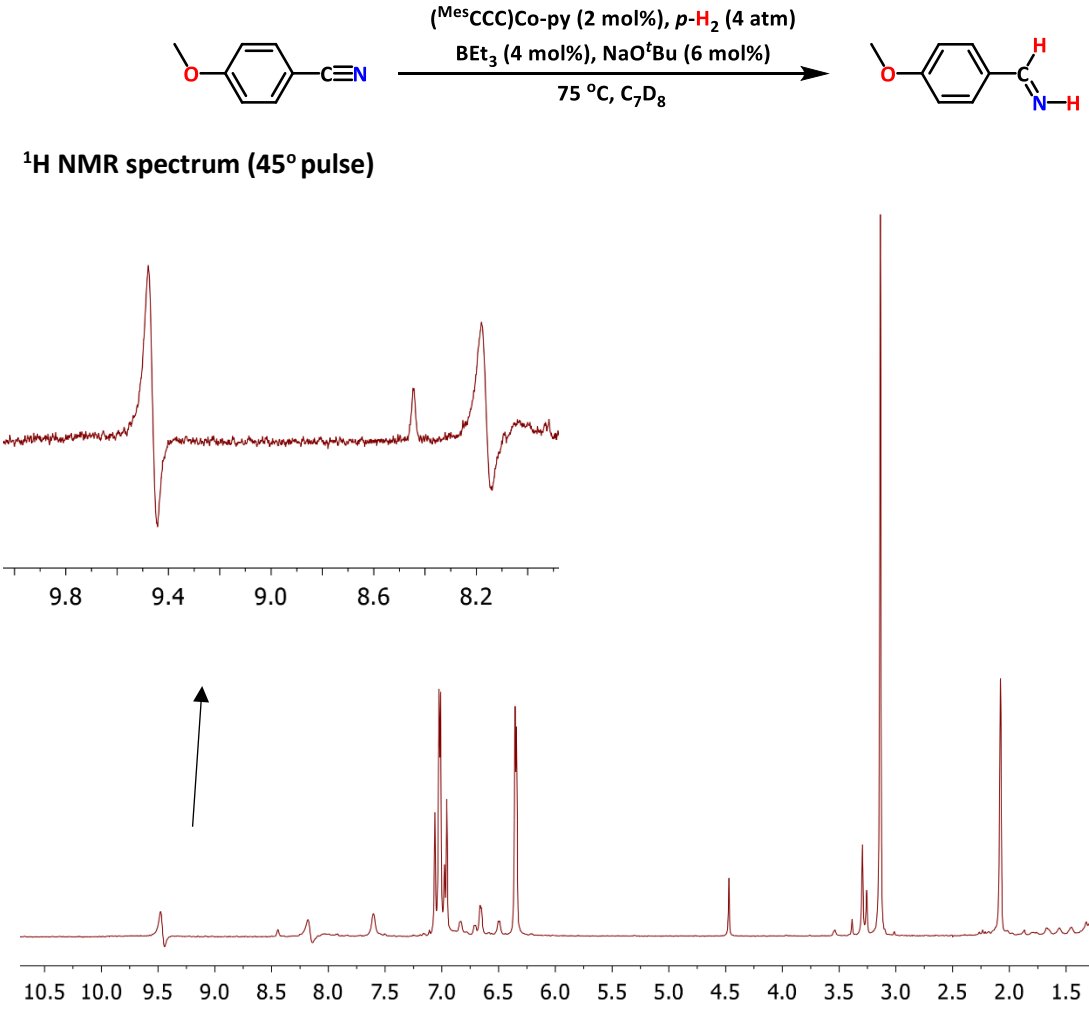

Figure 5.14 ^{1}H NMR (C_7D_8, 600 MHz, 45° pulse) spectrum of **(^{Mes}CCC)Co-py** (2 mol%), BEt_3 (4 mol%), NaO^{t}Bu (6 mol%) and 4-methoxybenzonitrile under 4 atm of *p*-H_2 at 75 °C.

Amine concentration experiment with 4-methoxybenzylamine and 4-tolunitrile or 4-methoxybenzonitrile

A standard J. Young NMR tube was charged with 4-tolunitrile (4.3 mg, 0.0367 mmol) or 4-methoxybenzonitrile (4.9 mg, 0.0367 mmol), 4-methoxybenzylamine (5 µL, 0.367 mmol), NaO^{t}Bu (0.2 mg, 0.002 mmol), **(^{Mes}CCC)Co-py** (0.5 mg, 0.0007 mmol) and BEt_3 (1.0 M in hexane, 1.5 µL, 0.0015 mmol) in *ca.* ½ mL of toluene-d_8. The sample was subjected to two freeze-pump-thaw cycles and H_2 gas (1 atm) was added at 77K on a high-vacuum line. After heating the reaction for 9 h in at 115 °C, the H_2 was vented and complete conversion to the primary amine product was observed for 4-tolunitrile by GC-MS analysis. When 4-methoxybenzonitrile was used, only the amine product was observed by GC-MS.

***In situ* NMR monitoring of a catalytic run**

A standard J. Young NMR tube was charged with 4-methoxybenzonitrile (4.9 mg, 0.0365 mmol), NaO^{t}Bu (0.2 mg, 0.002 mmol), **(^{Mes}CCC)Co-py** (0.5 mg, 0.0007 mmol), BEt_3 (1.0 M in hexane, 1.5 µL, 0.0015 mmol) and triphenyl methane (4.46 mg, 0.0182 mmol, internal standard) in *ca.* ½ mL of toluene-d_8. The sample was subjected to two freeze-pump-thaw cycles and H_2 gas (1 atm) was added at 77K on a high-vacuum line. After warming the NMR tube to ambient temperature, the reaction was heated in a 115 °C oil bath. For each time point, the reaction was removed from the oil bath, allowed to cool to ambient temperature, washed with hexanes to remove the excess oil and a ^{1}H NMR spectrum was recorded (**Figure 5.15**).

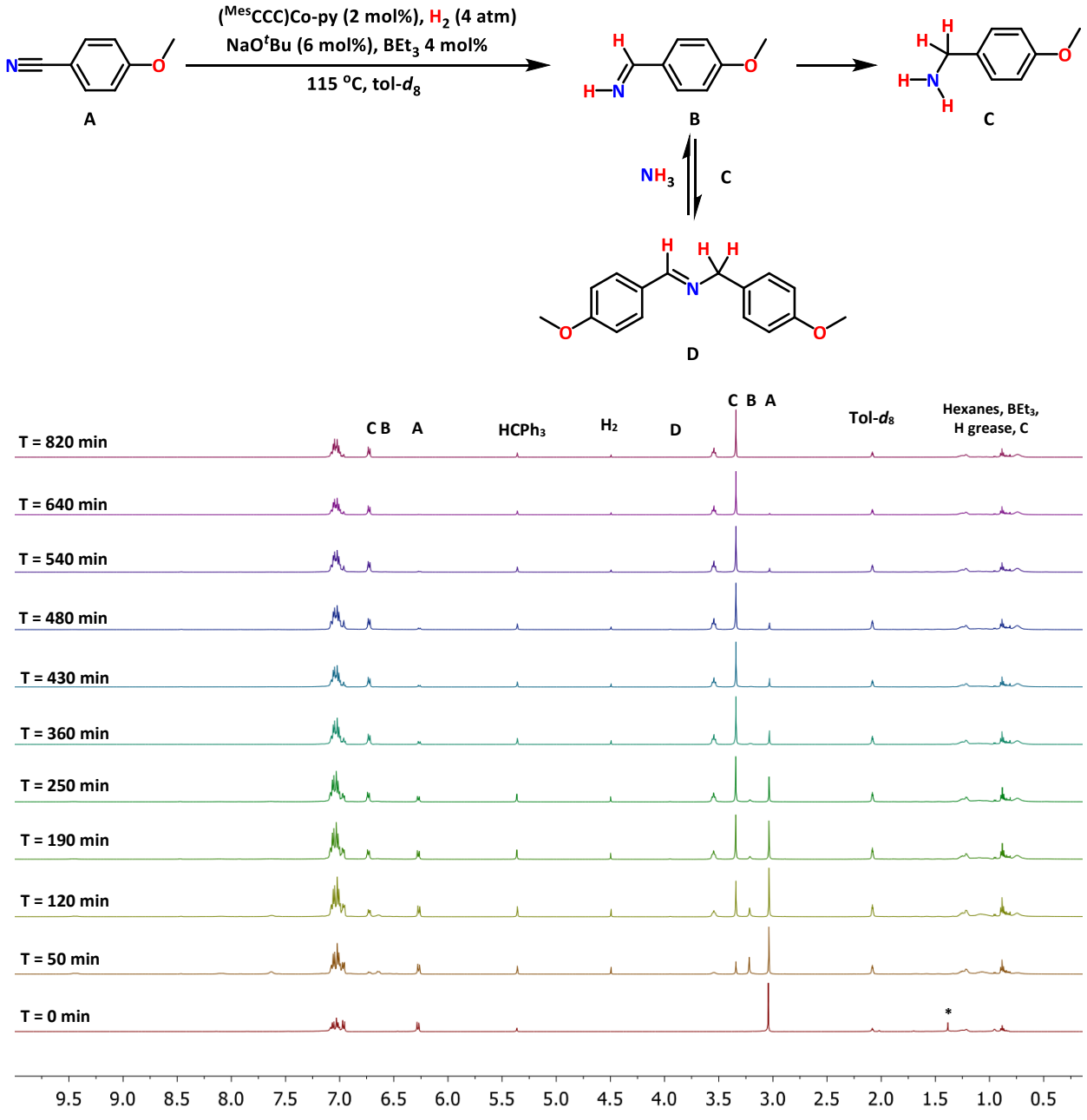

Figure 5.15 ^{1}H NMR (C_7D_8, 500 MHz) spectra of **(^{Mes}CCC)Co-py** (2 mol%), BEt_3 (4 mol%), NaO^{t}Bu (6 mol%) and 4-methoxybenzonitrile under 4 atm of H_2 taken a different timepoints during the hydrogenation reaction.

5.13 References

1. In Organotransition Metal Chemistry: From Bonding to Reactivity; Hartwig, J. F., Ed.; University Science Books: Sausalito, CA, 2010.
2. In Handbook of Homogenous Hydrogenation; de Vries, J. G., Elsevier, C. J., Eds. Wiley-VCH: New York, 2007.
3. Osborn, J. A.; Jardine, F. H.; Young, J. F.; Wilkinson, G. The preparation and properties of tris(triphenylphosphine)halogenorhodium(I) and some reactions thereof including catalytic homogeneous hydrogenation of olefins and acetylenes and their derivatives. *J. Chem. Soc. A* **1966**, 1711−1732.
4. Noyori, R.; Ohkuma, T.; Kitamura, M.; Takaya, H.; Sayo, N.; Kumobayashi, H.; Akutagawa, S. Asymmetric Hydrogenation of ß-Keto Carboxylic Esters. A Practical, Purely Chemical Access to ß-Hydroxy Esters in High Enantiomeric Purity. *J. Am. Chem. Soc.* **1987**, *109*, 5856-5858.
5. Crabtree, R. H. *The Organometallic Chemistry of the Transition Metals,* 5th ed.; John Wiley & Sons: New York, 2009.
6. Bagal, D. B.; Bhanage, B. Recent Advances in Transition Metal-Catalyzed Hydrogenation of Nitriles. *Adv. Synth. Catal.* **2015**, *357*, 883−900 and references therein.
7. Blaser, H.; Malan, C.; Pugin, B.; Spindler, F.; Steiner, H.; Studer, M. Selective Hydrogenation for Fine Chemicals: Recent Trends and New Developments. *Adv. Synth. Catal.* **2003**, *345*, 103−151.
8. Banwell, M. G.; Jones, M. T.; Reekie, T. A.; Schwartz, B. D.; Tan, S. H.; White, L. V. RANEY® cobalt – an underutilized reagent for the selective cleavage of C–X and N–O bonds. *Org. Biomol. Chem.* **2014**, *12*, 7433−7444.
9. Amundsen, L. H.; Nelson, L. S. Reduction of Nitriles to Primary Amines with Lithium Aluminum Hydride. *J. Am. Chem. Soc.* **1951**, *73*, 242− 244.
10. Hudlicky, M. Reductions in Organic Chemistry; John Wiley & Sons: New York, 1984.
11. Rajesh, K.; Dudle, B.; Blacque, Ol.; Berke, H. Homogeneous Hydrogenations of Nitriles Catalyzed by Rhenium Complexes. *Adv. Synth. Catal.* **2011**, *353*, 1479−1484.
12. Li, T.; Bergner, I.; Haque, F. N.; Zimmer-De Iuliis, M.; Song, D.; Morris, R. H. Hydrogenation of Benzonitrile to Benzylamine Catalyzed by Ruthenium Hydride Complexes with P−NH−NH−P Tetradentate Ligands: Evidence for a Hydridic−Protonic Outer Sphere Mechanism. *Organometallics* **2007**, *26*, 5940−5949.
13. Enthaler, S.; Junge,K.; Addis, D.;Erre,G.; Beller, M. A Practical and Benign Synthesis of Primary Amines through Ruthenium-Catalyzed Reduction of Nitriles. *ChemSusChem* **2008**, *1*, 1006−1010.

14. Addis, D.; Enthaler, S.; Junge, K.; Wendt, B.; Beller, M. Ruthenium N-heterocyclic carbene catalysts for selective reduction of nitriles to primary amines. *Tetrahedron Lett.* **2009**, *50*, 3654−3656.
15. Gunanathan, C.; Holscher, M.; Leitner, W. Reduction of Nitriles to Amines with H_2 Catalyzed by Nonclassical Ruthenium Hydrides – Water-Promoted Selectivity for Primary Amines and Mechanistic Investigations. *Eur. J. Inorg. Chem.* **2011**, *2011*, 3381−3386.
16. Miao, X.; Bidange, J.; Dixneuf, P. H.; Fischmeister, C.; Bruneau, C.; Dubois, J.; Couturier, J. Ruthenium–Benzylidenes and Ruthenium–Indenylidenes as Efficient Catalysts for the Hydrogenation of Aliphatic Nitriles into Primary Amines. *ChemCatChem* **2012**, *4*, 1911−1916.
17. Werkmeister, S.; Junge, K.; Wendt, B.; Spannenberg, A.; Jiao, H.; Bornschein, C.; Beller, M. Ruthenium/Imidazolylphosphine Catalysis: Hydrogenation of Aliphatic and Aromatic Nitriles to Form Amines. *Chem. - Eur. J.* **2014**, *20*, 4227−4231.
18. Adam, R.; Bheeter, C. B.; Jackstell, R.; Beller, M. A Mild and Base-Free Protocol for the Ruthenium-Catalyzed Hydrogenation of Aliphatic and Aromatic Nitriles with Tridentate Phosphine Ligands. *ChemCatChem* **2016**, *8*, 1329−1334.
19. Reguillo, R.; Grellier, M.; Vautravers, N.; Vendier, L.; Sabo- Etienne, S. Ruthenium-Catalyzed Hydrogenation of Nitriles: Insights into the Mechanism. *J. Am. Chem. Soc.* **2010**, *132*, 7854−7855.
20. Yoshida, T.; Okano, T.; Otsuka, S. Catalytic hydrogenation of nitriles and dehydrogenation of amines with the rhodium(I) hydrido compounds $[RhH(PPr^i_3)_3]$ and $[Rh_2H_2(\mu\text{-}N_2)\{P(cyclohexyl)_3\}_4]$. *J. Chem. Soc., Chem. Commun.* **1979**, 870−871.
21. Xie, X.; Liotta, C. L.; Eckert, C. CO_2-Protected Amine Formation from Nitrile and Imine Hydrogenation in Gas-Expanded Liquids. *Ind. Eng. Chem. Res.* **2004**, *43*, 7907−7911.
22. Anastas, P. T.; Kirchhoff, M. M. Origins, Current Status, and Future Challenges of Green Chemistry. *Acc. Chem. Res.* **2002**, *35*, 686− 694.
23. Bullock, R. M. Abundant Metals Give Precious Hydrogenation Performance. *Science* **2013**, *342*, 1054−1055.
24. Bornschein, C.; Werkmeister, S.; Wendt, B.; Jiao, H.; Alberico, E.; Baumann, W.; Junge, H.; Junge, K.; Beller, M. Mild and selective hydrogenation of aromatic and aliphatic (di)nitriles with a well-defined iron pincer complex. *Nat. Commun.* **2014**, *5*, 4111.
25. Lange, S.; Elangovan, S.; Cordes, C.; Spannenberg, A.; Jiao, H.; Junge, H.; Bachmann, S.; Scalone, M.; Topf, C.; Junge, K.; Beller, M. Selective catalytic hydrogenation of nitriles to primary amines using iron pincer complexes. *Catal. Sci. Technol.* **2016**, *6*, 4768−4772.

26. Elangovan, S.; Topf, C.; Fischer, S.; Jiao, H.; Spannenberg, A.; Baumann, W.; Ludwig, R.; Junge, K.; Beller, M. Selective Catalytic Hydrogenations of Nitriles, Ketones, and Aldehydes by Well-Defined Manganese Pincer Complexes. *J. Am. Chem. Soc.* **2016**, *138*, 8809−8814.
27. Mukherjee, A.; Srimani, D.; Chakraborty, S.; Ben-David, Y.; Milstein, D. Selective Hydrogenation of Nitriles to Primary Amines Catalyzed by a Cobalt Pincer Complex. *J. Am. Chem. Soc.* **2015**, *137*, 8888−8891.
28. Chakraborty, S.; Leitus, G.; Milstein, D. Selective hydrogenation of nitriles to primary amines catalyzed by a novel iron complex. *Chem. Commun.* **2016**, *52*, 1812−1815.
29. Adam, R.; Bheeter, C. B.; Cabrero-Antonino, J. R.; Junge, K.; Jackstell, R.; Beller, M. Selective Hydrogenation of Nitriles to Primary Amines by using a Cobalt Phosphine Catalyst. *ChemSusChem* **2017**, *10*, 842−846.
30. Tokmic, K.; Markus, C. R.; Zhu, L.; Fout, A. R. Well-Defined Cobalt(I) Dihydrogen Catalyst: Experimental Evidence for a Co(I)/Co(III) Redox Process in Olefin Hydrogenation. *J. Am. Chem. Soc.* **2016**, *138*, 11907-11913.
31. Tokmic, K.; Fout, A. R. Alkyne Semihydrogenation with a Well-Defined Nonclassical Co-H_2 Catalyst: A H_2 Spin on Isomerization and *E*-Selectivity. *J. Am. Chem. Soc.* **2016**, *138*, 13700-13705.
32. Friedfeld, M. R.; Shevlin, M.; Hoyt, J. M.; Krska, S. W.; Tudge, M. T.; Chirik, P. J. Cobalt Precursors for High-Throughput Discovery of Base Metal Asymmetric Alkene Hydrogenation Catalysts. *Science* **2013**, *342*, 1076−1080.
33. Greenhalgh, M. D.; Thomas, S. P. Chemo-, regio-, and stereoselective iron-catalysed hydroboration of alkenes and alkynes. *Chem. Commun.* **2013**, *49*, 11230−11232.
34. Chen, C.; Hecht, M. B.; Kavara, A.; Brennessel, W. W.; Mercado, B. Q.; Weix, D. J.; Holland, P. L. Rapid, Regioconvergent, Solvent-Free Alkene Hydrosilylation with a Cobalt Catalyst. *J. Am. Chem. Soc.* **2015**, *137*, 13244−13247.
35. Léonard, N. G.; Bezdek, M. J.; Chirik, P. J. Cobalt-Catalyzed C(sp^2)–H Borylation with an Air-Stable, Readily Prepared Terpyridine Cobalt(II) Bis(acetate) Precatalyst. *Organometallics* **2017**, *36*, 142−150.
36. Obligacion, J. V.; Bezdek, M. J.; Chirik, P. J. C(sp^2)–H Borylation of Fluorinated Arenes Using an Air-Stable Cobalt Precatalyst: Electronically Enhanced Site Selectivity Enables Synthetic Opportunities. *J. Am. Chem. Soc.* **2017**, *139*, 2825−2832.
37. Docherty, J. H.; Peng, J.; Dominey, A. P.; Thomas, S. P. Activation and discovery of earth-abundant metal catalysts using sodium tert-butoxide. *Nat. Chem.* **2017**, *9*, 595−600.

38. Ibrahim, A. D.; Tokmic, K.; Brennan, M. B.; Kim, D. Matson, E. M.; Nilges, M. J.; Bertke, J. A.; Fout, A. R. Monoanionic bis(carbene) pincer complexes featuring cobalt(I-III) oxidation states. *Dalton Trans.* **2016**, *45*, 9805-9811.
39. Tokmic, K.; Jackson, B. J.; Salazar, A.; Woods, T. J.; Fout, A. R. Cobalt-Catalyzed and Lewis Acid-Assisted Nitrile Hydrogenation to Primary Amines: A Combined Effort. *J. Am. Chem. Soc.* **2017**, *139*, 13554-13561.
40. Kovtunov, K. V.; Beck, I. E.; Bukhtiyarov, V. I.; Koptyug, I. V. Observation of Parahydrogen-Induced Polarization in Heterogeneous Hydrogenation on Supported Metal Catalysts. *Angew. Chem., Int. Ed.* **2008**, *47*, 1492−1495.
41. Balu, A. M.; Duckett, S. B.; Luque, R. Para-hydrogen induced polarisation effects in liquid phase hydrogenations catalysed by supported metal nanoparticles. *Dalton Trans.* **2009**, 5074−5076.
42. Irfan, M.; Eshuis, N.; Spannring, P.; Tessari, M.; Feiters, M. C.; Rutjes, F. P. J. T. Liquid-Phase Parahydrogen-Induced Polarization (PHIP) with Ligand-Capped Platinum Nanoparticles. *J. Phys. Chem. C* **2014**, *118*, 13313−13319.
43. Burueva, D. B.; Salnikov, O. G.; Kovtunov, K. V.; Romanov, A. S.; Kovtunova, L. M.; Khudorozhkov, A. K.; Bukhtiyarov, A. V.; Prosvirin, I. P.; Bukhtiyarov, V. I.; Koptyug, I. V. Hydrogenation of Unsaturated Six-Membered Cyclic Hydrocarbons Studied by the Parahydrogen-Induced Polarization Technique. *J. Phys. Chem. C* **2016**, *120*, 13541−13548.
44. Salnikov, O. G.; Liu, H.; Fedorov, A.; Burueva, D. B.; Kovtunov, K. V.; Copéret, C.; Koptyug, I. V. Pairwise hydrogen addition in the selective semihydrogenation of alkynes on silica-supported Cu catalysts. *Chem. Sci.* **2017**, *8*, 2426−2430.
45. Eisenberg, R. Parahydrogen-induced polarization: a new spin on reactions with molecular hydrogen. *Acc. Chem. Res.* **1991**, *24*, 110−116.
46. Duckett, S. B.; Wood, N. J. Parahydrogen-based NMR methods as a mechanistic probe in inorganic chemistry. *Coord. Chem. Rev.* **2008**, *252*, 2278− 2291.
47. Duckett, S. B.; Mewis, R. E. Application of Parahydrogen Induced Polarization Techniques in NMR Spectroscopy and Imaging. *Acc. Chem. Res.* **2012**, *45*, 1247− 1257 and references therein.
48. Leutzsch, M.; Wolf, M. L.; Gupta, P.; Fuchs, M.; Thiel, W.; Farès, C.; Fürstner, A. Formation of Ruthenium Carbenes by *gem*-Hydrogen Transfer to Internal Alkynes: Implications for Alkyne *trans*-Hydrogenation. *Angew. Chem., Int. Ed.* **2015**, *54*, 12431−12436.

49. Guan, D.; Holmes, A. J.; Lopez-Serrano, J.; Duckett, S. B. Following palladium catalyzed methoxycarbonylation by hyperpolarized NMR spectroscopy: a parahydrogen based investigation. *Catal. Sci. Technol.* **2017**, *7*, 2101−2109.
50. Zhivonitko, V. V.; Telkki, V. V.; Chernichenko, K.; Repo, T.; Leskela, M.; Sumerin, V.; Koptyug, I. V. Tweezers for Parahydrogen: A Metal-Free Probe of Nonequilibrium Nuclear Spin States of H_2 Molecules. *J. Am. Chem. Soc.* **2014**, *136*, 598−601.
51. Longobardi, L. E.; Russell, C. A.; Green, M.; Townsend, N. S.; Wang, K.; Holmes, A. J.; Duckett, S. B.; McGrady, J. E.; Stephan, D. W. Hydrogen Activation by an Aromatic Triphosphabenzene. *J. Am. Chem. Soc.* **2014**, *136*, 13453−13457.
52. Aguilar, J. A.; Elliott, P. I. P.; López-Serrano, J.; Adams, R. W.; Duckett, S. D. Only *para*-hydrogen spectroscopy (OPSY), a technique for the selective observation of *para*-hydrogen enhanced NMR signals. *Chem. Commun.* **2007**, 1183−1185.
53. Theis, T.; Truong, M. L.; Coffey, A. M.; Shchepin, R. V.; Waddell, K. W.; Shi, F.; Goodson, B. M.; Warren, W. S.; Chekmenev, E. Y. Microtesla SABRE Enables 10% Nitrogen-15 Nuclear Spin Polarization. *J. Am. Chem. Soc.* **2015**, *137*, 1404−1407.
54. Truong, M. L.; Theis, T.; Coffey, A. M.; Shchepin, R. V.; Waddell, K. W.; Shi, F.; Goodson, B. M.; Warren, W. S.; Chekmenev, E. Y. ^{15}N Hyperpolarization by Reversible Exchange Using SABRE-SHEATH. *J. Phys. Chem. C* **2015**, *119*, 8786−8797.
55. Zhivonitko, V. V.; Skovpin, I. V.; Koptyug, I. V. Strong ^{31}P nuclear spin hyperpolarization produced via reversible chemical interaction with parahydrogen. *Chem. Commun.* **2015**, *51*, 2506−2509.
56. Pravdivtsev, A. N.; Yurkovskaya, A. V.; Zimmermann, H.; Vieth, H.; Ivanov, K. L. Transfer of SABRE-derived hyperpolarization to spin-1/2 heteronuclei. *RSC Adv.* **2015**, *5*, 63615−63623.
57. Mewis, R. E.; Green, R. A.; Cockett, M. C. R.; Cowley, M. J.; Duckett, S. B.; Green, G. G. R.; John, R. O.; Rayner, P. J.; Williamson, D. C. Strategies for the Hyperpolarization of Acetonitrile and Related Ligands by SABRE. *J. Phys. Chem. B* **2015**, *119*, 1416−1425.
58. Logan, A. W. J.; Theis, T.; Colell, J. F. P.; Warren, W. S.; Malcolmson, S. J. Hyperpolarization of Nitrogen-15 Schiff Bases by Reversible Exchange Catalysis with *para*-Hydrogen. *Chem. - Eur. J.* **2016**, *22*, 10777−10782.
59. Colell, J. F. P.; Emondts, M.; Logan, A. W. J.; Shen, K.; Bae, J.; Shchepin, R. V.; Ortiz, G. X.; Spannring, P.; Wang, Q.; Malcolmson, S. J.; Chekmenev, E. Y.; Feiters, M. C.; Rutjes, F. P. J. T.; Blümich, B.; Theis, T.; Warren, S. W. Direct Hyperpolarization of Nitrogen-15 in Aqueous Media with Parahydrogen in Reversible Exchange. *J. Am. Chem. Soc.* **2017**, *139*, 7761−7767.

60. Clapham, S. E.; Hadzovic, A.; Morris, R. H. Mechanisms of the H_2-hydrogenation and transfer hydrogenation of polar bonds catalyzed by ruthenium hydride complexes. *Coord. Chem. Rev.* **2004**, *248*, 2201−2237.
61. Takemoto, S.; Kawamura, H.; Yamada, Y.; Okada, T.; Ono, A.; Yoshikawa, E.; Mizobe, Y.; Hidai, M. Ruthenium Complexes Containing Bis(diarylamido)/Thioether Ligands: Synthesis and Their Catalysis for the Hydrogenation of Benzonitrile. *Organometallics* **2002**, *21*, 3897− 3904.
62. Eisenberg, R.; Eisenschmid, T. C.; Chinn, M. S.; Kirss, R. U. Parahydrogen-Induced Polarization and Polarization Transfer in Hydrogenation and Oxidative Addition Reactions. *Adv. Chem. Ser.* **1992**, *230*,47−74.
63. Eisenberg, R. Parahydrogen Induced Polarization: A New Magnifying Glass for Examining Reactions with Hydrogen. *J. Chin. Chem. Soc.* **1995**, *42*, 471−481.
64. Michelin, R. A.; Mozzon, M.; Bertani, R. Reactions of transition metal-coordinated nitriles. *Coord. Chem. Rev.* **1996**, *147*, 299−338.
65. Addison, A. W.; Rao, T. N.; Reedijk, J.; Van Rijn, J.; Verschoor, G. C. Synthesis, structure, and spectroscopic properties of copper(II) compounds containing nitrogen–sulphur donor ligands; the crystal and molecular structure of aqua[1,7-bis(N-methylbenzimidazol-2'-yl)-2,6-dithiaheptane]copper(II) perchlorate. *J. Chem. Soc., Dalton Trans.* **1986**, 1349-1356.
66. Lesley, M. J. G.; Pineau, M. R.; Hunter, A. D.; Zeller, M. *p*-Anisolecarbonitrile. *Acta Crystallogr., Sect. E: Struct. Rep. Online* **2004**, *E60*, o1937−o1938.
67. Ateşin, T. A.; Li, T.; Lachaize, S.; García, J. J.; Jones, W. D. Experimental and Theoretical Examination of C−CN Bond Activation of Benzonitrile Using Zerovalent Nickel. *Organometallics* **2008**, *27*, 3811−2817.
68. Lu, Z.; Williams, T. J. A dual site catalyst for mild, selective nitrile reduction. *Chem. Commun.* **2014**, *50*, 5391−5393.
69. Paul, B.; Chakrabarti, K.; Kundu, S. Optimum bifunctionality in a 2-(2-pyridyl-2-ol)-1,10-phenanthroline based ruthenium complex for transfer hydrogenation of ketones and nitriles: impact of the number of 2-hydroxypyridine fragments. *Dalton Trans.* **2016**, *45*, 11162−11171.
70. Guyon, C.; Baron, M.; Lemaire, M.; Popowycz, F.; Métay, E. Commutative reduction of aromatic ketones to arylmethylenes/alcohols by hypophosphites catalyzed by Pd/C under biphasic conditions. *Tetrahedron* **2014**, *70*, 2088−2095.
71. Smith, E. L.; Sadowsky, D.; Cramer, C. J.; Phillips, J. A. Structure, Bonding, and Energetic Properties of Nitrile−Borane Complexes: RCN−BH_3. *J. Phys. Chem. A* **2011**, *115*, 1955−1964.

72. Jacobsen, H.; Berke, H.; Döring, S.; Kehr, G.; Erker, G.; Fröhlich, R.; Meyer, O. Lewis Acid Properties of Tris(pentafluorophenyl)borane. Structure and Bonding in L−B(C_6F_5)$_3$ Complexes. *Organometallics* **1999**, *18*, 1724−1735.
73. García, J. J.; Jones, W. D. Reversible Cleavage of Carbon−Carbon Bonds in Benzonitrile Using Nickel(0). *Organometallics* **2000**, *19*, 5544−5545.
74. García, J. J.; Brunkan, N. M.; Jones, W. D. Cleavage of Carbon−Carbon Bonds in Aromatic Nitriles Using Nickel(0). *J. Am. Chem. Soc.* **2002**, *124*, 9547−9555.
75. Huo, C.; Zeng, T.; Li, Y.; Beller, M.; Jiao, H. Switching End-on into Side-on C⁝N Coordination: A Computational Approach. *Organometallics* **2005**, *24*, 6037−6042.
76. Pangborn, A.B.; Giardello, M.A.; Grubbs, R. H.; Rosen, R. K.; Timmers, F. J. Safe and Convenient Procedure for Solvent Purification. *Organometallics*, **1996**, *15*, 1518−1520.
77. Wietz, I. S.; Rabinovitz, M. The application of C_8K for organic synthesis: reduction of substituted naphthalenes. *J. Chem. Soc. Perkin Trans.* **1993**, *1*, 117-120.
78. Buchwald, S. L.; LaMaire, S. J.; Nielsen, R. B.; Watson, B. T.; King, S. M. SCHWARTZ'S REAGENT. *Org. Synth*. **1993**, *71*, 77.
79. Aguilar, J. A.; Adam, R. W.; Duckett, S. B.; Green, G. G. R.; Kandiah, R. Selective detection of hyperpolarized NMR signals derived from para-hydrogen using the Only Para-hydrogen SpectroscopY (OPSY) approach. *J. Magn. Reson.* **2011**, *208*, 49-57.
80. Duckett, S. B.; Green, G. G. R.; Cowley, M. J. Pulse sequencing with hyperpolarisable nuclei. US Patent 20,110,274,626, November 10, 2011.
81. Tom, B. A.; Bhasker, S.; Miyamoto, Y.; Momose, T.; McCall, B. J. Producing and quantifying enriched *para*-H_2. *Rev. Sci. Instrum.* **2009**, *80*, 016108.

CHAPTER 6: COBALT-MEDIATED ^{1}H AND ^{13}C NMR SIGNAL ENHANCEMENT USING *PARA*HYDROGEN INDUCED POLARIZATION

6.1 Introduction

Nuclear magnetic resonance (NMR) is one of the most widely utilized techniques for the characterization of a wide variety of compounds and magnetic resonance imaging (MRI) is a diagnostic tool in the biomedical field. Even with their extensive use, the full potential of NMR and MRI is limited due to the inherent low sensitivity of these spectroscopic tools. A variety of hyperpolarization methods have been developed to produce a larger difference in the population of nuclear spin states, e.g. a non-Boltzmann distribution of spins, to increase the NMR and MRI signal intensity, thereby increasing the sensitivity of these instruments.[1-3] Among the hyperpolarization methods,[3] dynamic nuclear polarization (DNP) has advanced over the past few decades to successfully hyperpolarize contrast agents and apply them in clinical studies for metabolic imaging.[4] However, the excessive cost and difficulty in quickly generating hyperpolarized material remains a limitation for the widespread use of DNP. *Para*hydrogen Induced polarization (PHIP) involves the catalytic pairwise addition of *para*hydrogen (*p*-H_2) to an unsaturated substrate, typically carbon-carbon multiple bonds, using a transition metal catalyst. PHIP is a cheaper and faster alternative for the generation hyperpolarized substances compared to DNP.[5]

To prolong the signal enhancement gained from PHIP and enable its use for biomedical applications, the transfer of the polarization from added protons to slow relaxing nuclei heteronuclei, such as carboxylate ^{13}C or ^{15}N groups, is required. Although this requirement is certainly a limitation to the scope of biologically relevant substrates PHIP is compatible with, methods such as PHIP-SAH[6,7] (PHIP via the side arm hydrogenation), which incorporate unsaturated sites up to five chemical bonds away from slow relaxing nuclei (carboxylate ^{13}C or ^{15}N groups), have expanded the number of substrates amenable toward hyperpolarization using PHIP.[8,9]

Currently, one major limitation of generating hyperpolarized species using PHIP for *in vivo* biomedical applications or translation into clinical trials is the presence of the toxic hydrogenation catalyst in the solution of the hyperpolarized product.[5] The removal of the hydrogenation catalyst by means of filtration on ionic resins[10] or phase extraction[6,11] are promising and have been met with limited polarization loss to the substrate. Heterogenous catalysts[12-18] have also been considered as a tool to address this shortcoming, but further work is needed to increase the polarization levels. An alternative strategy to alleviate this limitation involves developing more benign hydrogenation catalytic systems, which would involve the incorporation of bioavailable transition metals, in lieu of currently employed toxic, but functional rhodium

catalysts.[5] In this regard, Earth-abundant hydrogenation catalysts are attractive alternatives. However, due to the requirements of PHIP,[19] few first-row transition metal complexes[20-25] have been studied using PHIP and none have been reported to hyperpolarize ^{13}C NMR signals using *p*-H_2.

The cobalt-based hydrogenation catalysts, **(^{Mes}CCC)Co(H_2)(PPh_3)** and **(^{Mes}CCC)Co-py** (^{Mes}CCC = bis(mesityl-benzimidazol-2-ylidene)phenyl; py = pyridine), that are active for the hydrogenation of carbon-carbon multiple bonds[23,24] and nitriles to primary amines,[22] respectively, have been previously described. Mechanistic studies of the hydrogenation catalysis elucidated catalytically pertinent intermediates and established a two-electron redox process, Co(I)/Co(III), was operative. Furthermore, given the robust functional group tolerance of the catalytic systems and ability to enhance ^1H NMR signals of hydrogenated products using PHIP, the ability of the low-valent cobalt complexes to effectively enhance the ^{13}C signals using PHIP was questioned. Herein the hydrogenation of olefins featuring carbon-carbon double bonds adjacent to carboxylate moieties were targeted using **(^{Mes}CCC)Co-py** and *p*-H_2. Furthermore, comparative ^{13}C NMR signal enhancement studies between a commercially available rhodium(I) PHIP catalyst, [(dppb)Rh(COD)]BF_4 (dppb = 1,4-bis(diphenylphosphino)butane; COD = 1,5-cyclooctadiene), and **(^{Mes}CCC)Co-py**, demonstrates that the cobalt system is a viable PHIP catalyst alternative (Figure 6.1).

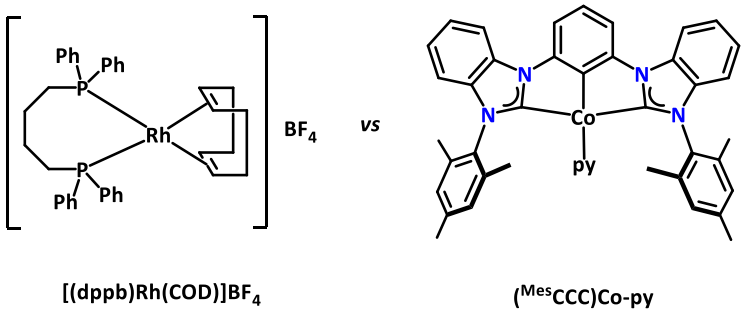

[(dppb)Rh(COD)]BF_4 **(^{Mes}CCC)Co-py**

Figure 6.1 Hydrogenation catalysts, [(dppb)Rh(COD)]BF_4 (left) and **(^{Mes}CCC)Co-py** (right), examined in these studies.

6.2 Hydrogenation of ethyl acrylate using (^{Mes}CCC)Co-py and *p*-H_2: A ^1H NMR spectroscopic study

PHIP studies using **(^{Mes}CCC)Co-py** were commenced following the conditions previously reported in the hydrogenation of ethyl acrylate using *p*-H_2 and [(dppb)Rh(COD)]BF_4.[7] The 16-electron **(^{Mes}CCC)Co-py** complex was chosen instead of the 18-electron **(^{Mes}CCC)Co(N_2)(PPh_3)** complex because the presence of triphenyl phosphine was previously demonstrated to inhibit catalysis.[23,24] Acetone-d_6 was chosen as the solvent to carry out the hydrogenation studies so that direct comparisons to the rhodium system[7] could be made. In our studies, ALTADENA[26] conditions were followed (see description in Chapter 1).

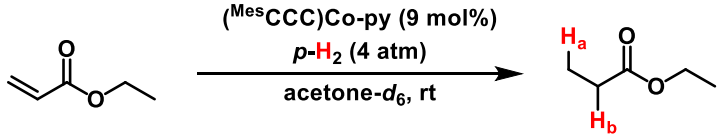

Scheme 6.1 Hydrogenation of ethyl acrylate using **(MesCCC)Co-py** (9 mol%) and *p*-H_2 (4 atm).

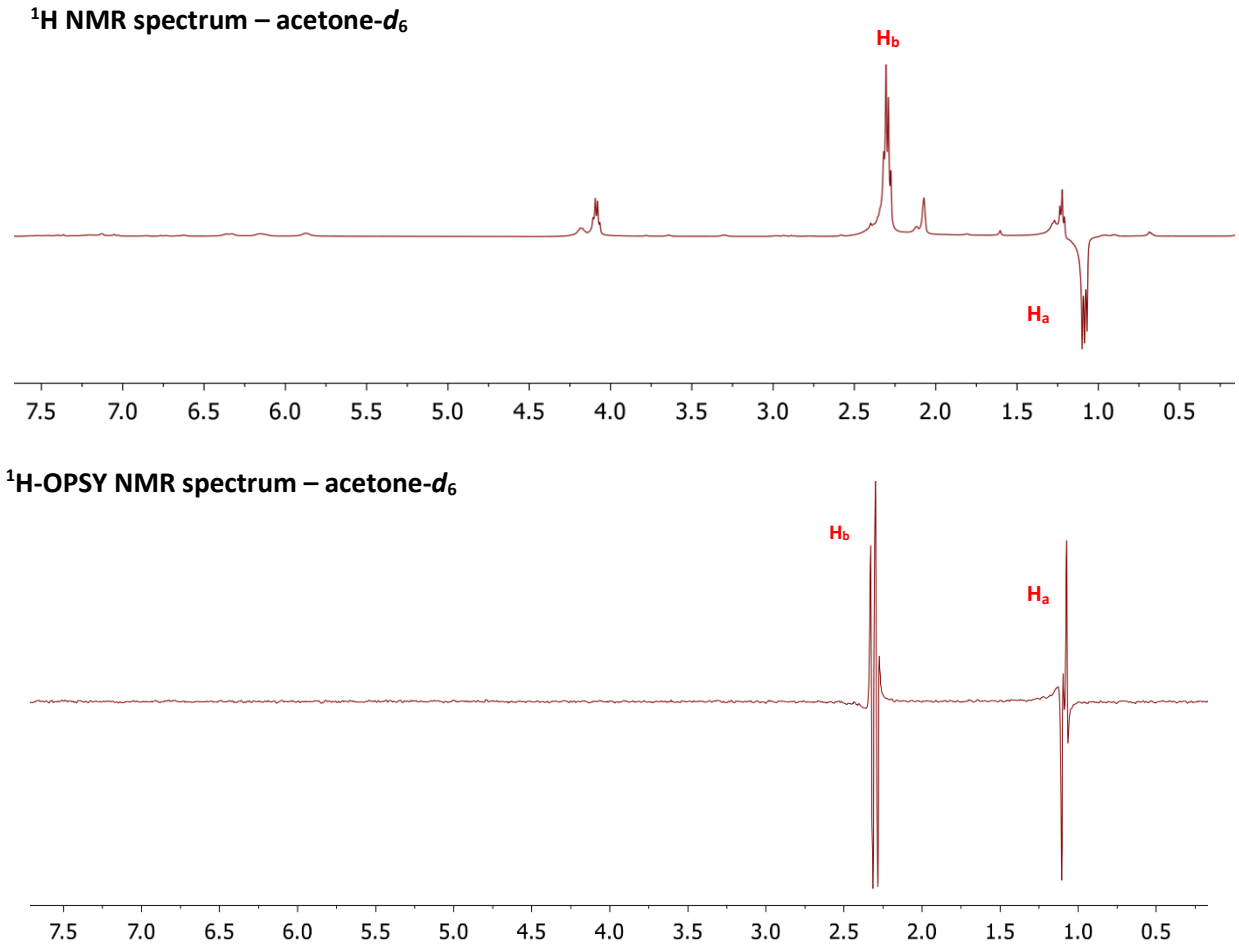

Figure 6.2 ^{1}H NMR using a 45° pulse (top) and ^{1}H-OPSY NMR (bottom) of hydrogenation of ethyl acrylate using **(MesCCC)Co-py** (9 mol%) and *p*-H_2 (4 atm) in acetone-d_6.

The addition of 4 atm of *p*-H_2 to a solution of ethyl acrylate (64 mM) and **(MesCCC)Co-py** (9 mol%) (Scheme 6.1) resulted in the hyperpolarization of the ^{1}H NMR signals of ethyl propionate (Figure 6.2, top). In addition, the observation of the anti-phase signals of the ethyl propionate was also observed in the ^{1}H-OPSY (only parahydrogen spectroscopy)[27] NMR spectrum (Figure 6.2, bottom). This illustrates the pairwise addition in the hydrogenation of ethyl acrylate is feasible using the low-valent cobalt system. Furthermore, the catalysis is not inhibited by acetone or the ester functionality of the substrate.

6.3 Hydrogenation of ethyl acrylate using (^{Mes}CCC)Co-py and *p*-H_2: A ^{13}C NMR spectroscopic study

Encouraged by the ability of **(^{Mes}CCC)Co-py** to hydrogenate ethyl acrylate in a pairwise manner, the collection of ^{13}C NMR data was pursued next to probe if the hyperpolarization transfer from the protons

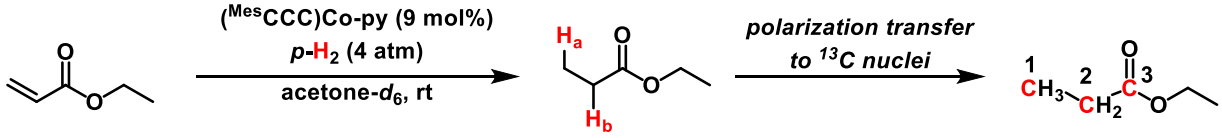

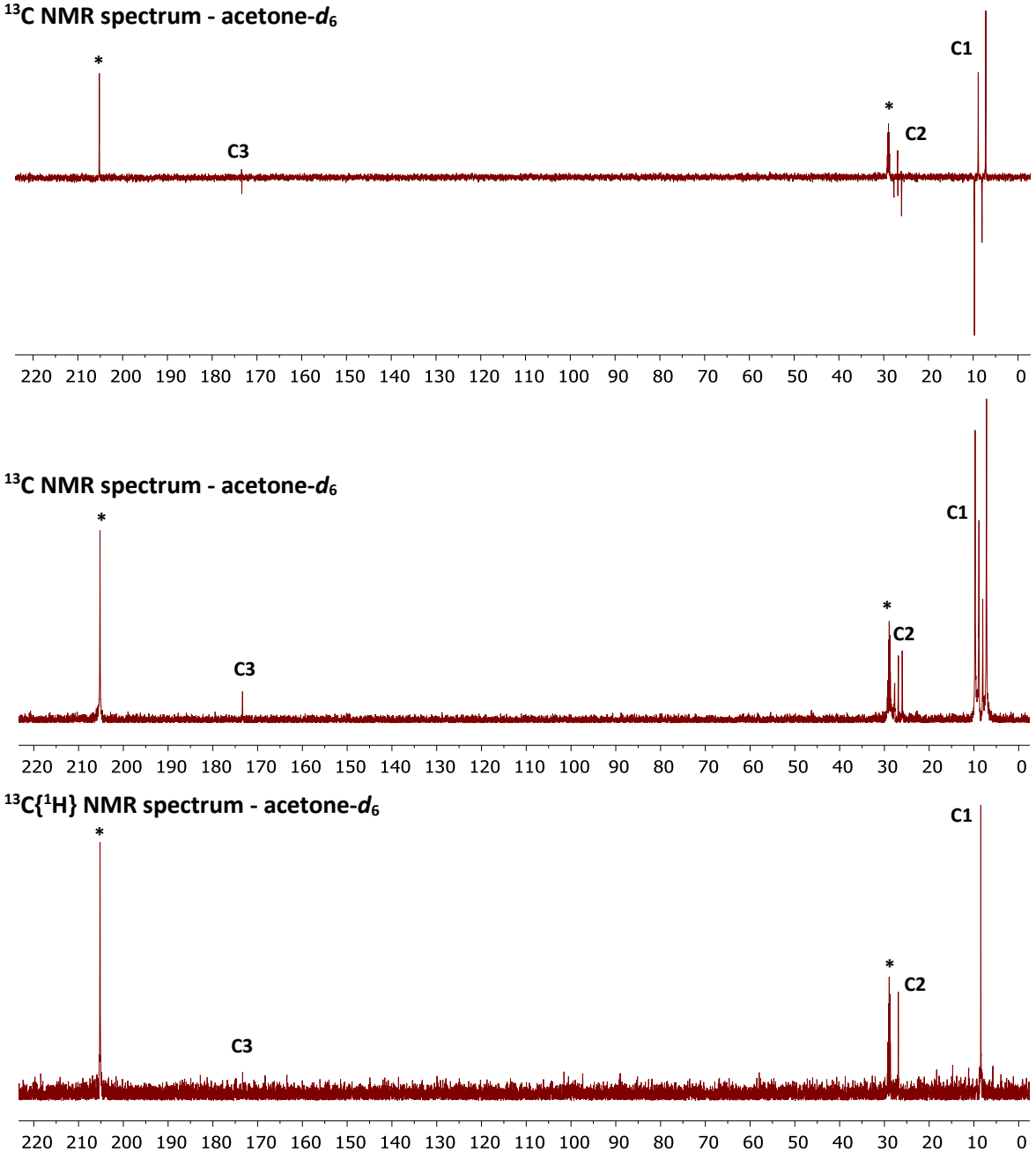

Figure 6.3 ^{13}C NMR spectrum (1 scan) of hydrogenation of ethyl acrylate using **(^{Mes}CCC)Co-py** (9 mol%) and *p*-H_2 (4 atm) in acetone-d_6 (*) (top), displayed in absolute mode (middle) and ^{13}C{^{1}H} NMR spectrum of the same reaction (bottom).

to ^{13}C signals could be accomplished. The transfer of hyperpolarization from ^{1}H to heteronuclei occurs through scalar coupling[28] and the transfer efficiency has been improved by a variety of different methods, namely by application of pulse sequences,[29-31] magnetic field cycling[32,33] and adiabatic passage through level anticrossing.[34] Because the resonance frequencies of all nuclei are the virtually the same at low field (either Earth's magnetic field or zero field inside a mu-metal cylinder), the nuclear polarization is transferred to all magnetically active nuclei.[35] Moreover, since the difference between ^{13}C and ^{1}H resonance frequency is negligible compared to the coupling constants of the two nuclei, the efficient polarization transfer from ^{1}H to ^{13}C nuclei occurs at low magnetic fields without the application of tailored pulse sequences.[5,35] In the following studies, the addition of *p*-H_2 and subsequent hydrogenation occurs at Earth's magnetic field (ALTADENA conditions), then the sample is subjected to ^{13}C NMR data collection.

The hydrogenation of ethyl acrylate using **(^{Mes}CCC)Co-py** and *p*-H_2 under 4 atm was performed at Earth's magnetic field with vigorous shaking (*ca.* 5 seconds) and then the sample was quickly transferred to the NMR spectrometer for ^{13}C data acquisition at room temperature (*ca*. 15 seconds) (Figure 6.3). The ^{13}C NMR spectrum shows the enhancement of the ^{13}C signals corresponding to the C1, C2 and C3 position of ethyl propionate (Figure 6.3, top & middle). Furthermore, the hyperpolarization is also observed in the $^{13}C\{^{1}H\}$ NMR spectrum, albeit with a lower signal enhancement for the C3 carbon atom. The signal-to-noise ratio in the ^{13}C NMR spectrum (Figure 6.3, bottom) for C1, C2, C3 was found to be 108, 29 and 12, respectively. The signal-to-noise ratio in the $^{13}C\{^{1}H\}$ NMR spectrum (Figure 6.3, bottom) for C1 and C2 was found to be 62 and 23, while C3 resonance was not resolved.

A recent study using a rhodium catalyst for PHIP of amino acid derivatives demonstrated that the efficacy of hyperpolarization arising from *p*-H_2 addition[36] can be increased at elevated temperatures. Considering a related hydrogenation catalyst, **(^{Mes}CCC)Co(N_2)(PPh_3)**, was demonstrated to be stable at 80 °C,[23] and **(^{Mes}CCC)Co-py** was also demonstrated to operate at 115 °C for the hydrogenation of nitriles,[22] the temperature of the hydrogenation of ethyl acrylate using **(^{Mes}CCC)Co-py** was increased to determine if higher polarization levels of the ^{13}C NMR signals could be achieved. The temperature of the reaction was increased to 37 °C (body temperature) considering the potential use of the catalysts for biomedical applications.

Upon heating the reaction mixture (ethyl acrylate, **(^{Mes}CCC)Co-py** (9 mol%), and *p*-H_2 (4 atm)) in the NMR spectrometer at 37 °C, the sample was quickly removed, transferred to at Earth's magnetic field, shaken vigorously (*ca.* 5 seconds) and then the sample was transferred back to the NMR spectrometer for ^{13}C data acquisition at 37 °C (*ca*. 15 seconds). The ^{13}C and $^{13}C\{^{1}H\}$ NMR spectra show the enhancement of C1, C2, and C3 positions of ethyl propionate (Figure 6.4). Unlike at 20 °C, the C3 resonance of ethyl

propionate in the $^{13}C\{^{1}H\}$ spectrum was observed (Figure 6.4, bottom). In the ^{13}C NMR spectrum (Figure 6.4, top) the signal-to-noise ratio for C1, C2, C3 increased to 150, 40 and 22, respectively. Similarly, in the

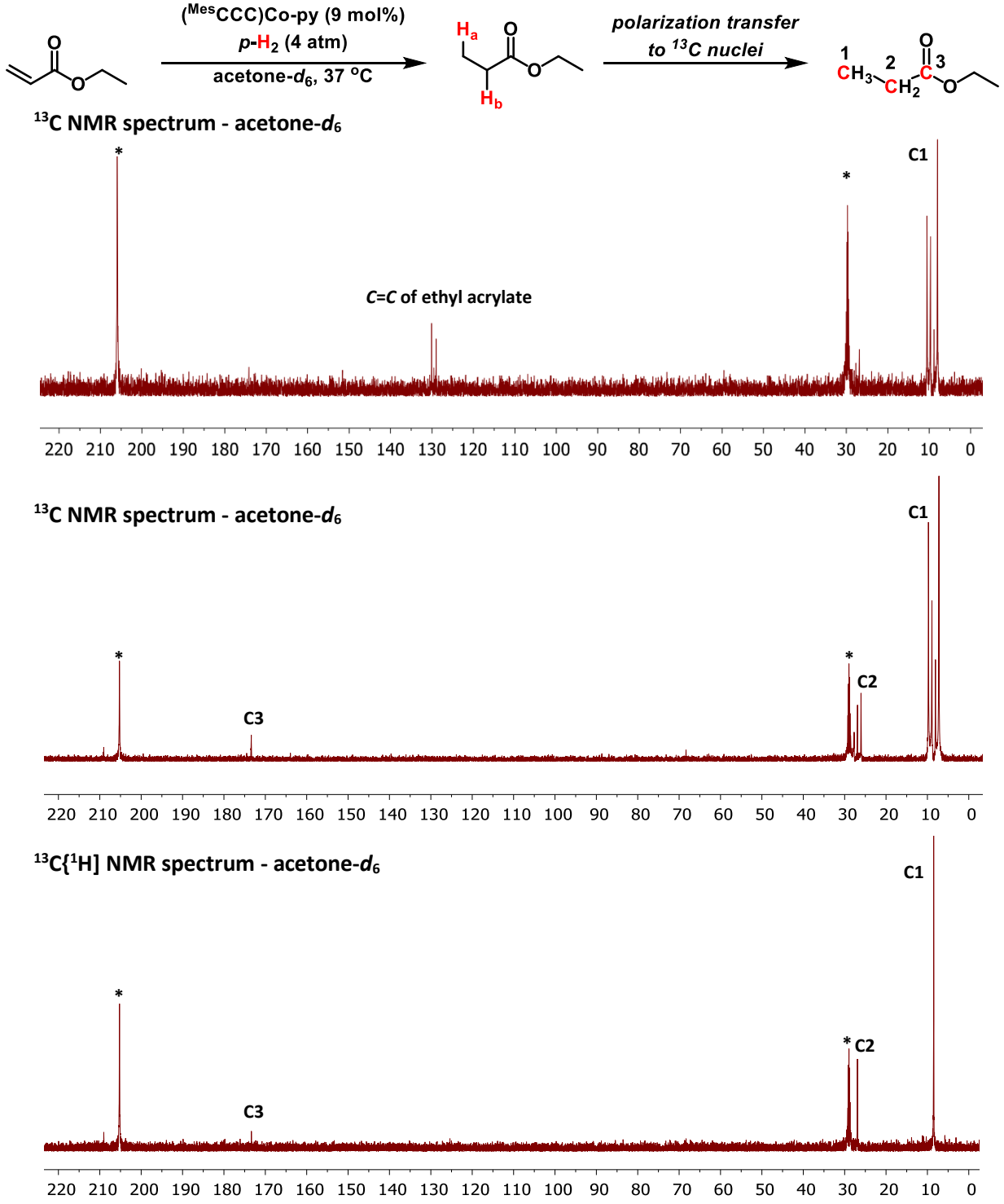

Figure 6.4 ^{13}C NMR spectra (1 scan) (displayed in absolute mode) of the hydrogenation of ethyl acrylate using **(^{Mes}CCC)Co-py** (9 mol%) and *p*-H_2 (4 atm) in acetone-d_6 (*) at 37 °C (1st shake – top, 2nd- shake middle). $^{13}C\{^{1}H\}$ NMR spectrum of the same reaction (3rd - shake bottom).

$^{13}C\{^{1}H\}$ NMR spectrum (Figure 6.4, bottom) the signal-to-noise ratio C1 and C2 increased to 140 and 44 and resonance C3 was resolved with a signal-to-noise ratio of 8.

6.4 Hydrogenation comparisons to [(dppb)Rh(COD)]BF_4 using NMR Studies

Not only does **(^{Mes}CCC)Co-py** hydrogenate and enable the hyperpolarization of the ^{1}H NMR signals in the product of ethyl acrylate using *p*-H_2, but the complex is also effective in enabling the signal enhancement of ^{13}C resonances of ethyl propionate. To further realize the potential of **(^{Mes}CCC)Co-py** as a PHIP catalyst and possibly serve as alternative to the widely utilized rhodium system,[7] a comparative *para*hydrogenation study between the two group 9 metal complexes was undertaken.

Under the identical catalytic conditions using [(dppb)Rh(COD)]BF_4 (9 mol%) (Figure 6.5, top) and **(^{Mes}CCC)Co-py** (9 mol%) (Figure 6.5, bottom) as the catalyst, the *para*hydrogenation of ethyl acrylate at 37 °C was carried out using the previously described protocol and the ^{13}C NMR spectra were acquired after 1 scan and are depicted in Figure 6.5. The ^{13}C signal enhancement for the carboxylate carbon, C3, in ethyl propionate appear identical using the cobalt or rhodium catalyst but differences in intensity arise for the C2 and C1 carbon positions.

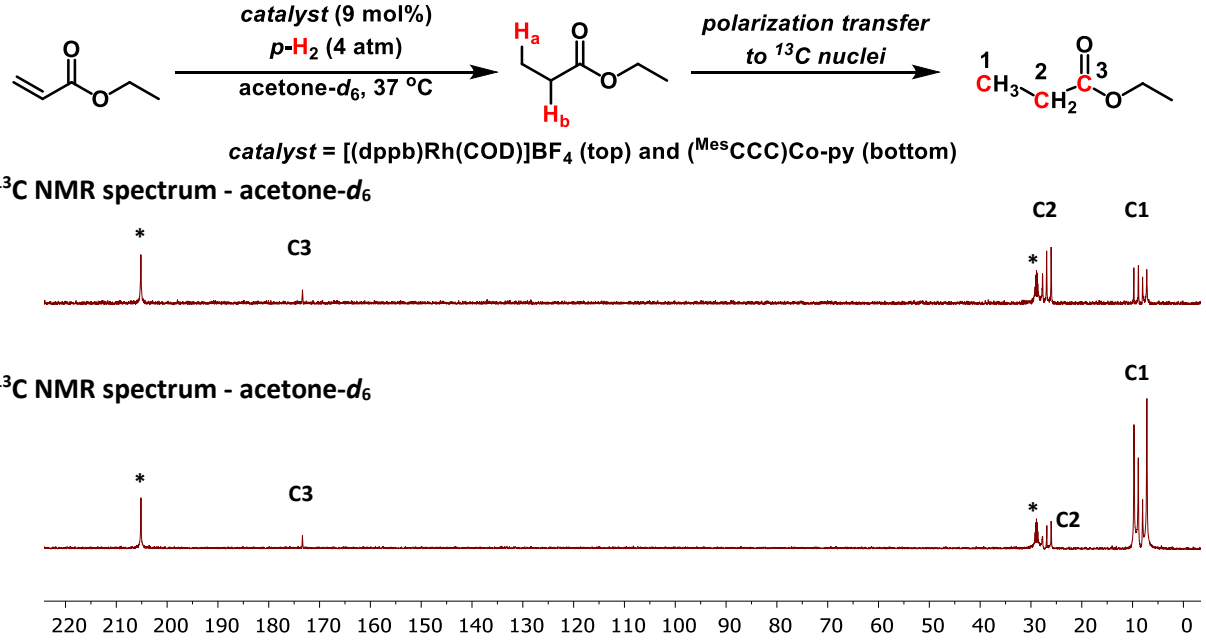

Figure 6.5 ^{13}C NMR spectrum (1 scan) (displayed in absolute mode) of the hydrogenation of ethyl acrylate using [(dppb)Rh(COD)]BF_4 (top) and **(^{Mes}CCC)Co-py** (bottom) and *p*-H_2 (4 atm) in acetone-d_6 (*) at 37 °C.

To understand the magnitude of the enhancement, integration of each hyperpolarized ^{13}C position was compared to a single scan of a 500 mM ethyl propionate standard and enhancement factors were calculated (Figure 6.6). Excitingly, the carboxylate carbon, C3, showed identical signal enhancement

factors for the cobalt and rhodium catalytic systems (Figure 6.6). This demonstrates that the cobalt system is equally effective for the generation of hyperpolarized ^{13}C signals of the carboxylate carbon as the rhodium(I) complex. Interestingly, the signal enhancement factor for position C2 is larger for the rhodium system, while the opposite is true for the C1 position (Figure 6.6).

These differences may arise from the catalytic pathway each metal undergoes during the

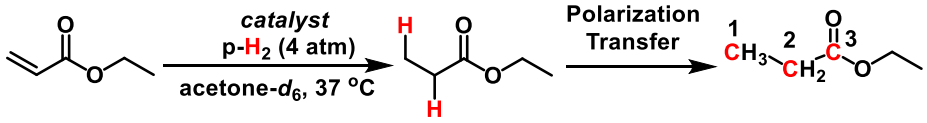

Catalyst	*^{13}C Position*			*Type of Enhancement*
	1	**2**	**3**	
(^{Mes}CCC)Co-py	4,773	755	148	Signal area
[(dppb)Rh(COD)]BF_4	751	800	145	

Figure 6.6 Comparison of the ^{13}C NMR signal enhancement of ethyl propionate using [(dppb)Rh(COD)]BF_4 and **(^{Mes}CCC)Co-py** at 37 °C.

hydrogenation process. Extensive mechanistic studies regarding the operative mechanism of chelating diphosphine rhodium(I) hydrogenation catalysts have elucidated that the coordination of the olefin, followed by irreversible addition of H_2 occurs, yielding the hyperpolarized product.[37,38] The operative hydrogenation mechanism for **(^{Mes}CCC)Co-py** has not been fully examined. Such studies may offer insights into the observed differences in the ^{13}C NMR signal enhancement and future catalyst design.

6.5 Mechanistic studies – stochiometric studies

To probe the potential distinctions between the rhodium and cobalt systems, mechanistic studies of the hydrogenation process using **(^{Mes}CCC)Co-py** were undertaken. To this end, the coordination of the olefin to the metal center was examined. The addition of 10 equiv of ethyl acrylate to **(^{Mes}CCC)Co-py** resulted in the formation of a yellow solution after 2 h, and following work up, **(^{Mes}CCC)Co(η^2-H_2C=CHCOOCH_2CH_3)$_2$** was isolated as a yellow solid in 81% yield (Scheme 6.2).

Characterization of **(^{Mes}CCC)Co(η^2-H_2C=CHCOOCH_2CH_3)$_2$** by ^1H NMR spectroscopy revealed a diamagnetic spectrum with 15 resonances (Figure 6.7). Three singlets integrating to 6H each, corresponded to the mesityl methyl groups on the ligand periphery, while the downfield resonances, integrating to 15H, were assigned to the aryl backbone of the pincer ligand. Integration of the remaining ^1H NMR resonances were assigned to the bound olefin, which are shifted upfield from the free olefin.

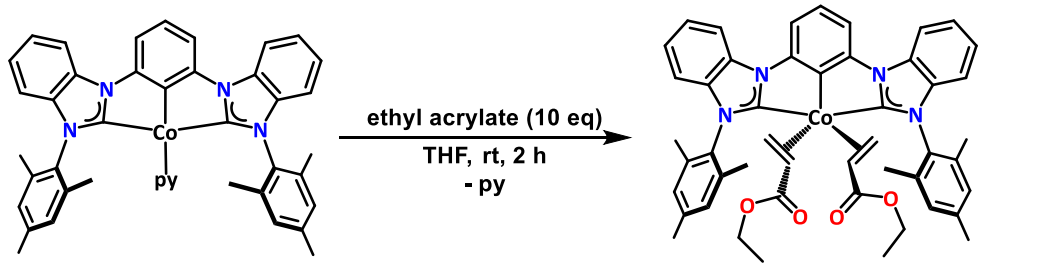

(^{Mes}CCC)Co(η^2-H_2C=CHCOOCH$_2$CH$_3$)$_2$

81%

Scheme 6.2 Synthesis of **(^{Mes}CCC)Co(η^2-H$_2$C=CHCOOCH$_2$CH$_3$)$_2$** from **(^{Mes}CCC)Co-py**.

^{1}H NMR spectrum – C$_6$D$_6$

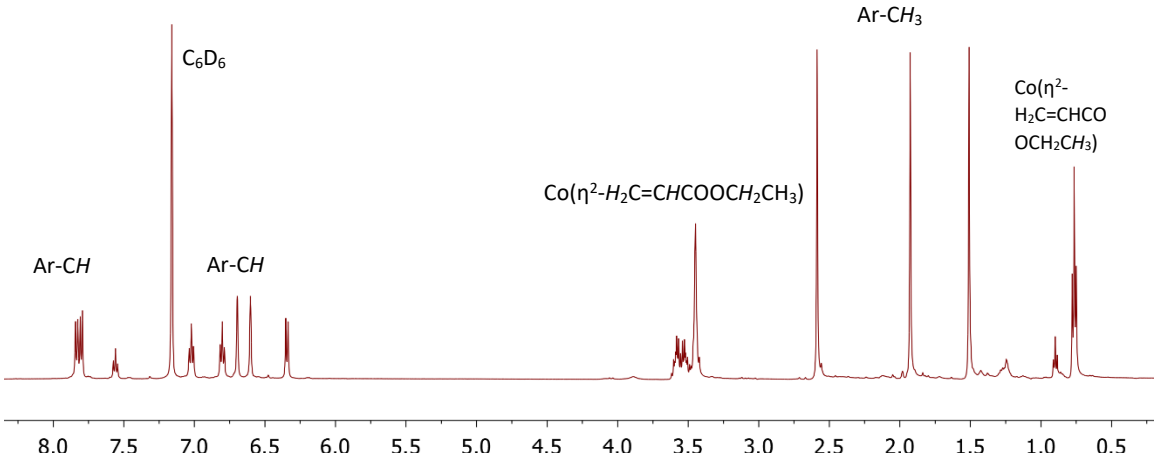

Figure 6.7 ^{1}H NMR spectrum of **(^{Mes}CCC)Co(η^2-H$_2$C=CHCOOCH$_2$CH$_3$)$_2$**.

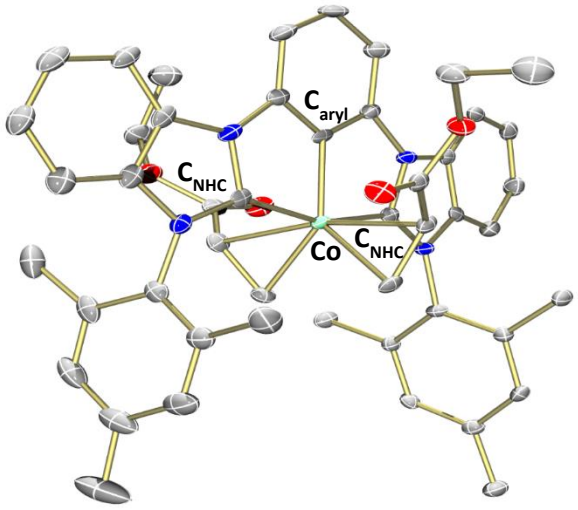

Figure 6.8 Molecular structure of **(^{Mes}CCC)Co(η^2-H$_2$C=CHCOOCH$_2$CH$_3$)$_2$** with 50% probability ellipsoids. Solvent molecules and hydrogen atoms have been omitted for clarity.

Based on the integration, it was concluded that 2 olefins were bound to the metal complex, furnishing an 18-electron Co(I) species. Additional characterization of **(^{Mes}CCC)Co(η^2-H$_2$C=CHCOOCH$_2$CH$_3$)$_2$** by X-ray diffraction studies confirmed the formulation of the complex (Figure 6.8, Tables 6.1 and 6.2). Interestingly,

no interaction between the metal center and C=O functionality is observed and bonding to the cobalt center is engaged through the carbon-carbon double bond of ethyl acrylate. This resembles the first step of rhodium hydrogenation catalysis, where olefin coordination occurs first.[37,38]

6.6 Mechanistic studies – catalytic studies

Under catalytic conditions, an ethyl acrylate molecule is assumed to displace the pyridine ligand from the metal center for hydrogenation to occur. To examine if pyridine is necessary for catalysis, **(^{Mes}CCC)Co(η^2-H_2C=CHCOOCH_2CH_3)$_2$** was used instead of **(^{Mes}CCC)Co-py** in a catalytic run. The observation of hyperpolarized ethyl propionate resonances in the ^{1}H NMR spectrum demonstrates pyridine is not necessary for the catalysis to occur. A closer examination of the ^{1}H NMR spectrum of a solution of ethyl acrylate, **(^{Mes}CCC)Co-py** and *p*-H_2 in benzene-d_6 confirms the loss of pyridine as evidenced by the resonance at 8.53 ppm, corresponding to the *ortho*-hydrogen atoms on pyridine, while the *meta* and *para* hydrogen atoms of pyridine could not be resolved (Figure 6.9). Furthermore, the singlets corresponding to the mesityl methyl groups observed at 2.57, 1.92 and 1.49 ppm are evidence of the presence of **(^{Mes}CCC)Co(η^2-H_2C=CHCOOCH_2CH_3)$_2$** in solution (Figure 6.9). Each of the mesityl methyl resonances integrate to 6H each, while the resonance at 8.53, ppm, assigned to pyridine, corresponds to 2H.

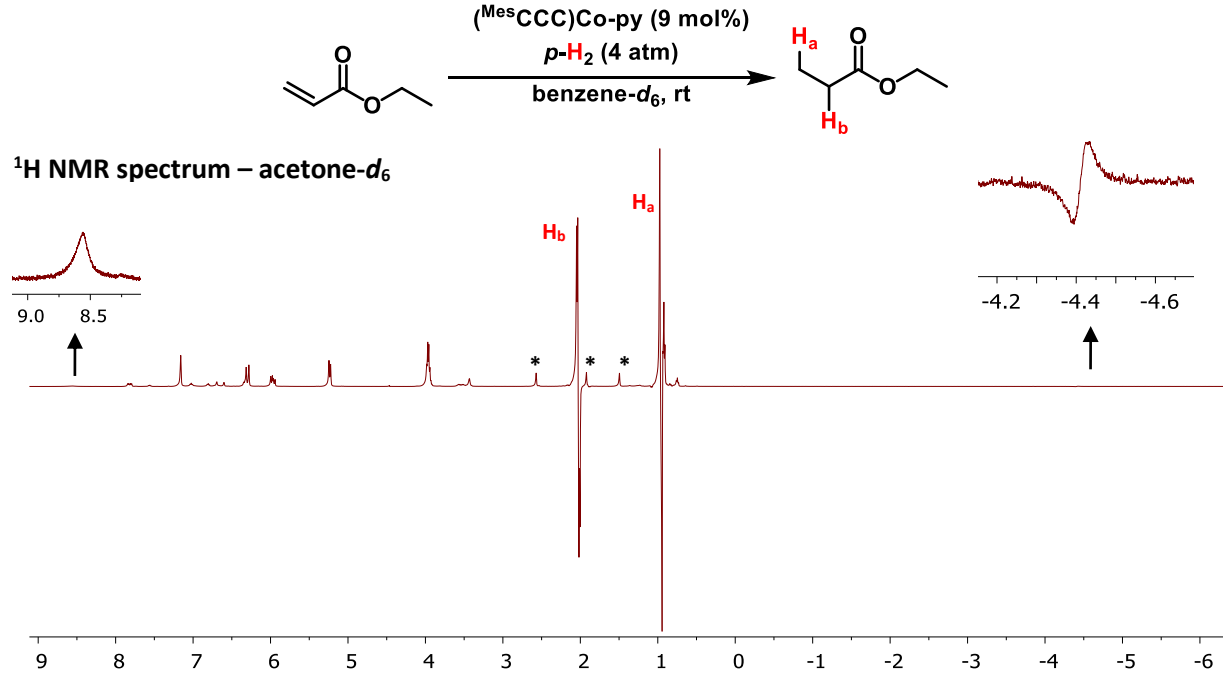

Figure 6.9 ^{1}H NMR spectrum of **(^{Mes}CCC)Co-py**, ethyl acrylate under 4 atm of *p*-H_2. (*denotes mesityl methyl groups of **(^{Mes}CCC)Co(η^2-H_2C=CHCOOCH_2CH_3)$_2$**).

Although **(^{Mes}CCC)Co(η^2-H_2C=CHCOOCH_2CH_3)$_2$** was observed during the catalytic reaction (Figure 6.9), for a PHIP effect to be observed, *p*-H_2 must displace one of the olefins to generate the active species, thereby allowing for oxidative addition of *p*-H_2 onto the metal center. A closer examination of the hydridic region of the ^{1}H NMR spectrum (Figure 6.9) revealed a singlet antiphase resonance at -4.41 ppm in benzene-d_6. Based on the chemical shift, the antiphase resonance was assigned as a transient cobalt-hydride (Figure 6.9 and 6.10). However, an additional resonance from the pairwise addition of *p*-H_2 was not resolved in the hydridic (cobalt-hydride species) region of the ^{1}H NMR spectrum. Furthermore, based on the magnitude of the resonance at -4.41 ppm, a similar species in the aliphatic region would naturally be difficult to characterize on the account of the hyperpolarized ethyl propionate and additional ligand resonances present.

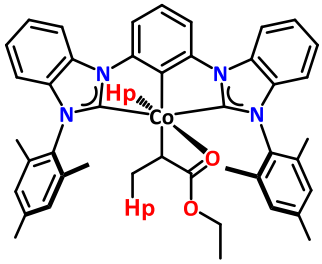

Figure 6.10 Proposed alkyl hydride cobalt intermediate.

Nonetheless, the greatly enhanced C1 ^{13}C signals of ethyl propionate (Figure 6.6) suggests a cobalt alkyl hydride species (Figure 6.10) may be involved in the hydrogenation process. From this proposed intermediate, hyperpolarized ethyl propionate could be released; reductive elimination or β-hydride elimination could yield hyperpolarized olefinic ^{13}C resonances of ethyl acrylate (Figure 6.4, top).

6.7 Substrate scope

Seeking to further develop **(^{Mes}CCC)Co-py** as a more general PHIP catalyst, additional substrates bearing carbon-carbon double bonds adjacent to a carboxylate or carbonyl group were examined. The hydrogenation of methyl acrylate using **(^{Mes}CCC)Co-py** (9 mol%) and *p*-H_2 (4 atm) was carried out using the previously described protocol at 37 °C. The ^{13}C NMR spectrum (Figure 6.11) displayed a similar signal enhancement pattern, albeit weaker, compared to that observed with ethyl propionate (Figure 6.4). The ^{13}C signal enhancement likely is due the lower solubility of the metal-olefin complex, as particulates in the J Young NMR tube were observed during the experiments. The use of methyl vinyl ketone as a substrate resulted in the hyperpolarization of the C1 position of butan-2-one, while the signal enhancement of the C2 or carbonyl carbon was not observed (Figure 6.12). The solubility of the metal-olefin complex is likely

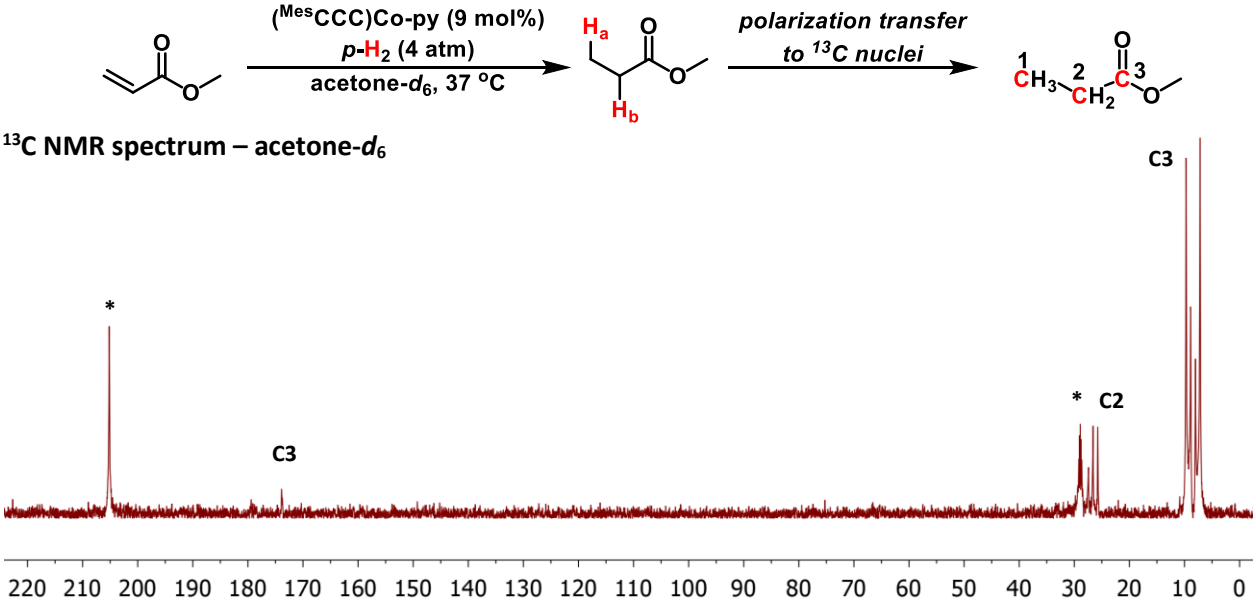

Figure 6.11 ^{13}C NMR spectrum (1 scan) (displayed in absolute mode) of the hydrogenation of methyl acrylate using **(MesCCC)Co-py** and *p*-H_2 (4 atm) in acetone-d_6 (*) at 37 °C.

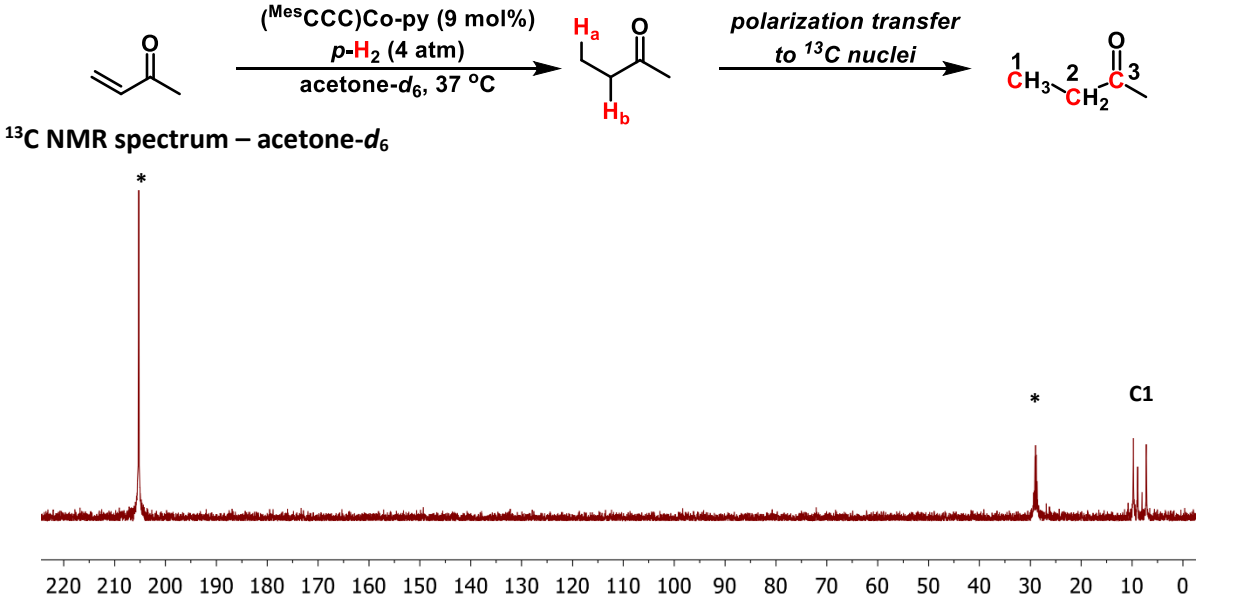

Figure 6.12 ^{13}C NMR spectrum (1 scan) (displayed in absolute mode) of the hydrogenation of methyl vinyl ketone using **(MesCCC)Co-py** (9 mol%) and *p*-H_2 (4 atm) in acetone-d_6 (*) at 37 °C.

the basis of the lower observed ^{13}C signal enhancement, as particulates were also observed during the catalytic studies.

To mitigate the influence of solubility of the metal-olefin complex in the generation of hyperpolarized ^{13}C resonances, the use of butyl acrylate was examined. It was hypothesized the longer alkyl chain would increase solubility of the metal-olefin precatalyst in acetone and allow for the improved ^{13}C signal

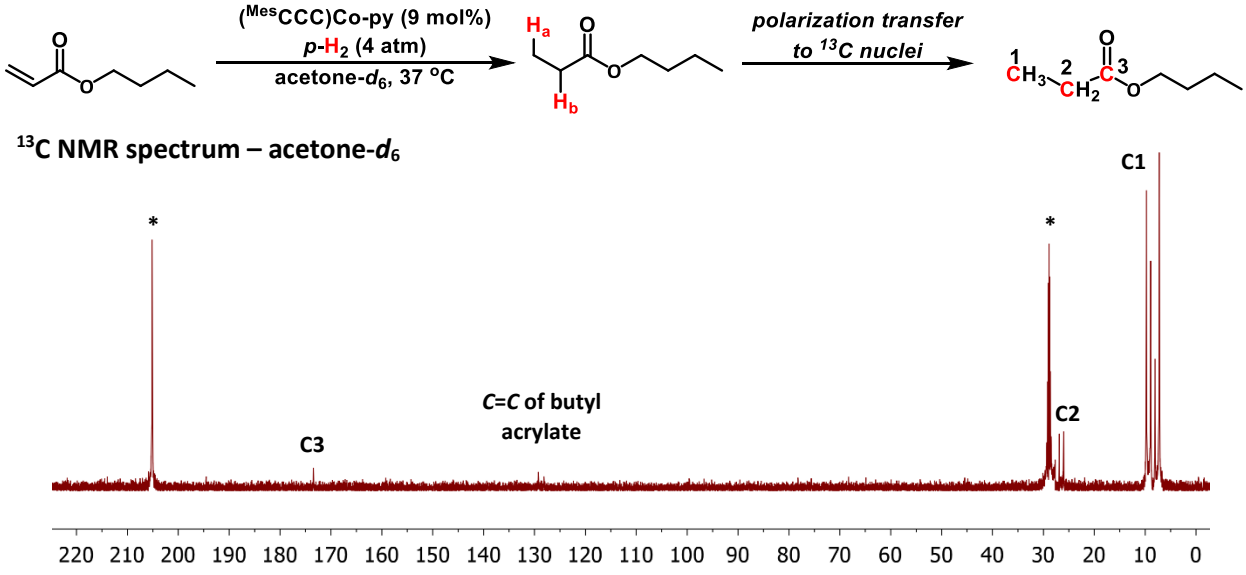

Figure 6.13 ^{13}C NMR spectrum (1 scan) (displayed in absolute mode) of the hydrogenation of butyl acrylate using **(MesCCC)Co-py** (9 mol%) and *p*-H_2 (4 atm) in acetone-d_6 (*) at 37 °C.

hyperpolarization. To this end, the hydrogenation of butyl acrylate using **(MesCCC)Co-py** (9 mol%) and *p*-H_2 (4 atm) was carried out following the previously described protocol in acetone-d_6. The ^{13}C NMR spectrum (Figure 6.13) displayed the ^{13}C signal enhancement for C1, C2, and C3 position of butyl propionate, as well as the olefinic carbon atoms, 129.2 and 128.1 ppm, of butyl acrylate. The signal-to-noise ratio for the C1, C2, and C3 position was 98, 23, and 9, respectively. Compared to the signal-to-noise ratio of hyperpolarized ^{13}C resonances in ethyl propionate, the increased solubility of butyl acrylate did not correlate with increased ^{13}C signal enhancement. In this case, the butyl group may influence the β-hydride elimination pathway, as seen in the hyperpolarized olefinic ^{13}C resonances of butyl acrylate.

Seeking to further increase the utility of the cobalt system as a PHIP catalyst, the functional group tolerance[22-24] of **(MesCCC)Co-py** was extended to include biologically relevant functionalities. The hyperpolarization of propanamide in the ^{1}H NMR spectrum from the *para*hydrogenation of acrylamide using **(MesCCC)Co-py** (9 mol%) as the catalyst is indicative of the robust functional group tolerance of the system (Figure 6.14). This signifies that future PHIP substrates featuring unprotected N atoms, such as NH_2 groups (present in amino acid derivatives),[36,39] will be amenable toward PHIP with **(MesCCC)Co-py**. The collection of ^{13}C NMR data was pursued next to probe if the polarization transfer to ^{13}C signals could be achieved in propanamide. Unfortunately, corresponding ^{13}C NMR signals of propanamide or acrylamide were not observed in the ^{13}C NMR spectrum. Even though hyperpolarization is observed in the ^{1}H NMR spectrum, the low solubility of the olefin-metal complex likely contributes to lower hydrogenation

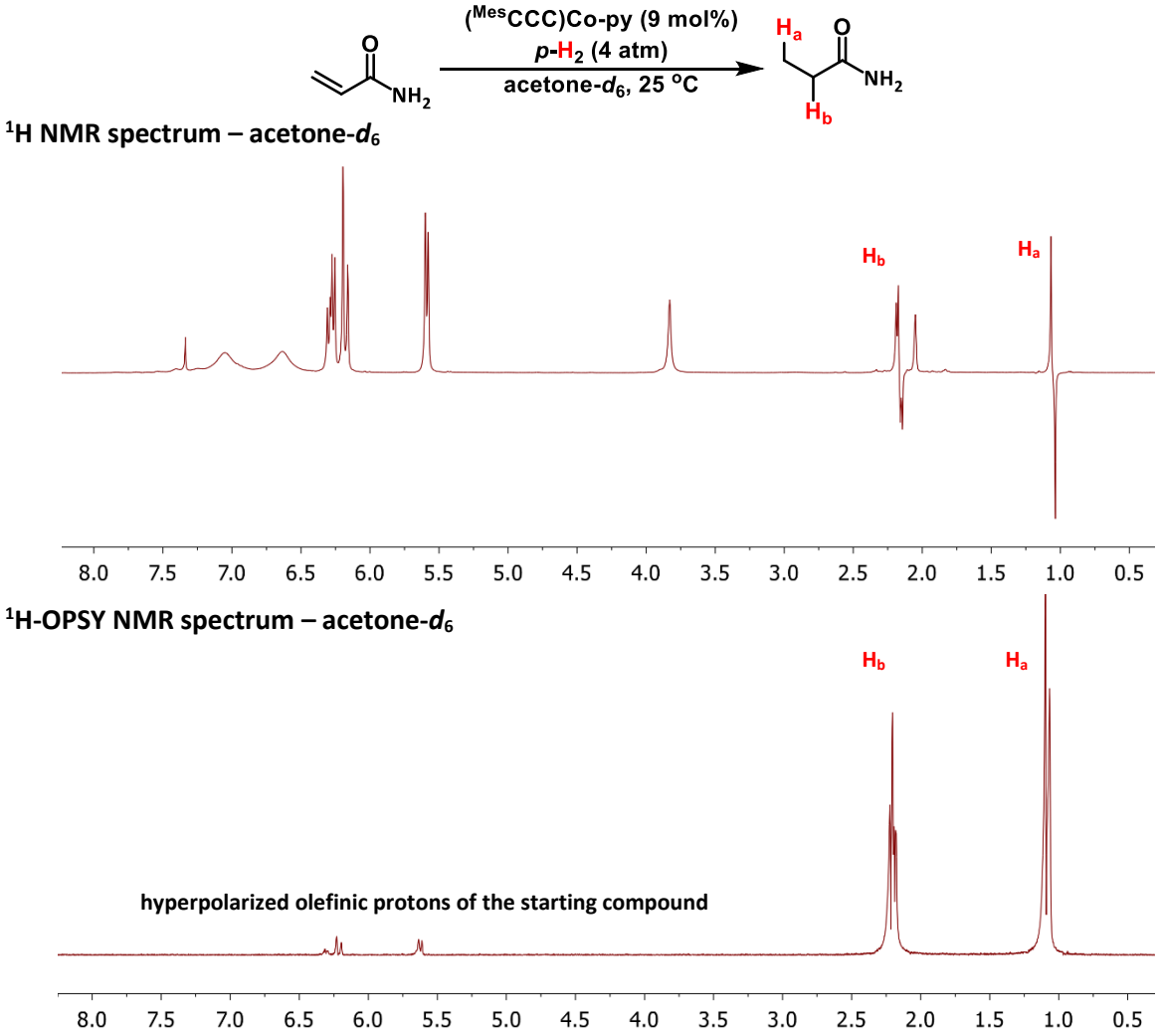

Figure 6.14 ^{1}H NMR spectrum using a 45° pulse (top) and ^{1}H-OPSY NMR (bottom) hydrogenation of acryl amide using **(^{Mes}CCC)Co-py** (9 mol%) and *p*-H_2 (4 atm) in acetone-d_6 (*) at 25 °C.

efficiency of the active catalyst precluding the observation of a ^{13}C signal enhancement by NMR spectroscopy.

6.8 Air-stable cobalt catalyst – (^{Mes}CCC)$CoCl_2$py

The capacity of **(^{Mes}CCC)Co-py** to hyperpolarize ^{13}C NMR signals of the hydrogenation products of ethyl, methyl, and butyl acrylate, as well as methyl vinyl ketone, with *p*-H_2 offers a potential alternative to the rhodium catalysts currently employed. The 16-electron cobalt(I) complex, **(^{Mes}CCC)Co-py**, is stable toward hydrogenation in acetone, however, catalyst's sensitivity to air limits the potential of this system. The bench-stable 18-electron cobalt(III) precursor, **(^{Mes}CCC)$CoCl_2$py**, was shown to selectivity hydrogenate nitriles to primary amines upon the *in situ* activation with $NaHBEt_3$.[22] A similar approach was envisioned

to determine if starting with the Co(III) precursor was a feasible route toward the generation of the hyperpolarized ^{13}C signals of the hydrogenation product of ethyl acrylate.

To this end, the hydrogenation of ethyl acrylate using **(^{Mes}CCC)CoCl$_2$py** (9 mol%), NaHBEt$_3$ (19 mol%) and *p*-H$_2$ (4 atm) was carried out following the previously described protocol in acetone-d_6 (Figure 6.15). The ^{13}C NMR spectrum shows the enhancement of the C1, C2, and C3 position of ethyl propionate as well as the olefinic C atoms of ethyl acrylate after the first set of data was collected (Figure 6.15, top). During the second shake of the sample following the same hydrogenation protocol, signal enhancement of C1, C2, and C3 positions of ethyl propionate were observed (Figure 6.15, middle). The signal-to-noise ratio of

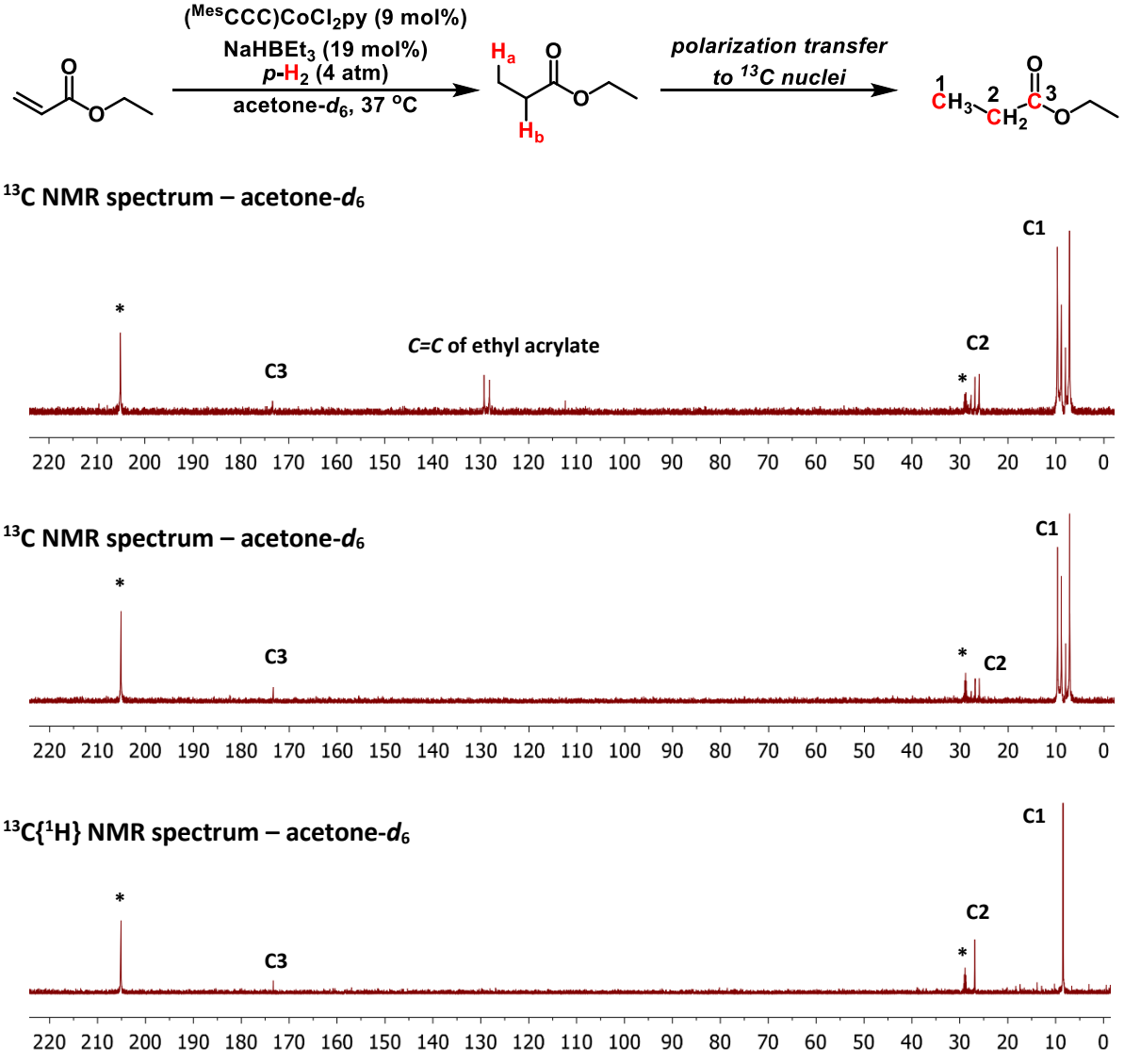

Figure 6.15 ^{13}C NMR spectrum (1 scan) of hydrogenation of ethyl acrylate using **(^{Mes}CCC)CoCl$_2$py** (9 mol%), NaHBEt$_3$ (19 mol%) and *p*-H$_2$ (4 atm) in acetone-d_6 (*) (top), displayed in absolute mode (middle) and $^{13}C\{^1H\}$ NMR spectrum of the same reaction (bottom).

C1, C2, and C3 were determined to be 105, 27, and 7, respectively. This signifies that the bench-stable cobalt(III) precursor can serve as a viable starting complex for the generation of hyperpolarized ^{13}C NMR signals through PHIP.

6.9 Conclusion

In conclusion, **(^{Mes}CCC)Co-py** was shown to hyperpolarize the ^{13}C NMR signals of ethyl propionate by the *para*hydrogenation of ethyl acrylate. Comparisons of the carboxylate ^{13}C signal enhancement of ethyl propionate using [(dppb)Rh(COD)]BF_4 and **(^{Mes}CCC)Co-py**, demonstrated that the cobalt complex hyperpolarization efficiency is comparable with the rhodium system. Stochiometric studies revealed the coordination mode of the olefin with the cobalt center and *in situ* ^1H NMR studies showed cobalt-olefin complexes can serve as the precatalysts. Furthermore, based on ^1H and ^{13}C NMR spectroscopic data, the binding of the olefin with the metal center is a reversible process and is proposed to transpire through a cobalt-alkyl hydride intermediate. Lastly, the success of a bench-stable cobalt precursor, **(^{Mes}CCC)CoCl$_2$py**, activated *in situ* with $NaHBEt_3$ along with the robust functional group tolerance demonstrates that this cobalt bis(carbene) pincer system is a viable alternative to the widely employed rhodium PHIP catalyst.

6.10 Experimental section

General considerations. All manipulations of air- and moisture-sensitive compounds were carried out in the absence of water and dioxygen in an MBraun inert atmosphere drybox under a dinitrogen atmosphere except where specified otherwise. All glassware was oven dried for a minimum of 8 h and cooled in an evacuated antechamber prior to use in the drybox. Solvents for sensitive manipulations were dried and deoxygenated on a Glass Contour System (SG Water USA, Nashua, NH) and stored over 4 Å molecular sieves purchased from Strem following a literature procedure prior to use.[40] Acetone-d_6 and benzene-d_6 were purchased from Cambridge Isotope Labs and were degassed and stored over 4 Å molecular sieves prior to use. Sodium triethylborohydride solution (1.0 M in toluene) was purchased from Sigma-Aldrich. Celite® 545 (J. T. Baker) was dried in a Schlenk flask for 24 h under dynamic vacuum while heating to at least 150˚C prior to use in a glovebox. NMR Spectra were recorded at room temperature on a Varian spectrometer operating at 500 MHz (^1H NMR) and 126 MHz (^{13}C NMR) (UI500NB) and 600 MHz (^1H NMR) and 150 MHz (^{13}C NMR) (UI600) and referenced to the residual HD_2COCD_3 and C_6D_5H resonance (δ in parts per million, and *J* in Hz). (^{Mes}CCC)CoCl$_2$py[41] and (^{Mes}CCC)Co-py[22] were prepared according to literature procedures.

Synthesis of cobalt(I) complexes

Preparation of (^{Mes}CCC)Co(η^2-H_2C=CHCOOEt)$_2$: A 20 mL scintillation vial was charged with **(^{Mes}CCC)Co-py** (0.036 g, 0.053 mmol) and THF (10 mL). Ethyl acrylate (55 uL, 0.530 mmol, 10 eq) was added and the solution was stirred for 2 h. After removing the THF was removed under reduced pressure and washing the solid was washed with Et_2O (2 x 5 mL), the remaining residue was extracted with benzene (10 mL). Removal of the solvent under reduced pressure resulted in a fine yellow powder (0.034 g, 0.042 mmol, 81%). NMR data (in benzene-d_6, 25 °C): ^{1}H δ = 7.87-7.77 (m, 4H), 7.56 (t, J = 7.3, 1H), 7.02 (t, J = 7.8, 2H), 6.80 (t, J = 7.8, 2H), 6.70 (s, 2H), 6.60 (s, 2H), 6.34 (d, J = 7.9, 2H), 3.62-3.47 (m, 4H), 3.45 (s, 6H), 2.59 (s, 6H), 1.93 (s, 6H), 1.51 (s, 6H), 0.76 (t, J = 7.4, 6H). ^{13}C δ = 204.3, 181.3, 176.3, 148.7, 138.9, 138.6, 138.3, 137.1, 132.6, 131.5, 130.4, 129.1, 128.6, 123.0, 122.7, 122.5, 110.8, 110.0, 108.4, 59.0, 50.3, 39.1, 20.8, 19.4, 18.5, 14.5.

Mechanistic studies

***Para*hydrogen induced polarization NMR studies**

Sample preparation using (^{Mes}CCC)Co-py. A standard 4 mL scintillation vial was charged with **(^{Mes}CCC)Co-py** (2.0 mg, 0.00294 mmol), ethyl acrylate (3.5 µL mg, 0.032 mmol) and dissolved in ½ mL of acetone-d_6 and transferred to a J. Young NMR tube. The sample was subjected to two freeze-pump-thaw cycles and *p*-H_2 gas (1 atm) was added at 77K on a high-vacuum line. The sample was kept frozen in liquid nitrogen and warmed to ambient temperature and shaken immediately at Earth's magnetic field for *ca.* 5 seconds prior to inserting into the NMR spectrometer. For the reactions carried out at 37 °C, the temperature of NMR probe was set to 37 °C and sample was warmed to ambient temperature, then inserted into the NMR and warmed for 2 minutes. The sample was removed from the spectrometer, shaken at Earth's magnetic field for 5 seconds and inserted into the NMR spectrometer and a single ^{13}C scan was acquired (ca. 15 sec).

Sample preparation using (^{Mes}CCC)CoCl$_2$py. To a standard 4 mL scintillation vial charged with **(^{Mes}CCC)CoCl$_2$py** (2.2 mg, 0.00294 mmol), a solution $NaHBEt_3$ (1.0 M in toluene, 6.2 µL, 0.0062 mmol) was added resulting effervesce of the brown suspension. The brown mixture was dissolved in ½ mL of acetone-d_6 and ethyl acrylate (3.5 µL mg, 0.032 mmol) was added and the resulting yellow solution was transferred to a J. Young NMR tube. The addition of *p*-H_2 and collection of ^{13}C NMR data was identical to the protocol described above.

NMR spectrometer. All PHIP ^{1}H NMR data presented herein were collected on a Varian UNITY INOVA 500 NB High-Resolution NMR Console with a 5mm Varian ^{1}H{^{13}C/^{15}N} PFG Z probe. All PHIP ^{13}C data presented herein were collected on a Varian UNITY INOVA 600 NB High-Resolution NMR Console with a 5mm Varian AutoTuneX ^{1}H/X PFG Z probe, X=^{31}P-^{15}N. All spectra ^{1}H NMR data were collected in acetone-d_6 or benzene-d_6 and the residual solvent resonance was referenced to 2.05 or 7.16 ppm, respectively. All ^{13}C NMR data were collected using acetone-d_6 and the residual solvent was referenced to 206.26. ^{1}H NMR spectra were recorded using 45° pulse angle. ^{13}C NMR spectra were recorded using a standard 90° pulse. The spectral window of 30 ppm was used in both proton and ^{1}H-OPSY experiments and 245 ppm in the ^{13}C NMR experiments. ^{1}H-OPSY NMR data was collected via a double quantum coherence pathway using the pulse sequence below (**Figure 6.16**). The OPSY spectra are anti-phase peaks, and they are generally displayed with absolute mode in the following spectra.[42,43]

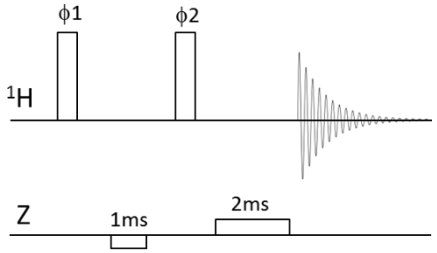

Figure 6.16 Double quantum OPSY pulse sequence (OPSY-d): the vertical bar at ^{1}H channel represents $\pi/2$ pulse. Phase cycle: $\phi1$: $(y)_4(x)_4$, $\phi2$: $(x)_4(y)_4$, rec: $(x)_4(y)_4$. Z Gradient: 50 G/cm rectangular gradient was used. First gradient was applied for 1ms in the opposite direction of the second gradient which was applied for 2ms. 0.5ms gradient recovery delays were used after each gradient. The acquisition time was 4 seconds and no delay between scans was used.

Generation of *para*-hydrogen. A parahydrogen converter was used to generate the *para*-H_2 enriched hydrogen gas. This consisted of copper tubing filled with a hydrous ferric oxide catalyst that was cooled to 15 K using a closed-cycle ^{4}He cryostat. A detailed description of the converter can be found in Tom *et al.*, which was able to consistently convert naturally occurring hydrogen gas (3:1 *ortho*:*para*) to 99.99% *para*-H_2.[44]

Table 6.1 Crystallographic parameters for **(^{Mes}CCC)Co(η^2-H_2C=CHCOOCH_2CH_3)$_2$**.

	(^{Mes}CCC)Co(η^2-H_2C=CHCOOCH_2CH_3)$_2$ dd59h
Empirical Formula	C52 H59 Co N4 O5
Formula Weight	878.96
Temperature	100(2) K
Wavelength	0.71073 Å
Crystal system	Monoclinic
Space group	P 2_1/n
Unit Cell Dimensions	a = 9.4490(5) Å b = 27.3062(12) Å c = 17.6271(8) Å α= 90° β= 99.799(2)° γ = 90°
Volume	3381.7(4) Å^3
Z	4
Reflections collected	73827
Independent reflections	8220
Goodness-of-fit on F2	1.068
Final R indices [I>sigma(I)]	R1 = 0.0506 wR2 = 0.1151

Table 6.2 Selected bond lengths and angles for **(^{Mes}CCC)Co(η^2-H_2C=CHCOOCH$_2$CH$_3$)$_2$**.

	(^{Mes}CCC)Co(η^2-H_2C=CHCOOCH$_2$CH$_3$)$_2$
Bond Distances (Å)	
Co – C_{NHC}	1.954(3)
Co – C_{aryl}	1.902(3)
Co – C_{NHC}	1.1.961(3)
Co – $C_{C=C}$	2.1610(3)
Co – $C_{C=C}$	2.1701(3)
Bond Angles (°)	
C_{NHC}-Co-C_{NHC}	159.09(12)
C_{NHC}-Co-C_{aryl}	79.98(12)
C_{NHC}-Co-C_{aryl}	79.51(12)
C_{NHC}-Co-$C_{C=C}$	97.05(11)
C_{NHC}-Co-$C_{C=C}$	92.305(11)
C_{aryl}-Co-$C_{C=C}$	94.135(11)
C_{aryl}-Co-$C_{C=C}$	93.955(11)
$C_{C=C}$-Co-$C_{C=C}$	126.635(12)

6.11 References

1. Halse, M. E. Perspectives for hyperpolarization in compact NMR. *Trends Anal. Chem.* **2016**, *83*, 76-83.
2. Hirsch, M. L.; Kalechofsky, N.; Belzer, A.; Rosay, M.; Kempf, J. G. Brute-Force Hyperpolarization for NMR and MRI. *J. Am. Chem. Soc.* **2015**, *137*, 8428-8434.
3. Nikolaou, P.; Goodson, B. M.; Chekmenev, E. Y. NMR Hyperpolarization Techniques for Biomedicine. *Chem. Eur. J.* **2015**, *21*, 3156-3166.
4. Nelson, S. J.; Kurhanewicz, J.; Vigneron, D. B.; Larson, P. E. Z.; Harzstark, A. L.; Ferrone, M.; van Criekinge, M.; Change, J. W.; Bok, R.; Park, I.; Reed, G.; Carvajal, L.; Small, E. J.; Munster, P.; Weinberg, V. K.; Ardenkjaer-Larsen, J. H.; Chen, A. P.; Hurd, R. E.; Odegardstuen, L.; Robb, F. J.; Tropp, J.; Murray, J. A. Metabolic Imaging of Patients with Prostate Cancer Using Hyperpolarized [1-13C]Pyruvate. *Sci. Transl. Med.* **2013**, *5*, 198ra108.
5. Cavallari, E.; Carrera, C.; Reineri, F. ParaHydrogen Hyperpolarized Substrates for Molecular Imaging Studies. *Isr. J. Chem.* **2017**, *57*, 833-842.
6. Reineri, F.; Boi, T.; Aime, S. ParaHydrogen Induced Polarization of ^{13}C carboxylate resonance in acetate and pyruvate. *Nat. Commun.* **2015**, *6*, 5858.
7. Cavallari, E.; Carrera, C.; Boi, T.; Aime, S.; Reineri, F. Effects of Magnetic Field Cycle on the Polarization Transfer from Parahydrogen to Heteronuclei through Long-Range J-Couplings. *J. Phys. Chem. B* **2015**, *119*, 10035-10041.
8. Shchepin, R. V.; Chekmenev, E. Y. Synthetic approach for unsaturated precursors for parahydrogen induced polarization of choline and its analogs. *J. Label Compd. Radiopharm* **2013**, *56*, 655-662.
9. Reineri, F.; Viale, A.; Ellena, S.; Alberti, D.; Boi, T.; Giovenzana, G. B.; Gobetto, R.; Premkumar, S. S. D.; Aime, S. ^{15}N Magnetic Resonance Hyperpolarization via the Reaction of Parahydrogen with ^{15}N-Propargylcholine. *J. Am. Chem. Soc.* **2012**, *134*, 11146-11152.
10. Goldman, M.; Jóhannesson, H.; Axelsson, O.; Karlsson, M. Hyperpolarization of 13C through order transfer from parahydrogen: A new contrast agent for MRI. *Magn. Reson. Imaging* **2005**, *23*, 153-157.
11. Reineri, F.; Viale, A.; Ellena, S.; Boi, T.; Daniele, V.; Gobetto, R.; Aime, S. Use of Labile Precursors for the Generation of Hyperpolarized Molecules from Hydrogenation with Parahydrogen and Aqueous-Phase Extraction. *Angew. Chem. Int. Ed.* **2011**, *50*, 7350-7353.

12. Kovtunov, K. V.; Barskiy, D. A.; Shchepin R. V.; Coffey, A. M.; Waddell, K. W.; Koptyug, I. V.; Chekmenev, E. Y. Demonstration of Heterogeneous Parahydrogen Induced Polarization Using Hyperpolarized Agent Migration from Dissolved Rh(I) Complex to Gas Phase. *Anal. Chem.* **2014**, *86*, 6192-6196.
13. Kovtunov, K. V.; Barskiy, D. A.; Salnikov, O. G.; Shchepin, R. V.; Coffey, A. M.; Kovtunova, L. M.; Bukhitiyarov, V. I.; Koptyug, I. V.; Chekmenev, E. Y. Toward production of pure ^{13}C hyperpolarized metabolites using heterogeneous parahydrogen-induced polarization of ethyl[1-^{13}C]acetate. *RSC Adv.* **2016**, *6*, 69278-69732.
14. Koptyug, I. V.; Zhivonitko, V. V.; Kovtunov, D. V. New Perspectives for Parahydrogen-Induced Polarization in Liquid Phase Heterogeneous Hydrogenation: An Aqueous Phase and ALTADENA Study. *ChemPhysChem* **2010**, *11*, 3086-3088.
15. Salnikov, O. G.; Kovtunov, K. V.; Koptyug, I. V. Production of Catalyst-Free Hyperpolarised Ethanol Aqueous Solution via Heterogeneous Hydrogenation with Parahydrogen. *Sci. Rep.* **2015**, *5*, 13930.
16. Kovtunov, D. V.; Kovtunova, L. M.; Gemeinhardt, M. E.; Bukhtiyarov, A. V.; Gesiorski, J.; Bukhityarov, V. I.; Chekmenev, E. Y.; Koptyug, I. V.; Goodson, B. M. Heterogeneous Microtesla SABRE Enhancement of ^{15}N NMR Signals. *Angew. Chem. Int. Ed.* **2015**, *54*, 2452-2456.
17. Glögger, S.; Grunfeld, A. M.; Ertas, Y. N.; McCormick, J.; Wagner, S.; Bouchard, L. -S. Surface ligand-directed pair-wise hydrogenation for heterogeneous phase hyperpolarization. *Chem. Commun.* **2016**, *52*, 605-608.
18. Kovtunov, K. V.; Barskiy, D. A.; Shchepin, R. V.; Salnikov, O. G.; Prosvirin, I. P.; Kukhtiyarov, A. V.; Kovtunova, L. M.; Bukhitiyarov, V. I.; Koptyug, I. V.; Chekmenev, E. Y. Production of Pure Aqueous ^{13}C-Hyperpolarized Acetate Via Heterogeneous Parahydrogen-Induced Polarization. *Chem. Eur. J.* **2016**, *22*, 16446-16449.
19. Duckett, S. B.; Mewis, R. E. Application of *Para*hydrogen Induced Polarization Techniques in NMR Spectroscopy and Imaging. *Acc. Chem. Res.* **2012**, *45*, 1247-1257.
20. Godard, C.; Duckett, S. B.; Polas, S.; Tooze, R.; Whitwood, A. C. An NMR study of cobalt-catalyzed hydroformylation using *para*-hydrogen induced polarization. *Dalton Trans.***2009**, 2496-2509.
21. Godard, C.; Duckett, S. B.; Polas, S.; Tooze, R.; Whitwood, A. C. Detection of Intermediates in Cobalt-Catalyzed Hydroformylation Using *para*-Hydrogen-Induced Polarization. *J. Am. Chem. Soc.* **2005**, *127*, 4994−4995.

22. Tokmic, K.; Jackson, B. J.; Salazar, A.; Woods, T. J.; Fout, A. R. Cobalt-Catalyzed and Lewis Acid-Assisted Nitrile Hydrogenation to Primary Amines: A Combined Effort. *J. Am. Chem. Soc.* **2017**, *139*, 13554-13561.
23. Tokmic, K.; Markus, C. R.; Zhu, L.; Fout, A. R. Well-Defined Cobalt(I) Dihydrogen Catalyst: Experimental Evidence for a Co(I)/Co(III) Redox Process in Olefin Hydrogenation. *J. Am. Chem. Soc.* **2016**, *138*, 11907-11913.
24. Tokmic, K.; Fout, A. R. Alkyne Semihydrogenation with a Well-Defined Nonclassical Co-H_2 Catalyst: A H_2 Spin on Isomerization and *E*-Selectivity. *J. Am. Chem. Soc.* **2016**, *138*, 13700-13705.
25. Salnikov, O. G.; Liu, H.; Fedorov, A.; Burueva, D. B.; Kovtunov, K. V.; Copéret, C.; Koptyug, I. V. Pairwise hydrogen addition in the selective semihydrogenation of alkynes on silica-supported Cu catalysts. *Chem. Sci.* **2017**, *8*, 2426-2430.
26. Pravica, M. G.; Weitekamp, D. P. Net NMR alignment by adiabatic transport of parahydrogen addition products to high magnetic field. *Chem. Phys. Lett.* **1988**, *145*, 255−258.
27. Aguilar, J. A.; Elliott, P. I. P.; López-Serrano, J.; Adams, R. W.; Duckett, S. D. Only *para*-hydrogen spectroscopy (OPSY), a technique for the selective observation of *para*-hydrogen enhanced NMR signals. *Chem. Commun.* **2007**, 1183−1185.
28. Barkemeyer, J.; Haake, M.; Bargon, J. Hetero-NMR Enhancement via Parahydrogen Labeling. *J. Am. Chem. Soc.* **1995**, *117*, 2927-2928.
29. Goldman, M.; Johannesson, H. Conversion of a Proton Pair Para Order into C-13 Polarization by Rf Irradiation, for Use in Mri. *C. R. Phys.* **2005**, *6*, 575−581.
30. Goldman, M.; Johannesson, H.; Axelsson, O.; Karlsson, M. Design and Implementation of C-13 Hyperpolarization from Para- Hydrogen, for New MRI Contrast Agents. *C. R. Chim.* **2006**, *9*, 357−363.
31. Bär, S.; Lange, T.; Leibfritz, D.; Hennig, J.; von Elverfeldt, D.; Hövener, J. B. On the Spin Order Transfer from Parahydrogen to Another Nucleus. *J. Magn. Reson.* **2012**, *225*,25−35.
32. Jóhannesson, H.; Axelsson, O.; Karlsson, M. Transfer of Para- Hydrogen Spin Order into Polarization by Diabatic Field Cycling. *C. R. Phys.* **2004**, *5*, 315−324.
33. Olsson, L. E.; Chai, C. M.; Axelsson, O.; Karlsson, M.; Golman, K.; Petersson, S. MR Coronary Angiography in Pigs With Intraarterial Injections of a Hyperpolarized ^{13}C Substance. *Magn. Reson. Med.* **2006**, *55*, 731−737.

34. Pravdivtsev, A. N; Yurkovskaya, A. V.; Lukzen, N. N.; Ivanov, K. L.; Vieth, H. M.; Highly Efficient Polarization of Spin-1/2 Insensitive NMR Nuclei by Adiabatic Passage through Level Anticrossings. *J. Phys. Chem. Lett.* **2014**, *5*, 3421-3426.
35. Stephan, M.; Kohlmann, O.; Niessen, H. G.; Eichhorn, A.; Bargon, J. ^{13}C PHIP NMR spectra and polarization transfer during the homogeneous hydrogenation of alkynes with parahydrogen. *Magn. Reson. Chem.* **2002**, *40*, 157-160.
36. Glöggler, S.; Wagner, S.; Bouchard, L. S. Hyperpolarization of amino acid derivatives in water for biological applications. *Chem. Sci.* **2015**, *6*, 4261-4266.
37. Sánchez-Delgado, R. A. ; Rosales, M. Kinetic studies as a tool for the elucidation of the mechanisms of metal complex-catalyzed homogeneous hydrogenation reactions. *Coord. Chem. Rev.* **2000**, *196*, 249–280.
38. Giernoth, R.; Heinrich, H.; Adams, N. J.; Deeth, R. J.; Bargon, J.; Brown, J. M. PHIP Detection of a Transient Rhodium Dihydride Intermediate in the Homogeneous Hydrogenation of Dehydroamino Acids. *J. Am. Chem. Soc.* **2000**, *122*, 12381–12382.
39. Cerutti, E.; Viale, A.; Nervi, C.; Gobetto, R.; Aime, S. The Role of the Amino Protecting Group during Parahydrogenation of Protected Dehydroamino Acids. *J. Phys. Chem. A* **2015**, *119*, 11271-11279.
40. Pangborn, A.B.; Giardello, M.A.; Grubbs, R. H.; Rosen, R. K.; Timmers, F. J. Safe and Convenient Procedure for Solvent Purification. *Organometallics*, **1996**, *15*, 1518−1520.
41. Ibrahim, A. D.; Tokmic, K.; Brennan, M. B.; Kim, D. Matson, E. M.; Nilges, M. J.; Bertke, J. A.; Fout, A. R. Monoanionic bis(carbene) pincer complexes featuring cobalt(I-III) oxidation states. *Dalton Trans.* **2016**, *45*, 9805-9811.
42. Aguilar, J. A.; Adam, R. W.; Duckett, S. B.; Green, G. G. R.; Kandiah, R. Selective detection of hyperpolarized NMR signals derived from para-hydrogen using the Only Para-hydrogen SpectroscopY (OPSY) approach. *J. Magn. Reson.* **2011**, *208*, 49-57.
43. Duckett, S. B.; Green, G. G. R.; Cowley, M. J. Pulse sequencing with hyperpolarisable nuclei. US Patent 20,110,274,626, November 10, 2011.
44. Tom, B. A.; Bhasker, S.; Miyamoto, Y.; Momose, T.; McCall, B. J. Producing and quantifying enriched *para*-H_2. *Rev. Sci. Instrum.* **2009**, *80*, 016108.

CHAPTER 7: OXIDATIVE ADDITION, MIGRATORY INSERTION AND REDUCITVE ELIMINATION CHEMISTRY WITH PINCER BIS(CARBENE) COBALT COMPLEXES[†]

7.1 Introduction

Predictable two-electron chemistry is an attractive feature of late second- and third-transition metal complexes.[1] Along with the ease of handling and conferred high activity, numerous catalytic systems are based on the applications of such transition metal complexes.[2] Due to the well-defined nature of these complexes, detailed mechanistic insights about the operative reaction pathways have facilitated improvements of these catalytic systems.

Recently, the use of electron-rich pincer ligand systems has emerged as a prominent tactic to allow similar reactivity profiles with more abundant and relatively less toxic first-row transition metals.[3-7] In our group, the strongly σ-donating CCC pincer ligand platform complexed with cobalt has demonstrated well-defined two-electron chemistry in the hydrosilylation of alkenes,[8] hydroboration of alkenes and nitriles[9] and hydrogenation of olefins,[10] alkynes[11] and nitriles.[12] Based on the *para*Hydrogen Induced Polarization (PHIP) NMR studies of these catalytic hydrogenation processes,[10-12] the predictable two-electron reactivity of the low-valent cobalt complexes emboldened us to apply these compounds as PHIP catalysts to enhance ^{13}C NMR signals using *para*hydrogen (*p*-H_2).

To further examine the potential of these cobalt CCC complexes, stoichiometric studies toward two electron oxidants and reductants were necessary. The proposed mechanistic steps of the hydrogenation reactions in this system (oxidative addition, migratory insertion and reductive elimination), were postulated because of the observation of a PHIP effect in the hydrogenation studies, rather than the direct observation of such intermediates. In this chapter efforts toward the synthesis of new cobalt complexes supported by the ^{Mes}CCC ligand platform to study fundamental organometallic reactions,[13] specifically those proposed in the catalytic cycle of the hydrogenation of carbon-carbon multiple bonds, were undertaken.

7.2 Synthesis of (^{Mes}CCC)Co-HCl(PMe_3)

In the (^{Mes}CCC)Co system, the cleavage of the H-H bond by the low valent cobalt complexes transpires throughout the catalytic hydrogenation of olefins,[10] alkynes,[11] and nitriles;[12] however, the oxidative

[†] Portions of this chapter are reproduced from the following publications with permission from the authors. Tokmic, K.; Markus, C. R.; Zhu, L.; Fout, A. R. Well-Defined Cobalt(I) Dihydrogen Catalyst: Experimental Evidence for a Co(I)/Co(III) Redox Process in Olefin Hydrogenation. *J. Am. Chem. Soc.* **2016**, *138*, 11907-11913.

addition product (Co-$(H)_2$ species) has not been isolated. An alternative synthetic route to further understand H_2 reactivity with the cobalt complexes was sought. The addition of 1 equiv of HCl•Et_2O to **(^{Mes}CCC)Co(N_2)(PPh_3)**[14] led to the formation of an orange solution and following workup, the ^{1}H NMR spectrum of the orange solid in benzene-d_6 displayed broad paramagnetic resonances. The IR spectrum did not display an absorption characteristic of a cobalt-hydride. After unsuccessful efforts to crystallographically characterize the newly formed species, 1 equiv of HCl·Et_2O was added to a THF solution **(^{Mes}CCC)Co(N_2)(PMe_3)**. A color change of the solution resulted and after work up, an orange solid, **(^{Mes}CCC)Co-HCl(PMe_3)** was isolated in 80% yield (Scheme 7.1).

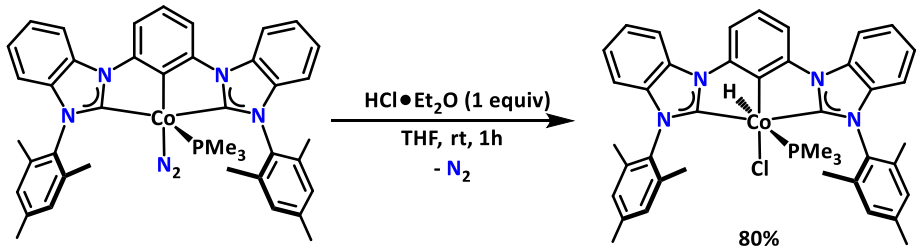

Scheme 7.1 Synthesis of **(^{Mes}CCC)Co-HCl(PMe_3)** via the oxidative addition of **(^{Mes}CCC)Co(N_2)(PMe_3)** using HCl.

Characterization of **(^{Mes}CCC)Co-HCl(PMe_3)** by ^{1}H NMR spectroscopy in benzene-d_6 revealed a C_s-symmetric molecule in solution, (Figure 7.1) similar to that of **(^{Mes}CCC)Co(N_2)(PMe_3)**. A doublet at −10.0 ppm corresponding to 1H with a T_1(min) value of 139 ms was assigned as a hydride and the large J value of this resonance ($^2J_{HP}$ = 109 Hz) indicated a *trans* substitution of the hydride with respect to the phosphine. The observation of a similar resonance for the analogous reaction with DCl·Et_2O at −10.0 ppm ($^2J_{DP}$ = 16.4 Hz) in the ^{2}H NMR spectrum further established that the source of the cobalt-hydride was the

^{1}H NMR spectrum – C_6D_6

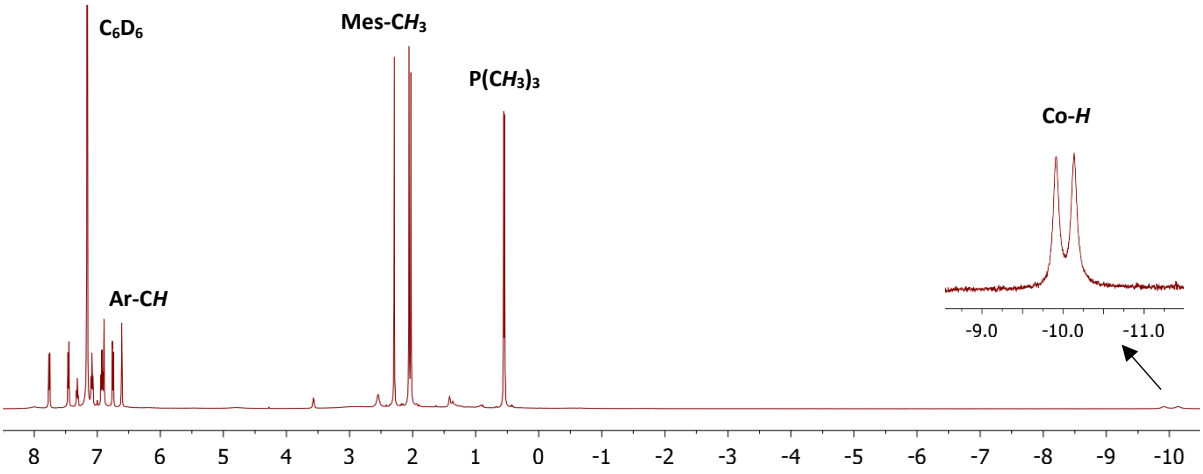

Figure 7.1 ^{1}H NMR spectrum of **(^{Mes}CCC)Co-HCl(PMe_3)**.

added acid (no resonances indicative of the protonation of the carbene moiety or pincer framework were observed) (Figure 7.2). The presence of an absorption band at 1828 cm^{-1} in the IR spectrum was also consistent with a Co−H vibration mode, while the Co−D absorption band (calculated 1304 cm^{-1}) was not resolved in the fingerprint region of the IR spectrum.

^{2}H NMR spectrum – C_6H_6

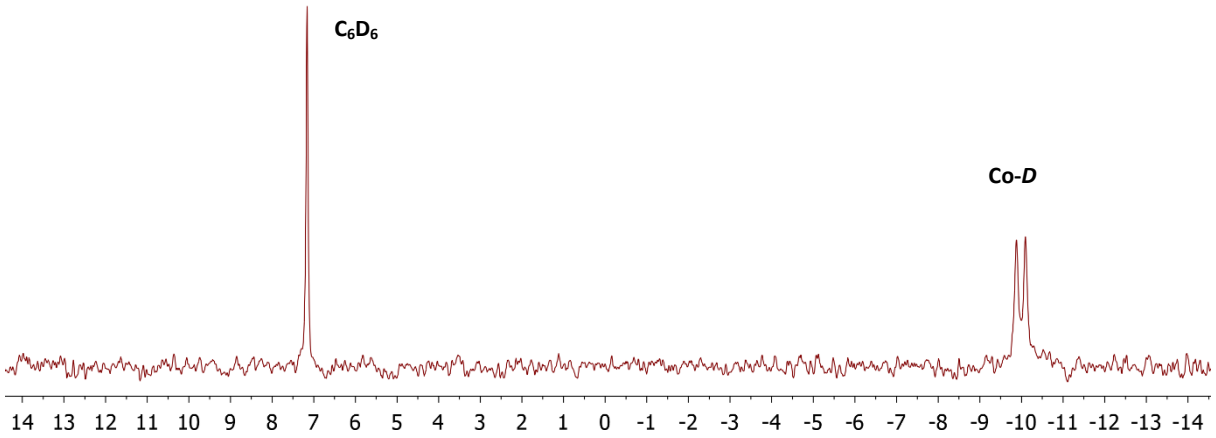

Figure 7.2 ^{2}H NMR spectrum of **(^{Mes}CCC)Co-DCl(PMe$_3$)** in benzene.

Single crystals suitable for X-ray structure determination were grown from a concentrated diethyl ether solution of **(^{Mes}CCC)Co-HCl(PMe$_3$)** and supported the oxidative addition of HCl onto **(^{Mes}CCC)Co-(N$_2$)(PMe$_3$)** (Figure 7.3). The octahedral cobalt complex has a slightly elongated Co−C_{NHC} (1.922(3) and 1.919(3) Å) and Co−P (2.2229(8) Å) bond lengths and a mildly shorter Co−C_{aryl} bond length (1.857(3) Å) when compared to **(^{Mes}CCC)Co-(N$_2$)(PMe$_3$)** (Table 7.1 and 7.2). The Co− Cl bond distance of 2.3057(7) Å is longer than the two Co−Cl bond lengths in **(^{Mes}CCC)CoCl$_2$py**[14] (2.2751(13) and 2.2651(12) Å), likely due to the C_{aryl} *trans* influence. The hydride was found in the difference map with 88% occupancy and a bond

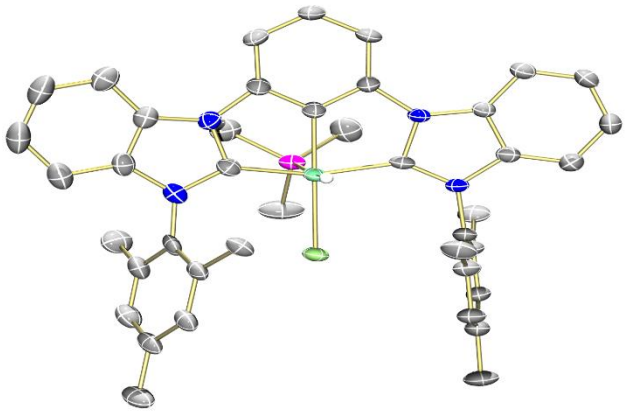

Figure 7.3 Molecular structure of **(^{Mes}CCC)Co-HCl(PMe$_3$)** with 50% probability ellipsoids. Solvent molecules and H atoms have been removed for clarity.

length of 1.40(5) Å from the metal center. The remainder of the electron density was modeled as a chloride atom with a bond length of 2.486(6) Å from the metal center, giving rise to a new Co(III) species, **(^{Mes}CCC)CoCl$_2$(PMe$_3$)** (Figure 7.4 and Table 7.1 and 7.2).

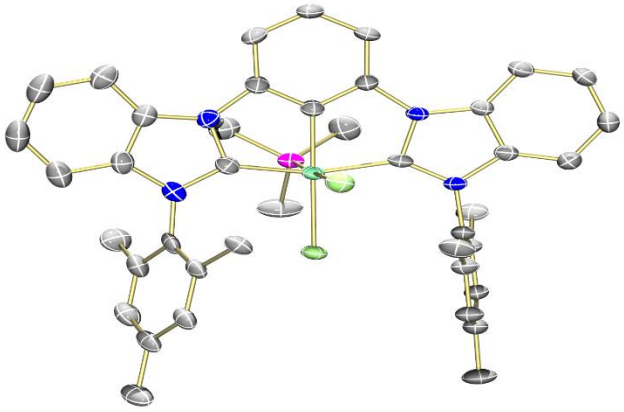

Figure 7.4 Molecular structure of **(^{Mes}CCC)CoCl$_2$(PMe$_3$)** with 50% probability ellipsoids. Solvent molecules and H atoms have been removed for clarity.

The formation of **(^{Mes}CCC)CoCl$_2$(PMe$_3$)** likely coincided with the addition of a slight excess of 1 equiv of HCl to **(^{Mes}CCC)Co-(N$_2$)(PMe$_3$)**. This was corroborated by the addition of another equivalent of HCl·Et$_2$O to a solution of **(^{Mes}CCC)Co-HCl(PMe$_3$)** in benzene-d_6 (Scheme 7.2 and Figure 7.23). The appearance of resonances corresponding to **(^{Mes}CCC)CoCl$_2$(PMe$_3$)**, as well as H_2 gas observed in the ^{1}H NMR spectrum, supports that **(^{Mes}CCC)CoCl$_2$(PMe$_3$)** is generated by the addition excess of HCl to **(^{Mes}CCC)Co-(N$_2$)(PMe$_3$)** (Figure 7.23). **(^{Mes}CCC)CoCl$_2$(PMe$_3$)** was also independently prepared by the addition of 2 equiv of ClCPh$_3$ to **(^{Mes}CCC)Co-(N$_2$)(PMe$_3$)**.

7.3 Synthesis of (^{Mes}CCC)Co-HClpy

Mechanistic insights from PHIP NMR studies provide evidence that the addition of H_2 onto the cobalt center occurs via *cis*-addition in a concerted fashion.[11,12] The addition of HCl onto the square pyramidal cobalt complex, **(^{Mes}CCC)Co(N$_2$)(PMe$_3$)**, yielded the octahedral cobalt complex, **(^{Mes}CCC)Co-HCl(PMe$_3$)**.

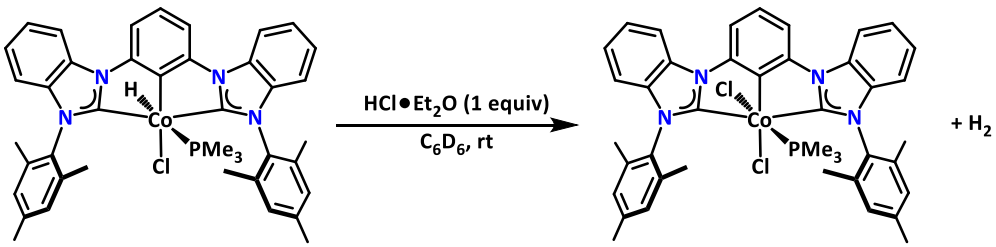

(^{Mes}CCC)Co-HCl(PMe$_3$) (^{Mes}CCC)Co-Cl$_2$(PMe$_3$)

Scheme 7.2 Synthesis of **(^{Mes}CCC)Co-Cl$_2$(PMe$_3$)** via the addition HCl to **(^{Mes}CCC)Co-HCl(PMe$_3$)**.

Even though a *cis*-addition product was observed, the nature of the HCl addition process remains unclear. Presumably an ionic mechanism is followed, and the *cis*-addition product may also be dictated by the steric factors of the PMe_3 ligand. The addition of HCl onto a square planer cobalt(I) species, **(^{Mes}CCC)Co-py**, was explored to provide further insight into the manner in which HCl is added to the cobalt center.

To this end, 1 equiv of HCl was added to a cold THF solution of **(^{Mes}CCC)Co-py** and upon work-up, **(^{Mes}CCC)Co-HCl(py)**, was isolated as a yellow solid in 60% yield (Scheme 7.3). Characterization by ^{1}H NMR spectroscopy in benzene-d_6 revealed a C_s-symmetric species present in solution, analogues to **(^{Mes}CCC)Co-HCl(PMe_3)** (Figure 7.5). A singlet at -23.53 ppm integrating to 1H with a T_1(min) value of 115 ms at 293K was assigned as a cobalt-hydride. The presence of an absorption band at 1895 cm^{-1} in the IR spectrum was consistent with a Co−H vibration mode.

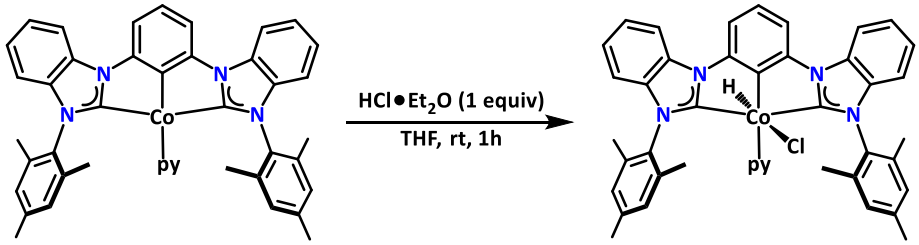

(^{Mes}CCC)Co-py (^{Mes}CCC)Co-HCl(py)

Scheme 7.3 Synthesis of **(^{Mes}CCC)Co-HCl(py)** via the addition HCl to **(^{Mes}CCC)Co-py**.

^{1}H NMR spectrum – C_6D_6

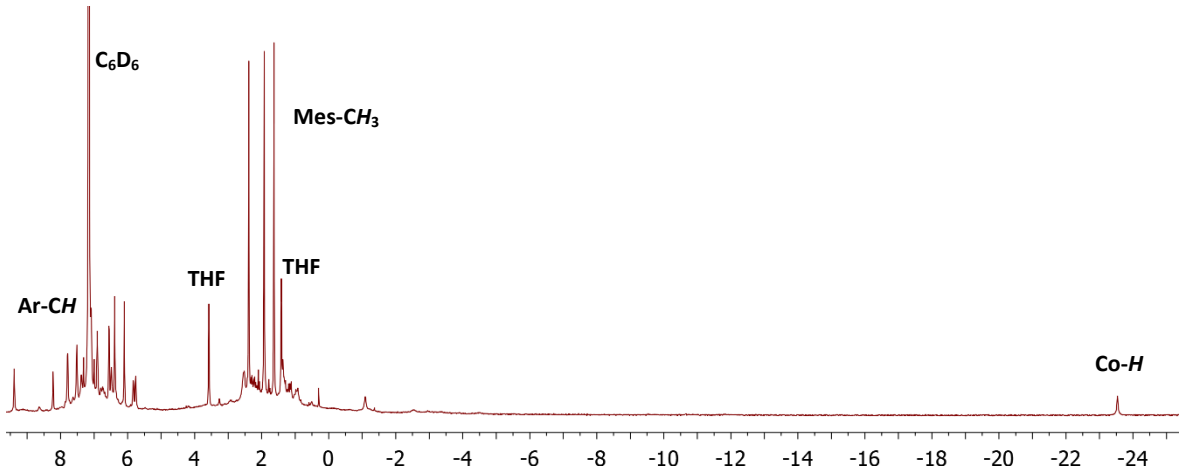

Figure 7.5 ^{1}H NMR spectrum of **(^{Mes}CCC)Co-HCl(py)** in benzene-d_6.

To further examine the nature of HCl addition on the square planar cobalt complex, single crystals suitable for X-ray diffraction studies were grown from a saturated benzene solution of **(^{Mes}CCC)Co-HCl(py)**. Despite the poor crystal quality, the connectivity of the complex shows the octahedral cobalt center bound by the pincer ligand, pyridine, chloride and a hydride moiety (Figure 7.6). Unlike in **(^{Mes}CCC)Co-**

HCl(PMe$_3$), the chloride and hydride are *trans* to one another in **(^{Mes}CCC)Co-HCl(py)**, demonstrating that HCl addition follows the expected ionic mechanism of oxidative addition.

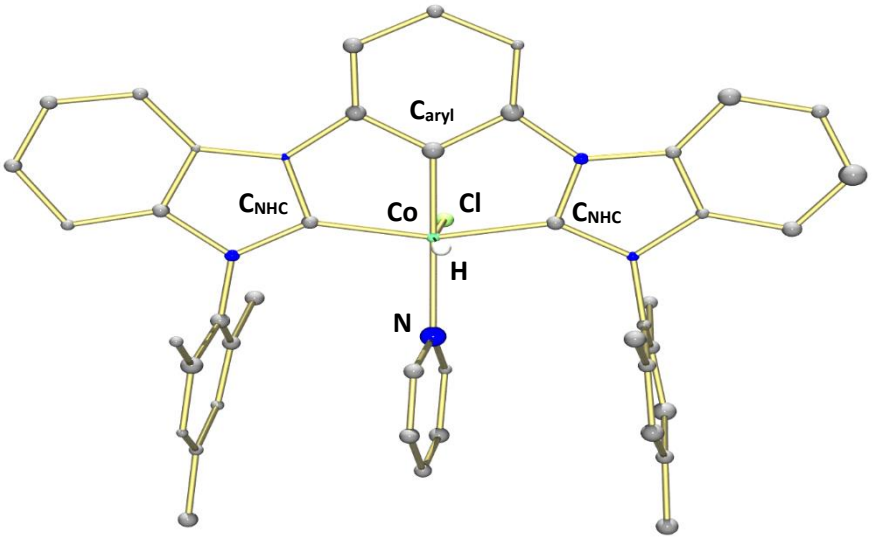

Figure 7.6 Connectivity of **(^{Mes}CCC)Co-HCl(py)**. Solvent molecules and H atoms have been omitted for clarity.

7.4 Alternative route to (^{Mes}CCC)Co-HCl(PMe$_3$)

The addition of HCl proved to be a synthetically viable route toward the generation of cobalt(III)-hydride precursors on the bis(carbene) ligand platform for further reactivity studies. However, the generation of **(^{Mes}CCC)CoCl$_2$(PMe$_3$)** from the slight excess of HCl addition, motivated us to find alternative protocols for the synthesis of cobalt(III)-hydride complexes and also investigate metalation protocols of the ligand precursor, [H$_3$(^{Mes}CCC)]Cl$_2$. In parallel to our group's work with iron CCC chemistry,[15] **(^{Mes}CCC)Co-HCl(PMe$_3$)** was prepared in a two-step procedure starting with the imidazolium salt, [H$_3$(^{Mes}CCC)]Cl$_2$ (Scheme 7.4).

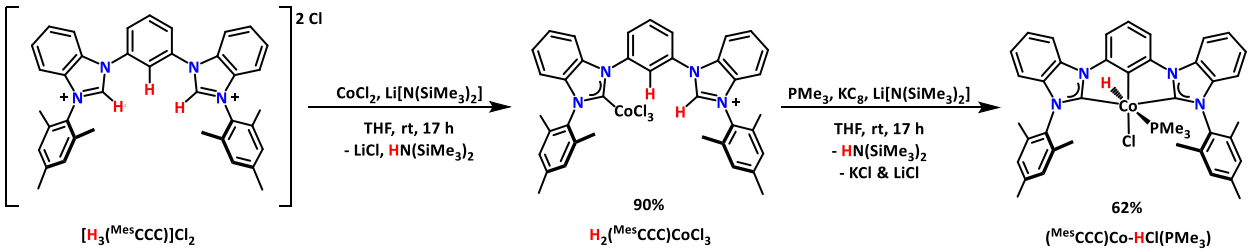

Scheme 7.4 Two-step synthesis of **(^{Mes}CCC)Co-HCl(PMe$_3$)** from [H$_3$(^{Mes}CCC)]Cl$_2$.

^{1}H NMR spectrum – $CDCl_3$

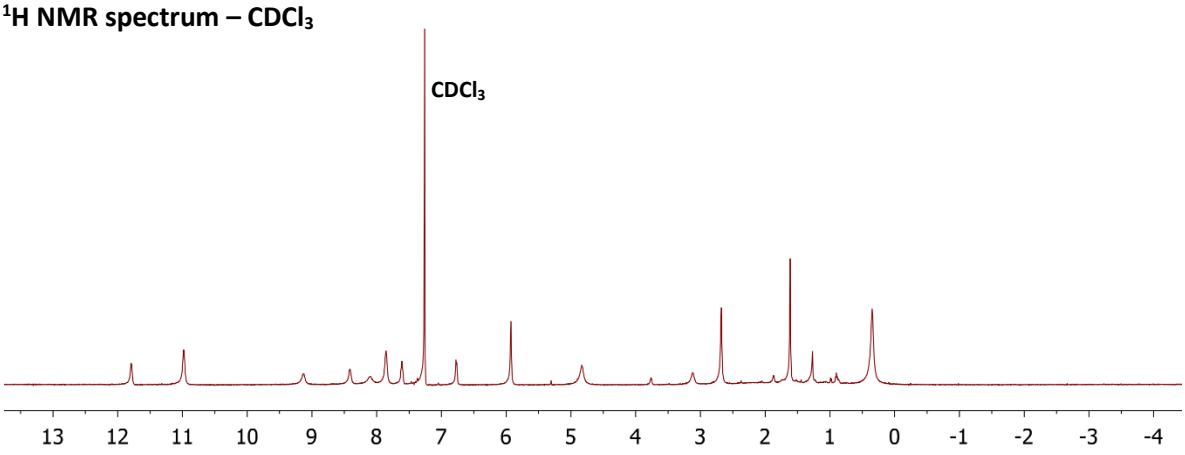

Figure 7.7 ^{1}H NMR spectrum of **H_2(^{Mes}CCC)$CoCl_3$** in $CDCl_3$.

The addition of lithium hexamethyldisilazide ($LiN(SiMe_3)_2$) to a THF suspension of $[H_3(^{Mes}CCC)]Cl_2$ and $CoCl_2$ resulted in the formation of a light-blue complex, **H_2(^{Mes}CCC)$CoCl_3$**, in 90% yield after workup (Scheme 7.4). Characterization of **H_2(^{Mes}CCC)$CoCl_3$** by ^{1}H NMR spectroscopy revealed 16 broadened resonances ranging from 12 to 0 ppm (Figure 7.7). Single crystals suitable for X-ray diffraction studies were grown from a saturated solution of **H_2(^{Mes}CCC]$CoCl_3$** in THF. The metal center adopts a distorted trigonal pyramidal ($\tau = 0.9$)[16] geometry (Figure 7.8 and Tables 7.1 and 7.2). The cobalt(II) center in the zwitterionic complex, **H_2(^{Mes}CCC]$CoCl_3$**, is ligated by one C_{NHC} atom and three chloride moieties.

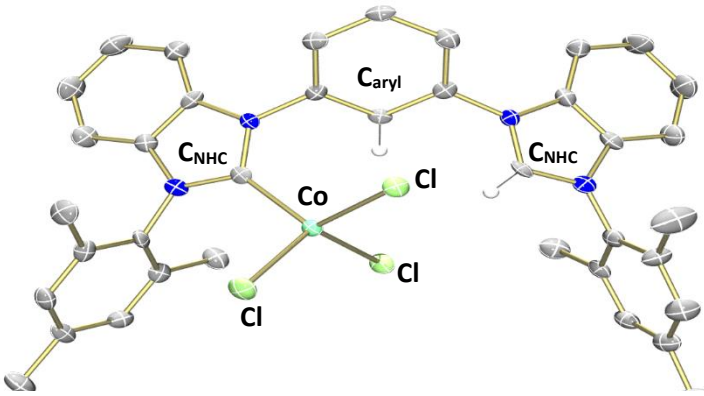

Figure 7.8 Molecular structure of **H_2(^{Mes}CCC)$CoCl_3$** with 50% probability ellipsoids. Solvent molecules and H atoms have been omitted for clarity.

Following the characterization **H_2(^{Mes}CCC]$CoCl_3$**, we turned our attention to the synthesis of the cobalt(III)-hydride complex. The addition of a mixture of $LiN(SiMe_3)_2$ (1 equiv) and KC_8 (1 equiv) in THF to a THF suspension of **H_2(^{Mes}CCC]$CoCl_3$** and PMe_3 (1 equiv) resulted in the formation of an orange solid after work-up in 69% yield (Scheme 7.4). The ^{1}H NMR spectrum of the orange species matched that of **(^{Mes}CCC)Co-HCl(PMe_3)** (Figure 7.1). The overall yield of the synthetic route (Scheme 7.4) is 62% and provides an alternative synthetic for the preparation of the cobalt(III)-hydride complex.

7.5 Reductive elimination of H_2 and methane from (^{Mes}CCC)Co-HCl(PMe_3)

With **(^{Mes}CCC)Co-HCl(PMe_3)** in hand, a hydride transfer reagent was added to the metal center to determine if a Co(III)-$(H)_2$ complex could be accessed. Under a dinitrogen atmosphere, the addition of Cp_2ZrHCl to a benzene-d_6 solution of **(^{Mes}CCC)Co-HCl(PMe_3)** immediately resulted in the formation of **(^{Mes}CCC)Co-(N_2)(PMe_3)** and Cp_2ZrCl_2 as well as H_2 gas (Scheme 7.5), as evidenced by ^{1}H NMR spectroscopy (Figure 7.22). The reaction likely proceeds through salt metathesis to generate a transient Co(III)-*cis*$(H)_2$ species, followed by reductive coupling of dihydrogen and coordination of N_2 to yield **(^{Mes}CCC)Co-(N_2)(PMe_3)**. This rapid reductive coupling suggests H_2/D_2 scrambling may in fact proceed via a Co(III)-dihydride, but this species is thermally unstable and, therefore, not easily detected via conventional characterization methods.

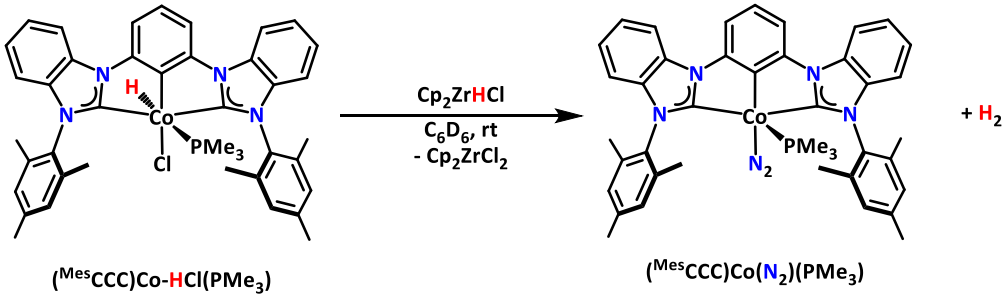

Scheme 7.5 Addition of Cp_2ZrHCl to **(^{Mes}CCC)Co-HCl(PMe_3)**.

To determine if a unimolecular process is operative during the addition of a hydride source to **(^{Mes}CCC)Co-HCl(PMe_3)**, we turned our attention to the use of the isotopically labeled cobalt-deuteride, **(^{Mes}CCC)Co-DCl(PMe_3)**, complex. The addition of Cp_2ZrHCl to **(^{Mes}CCC)Co-DCl(PMe_3)** resulted in the formation of **(^{Mes}CCC)Co-(N_2)(PMe_3)** and H_2 and HD gas, as observed by ^{1}H NMR spectroscopy. This is not indicative that elimination process in unimolecular or bimolecular since the cobalt(I) complex, **(^{Mes}CCC)Co-(N_2)(PMe_3)**, formed in the reaction scrambles H_2/D_2.

Following a similar reaction scheme, alkylation of **(^{Mes}CCC)Co-HCl(PMe_3)** with methyllithium in benzene-d_6 furnished **(^{Mes}CCC)Co-(N_2)(PMe_3)** and methane gas (Figure 7.9). To rule out the bimolecular process, alkylation of **(^{Mes}CCC)Co-DCl(PMe_3)** with methyllithium resulted in the formation of CH_3D gas, confirmed by ^{1}H and ^{2}H NMR spectroscopy (Figure 7.9). The formation of CH_3D is direct evidence for a unimolecular reductive elimination process from the Co(III)-hydride species is operative.

Stoichiometric two-electron chemistry on the cobalt CCC ligand system via the oxidative addition of HCl and the concerted reductive elimination of H_2 and methane support the proposed catalytic steps and proposed redox changes in the catalytic cycle of the hydrogenation of carbon-carbon multiple bonds[10,11] and nitriles[12] with the cobalt complexes. To probe if additional steps, such as migratory insertion, in the

proposed catalytic cycle could be characterized and further provide mechanistic evidence of H_2 / D_2 exchange, additional complexes to support such studies were synthesized.

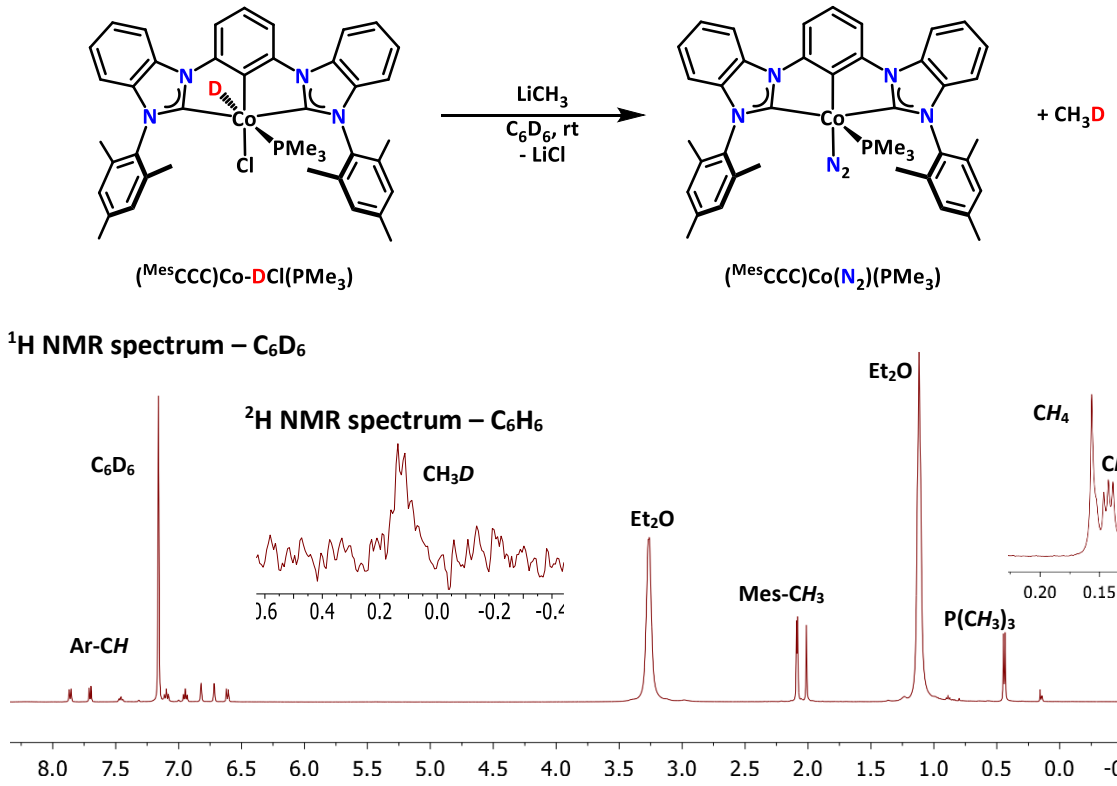

Figure 7.9 ^{1}H NMR spectrum the addition of MeLi (1.6M, Et_2O) to a C_6D_6 solution of **(MesCCC)Co-DCl(PMe3)**. Middle inset is the ^{2}H NMR in benzene of the same reaction.

7.6 Synthesis of [(MesCCC)Co(H)(N2)(PMe3)][B(ArF)4]

To gain insights into migratory insertion and H_2 / D_2 exchange pathways proposed in our catalytic studies, attention was turned to the octahedral **(MesCCC)Co-HCl(PMe3)** complex. We reasoned that the Co(III) species, which features a reactive hydride ligand, could serve as a platform to carry out such reactivity studies. Addition of olefins, alkynes, H_2 or D_2 to the coordinatively saturated 18-electron **(MesCCC)Co-HCl(PMe3)** complex resulted in no reaction. The ligand displacement of the *cis*-position chloride most likely inhibits the desired reactivity.

To circumvent this issue, displacement of the chloride ligand from the metal complex was explored. The addition of sodium tetrakis(3,5-bis(trifluoromethyl)phenyl)borate ($Na[BAr^F]_4$) (Ar^F = 3,5-$(CF_3)_2C_6H_3$) to a solution of **(MesCCC)Co-HCl(PMe3)** in benzene-d_6 resulted in the formation of a yellow oil (Scheme 7.6). Characterization of the crude mixture by ^{1}H NMR spectroscopy revealed a small upfield shift of the mesityl and $P(CH_3)_3$ methyl resonances. The upfield shift of the hydride resonance to -10.67 ppm with a smaller

$^{1}H\{^{31}P\}$ coupling constant, $^{2}J_{HP}$ = 96 Hz, compared to **(^{Mes}CCC)Co-HCl(PMe$_3$)** were consistent with the formation of a new species (Figure 7.10). Based the coupling constant, the hydride is presumed to remain *trans* to the phosphine ligand. The presence of an absorption band at 1828 cm^{-1} in the IR spectrum is consistent with a cobalt-hydride and is similar to **(^{Mes}CCC)Co-HClL** (L = PMe$_3$ (1828 cm^{-1}) & pyridine (1895 cm^{-1})). Interestingly, an intense absorption band at 2251 cm^{-1} was also observed, suggesting coordination of an N_2 ligand to the electrophilic cobalt center, blue-shifted from ν_{N2} = 2114 cm^{-1} observed in **(^{Mes}CCC)Co(N$_2$)(PMe$_3$)**.

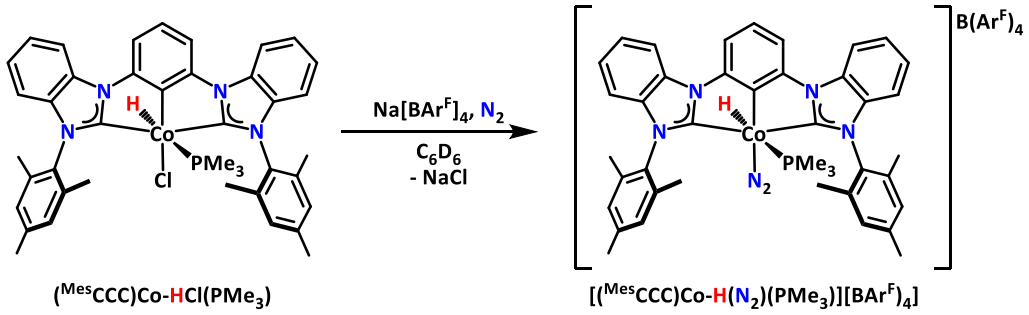

Scheme 7.6 Synthesis of **[(^{Mes}CCC)Co(H)(N$_2$)(PMe$_3$)][B(Ar^F)$_4$]**.

^{1}H NMR spectrum – C$_6$D$_6$

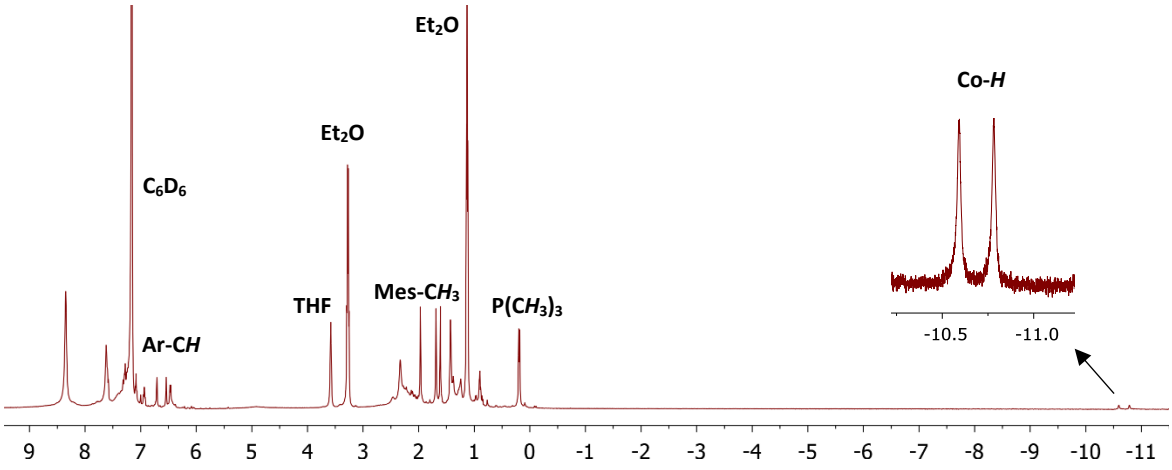

Figure 7.10 ^{1}H NMR spectrum of **[(^{Mes}CCC)Co-H(N$_2$)(PMe$_3$)][B(Ar^F)$_4$]** in benzene-d_6.

The formation of NaCl via the salt metathesis of the chloride ligand on the cobalt center with Na[B(Ar^F)$_4$] likely transpired throughout the reaction, thus the coordination of an alternative ligand such as N_2 or the formation of a square pyramidal 16-electron cobalt(III) species also remained a possibility. To unambiguously determine the molecular structure of the new species, single crystals suitable for X-ray diffraction studies were grown from a benzene and hexanes mixture of the target complex. The molecular structure of **[(^{Mes}CCC)Co-H(N$_2$)(PMe$_3$)][B(Ar^F)$_4$]** confirms the coordination of N_2 to the octahedral cobalt

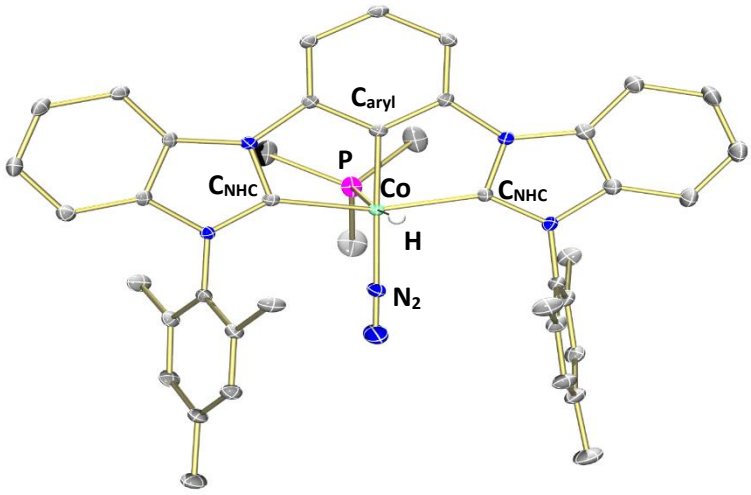

Figure 7.11 Molecular structure of **[(^{Mes}CCC)Co-H(N_2)(PMe_3)][$B(Ar^F)_4$]** with 50% probability ellipsoids. Solvent molecules, $B(Ar^F)_4$ counter anion and remaining H atoms have been omitted for clarity.

complex across the from the C_{aryl} carbon and is in agreement with the predicted reactivity (Figure 7.11). Furthermore, the hydride was found in the difference map and lies *trans* to the PMe_3 moiety.

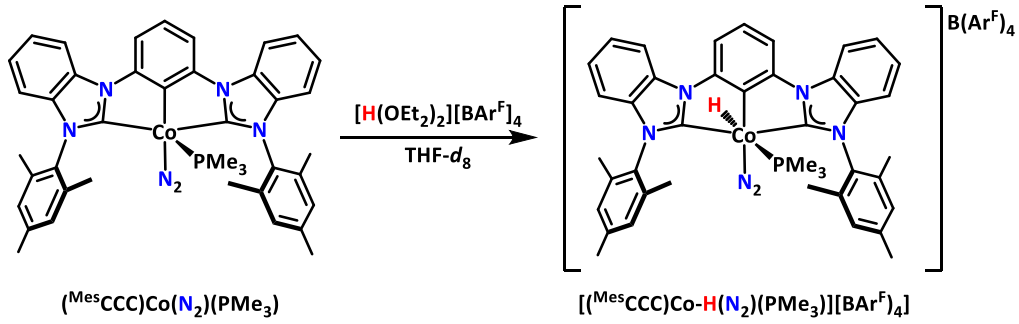

^{1}H NMR spectrum – THF-d_8

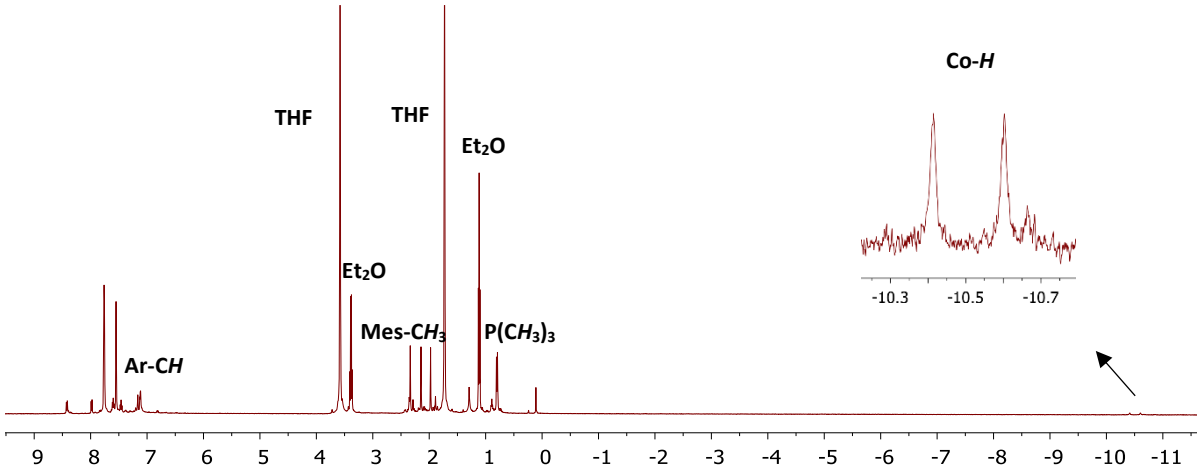

Figure 7.12 ^{1}H NMR spectrum of **[(^{Mes}CCC)Co-H(N_2)(PMe_3)][$B(Ar^F)_4$]** in THF-d_8.

Due to unsuccessful attempts to remove intractable impurities from the oily complex, alternative approaches to prepare **[(^Mes^CCC)Co-H(N$_2$)(PMe$_3$)][B(Ar^F)$_4$]** were undertaken. To this end, the addition of Brookhart's acid, **[H(OEt$_2$)$_2$][B(Ar^F)$_4$]**, to a THF-d_8 solution of **(^Mes^CCC)Co(N$_2$)(PMe$_3$)** resulted in the formation of **[(^Mes^CCC)Co-H(N$_2$)(PMe$_3$)][B(Ar^F)$_4$]**. Characterization by ^{1}H NMR spectroscopy confirmed the formation of the desired product (Figure 7.12). The presence of a doublet at -10.51 ppm with a $^2J_{DP}$ = 15 Hz coupling constant in the ^{2}H NMR spectrum following the addition of [D(OEt$_2$)$_2$][B(Ar^F)$_4$] to **(^Mes^CCC)Co(N$_2$)(PMe$_3$)** in THF further confirmed the resonance was due to the added acid (Figure 7.13).

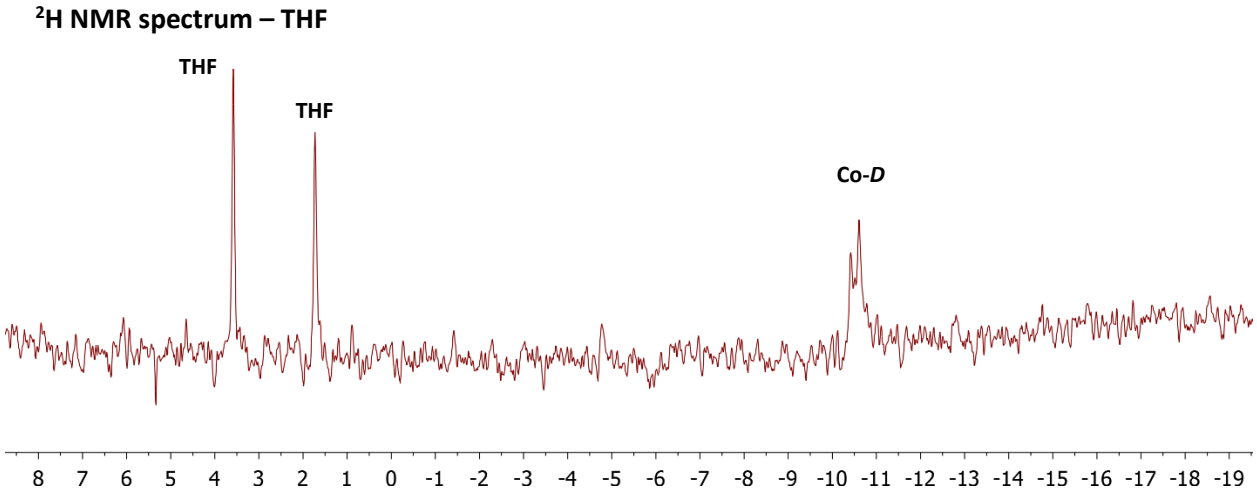

Figure 7.13 ^{2}H NMR spectrum of **[(^Mes^CCC)Co-D(N$_2$)(PPh$_2$Me)][B(Ar^F)$_4$]** in THF.

7.7 Addition of H_2 to [(^Mes^CCC)Co(H)(N$_2$)(PMe$_3$)][B(Ar^F)$_4$]

With **[(^Mes^CCC)Co-H(N$_2$)(PMe$_3$)][B(Ar^F)$_4$]** in hand, studies into the scrambling of H_2 / D_2 by the cobalt(III) complex were pursued. The addition of H_2 to a THF-d_8 solution of **[(^Mes^CCC)Co-H(N$_2$)(PMe$_3$)][B(Ar^F)$_4$]** resulted in the shift of the mesityl methyl resonances in the ^{1}H NMR spectrum from 1.97, 2.14 and 2.34 to 1.88, 2.08 and 2.38 ppm, indicating the formation of a new species. The presence of a broad resonance at -5.57 ppm with a T_1 (min) value of 18 ms at 298K integrating to 2H suggests Co-(H_2) is present in solution. The T_1(min) relaxation rate of the assigned dihydrogen resonance is similar to the rate in **(^Mes^CCC)Co(H$_2$)(PR$_3$)** (R = PPh$_3$, 12 ms; PMe$_3$, 14 ms)[12] and shorter than the rate in related electrophilic cobalt(III) complexes of the general formula [Cp*Co(L)(H)(H$_2$)][B(Ar^F)$_4$] (Cp* = C$_5$Me$_5$; L = P(OMe)$_3$, 22 ms; PMe$_3$, 52 ms).[17] However, relaxation rate alone is not indicative of an explicit cobalt-dihydrogen molecule since contributions from the cobalt and phosphine nuclei effect the relaxation rate of the bound H_2 ligand,[18] therefore the actual Co-(H_2) T_1(min) value is likely shorter. In addition, an upfield shift and

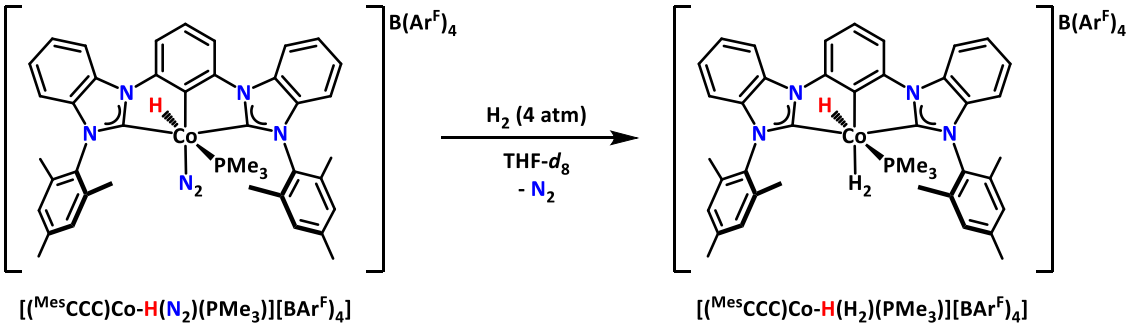

^{1}H NMR spectrum – THF-d_8

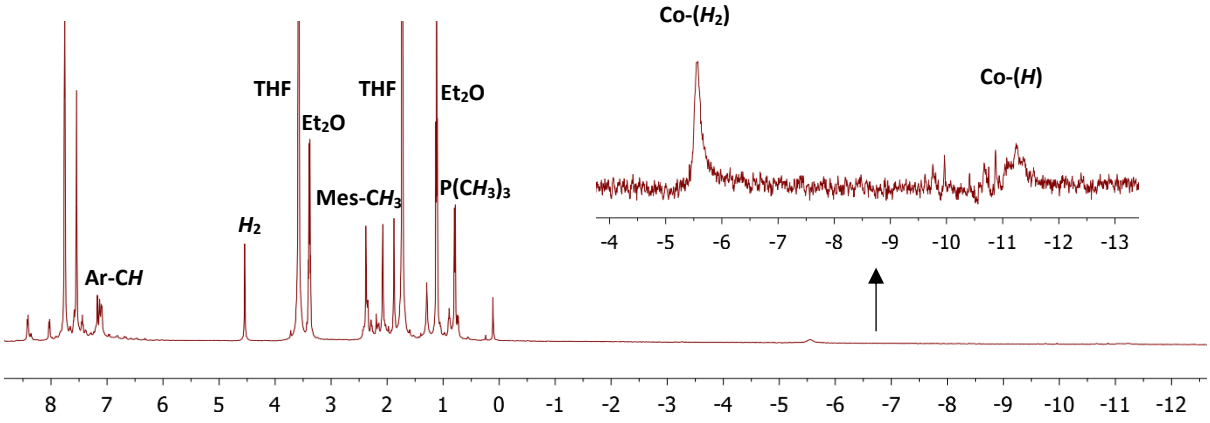

Figure 7.14 ^{1}H NMR spectrum of **[(^{Mes}CCC)Co-H(H_2)(PMe_3)][$B(Ar^F)_4$]** in THF-d_8.

broadening of the hydride resonance to *ca.* -11.20 ppm suggests the formation of a cobalt(III) dihydrogen hydride complex in solution. Due to the broadening of the resonance, a $^1H\{^{31}P\}$ coupling constant could not be resolved with confidence ($^2J_{HP}$ ~ 75 Hz). In this case, the broadening of the hydride resonance may be a result of the dynamic exchange between the dihydrogen and hydride ligands on the metal center.[19]

To further understand the nature of H_2 reactivity with **[(^{Mes}CCC)Co-H(N_2)(PMe_3)][$B(Ar^F)_4$]**, D_2 was used in place of H_2 to extract J_{HD} coupling values in order to more accurately assign the new complex. The formation of HD gas in the ^{1}H NMR spectrum following the addition of D_2 gas to a THF-d_8 solution of **[(^{Mes}CCC)Co-H(N_2)(PMe_3)][$B(Ar^F)_4$]** coincided with the disappearance of the hydride resonance at -10.5 ppm, confirming the exchange of H with D_2. Furthermore, the ligand based resonances observed in the ^{1}H NMR spectrum were identical those of **[(^{Mes}CCC)Co-H(H_2)(PMe_3)][$B(Ar^F)_4$]**. To support the assignment of resonances at -5.57 and -10.5 ppm arising from H_2, D_2 was added to a THF solution of **[(^{Mes}CCC)Co-H(N_2)(PMe_3)][$B(Ar^F)_4$]**. This resulted in the appearance of a resonance at -5.36 ppm, assigned as a Co(D_2) species and a broad feature -10.08 to -11.35 ppm, assigned as the cobalt-deuteride ligand moiety, in the ^{2}H NMR spectrum (Figure 7.15). Due to the broadening of the resonances, no HD coupling values were

obtained; however, based on the ^{1}H and ^{2}H NMR data, it is proposed that **[(^{Mes}CCC)Co-H(H_2)(PMe_3)][$B(Ar^F)_4$]** is formed from N_2 displacement in **[(^{Mes}CCC)Co-H(N_2)(PMe_3)][$B(Ar^F)_4$]** by H_2.

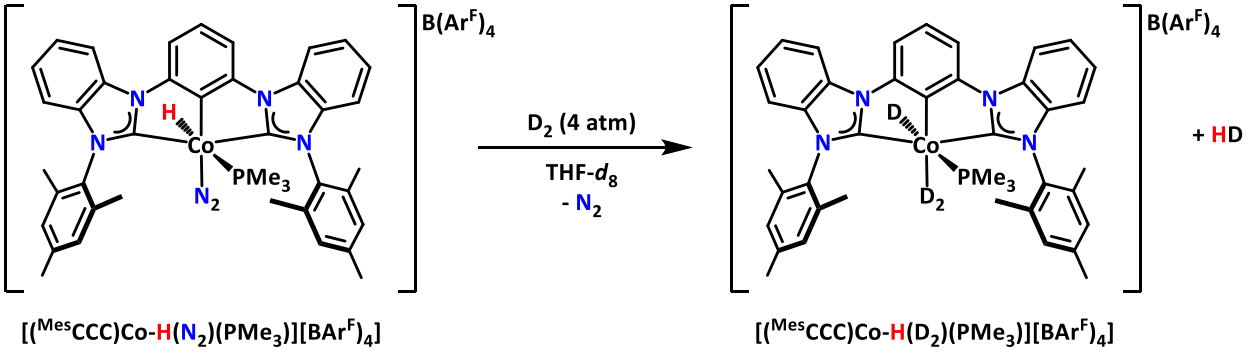

[(^{Mes}CCC)Co-H(N_2)(PMe_3)][$BAr^F)_4$] [(^{Mes}CCC)Co-H(D_2)(PMe_3)][$BAr^F)_4$]

^{2}H NMR spectrum – THF

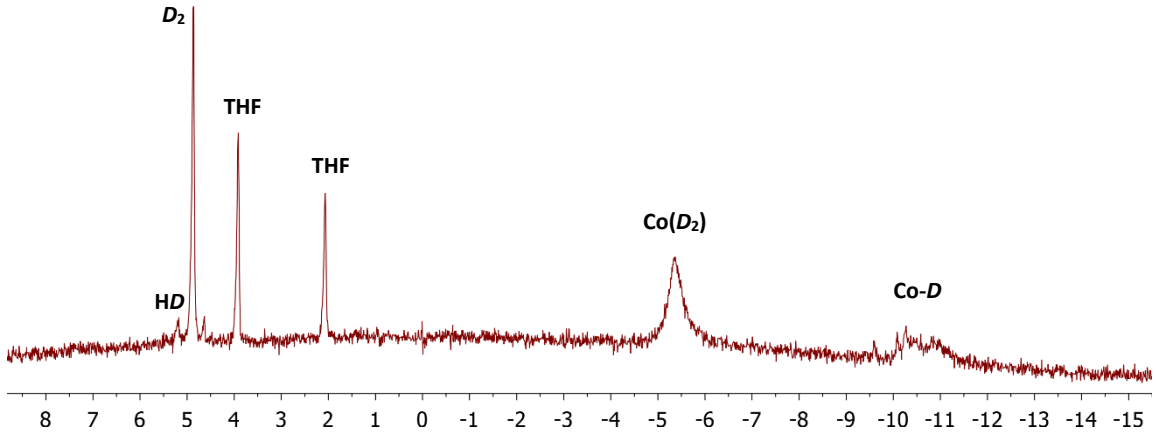

Figure 7.15 ^{2}H NMR spectrum of **[(^{Mes}CCC)Co-D(D_2)(PMe_3)][$B(Ar^F)_4$]** in THF.

These studies suggest that the H_2 / D_2 scrambling observed with **(^{Mes}CCC)Co(N_2)(PR_3)** (R = Ph, Me)[10] likely occurs via the Co(III) dihydrogen hydride intermediates proposed previously. Interestingly, throughout the course of these studies, the addition of either HCl or $[H(OEt_2)_2][B(Ar^F)_4]$ to **(^{Mes}CCC)Co(N_2)(PPh_3)** resulted in ambiguous products, while similar reactivity with **(^{Mes}CCC)Co(N_2)(PMe_3)** resulted in well-defined oxidative addition complexes. To further examine the electronic or steric influence of the phosphine ligand employed, the synthesis of the PPh_2Me and PPh_2Me Co(I) complexes with the same ligand platform were pursued.

7.8 Synthesis of (^{Mes}CCC)Co(N_2)(L) (L = PPh_2Me and $PPhMe_2$)

Following a similar protocol for the preparation of **(^{Mes}CCC)Co(N_2)(PR_3)** (R = Ph, Me)[10] complexes, **(^{Mes}CCC)Co(N_2)(L)** (L = PPh_2Me or $PPhMe_2$) were isolated in 81% and 59% yield, respectively, as dark red solids (Scheme 7.7). Characterization by ^{1}H NMR spectroscopy revealed a C_s-symmetric ligand

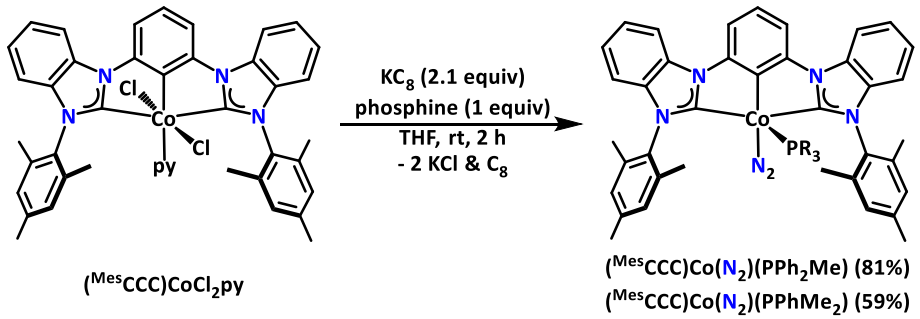

Scheme 7.7 Synthesis of **(^{Mes}CCC)Co(N_2)(L)** (L = PPh_2Me or $PPhMe_2$).

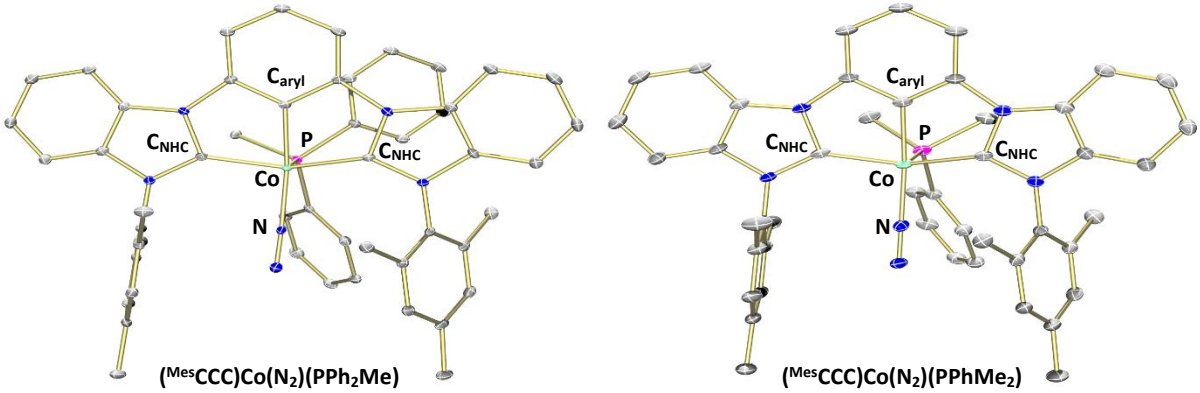

Figure 7.16 Molecular structures of **(^{Mes}CCC)Co(N_2)(L)** (L = PPh_2Me (left) and $PPhMe_2$ (right)) with 50% probability ellipsoids. H atoms have been omitted for clarity.

environment, similar to that of **(^{Mes}CCC)Co(N_2)(PR_3)** (R = Ph, Me).[10] Characterization of **(^{Mes}CCC)Co(N_2)(L)** (L = PPh_2Me or $PPhMe_2$) by IR spectroscopy revealed an absorption band at 2118 and 2114 cm^{-1}, respectively, assigned to a bound N_2 ligand. X-ray crystallographic characterization of **(^{Mes}CCC)Co(N_2)(L)** (L = PPh_2Me or $PPhMe_2$) established the connectivity of the square pyramidal (τ = 0.17 and 0.18, respectively) complexes and was in agreement with IR spectroscopy. The N_2 bond distances (1.111(5) and 1.107(2) Å) in **(^{Mes}CCC)Co(N_2)(L)** (L = PPh_2Me or $PPhMe_2$, respectively) remain largely unactivated (Figure 7.16 and Tables 7.3 and 7.4).

7.9 Oxidative addition of (^{Mes}CCC)Co(N_2)(L) (L = PPh_2Me and $PPhMe_2$)

With the **(^{Mes}CCC)Co(N_2)(L)** (L = PPh_2Me or $PPhMe_2$) complexes in hand, the preparation of electrophilic Co(III)-hydride complexes were next examined. The addition of $[H(OEt_2)_2][B(Ar^F)_4]$ to a THF-d_8 solution of **(^{Mes}CCC)Co(N_2)(L)** (L = PPh_2Me or $PPhMe_2$) resulted in the formation of **[(^{Mes}CCC)Co-H(N_2)(PR_3)][$B(Ar^F)_4$]** (R = PPh_2Me, $PPhMe_2$) as observed by ^{1}H NMR spectroscopy (Figure 7.17). Based on the three mesityl methyl resonances, both complexes adopt a C_s-symmetric structure in solution, similar to the ^{1}H NMR spectrum of **[(^{Mes}CCC)Co-H(N_2)(PMe_3)][$B(Ar^F)_4$]** (Figure 7.12). Interestingly, a close

examination of the ^{1}H NMR spectrum of **[(^{Mes}CCC)Co-H(N_2)($PPhMe_2$)][$B(Ar^F)_4$]** displayed additional minor resonances, indicating the possible formation of additional products. Conversely, **[(^{Mes}CCC)Co-H(N_2)(PPh_2Me)][$B(Ar^F)_4$]** appears to be the only species present in solution by ^{1}H NMR spectroscopy and exhibits only one doublet at -11.62 ppm with a $^{2}J_{HP}$ = 97 Hz, consistent with that observed for **[(^{Mes}CCC)Co-H(N_2)(PMe_3)][$B(Ar^F)_4$]** (Figure 7.17). Treatment of **(^{Mes}CCC)Co(N_2)(PPh_3)** with both HCl and $[H(OEt_2)_2][B(Ar^F)_4]$ yielded different reactivity compared to the PPh_2Me and $PPhMe_2$ derivatives and the outcome of the reactions remain unresolved. Nevertheless, the three ionic cobalt(III)-hydride complexes, **[(^{Mes}CCC)Co-H(N_2)(PR_3)][$B(Ar^F)_4$]** (R = PPh_2Me, $PPhMe_2$, PMe_3), were successfully synthesized and the corresponding structures provide possible explanations to the divergent reactivity. The larger cone angle of PPh_3 (145°) versus the other phosphines (PPh_2Me, $PPhMe_2$ and PMe_3 (136, 122 and 118°, respectively)) may inhibit the formation of the 18-electron octahedral complex. This suggests that steric hindrance of the phosphine likely influences the stability of the Co(III)-hydride complexes.[20] Electronic differences between the phosphines are not likely a large contributor to stability of these cobalt(III)-hydride complexes, evidenced by the pyridine derivative **(^{Mes}CCC)Co-py**, which was shown to be amenable to acid addition.

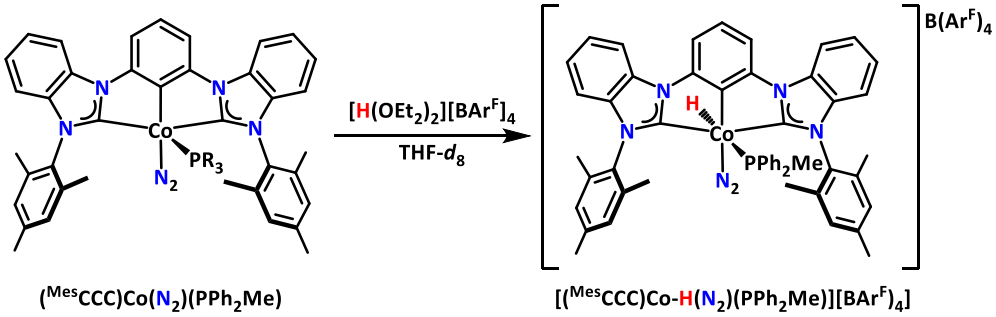

(^{Mes}CCC)Co(N_2)(PPh_2Me) [(^{Mes}CCC)Co-H(N_2)(PPh_2Me)][$BAr^F)_4$]

^{1}H NMR spectrum – THF-d_8

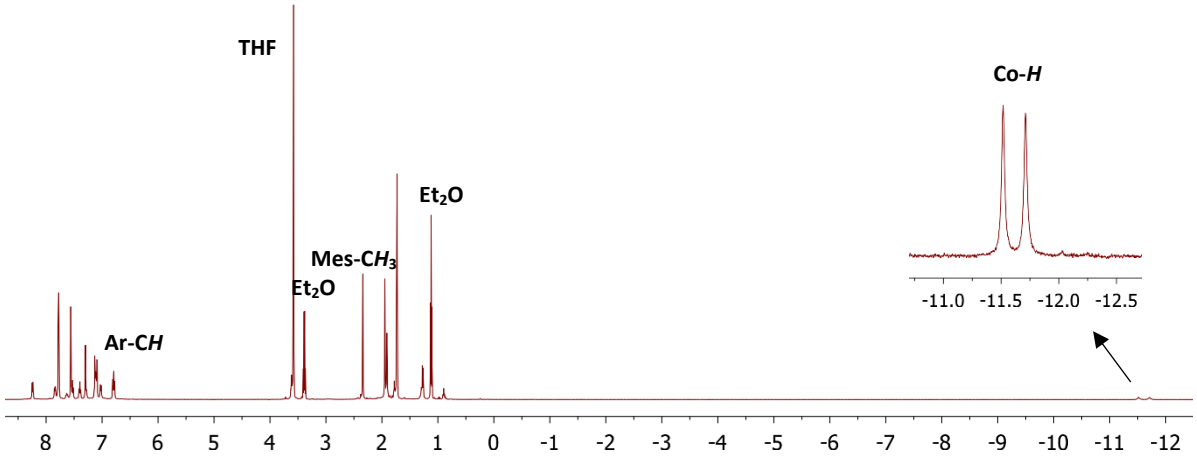

Figure 7.17 ^{1}H NMR spectrum of **[(^{Mes}CCC)Co-H(N_2)(PPh_2Me)][$B(Ar^F)_4$]** in THF-d_8.

7.10 Migratory insertion: ethylene and ethyl acrylate

In the olefin and alkyne hydrogenation studies employing the cobalt catalyst, **(^{Mes}CCC)Co(N_2)(PPh_3)**, migratory insertion of a carbon-carbon double or triple bond into the cobalt hydride fragment is proposed to occur. To this end, efforts to isolate or observe potential intermediates arising from migratory insertion using the electrophilic cobalt complexes, **[(^{Mes}CCC)Co-H(N_2)(PR_3)][$B(Ar^F)_4$]** (R = PPh_2Me, $PPhMe_2$, PMe_3) were undertaken. In these studies, **[(^{Mes}CCC)Co-H(N_2)(PPh_2Me)][$B(Ar^F)_4$]** was chosen since the phosphine derivate could be cleanly furnished, however, the other electrophilic Co(III)-hydride dinitrogen phosphine (PMe_3 or $PPhMe_2$) analogues are assumed to react in a similar manner.

The addition of styrene to a THF-d_8 solution of **[(^{Mes}CCC)Co-H(N_2)(PPh_2Me)][$B(Ar^F)_4$]** did not result in a change of the ^{1}H NMR spectrum suggesting no reaction took place. Undeterred by this shortcoming, the addition of 1 atm of ethylene to **[(^{Mes}CCC)Co-H(N_2)(PPh_2Me)][$B(Ar^F)_4$]** resulted in the disappearance of the hydridic resonance at -11.62 ppm and the appearance of six mesityl methyl resonances integrating to 3H each by ^{1}H NMR spectroscopy (Figure 7.18). Furthermore, the presence of a broad resonance at -

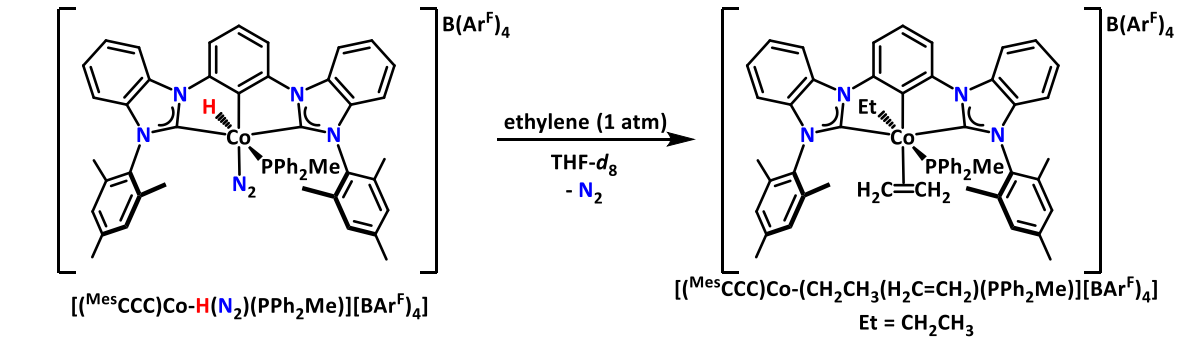

^{1}H NMR spectrum – THF-d_8

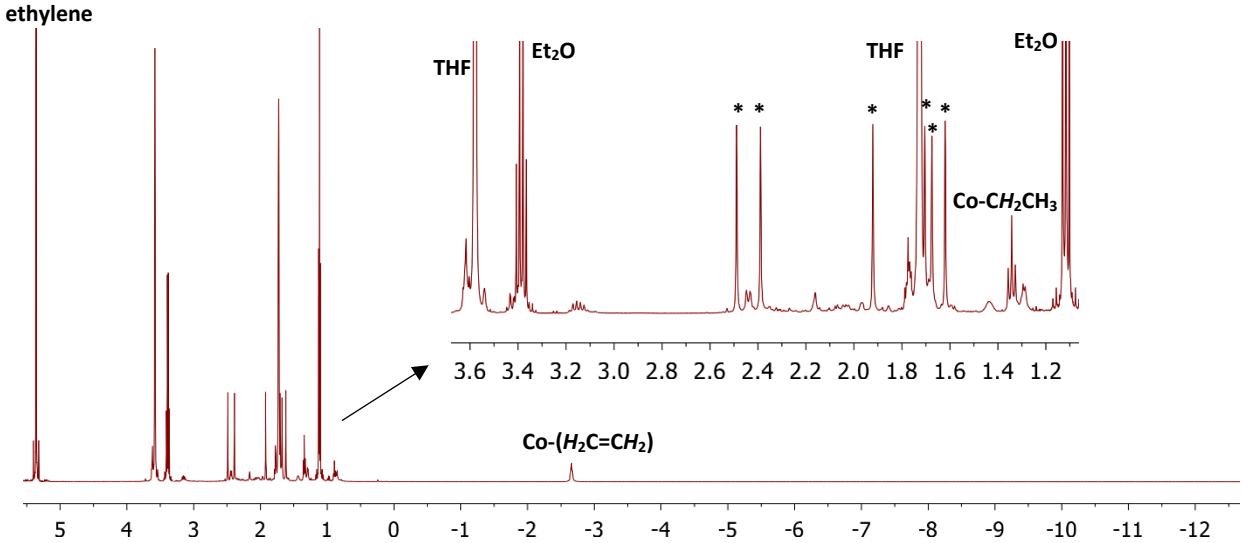

Figure 7.18 ^{1}H NMR spectrum of **[(^{Mes}CCC)Co-(CH_2CH_3)(η^2-H_2C=CH_2)(PPh_2Me)][$B(Ar^F)_4$]** in THF-d_8.

2.66 ppm, integrating to 4H suggested the formation of a Co(III)-(η^2-H_2C=CH_2) *in situ*. The chemical shift ^{1}H NMR resonances of the insertion product, a Co-CH_2CH_3 species, remained ambiguous. The formation of a new resonance at 1.3 ppm in the ^{2}H NMR spectrum (Figure 7.19) following the addition of ethylene to a THF solution of **[(^{Mes}CCC)Co-D(N_2)(PPh_2Me)][$B(Ar^F)_4$]** matched the chemical shift of new triplet in the ^{1}H NMR spectrum at 1.34 ppm with a $^3J_{CH}$ = 7.5 Hz integrating to 3H and was assigned to the β-hydride of the Co-CH_2CH_3 fragment. The chemical shift of the α carbon protons of Co-CH_2CH_3 could not be determined with confidence. Nevertheless, these results show that the olefin undergoes insertion into the cobalt-hydride species and further support such a process transpiring during catalysis. Unlike a similar cobalt(III) species reported by Brookhart and coworkers, [Cp*Co(L)(CH_2CH_2-μ-H)][$B(Ar^F)_4$][17] (L = PMe_3 or $P(OMe)_3$), **[(^{Mes}CCC)Co-(CH_2CH_3)(η^2-H_2C=CH_2)(PPh_2Me)][$B(Ar^F)_4$]** was not active for the polymerization ethylene, likely due to the lack of *β*-agostic C-H cobalt interactions of the ethyl group.

^{2}H NMR spectrum – THF

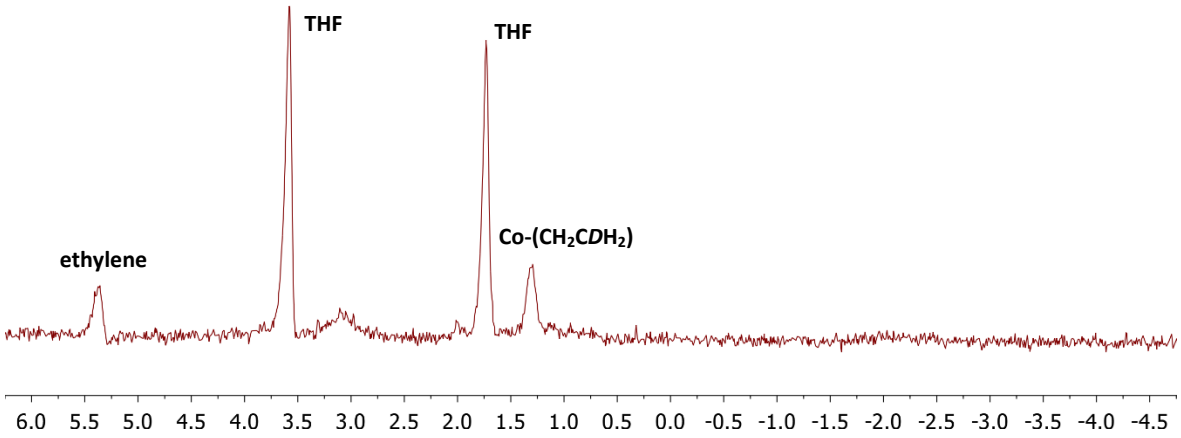

Figure 7.19 ^{2}H NMR spectrum of **[(^{Mes}CCC)Co-(CH_2CDH_2)(η^2-H_2C=CH_2)(PPh_2Me)][$B(Ar^F)_4$]** in THF.

A cobalt(III)-hydride intermediate was proposed to be involved in the *p*-H_2 transfer process in the ^{1}H and ^{13}C NMR signal enhancement studies using **(^{Mes}CCC)Co-py**. In these studies, migratory insertion of the olefin was proposed, therefore the use of ethyl acrylate to probe such a similar insertion step was investigated. The addition of ethyl acrylate to a THF-d_8 solution of **[(^{Mes}CCC)Co-H(N_2)(PPh_2Me)][$B(Ar^F)_4$]** resulted in the disappearance of the hydride resonance and the appearance of a resonance at 0.29 ppm in the ^{2}H NMR spectrum. This suggested that a reaction took place that was similar to that observed with ethylene (Figure 7.20). The presence of copious resonances in the aliphatic region of the ^{1}H NMR spectrum suggested multiple species were present in the solution and attempts to purify or assign the ^{1}H NMR spectrum of the crude mixture were not successful.

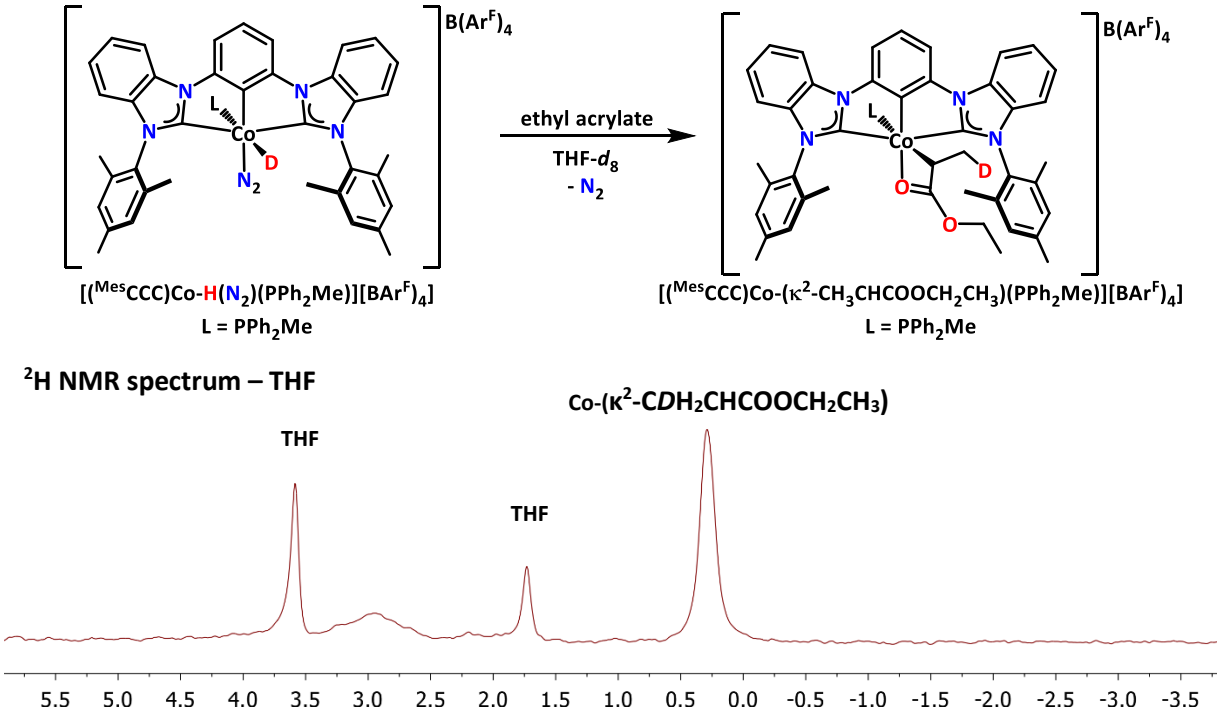

Figure 7.20 ^{2}H NMR spectrum of **[(^{Mes}CCC)Co-(κ^2-CDH$_2$CHCOOCH$_2$CH$_3$)(PPh$_2$Me)][B(Ar^F)$_4$]** in THF.

Single crystals suitable for X-ray diffraction studies were grown from a saturated diethyl ether and hexanes mixture of **[(^{Mes}CCC)Co-(κ^2-CH$_3$CHCOOCH$_2$CH$_3$)(PPh$_2$Me)][B(Ar^F)$_4$]** and confirmed the connectivity of the compound (Figure 7.21). The insertion of ethyl acrylate into the Co-H bond furnished an octahedral cobalt(III) complex. The C_α-Co bond lies *trans* to the phosphine ligand and the carbonyl oxygen atom is *trans* to the C_{aryl}-Co bond in the complex. Although a 4-membered chelate resulted from the 2,1-insertion of ethyl acrylate, isomerization to the more thermodynamically spices was not observed. In the case of [Cp*Co(L)(H$_2$)H][B(Ar^F)$_4$][17] (L = PMe$_3$ or P(OMe)$_3$), methyl acrylate displaces the bound H$_2$ ligand and products from both the 1,2 and 2,1-insertion are observed by ^{1}H NMR spectroscopy initially and over 24 hours, the thermodynamically favored 1,2-inserted product is formed via the standard β-hydride elimination, olefin rotation, insertion mechanism. Furthermore, 1,2-insertion products of methyl acrylate are well precedented with rhodium Cp (Cp = C$_5$H$_5$) or Cp* chemistry[21-23] and proposed intermediates in ruthenium-mediated head-to-tail dimerization of acrylates.[24]

The coordination of the olefin to the cobalt center likely proceeds first by the displacement of the N$_2$, followed the insertion of the olefin into the Co-H bond and chelation of the carbonyl oxygen atom. The addition of H$_2$ to a THF-d_8 solution of **[(^{Mes}CCC)Co-(κ^2-CH$_3$CHCOOCH$_2$CH$_3$)(PPh$_2$Me)][B(Ar^F)$_4$]** resulted in no reaction. Nevertheless, this system supports the proposed migratory insertion pathways proposed in catalytic hydrogenation and PHIP studies.

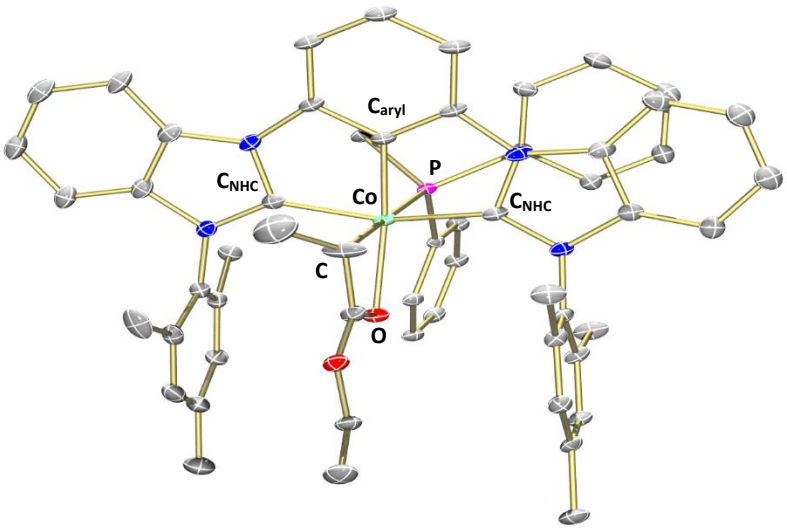

Figure 7.21 Molecular structure of **[(^{Mes}CCC)Co-(κ^2-CH$_3$CHCOOCH$_2$CH$_3$)(PPh$_2$Me)][B(Ar^F)$_4$]** with 50% probability ellipsoids. Solvent molecules, B(Ar^F)$_4$ counter anion and H atoms have been omitted for clarity.

7.11 Conclusion

In conclusion, stoichiometric oxidative addition and reductive elimination chemistry with the ^{Mes}CCC ligand platform demonstrate the viability of a Co(I)/Co(III) redox couple in the scrambling of H_2 and D_2 and further support the transient formation of Co(III)-$(H)_2$ intermediates in the hydrogenation catalysis observed with these complexes. Ionic cobalt(III)-hydride dinitrogen phosphine complexes were prepared from 1) the oxidative addition of [H(OEt$_2$)$_2$][B(Ar^F)$_4$] onto the Co(I)-N_2 precursors and 2) the salt metathesis of the Co-HCl phosphines complexes with NaB(Ar^F)$_4$. Addition of H_2 or D_2 to **[(^{Mes}CCC)Co-H(N$_2$)(PMe$_3$)][B(Ar^F)$_4$]** resulted in the formation of dynamic Co-(H_2)(H) complexes, which also proved to facilitate the scrambling of H_2 and D_2. Migratory insertion of ethylene or the carbon-carbon double bond of ethyl acrylate into the Co-H were observed and the resulting complexes were characterized by multinuclear NMR spectroscopy and X-ray crystallography. Taken together, these studies demonstrate that the ^{Mes}CCC cobalt complexes engage in many of the same mechanistic steps (oxidative addition, migratory insertion, and reductive elimination) for which noble metals are well known. This work also demonstrates that the ^{Mes}CCC ligand framework provides the appropriate support and spectroscopic handles to elucidate key mechanistic steps observed in the hydrogenation chemistry of the cobalt complexes.

7.12 Experimental section

General considerations. All manipulations of air- and moisture-sensitive compounds were carried out in the absence of water and dioxygen in an MBraun inert atmosphere drybox under a dinitrogen atmosphere except where specified otherwise. All glassware was oven dried for a minimum of 8 h and cooled in an evacuated antechamber prior to use in the drybox. Solvents for sensitive manipulations were dried and deoxygenated on a Glass Contour System (SG Water USA, Nashua, NH) and stored over 4 Å molecular sieves purchased from Strem following a literature procedure prior to use.[25] Chloroform-*d*, toluene-d_8 and benzene-d_6 were purchased from Cambridge Isotope Labs and were degassed and stored over 4 Å molecular sieves prior to use. Lithium hexamethyldisilazane was purchased from Sigma-Aldrich and recrystallized from toluene under an inert atmosphere prior to use. Celite® 545 (J. T. Baker) was dried in a Schlenk flask for 24 h under dynamic vacuum while heating to at least 150˚C prior to use in a glovebox. NMR Spectra were recorded at room temperature on a Varian spectrometer operating at 500 MHz (^{1}H NMR) and 126 MHz (^{13}C NMR) (U500, VXR500, UI500NB) and referenced to the residual $CHCl_3$ and C_6D_5H resonance (δ in parts per million, and *J* in Hz). Potassium graphite (KC_8),[26] **(^{Mes}CCC)CoCl$_2$py**,[14] **(^{Mes}CCC)Co(N$_2$)(PPh$_3$)**,[14] **(^{Mes}CCC)Co(N$_2$)(PMe$_3$)**,[10] **(^{Mes}CCC)Co-py**,[12] $NaB(Ar^F)_4$,[27] $[H(Et_2O)_2][B(Ar^F)_4]$[27] and $[D(Et_2O)_2][B(Ar^F)_4]$[27] were prepared according to literature procedures. HCl (2.0 M in Et_2O) and DCl (1.0 M in Et_2O) were purchased from the Sigma Aldrich Chemical Company.

Synthesis of metal complexes

Preparation of (^{Mes}CCC)Co-HCl(PMe$_3$): A 20 mL scintillation vial charged with **(^{Mes}CCC)Co(N$_2$)(PMe$_3$)** (0.024 g, 0.034 mmol) and *ca.* 5 mL of THF was cooled to -35°C. A solution of HCl·Et_2O (2.0 M, 17 µL, 0.034 mmol) was added and the mixture was stirred for 1 h. Following the removal of the volatiles under reduced pressure, the mixture was washed with Et_2O (2 x 5 mL), dissolved in C_6H_6 (10 mL), filtered over a plug of Celite and the solvent was removed *in vacuo* to give an orange solid (0.020 g, 0.027 mmol, 80%). Crystals suitable for X-ray diffraction were grown from slow evaporation of a concentrated solution of complex **(^{Mes}CCC)Co-HCl(PMe$_3$)** in Et_2O at room temperature. ^{1}H NMR data (in benzene-d_6): δ = 7.76 (d, J = 7.5, 2H), 7.45 (d, J = 7.5, 2H), 7.32 (t, ^{2}J = 6.5 1H), 7.08 (t, J = 7.3, 2H), 6.95-6.88 (m, 4H), 6.75 (d, J = 7.5, 2H) s (2H), 2.30 (s, 6H), 2.06 (s, 6H), 2.03 (s, 6H), 0.55 (d, J_{CH3P} = 7, 9H), -10.0 (d, $^2J_{HP}$ = 109, 1H). ^{13}C δ = 146.3, 138.5, 138.1, 137.9, 133.8, 131.5, 130.3, 123.1, 122.8, 122.1, 110.6, 110.4, 107.3, 21.1, 19.0, 18.9, 14.0, 13.8. T_1 (min): 139 ms (298K). HRMS (ESI), calc. for $C_{41}H_{42}ClCoN_4P$ $(M - H)^+$: calculated 715.2168; found 715.2161.

Preparation of (^{Mes}CCC)Co-DCl(PMe$_3$): A 20 mL scintillation vial charged with **(^{Mes}CCC)Co(N$_2$)(PMe$_3$)** (0.023 g, 0.032 mmol) and *ca.* 5 mL of THF was cooled to -35°C. A solution of DCl·Et$_2$O (1.0 M, 32 µL, 0.033 mmol) was added and the mixture was stirred for 1 h. Following the removal of the volatiles under reduced pressure, the mixture was washed with Et$_2$O (2 x 5 mL), dissolved in C$_6$H$_6$ (10 mL), filtered over a plug of Celite and the solvent was removed *in vacuo* to give an orange solid (0.019 g, 0.027 mmol, 82%). ^{1}H NMR data (in benzene-d_6): δ = 7.76 (d, J = 7.5, 2H), 7.45 (d, J = 7.5, 2H), 7.32 (t, J = 6.5 1H), 7.08 (t, J = 7.3, 2H), 6.95-6.88 (m, 4H), 6.75 (d, J = 7.5, 2H) s (2H), 2.30 (s, 6H), 2.06 (s, 6H), 2.03 (s, 6H), 0.55 (d, $^2J_{CH3P}$ = 7, 9H). ^{2}H NMR data (in benzene, 76.7 MHz, 25 °C): δ = -10.0 (d_{DP}, ^{2}J = 16.4, 1H).

Preparation of (^{Mes}CCC)Co-Cl$_2$(PMe$_3$): A 20 mL scintillation vial charged with **(^{Mes}CCC)Co(N$_2$)(PMe$_3$)** (0.0273 g, 0.0385 mmol) in *ca.* 5 mL of THF. A solution of ClCPh$_3$ (0.0220 g, 0.0789 mmol) in *ca.* 5 mL of THF was added to the mixture. After stirring the brown solution for 1 h, the THF was removed under reduced pressure. The solid residue was washed with THF (5 mL x 2) over a pad of Celite and the orange solid was dissolved in DCM (15 mL). Following the removal of solvent under reduced pressure, the solid residue was triturated with hexanes (5 mL) and dried *in vacuo* to yield an orange solid (0.0103 g, 0.0137 mmol, 36%). ^{1}H NMR data (in benzene-d$_6$): δ = 7.68 (d, J = 8.0, 2H), 7.40 (d, J = 7.5, 2H), 7.27 (t, J = 8, 1H), 7.05 (t, J = 7.5, 2H), 6.94-6.89 (m, 4H), 6.75 (d, J = 8, 2H), 6.68 (s, 2H), 2.58 (s, 6H), 2.13 (s, 6H), 1.94 (s, 6H), 0.40 (d, $^2J_{CH3P}$ = 11, 9H). ^{13}C (NMR data in CDCl$_3$) δ = 147.7, 138.8, 138.5, 138.0, 133.2, 133.1, 131.7, 130.43, 128.6, 125.2, 124.1, 123.7, 111.6, 109.7, 21.4, 20.1, 19.7, 16.4, 16.1. HRMS (ESI), calc. for C$_{41}$H$_{42}$ClCoN$_4$P (M – Cl)$^+$: calculated 715.2168; found 715.2164.

Preparation of (^{Mes}CCC)Co-HClpy: A 20 mL scintillation vial was charged with **(^{Mes}CCC)CoCl$_2$py** (0.070 g, 0.093 mmol) and THF (10 mL). A suspension of KC$_8$ (0.026 g, 0.195 mmol) in THF (5 mL) was added to the mixture. After stirring for 2 hours, the dark brown suspension was filtered over Celite and to the filtrate, a solution of HCl•Et$_2$O (2.0 M, *ca.* 0.044 µL, 0.088 mmol) was added dropwise to the mixture, resulting a yellow color change to the solution. After stirring the mixture for 30 min, the solvent was removed under reduced pressure. The product was washed with Et$_2$O (10 mL) and extracted into THF (20 mL). The THF solution was concentrated under reduced pressure to an orange-yellow solid (0.040 g, 0.056 mmol, 60%). Single crystals suitable for X-ray diffraction studies were grown from a saturated Et$_2$O solution of the complex by slow evaporation. ^{1}H NMR data (in benzene-d_6): δ = 9.38 (s, 1H), 8.22 (s, 1H), 7.80 (s, 2H), 7.51 (s, 2H), 7.38 (s, 1H), 7.10 (s, 2H), 6.90 (s, 2H), 6.56 (d, J = 7, 2H), 6.49 (s, 1H), 6.49 (s, 2H), 6.10 (s, 2H), 5.83 (s, 1H), 5.76 (s, 1H), 2.39 (s, 6H), 1.93 (s, 6H), 1.63 (s, 6H), -23.53 (s, 1H). The low solubility of the complex

precluded the collection of reliable ^{13}C NMR data. T_1(min) (298K) was found to be 115 ms. HRMS (ESI), calc. for $C_{43}H_{38}CoN_5$ $(M\text{-}HCl)^{2+}$: 683.2459; found 683.2455. IR: 1895 cm^{-1} (Co-H).

Preparation of ($H_2^{Mes}CCC$)$CoCl_3$: A 20 mL scintillation vial charged with **$[H_3(CCC^{Mes})]Cl_2$** (0.123 g, 0.199 mmol) and $CoCl_2$ (0.026 g, 0.200 mmol) in *ca.* 10 mL of THF were stirred at ambient temperature. A solution of lithium hexamethyldisilazide (0.034 g, 0.200 mmol) in *ca.* 5 mL of THF was added dropwise and the blue suspension was stirred for 17 h. After removing the volatiles under reduced pressure, the crude mixture was taken up in DCM (*ca.* 10 mL), cooled to -35°C and filtered over a plug of celite. A blue solid was isolated after the evaporation of DCM under reduced pressure. (0.128 mg, 0.179, 90%). ^1H NMR (500 MHz, $CDCl_3$) δ 11.79, 10.98, 9.14, 8.39, 8.14, 7.85, 7.60, 6.75, 5.93, 4.82, 3.76, 3.17, 2.68, 1.26, 0.90, 0.33.

Synthesis (^{Mes}CCC)Co-HCl(PMe_3) from ($H_2^{Mes}CCC$)$CoCl_3$: A 20 mL scintillation vial charged with **($H_2^{Mes}CCC$)$CoCl_3$** (0.030 g, 0.041 mmol) and PMe_3 (1.0 M, *ca.* 0.05 mL, 0.05 mmol) in *ca.* 10 mL of THF were stirred at ambient temperature for 5 min. A dropwise addition of a THF (*ca.* 6 mL) suspension of KC_8 (0.006 g, 0.041 mmol) and lithium hexamethyldisilazide (0.007 g, 0.041 mmol) resulted in the formation of orange solution after stirring at for 17 h. The volatiles were removed under reduced pressure and the crude solid was washed with Et_2O (2 x 5 mL), taken up in benzene (10 mL) and filtered over a plug of celite and lyophilized to an orange solid (0.021 mg, 0.029 mmol, 69%).

Preparation of (^{Mes}CCC)Co(N_2)(PPh_2Me): A 20 mL scintillation vial was charged with **(^{Mes}CCC)$CoCl_2$py** (0.080 g, 0.106 mmol) and THF (10 mL). A suspension of KC_8 (0.030 g, 0.223 mmol) in THF (5 mL) was added to the mixture. After stirring for 2 hours, the dark brown suspension was filtered over Celite and to the filtrate, PPh_2Me (0.021 g, 20 µL, 0.106 mmol) was added, resulting in the change of the mixture to dark red. The THF was removed under reduced pressure after stirring the solution for 5 min. The product was washed with hexanes (5 mL) and extracted into benzene (10 mL), filtered over Celite and concentrated under reduced pressure to a red solid. The solid was triturated with hexane (10 mL) and concentrated *in vacuo* to give a fine red powder (0.071 g, 0.086 mmol, 81%). The ^1H and ^{13}C NMR spectra match those of the reported compound. NMR data (in benzene-d_6, 25 °C): ^1H δ = 7.78 (d, J = 7.8, 2H), 7.63 (d, J = 7.7, 2H), 7.48 (dt, J = 7.5, J = 2.4, 1H), 7.07 (t, J = 7.5, 2H), 6.90-6.80 (m, 12H), 6.79 (s, 2H), 6.70 (s, 2H), 6.53 (d, J = 7.6, 2H), 2.02 (s, 6H), 2.01 (s, 6H), 1.87 (s, 6H), 0.91 (d, $J_{CH3\text{-}P}$ = 5.3, 3H). ^{13}C δ = 144.9, 144.0, 138.5, 138.4, 138.2, 136.3, 134.3, 132.0, 131.6, 131.5, 130.1, 128.9, 127.6, 127.6, 121.8, 121.7, 109.7, 108.4, 106.0, 21.1, 18.6, 18.26, 13.2, 12.8. IR: 2118 cm^{-1} (N_2).

Preparation of (^{Mes}CCC)Co(N_2)($PPhMe_2$): A 20 mL scintillation vial was charged with **(^{Mes}CCC)$CoCl_2$py** (0.080 g, 0.106 mmol) and THF (10 mL). A suspension of KC_8 (0.030 g, 0.223 mmol) in THF (5 mL) was added to the mixture. After stirring for 2 hours, the dark brown suspension was filtered over Celite and to the filtrate, $PPhMe_2$ (0.015 g, 15 µL, 0.106 mmol) was added, resulting in the change of the mixture to dark red. The THF was removed under reduced pressure after stirring the solution for 5 min. The product was washed with hexanes (5 mL) and extracted into diethyl ether (10 mL), filtered over Celite and concentrated under reduced pressure to a red solid. The solid was triturated with hexane (10 mL) and concentrated *in vacuo* to give a fine red powder (0.048 g, 0.063 mmol, 59%). NMR data (in benzene-d_6, 25 °C ^{1}H δ = 7.86 (d, J = 7.8, 2H), 7.72 (d, J = 7.2, 2H), 7.50 (dt, J = 7.5, J = 2.4, 1H), 7.09 (t, J = 7.8, 2H), 7.00-6,90 (m, 7H), 6.77 (s, 2H), 6.72 (s, 2H), 6.57 (d, J = 7.8, 2H), 2.07 (s, 6H), 2.00 (s, 6H), 1.92 (s, 6H), 0.63 (d, $J_{CH3\text{-}P}$ = 6.4, 6H). ^{13}C δ = 209.5, 163.6, 143.64, 143.6, 140.3, 140.2, 138.5, 138.4, 138.2, 136.0, 134.2, 132.1, 130.5, 130.4, 130.1, 128.0, 128.6, 121.9, 121.7, 118.9, 118.9, 109.7, 105.8, 105.6, 21.1, 18.5, 18.3, 14.5, 14.3. IR: 2114 cm^{-1} (N_2).

In situ preparation of **[(^{Mes}CCC)Co-H(N_2)(L)][$B(Ar^F)_4$] (L = PMe_3, PPh_2Me).** The deuterium analogues were prepared in an identical manner using [$D(OEt_2)_2$][$B(Ar^F)_4$] and show identical ^{1}H NMR spectra without the hydride present.

Preparation of [(^{Mes}CCC)Co-H(N_2)(PMe_3)][$B(Ar^F)_4$]: A THF-d_8 solution of **(^{Mes}CCC)Co(N_2)(PMe_3)** (0.005g, 0.0071 mmol) and [$H(OEt_2)_2$][$B(Ar^F)_4$] (0.07 g, 0.0071 mmol) was transferred to a J Young NMR tube. The resulting color change yellow color and 1H NMR spectrum indicated oxidation of the species *in situ*. ^{1}H NMR data in THF-d_8 δ 8.42 (d, J = 8.3, 2H), 7.98 (d, J = 7.9, 2H), 7.76 (s, 8H), 7.60 (t, J =7.8, 2H), 7.55 (s, 4H), 7.46 (t, J = 6.4, 2H), 7.20-7.08 (m, 7H), 2.34 (s, 6H), 2.15 (s, 6H), 1.98 (s, 6H), 0.80 ($^2J_{PH}$ = 8.9, 3H), -10.51 (d, $^2J_{HP}$ = 94, 1H). 2H NMR data THF δ -10.51 ($^2J_{DP}$ = 15 Hz, 1D)

Preparation of [(^{Mes}CCC)Co-H(N_2)(PPh_2Me)][$B(Ar^F)_4$]: A THF-d_8 solution of **(^{Mes}CCC)Co(N_2)(PPh_2Me)** (0.005 g, 0.006 mmol) and [$H(OEt_2)_2$][$B(Ar^F)_4$] (0.06 g, 0.006 mmol) was transferred to a J Young NMR tube. The resulting color change yellow color and 1H NMR spectrum indicated oxidation of the species *in situ*. ^{1}H NMR data in THF-d_8 δ 8.24 (d, J = 8.2, 2H), 7.84 (d, J = 7.7, 2H), 7.78 (s, 8H), 7.63 (t, J = 8.1, 1H), 7.56 (s, 4H), 7.53 (t, J = 8.3, 2H), 7.40 (t, 8.1, 2H), 7.29 (t, J = 7.2, 2H), 7.11 (m, 8H), 7.02 (d, J = 8.0, 2H), 6.79 (t, J = 8.9, 4H), 2.34 (2, 6H), 1.95 (s, 6H), 1.91 (s, 6H), 1.27 ($^2J_{PH}$ = 7.7, 3H), -11.61 (d, $^2J_{HP}$ = 97, 1H).

Determination of T_1: T_1 (minimum): Measurements were obtained on a 500 MHz spectrometer of

(^{Mes}CCC)Co-HCl(PMe$_3$), (^{Mes}CCC)Co-HClpy, in THF-d_8 by the standard inversion recovery pulse sequence method.

Stoichiometric reactivity studies

Reactivity with HCl: HCl·Et$_2$O (2.0 M, 6 µL, 0.0012 mmol) was added to a J. Young tube containing **(^{Mes}CCC)Co-HCl(PMe$_3$)** (0.009 g, 0.012 mmol) and ½ mL C_6D_6 then sealed. The resulting ^{1}H NMR spectrum showed resonances corresponding to the formation of H_2 gas and **(^{Mes}CCC)Co-Cl$_2$(PMe$_3$)**.

Reactivity with Cp$_2$ZrHCl: Cp$_2$ZrHCl (6 mg, 0.023 mmol) was added to a J. Young tube containing **(^{Mes}CCC)Co-HCl(PMe$_3$)** (0.05 g, 0.008 mmol) and ½ mL C_6D_6 then sealed. The resulting ^{1}H NMR spectrum showed resonances corresponding to the formation of H_2 gas, Cp$_2$ZrCl$_2$ and **(^{Mes}CCC)Co-(N$_2$)(PMe$_3$)**.

Reactivity of [(^{Mes}CCC)Co-H(N$_2$)(PMe$_3$)][B(Ar^F)$_4$] with H$_2$: A THF-d_8 solution of **(^{Mes}CCC)Co(N$_2$)(PMe$_3$)** (0.005 g, 0.006 mmol) and [H(OEt$_2$)$_2$][B(Ar^F)$_4$] (0.06 g, 0.006 mmol) was transferred to a J Young NMR tube and sealed. After subjecting the J Young NMR tube to two freeze-pump-thaw cycles, H_2 gas (1 atm) was added at 77K resulting 4 atm of gas pressure after warming the solution to room temperature. The color of the solution changed to a faint yellow color. ^{1}H NMR data in THF-d_8 δ 8.41 (d, J = 8.7, 2H), 8.03 (d, J = 8.5, 2H), 7.66 (t, J = 7.0, 1H), 7.44 (t, J = 7.7, 2H), 7.21-7.03 (m, 6H), 2.42 (s, 6H), 2.08 (s, 6H), 1.88 (s, 6H), 0.79 (d, $^2J_{HP}$ = 8l6, 9H), -5.55 (s, 2H), -11.1 to -11.2 (s, 1H).

Reactivity of [(^{Mes}CCC)Co-H(N$_2$)(PMe$_3$)][B(Ar^F)$_4$] with H$_2$: A THF-d_8 solution of **(^{Mes}CCC)Co(N$_2$)(PMe$_3$)** (0.007 g, 0.010 mmol) and [H(OEt$_2$)$_2$][B(Ar^F)$_4$] (0.011 g, 0.010 mmol) was transferred to a J Young NMR tube and sealed. After subjecting the J Young NMR tube to two freeze-pump-thaw cycles, D_2 gas (1 atm) was added at 77K resulting 4 atm of gas pressure after warming the solution to room temperature. The color of the solution changed to a faint yellow color. ^{2}H NMR data in THF δ -5.36 (s, 2D), -10.22 to -11.24 (m, 1H).

Reactivity of [(^{Mes}CCC)Co-H(N$_2$)(PPh$_2$Me)][B(Ar^F)$_4$] with ethylene: A THF-d_8 solution of **(^{Mes}CCC)Co(N$_2$)(PPh$_2$Me)** (0.005 g, 0.006 mmol) and [H(OEt$_2$)$_2$][B(Ar^F)$_4$] (0.06 g, 0.006 mmol) was transferred to a J Young NMR tube and sealed. After subjecting the J Young NMR tube to two freeze-pump-thaw cycles, ethylene gas (1 atm) was added. The color of the solution changed to a faint yellow color.

Reactivity of [(^{Mes}CCC)Co-D(N$_2$)(PPh$_2$Me)][B(Ar^F)$_4$] with ethylene: A THF solution of **(^{Mes}CCC)Co(N$_2$)(PPh$_2$Me)** (0.012 g, 0.0146 mmol) and [D(OEt$_2$)$_2$][B(Ar^F)$_4$] (0.014 g, 0.0146 mmol) was

transferred to a J Young NMR tube and sealed. After subjecting the J Young NMR tube to two freeze-pump-thaw cycles, ethylene gas (1 atm) was added. The color of the solution changed to a faint yellow color. ^{2}H NMR data in THF δ 1.30 (s, 1D).

Reactivity of [(^{Mes}CCC)Co-H(N_2)(PPh_2Me)][$B(Ar^F)_4$] with ethyl acrylate: A THF-d_8 solution of **(^{Mes}CCC)Co(N_2)(PPh_2Me)** (0.006 g, 0.007 mmol) and [$H(OEt_2)_2$][$B(Ar^F)_4$] (0.007 g, 0.007 mmol) was transferred to a J Young NMR tube. Ethyl acrylate (1 µL, 0.007 mmol) was transferred to the cobalt mixture in the J Young tube resulting in a faint yellow color change.

Reactivity of [(^{Mes}CCC)Co-D(N_2)(PPh_2Me)][$B(Ar^F)_4$] with ethyl acrylate: A THF solution of **(^{Mes}CCC)Co(N_2)(PPh_2Me)** (0.015 g, 0.018 mmol) and [$D(OEt_2)_2$][$B(Ar^F)_4$] (0.018 g, 0.018 mmol) was transferred to a J Young NMR tube. Ethyl acrylate (2 µL, 0.0014 mmol) was transferred to the cobalt mixture in the J Young tube resulting in a faint yellow color change. ^{2}H NMR data in THF δ 0.29 (s, 1D).

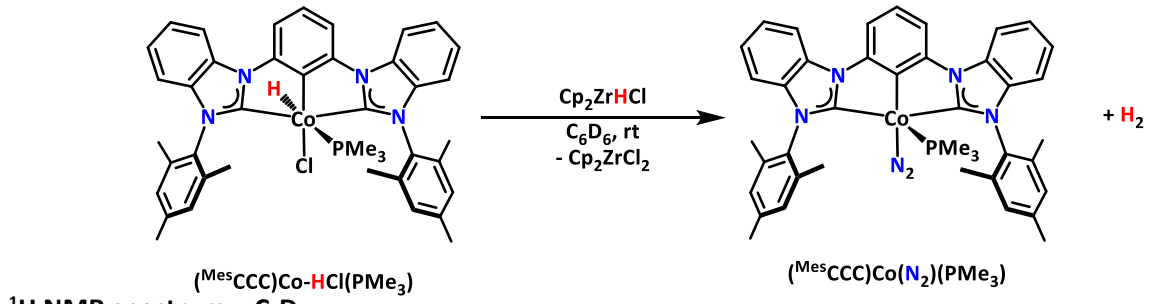

(^{Mes}CCC)Co-HCl(PMe$_3$) (^{Mes}CCC)Co(N$_2$)(PMe$_3$)

^{1}H NMR spectrum – C_6D_6

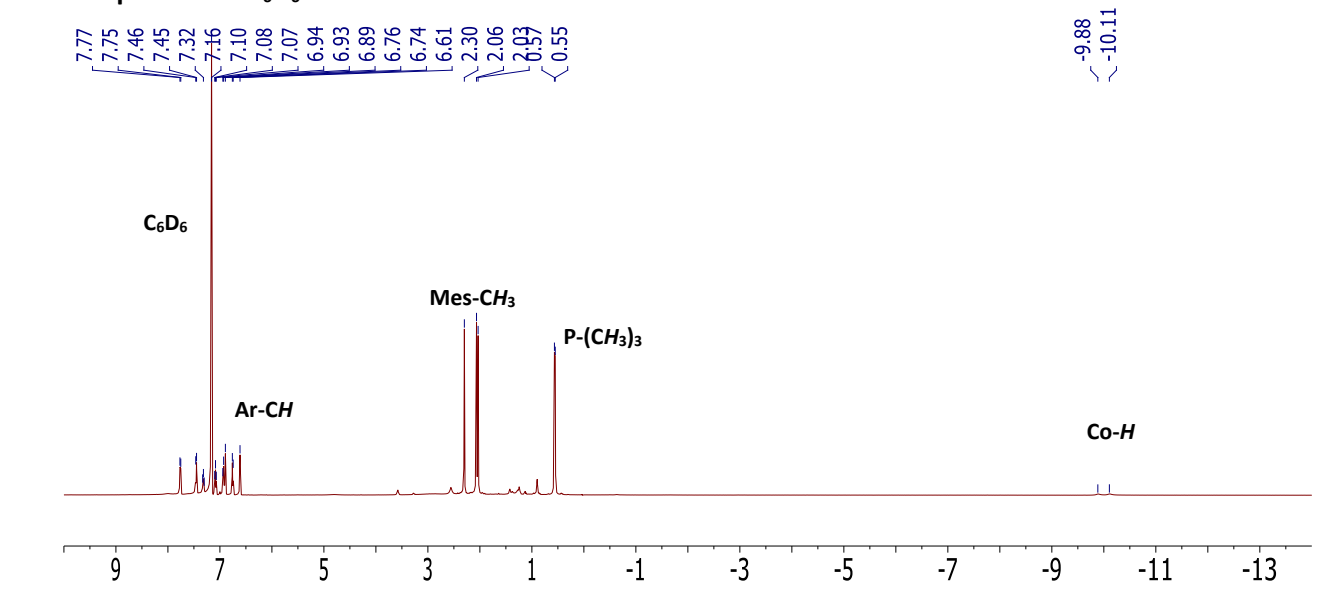

^{1}H NMR spectrum – C_6D_6

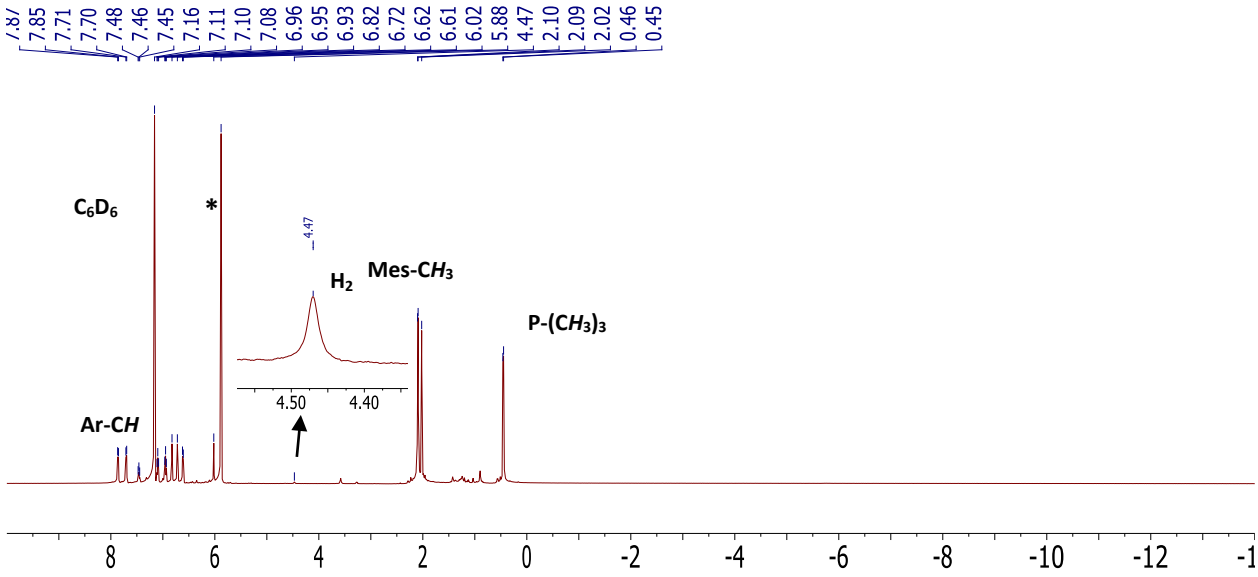

Figure 7.22 ^{1}H NMR (C_6D_6, 500 MHz) spectrum of **(^{Mes}CCC)Co-HCl(PMe$_3$)** (top) and the resulting ^{1}H NMR spectrum (bottom) following addition of Cp_2ZrHCl (3 eq.). (*denotes Cp_2ZrCl_2)

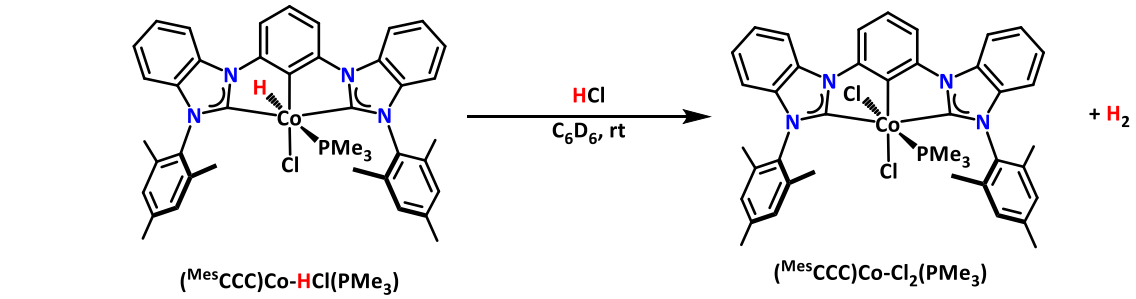

(^{Mes}CCC)Co-HCl(PMe$_3$) (^{Mes}CCC)Co-Cl$_2$(PMe$_3$)

^{1}H NMR spectrum – C_6D_6

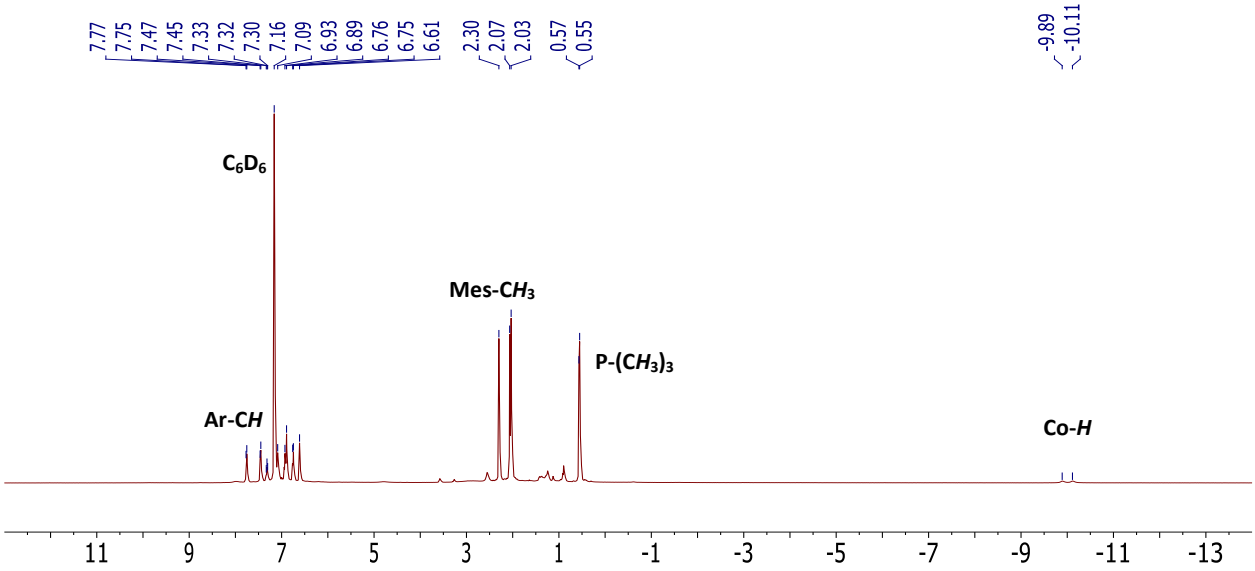

^{1}H NMR spectrum – C_6D_6

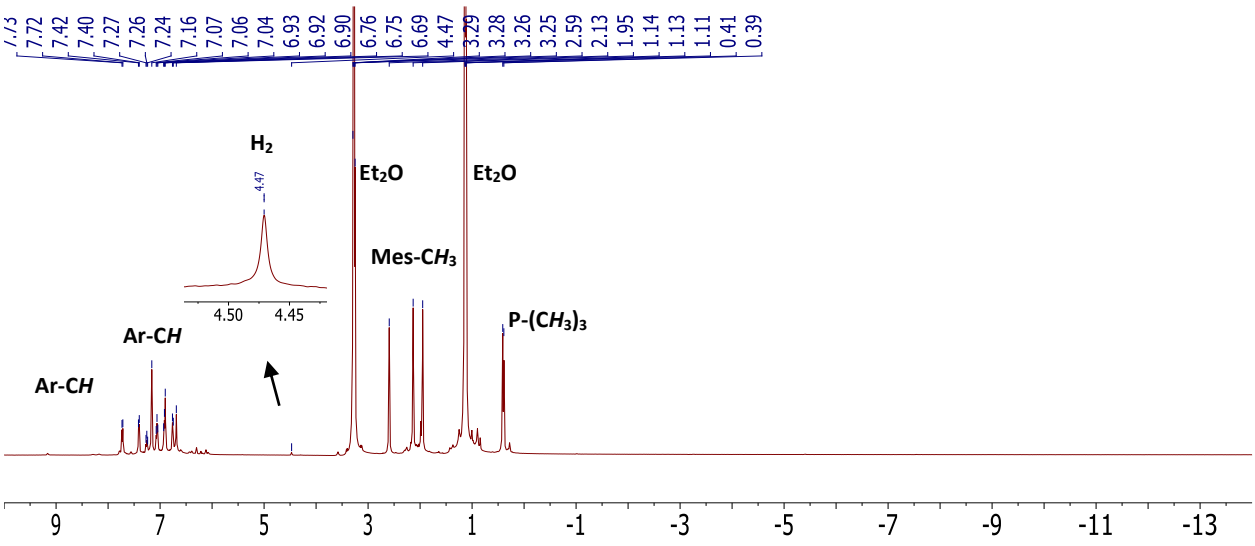

Figure 7.23 ^{1}H NMR (C_6D_6, 500 MHz) spectrum of **(^{Mes}CCC)Co-HCl(PMe$_3$)** (top) and the resulting ^{1}H NMR spectrum (bottom) following addition of HCl·Et$_2$O (1 eq.). (*denotes Et$_2$O)

Table 7.1 Crystallographic parameters for **H_2(^{Mes}CCC)$CoCl_3$** and **(^{Mes}CCC)Co-HCl(PMe_3)**.

	H_2(^{Mes}CCC)$CoCl_3$ cd75w	**(^{Mes}CCC)Co-HCl(PMe_3)** cm07w
Empirical Formula	C54 H66 Co N4 O4	C41 H42.18 Cl 1.12 Co N4 P
Formula Weight	1000.39	720.66
Temperature	100(2) K	100(2) K
Wavelength	0.71073 Å	0.71073 Å
Crystal system	Triclinic	Monoclinic
Space group	P-1	P 2_1/c
Unit Cell Dimensions	a = 11.5158(9) Å b = 13.5253(10) Å c = 18.1738(12) Å α= 104.582(3)° β= 98.135(3)° γ = 105.798(3)°	a = 12.2774(5) Å b = 18.0919(7) Å c = 16.3936(7) Å α = 90° β = 94.5253(17)° γ = 90°
Volume	2568.1(3) $Å^3$	3630.0(3) $Å^3$
Z	2	4
Reflections collected	50829	44035
Independent reflections	9506	6670
Goodness-of-fit on F2	1.123	1.016
Final R indices [I>sigma(I)]	R1 = 0.0875 wR2 = 0.1560	R1 = 0.0443 wR2 = 0.0915

Table 7.2 Crystallographic parameters for **(^{Mes}CCC)Co(N_2)(PPh_2Me)** and **(^{Mes}CCC)Co(N_2)($PPhMe_2$)**.

	(^{Mes}CCC)Co(N_2)(PPh_2Me) dd82f	**(^{Mes}CCC)Co(N_2)($PPhMe_2$)** dd67f
Empirical Formula	C51 H46 Co N6 P	C46 H44 Co N6 P
Formula Weight	832.84	770.77
Temperature	100(2) K	100(2) K
Wavelength	0.71073 Å	0.71073 Å
Crystal system	Monoclinic	Triclinic
Space group	P n	P-1
Unit Cell Dimensions	a = 10.3973(4) Å b = 25.1993(9) Å c = 16.0066(6) Å α = 90° β = 98.5741(10)° γ = 90°	a = 15.5791(7) Å b = 17.4213(8) Å c = 19.4108(9) Å α = 88.5420(14)° β = 88.7521(13)° γ = 72.9757(13)°
Volume	4146.9(3)(6) $Å^3$	5035.2(4) $Å^3$
Z	4	4
Reflections collected	80738	90030
Independent reflections	15225	18497
Goodness-of-fit on F2	1.048	1.032
Final R indices [I>sigma(I)]	R1 = 0.0324 wR2 = 0.0791	R1 = 0.0415 wR2 = 0.1110

Table 7.3 Selected bond lengths and angles for **$H_2(^{Mes}CCC)CoCl_3$** and **$(^{Mes}CCC)Co\text{-}HCl(PMe_3)$**.

	$H_2(^{Mes}CCC)CoCl_3$	$(^{Mes}CCC)Co\text{-}HCl(PMe_3)$
Bond Distances (Å)		
Co – C_{NHC}	2.070(5)	1.922(3)
Co – C_{aryl}	N/A	1.857(3)
Co – C_{NHC}	N/A	1.919(3)
Co-H	Cl1 2.2417(15)	1.40(5)
Co – Cl1	Cl2 2.2946(14)	2.3057(7)
Co – P	Cl3 2.2805(14)	2.2229(8)
Co-Cl2	N/A	2.483(6)
Bond Angles (°)		
C_{aryl}-Co-N	Cl1-Co-Cl2 116.75(6)	N/A
C_{NHC}-Co-C_{aryl}	Cl1-Co-Cl3 107.23(6)	80.77(11)
C_{aryl}-Co-C_{NHC}	Cl3-Co-Cl2 104.97(5)	80.76(11)
C_{NHC}-Co-C_{NHC}	C-Co-Cl1 107.44(14)	158.71(11)
C_{aryl}-Co-Cl1	C-Co-Cl2 105.29(13)	99.23(8)
N-Co-P	C-Co-Cl3 115.54(14)	N/A
P-Co-H	N/A	174.0(17)
Cl1-Co-Cl2	N/A	89.81(14)

Table 7.4 Selected bond lengths and angles for **(^{Mes}CCC)Co(N_2)(PPh_2Me)** and **(^{Mes}CCC)Co(N_2)($PPhMe_2$)**.

	(^{Mes}CCC)Co(N_2)(PPh_2Me)	(^{Mes}CCC)Co(N_2)($PPhMe_2$)
Bond Distances (Å)		
Co – C_{NHC}	1.901(4)	1.905(2)
Co – C_{aryl}	1.870(4)	1.870(2)
Co – C_{NHC}	1.915(4)	1.889(2)
Co – N	1.836(3)	1.8339(19)
Co – P	2.2183(11)	2.2058(6)
N – N	1.107(5)	1.103(3)
Bond Angles (°)		
C_{aryl}-Co-N	163.73(16)	164.00(9)
C_{NHC}-Co-C_{aryl}	79.18(17)	78.87(9)
C_{aryl}-Co-C_{NHC}	79.01(16)	79.64(9)
C_{NHC}-Co-C_{NHC}	153.57)16)	153.15(9)
N-Co-P	101.01(11)	103.24(7)

7.13 References

1. Ludwig, J. R.; Schindler, C. S. Catalyst: Sustainable Catalysis. *Chem*, **2017**, *2*, 313-316.
2. In Organotransition Metal Chemistry: From Bonding to Reactivity; Hartwig, J. F., Ed.; University Science Books: Sausalito, CA, 2010.
3. Chirik, P. J. Iron- and Cobalt-Catalyzed Alkene Hydrogenation: Catalysis with Both Redox-Active and Strong Field Ligands. *Acc. Chem. Res.* **2015**, *48*, 1687−1695.
4. Friedfeld, M. R.; Margulieux, G. W.; Schaefer, B. A.; Chirik, P. J. Bis(phosphine)cobalt Dialkyl Complexes for Directed Catalytic Alkene Hydrogenation. *J. Am. Chem. Soc.* **2014**, *136*, 13178−13181.
5. Ingleson, M.; Fan, H.; Pink, M.; Tomaszewski, J.; Caulton, K. Three-Coordinate Co(I) Provides Access to Unsaturated Dihydrido-Co(III) and Seven-Coordinate Co(V). *J. Am. Chem. Soc.* **2006**, *128*, 1804−1805.
6. Semproni, S. P.; Atienza, C. C. H.; Chirik, P. J. Oxidative addition and C-H activation chemistry with a PNP pincer-ligated cobalt complex. *Chem. Sci.* **2014**, *5*, 1956-1960.
7. Rozenel, S. S.; Padilla, R.; Camp, C.; Arnold, J. Unusual activation of H_2 by reduced cobalt complexes supported by a PNP pincer ligand. *Chem. Commun.* **2014**, *50*, 2612-2614.
8. Ibrahim, A. D.; Entsminger, S.; Zhu, L.; Fout, A. R. A Highly Chemoselective Cobalt Catalyst for the Hydrosilylation of Alkenes using Tertiary Silanes and Hydroxiloxanes. *ACS Catal.* **2016**, *6*, 3589-3593.
9. Ibrahim, A. D.; Entsminger, S.; Fout, A. R. Insights into a Chemoselective Cobalt Catalyst for the Hydroboration of Alkenes and Nitriles. *ACS Catal.* **2017**, *6*, 3730-3734.
10. Tokmic, K.; Markus, C. R.; Zhu, L.; Fout, A. R. Well-Defined Cobalt(I) Dihydrogen Catalyst: Experimental Evidence for a Co(I)/Co(III) Redox Process in Olefin Hydrogenation. *J. Am. Chem. Soc.* **2016**, *138*, 11907-11913.
11. Tokmic, K.; Fout, A. R. Alkyne Semihydrogenation with a Well-Defined Nonclassical Co-H2 Catalyst: A H2 Spin on Isomerization and E-Selectivity. *J. Am. Chem. Soc.* **2016**, *138*, 13700-13705.
12. Tokmic, K.; Jackson, B. J.; Salazar, A.; Woods, T. J.; Fout, A. R. Cobalt-Catalyzed and Lewis Acid-Assisted Nitrile Hydrogenation to Primary Amines: A Combined Effort. *J. Am. Chem. Soc.* **2017**, *139*, 13554-13561.
13. In Organotransition Metal Chemistry: From Bonding to Reactivity; Hartwig, J. F., Ed.; University Science Books: Sausalito, CA, 2010.

14. Ibrahim, A. D.; Tokmic, K.; Brennan, M. B.; Kim, D. Matson, E. M.; Nilges, M. J.; Bertke, J. A.; Fout, A. R. Monoanionic bis(carbene) pincer complexes featuring cobalt(I-III) oxidation states. *Dalton Trans.* **2016**, *45*, 9805-9811.
15. Matson, E. M.; Jackson, B. J.; Bertke, J. A.; Fout, A. R. Synthesis and Characterization of Monoanionic Pincer N-heterocyclic Carbene Iron Complexes. unpublished.
16. Yang, L.; Powell, D. R.; Houser, R. P. Structural Variation in Copper(I) Complexes with Pyridylmethylamide Ligands: Structural Analysis with a New Four-Coordinate Geometry Index, Tau4. *Dalton Trans.* **2007**, 955-964.
17. Doherty, M. D.; Grant, B.; White, P. S.; Brookhart, M. Reactions of H2 and R3SiH with Electrophilic Cobalt(III) Alkyl Complexes: Spectroscopic Characterization, Dynamics, and Chemistry of $[Cp^*Co(L)(H)(\eta^2\text{-}H_2)][B(Ar^F)_4]$ and $[Cp^*Co(L)(H)(\eta^2\text{-}HSiR_3)][B(Ar^F)_4]$. *Organometallics* **2007**, *26*, 5950-5960.
18. Desrosiers, P. J.; Cai, L.; Richards, R.; Halpern, J.; Lin, Z. Assessment of the "T1 criterion" for distinguishing between classical and nonclassical transition-metal hydrides: hydride relaxation rates in tris(triarylphosphine)osmium tetrahydrides and related polyhydrides. *J. Am. Chem. Soc.* **1991**, *113*, 4173−4184.
19. Nanishankar, H. V.; Dutta, S.; Nethaji, M.; Jagirdar, B. R. Dynamics of a cis-Dihydrogen/Hydride Complex of Iridium. *Inorg. Chem.* **2005**, *44*, 6203-6210.
20. Bilbrey, J. A.; Kazez, A. H.; Locklin, J.; Allen, W. D. Exact Ligand Cone Angles. *J. Comput. Chem.* **2013**, *34*, 1189-1197.
21. Hauptman, E.; Sabo-Etienne, S.; White, P. S.; Brookhart, M.; Garner, J. M.; Fagan, P. J.; Calabrese, J. C. Design and Study of Rh(III) Catalysts for the Selective Tail-to-Tail Dimerization of Methyl Acrylate. *J. Am. Chem. Soc.* **1994**, *116*, 8038-8060.
22. Brookhart, M.; Sabo-Etienne, S. Catalytic Tail-to-tail Dimerization of Methyl Acrylate Using Rh(III) Catalysts. *J. Am. Chem. Soc.* **1991**, *113*, 2777-2779.
23. Brookhart, M.; Hauptman, E. Mechanism of Rhodium(III)-Catalyzed Methyl Acrylate Dimerization. *J. Am. Chem. Soc.* **1992**, *114*, 4437-4439.
24. Yi, C. S.; Liu, N. Ruthenium-mediated selective head-to-tail dimerization of acrylic and α,β-unsaturated carbonyl compounds: generation of an acrylate-hydride complex $C_5Me_5Ru(PCy_3)(CH_2{=}CHCO_2Et)H$. *J. Organomet. Chem.* **1998**, *553*, 157-161.
25. Pangborn, A.B.; Giardello, M.A.; Grubbs, R. H.; Rosen, R. K.; Timmers, F. J. Safe and Convenient Procedure for Solvent Purification. *Organometallics*, **1996**, *15*, 1518−1520.

26. Wietz, I. S.; Rabinovitz, M. The application of C_8K for organic synthesis: reduction of substituted naphthalenes. *J. Chem. Soc. Perkin Trans.* **1993**, *1*, 117-120.
27. Brookhart, M.; Grant, B.; Volpe Jr., A. F. [(3,5-(CF3)2C6H3)4B]-[H(OEt2)2]+: a convenient reagent for generation and stabilization of cationic, highly electrophilic organometallic complexes. *Organometallics* **1992**, *11*, 3920-3922.